JOURNAL OF RESEARCH

OF THE U.S. GEOLOGICAL SURVEY

MAY–JUNE 1978
VOLUME 6, NUMBER 3

Scientific notes and summaries of investigations in geology, hydrology, and related fields

U.S. DEPARTMENT OF THE INTERIOR

UNITED STATES DEPARTMENT OF THE INTERIOR
CECIL D. ANDRUS, Secretary
GEOLOGICAL SURVEY
H. William Menard, Director

For sale by Superintendent of Documents, U.S. Government Printing Office, Washington, DC 20402. Annual subscription rate, $18.90 (plus $4.75 for foreign mailing). Make check or money order payable to Superintendent of Documents. Send all subscription inquiries and address changes to Superintendent of Documents at above address.

Purchase single copy ($3.15) from Branch of Distribution, U.S. Geological Survey, 1200 South Eads Street, Arlington, VA 22202. Make check or money order payable to U.S. Geological Survey.

Library of Congress Catalog-card No. 72-600241.

The Journal of Research is published every 2 months by the U.S. Geological Survey. It contains papers by members of the Geological Survey and their professional colleagues on geologic, hydrologic, topographic, and other scientific and technical subjects.

Correspondence and inquiries concerning the Journal (other than subscription inquiries and address changes) should be directed to Anna M. Orellana, Managing Editor, Journal of Research, Publications Division, U.S. Geological Survey, 321 National Center, Reston, VA 22092.

Papers for the Journal should be submitted through regular Division publication channels.

The Secretary of the Interior has determined that the publication of this periodical is necessary in the transaction of the public business required by law of this Department. Use of funds for printing this periodical has been approved by the Director of the Office of Management and Budget through June 30, 1980.

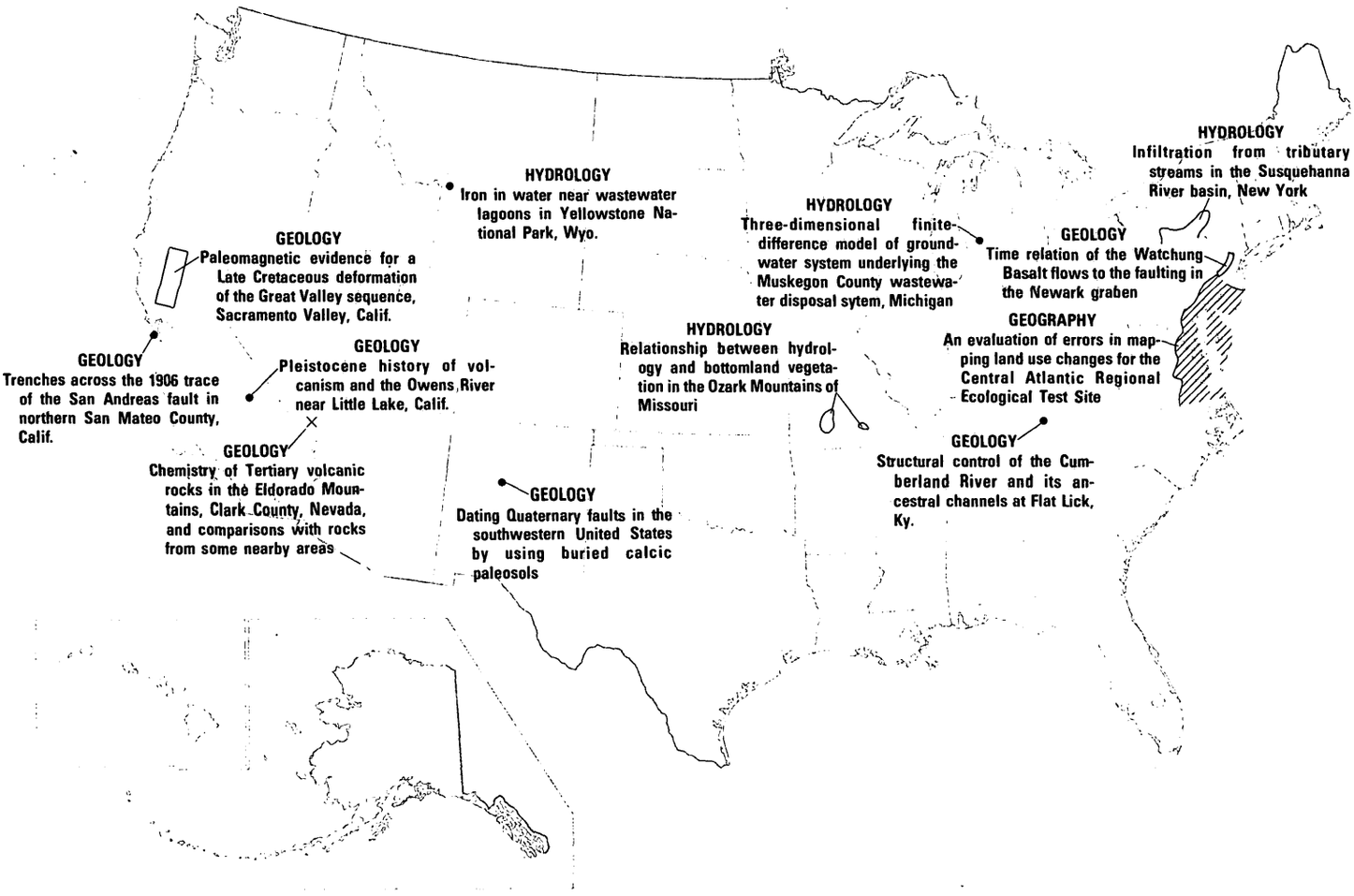

GEOGRAPHIC INDEX TO ARTICLES

See "Contents" for articles concerning areas outside the United States and articles without geographic orientation.

JOURNAL OF RESEARCH

of the

U.S. Geological Survey

Vol. 6 No. 3 May–June 1978

CONTENTS

SI UNITS AND U.S. CUSTOMARY EQUIVALENTS

[SI, International System of Units, a modernized metric system of measurement. All values have been rounded to four significant digits except 0.01 bar, which is the exact equivalent of 1 kPa. Use of hectare (ha) as an alternative name for square hectometer (hm^2) is restricted to measurement of land or water areas. Use of liter (L) as a special name for cubic decimeter (dm^3) is restricted to the measurement of liquids and gases; no prefix other than milli should be used with liter. Metric ton (t) as a name for megagram (Mg) should be restricted to commercial usage, and no prefixes should be used with it. Note that the style of $meter^2$ rather than square meter has been used for convenience in finding units in this table. Where the units are spelled out in text, Survey style is to use square meter]

SI unit		U.S. customary equivalent	
Length			
millimeter (mm)	=	0.039 37	inch (in)
meter (m)	=	3.281	feet (ft)
	=	1.094	yards (yd)
kilometer (km)	=	0.621 4	mile (mi)
	=	0.540 0	mile, nautical (nmi)
Area			
$centimeter^2$ (cm^2)	=	0.155 0	$inch^2$ (in^2)
$meter^2$ (m^2)	=	10.76	$feet^2$ (ft^2)
	=	1.196	$yards^2$ (yd^2)
	=	0.000 247 1	acre
$hectometer^2$ (hm^2)	=	2.471	acres
	=	0.003 861	section (640 acres or 1 mi^2)
$kilometer^2$ (km^2)	=	0.386 1	$mile^2$ (mi^2)
Volume			
$centimeter^3$ (cm^3)	=	0.061 02	$inch^3$ (in^3)
$decimeter^3$ (dm^3)	=	61.02	$inches^3$ (in^3)
	=	2.113	pints (pt)
	=	1.057	quarts (qt)
	=	0.264 2	gallon (gal)
	=	0.035 31	$foot^3$ (ft^3)
$meter^3$ (m^3)	=	35.31	$feet^3$ (ft^3)
	=	1.308	$yards^3$ (yd^3)
	=	264.2	gallons (gal)
	=	6.290	barrels (bbl) (petroleum, 1 bbl=42 gal)
	=	0.000 810 7	acre-foot (acre-ft)
$hectometer^3$ (hm^3)	=	810.7	acre-feet (acre-ft)
$kilometer^3$ (km^3)	=	0.239 9	$mile^3$ (mi^3)
Volume per unit time (includes flow)			
$decimeter^3$ per second (dm^3/s)	=	0.035 31	$foot^3$ per second (ft^3/s)
	=	2.119	$feet^3$ per minute (ft^3/min)
Volume per unit time (includes flow)—Continued			
$decimeter^3$ per second (dm^3/s)	=	15.85	gallons per minute (gal/min)
	=	543.4	barrels per day (bbl/d) (petroleum, 1 bbl=42 gal)
$meter^3$ per second (m^3/s)	=	35.31	$feet^3$ per second (ft^3/s)
	=	15 850	gallons per minute (gal/min)
Mass			
gram (g)	=	0.035 27	ounce avoirdupois (oz avdp)
kilogram (kg)	=	2.205	pounds avoirdupois (lb avdp)
megagram (Mg)	=	1.102	tons, short (2 000 lb)
	=	0.984 2	ton, long (2 240 lb)
Mass per unit volume (includes density)			
kilogram per $meter^3$ (kg/m^3)	=	0.062 43	pound per $foot^3$ (lb/ft^3)
Pressure			
kilopascal (kPa)	=	0.145 0	pound-force per $inch^2$ (lbf/in^2)
	=	0.009 869	atmosphere, standard (atm)
	=	0.01	bar
	=	0.296 1	inch of mercury at 60°F (in Hg)
Temperature			
temp kelvin (K)	=	[temp deg Fahrenheit (°F)+459.67]/1.8	
temp deg Celsius (°C)	=	[temp deg Fahrenheit (°F)−32]/1.8	

The policy of the "Journal of Research of the U.S. Geological Survey" is to use SI metric units of measurement except for the following circumstance:

When a paper describes either field equipment or laboratory apparatus dimensioned or calibrated in U.S. customary units and provides information on the physical features of the components and operational characteristics of the equipment or apparatus, then dual units may be used. For example, if a pressure gage is calibrated and available only in U.S. customary units of measure, then the gage may be described using SI units in the dominant position with the equivalent U.S. customary unit immediately following in parentheses. This also applies to the description of tubing, piping, vessels, and other items of field and laboratory equipment that normally are described in catalogs in U.S. customary dimensions.

S. M. LANG, *Metrics Coordinator,*
U.S. Geological Survey

Jour. Research U.S. Geol. Survey
Vol. 6, No. 3, May–June 1978, p. 285–297

INFILTRATION FROM TRIBUTARY STREAMS IN THE SUSQUEHANNA RIVER BASIN, NEW YORK

By ALLAN D. RANDALL, Albany, N.Y.

Work done in cooperation with the New York State Department of Environmental Conservation

Abstract.—As tributary streams in the Susquehanna River basin leave narrow upland valleys and enter larger valleys floored with permeable stratified glacial drift, they lose water by infiltration through streambeds. The infiltration rate is generally slow near the point of entering a larger valley, but farther downstream it is much faster and is approximately constant per unit distance along a given stream. A conservative average value of infiltration rate in the downstream reach is 10 liters per second per 100 meters of channel. Infiltration from these streams is little influenced by stream width, depth, or temperature and seems to be controlled by permeability distribution beyond the streambed in the alluvium or underlying glacial drift rather than by permeability at the streambed. Hydraulic conductivity of earth materials near each of the streams studied was calculated by applying models that describe steady-state saturated flow into isotropic materials with various boundary conditions. Hydraulic conductivities of 4 to 41 meters per day were obtained; 13 meters per day is suggested as a conservative average value for silty gravel alluvium in the Susquehanna River basin.

Broad valleys occupy about 15 percent of the Susquehanna River basin in New York. They are floored with stratified glacial drift that is at least 21 m thick and includes highly productive aquifers of sand and gravel in most localities (Hollyday, 1969). Small tributary streams originating in the adjacent till-mantled bedrock upland invariably lose water as they enter these valleys and flow across the stratified drift or across their own alluvial fans. The lower reaches of many such streams are dry for long periods during late summer and fall (Ku and others, 1975). Wetterhall (1959, p. 13) recognized that infiltration from tributary streams recharges aquifers in the major valleys of southwestern New York. Crain (1966) demonstrated that infiltration from tributary streams where they enter Cassadaga Creek valley near Jamestown, N.Y., is the principal source of recharge to a sand-and-gravel aquifer that underlies the center of the valley beneath 37 m of clay. All this information suggests that infiltration from tributary streams is a significant element in the hydrologic system of this region. Therefore, the magnitude and distribution of infiltration along several tributary streams were studied as part of an investigation of water resources in the Susquehanna River basin that was begun in 1965 by the U.S. Geological Survey in cooperation with the New York State Department of Environmental Conservation.

FIELD INVESTIGATIONS

Twelve stream reaches near the margins of major valleys were selected for study of infiltration. Along seven of these, several types of measurements were made on several dates during base-flow conditions in 1967 and 1968. Flow was measured at the most downstream point where the channel was known to be cut in till or bedrock, or at least was still clearly within its own upland valley, and at one or more points farther downstream within a major valley, where streamflow losses were expected. Each set of flow measurements was completed within 2 hours. Flow was measured by pygmy current meter or by chloride dilution, generally in cross sections graded or shaped by hand to create flow conditions suitable for precise measurement. In addition, stream length between points of measurement (including points of zero flow) was determined by pacing, stream width was taped, and average stream depth was estimated at regular intervals, usually of 15 to 30 m. Stream temperature was measured wherever flow was measured, and depth to water in nearby wells was taped. The flow measurements were published by the U.S. Geological Survey (1970). Average water losses and selected characteristics of the reaches studied are given in table 1.

Maps and longitudinal sections (fig. 1*A–F*) illustrate topography and subsurface geology along the seven reaches that were studied in detail. Drill cuttings from 10 test wells near these reaches showed the upper 5 to 9 m of sediment to be compact silty and sandy gravel that yields little water to drilled wells (Randall, 1972). The gravel, deposited in alluvial fans, is locally

TABLE 1.—*Summary of measured infiltration*

Stream		Infiltration			Casing depth and average depth to water in well below stream surface at point nearest well (m)				
					Wells ending near base of alluvium[3]		Deeper wells		
Stream name and station number at head of reach studied[1]	Estimated 50-percent flow duration for 1931-60[1] (L/s)	Number of measurement sets	Subreach in fig. 1[2]	Average loss per 100 m of channel (L/s)	Casing	Water	Casing	Water	Stream gradient[4]
Mulholland Creek 01-5264.95-------	42	10	upstream	0.9	---	-----	----	-----	0.031
			downstream	26	7.6	3.7	15.8	3.7	
Thorn Hollow Creek 01-5148.20-------	42	15	upstream	1.9	4.6	<.3	13.7	small	.017
			downstream	15	3.0	.9	16.5	6.7	
Pumpelly Creek[5] 01-5138.40-------	70	7	upstream	1.9	3.7	.3	----	-----	.013
			downstream	12?(>6)	---	small	----	-----	
Carter Creek 01-5155.80-------	79	8	upstream	.6	---	-----	17.4	>6.7	.013
			downstream	9.3	6.1	2.1			
Red Brook 01-5074.70-------	105	8	upstream	1.6	4.0	.5	----	-----	.025
			downstream	4.7	3.0	.6	5.2	1.1	
Little Choconut Creek 01-5131.90-	108	11	upstream	1.1	5.2	1.2	----	-----	.010
Finch Hollow Creek 01-5132.80-------	31	6	upstream	.5	---	-----	----	-----	.022
			downstream?[6]	.7	---	-----	16.8	>4.6	.007
Two other streams--	---	6	----------	<.9	---	<.3	----	-----	.004-.02
Three other streams	---	6	----------	6.5	---	-----	----	-----	.01 -.02

[1] From Ku and others, 1975.

[2] Boundaries of upstream and downstream subreaches, and average loss rates in each subreach, estimated from figure 2 or similar data. Upstream subreach heads at last till or bedrock in channel, if any; otherwise at measurement site farthest upstream.

[3] In several wells, an envelope of clean coarse sand surrounds a sand point and also extends slightly above bottom of casing.

[4] Determined from U.S. Geological Survey topographic quadrangle maps (figure 1).

[5] About 180 m of channel altered by highway construction; silted in 1967 and 1968, graded and cleaned early in 1968. Boundary between upstream and downstream subreaches, and rate of infiltration in downstream subreach, are poorly defined.

[6] Channel incised in organic-rich silt for at least 180 m downstream from head of downstream reach; channel further downstream partly choked with silt from highway construction.

interbedded with or replaced by dense silt containing organic matter. These materials constitute postglacial alluvium. Where streams enter major valleys, the alluvium overlies till or bedrock; downstream it commonly overlies sandy glaciofluvial gravel, and farther downstream a wedge of silt and very fine sand may overlie or replace the glaciofluvial gravel. The glaciofluvial gravel generally has a more varied lithology and a lower silt content than the alluvium and has much greater potential as an aquifer.

To reduce flooding, most tributary streams in the Susquehanna River basin have been deepened a few feet within the major valleys, and some have been straightened. The streams studied are no exception. Gravel that was pushed out of the channels by construction equipment forms artificial levees. The present streambed sediment is loose sandy gravel, slightly silty or free of silt in most places.

FACTORS INFLUENCING INFILTRATION

In general, flow of water through granular material varies directly with hydraulic conductivity, area perpendicular to flow, and hydraulic gradient (Darcy's law) and varies inversely with viscosity of water. The hydraulic conductivity of earth materials is constant with time below the water table but is a function of negative pressure head above the water table (Bouwer, 1964). Relying on these principles and some experimental observations, several authors have listed or evaluated specific environmental features that they expected would influence rates of infiltration from losing reaches of streams or canals (for example, Burkham, 1970; Walton, 1963; Bouwer, 1965). Among these features are the following:

1. Stream area (width times length) and depth.
2. Temperature (affects water viscosity).

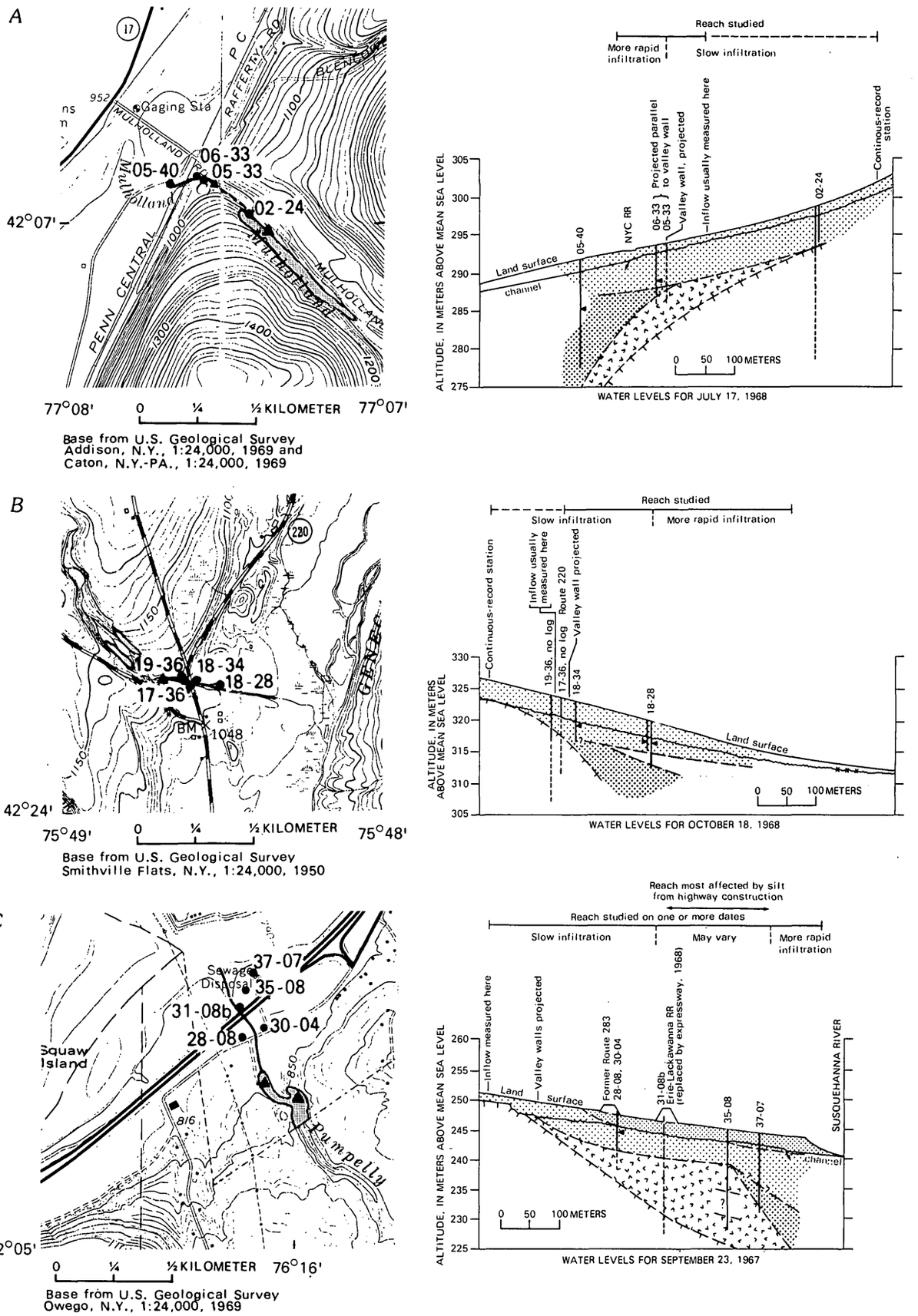

FIGURE 1.—Continued on following page.

D

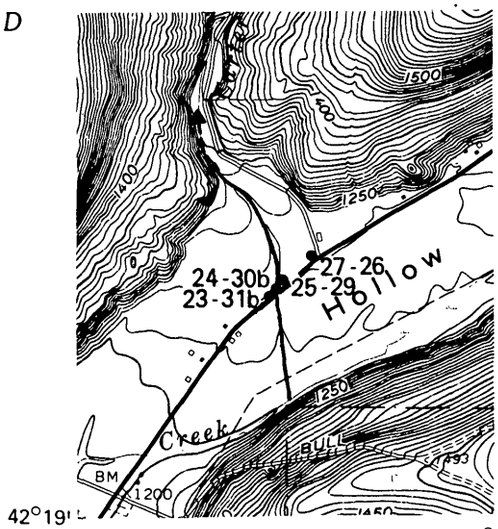

Base from U.S. Geological Survey
Alpine, N.Y., 1:24,000, 1969

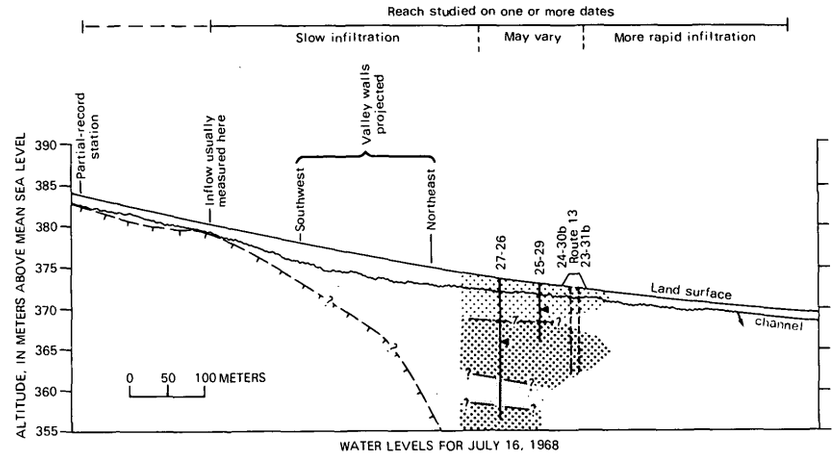

WATER LEVELS FOR JULY 16, 1968

E

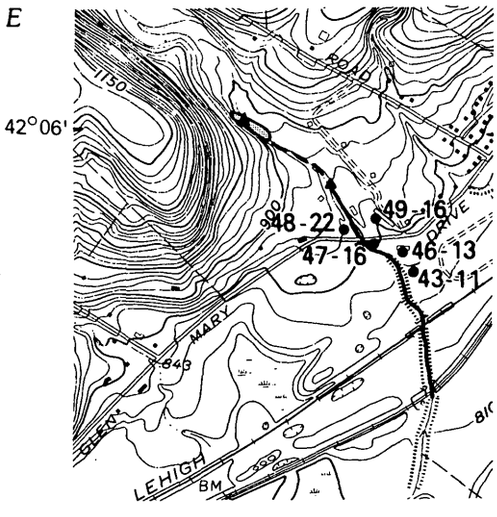

Base from U.S. Geological Survey
Owego, N.Y., 1:24,000, 1969

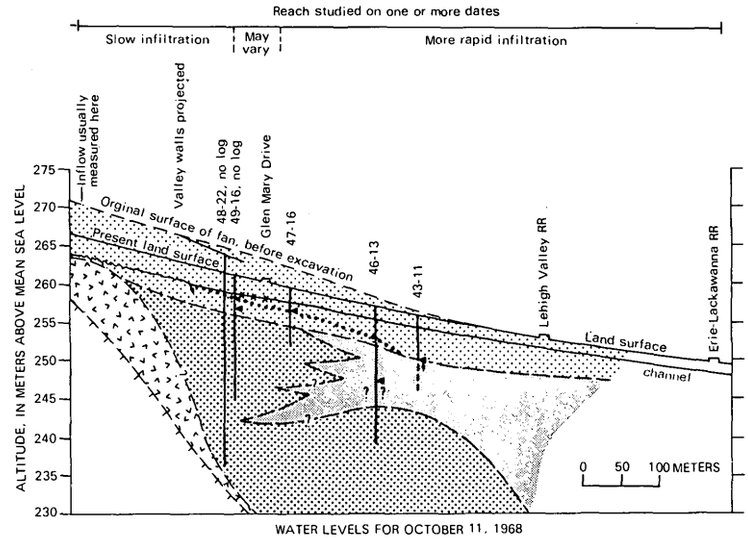

WATER LEVELS FOR OCTOBER 11, 1968

EXPLANATION

SYMBOLS IN CROSS SECTIONS

Line of section is along creek

- Silt, silt to fine sand, loam, or clay; river flood-plain alluvium
- Silty sandy gravel, yields little water to drilled wells; tributary creek alluvium
- Sandy gravel or sand, variably silty, in part water yielding; glaciofluvial valley-train deposits
- Silt to fine sand; lake-bottom deposits
- Glacial till
- ? Uncertain

- Top of bedrock
- Well or test boring, projected perpendicular to stream except as noted. Solid line represents casing, dashed where casing has been removed (test borings) or not used (bedrock). Log available (Randall, 1972) unless otherwise indicated
- Streambed cut in dense silt
- Stream and point of dryness
- Water level in well

} Only on date indicated

- Water table
- Contact between lithologic units

FIGURE 1.—Continued on following page.

F

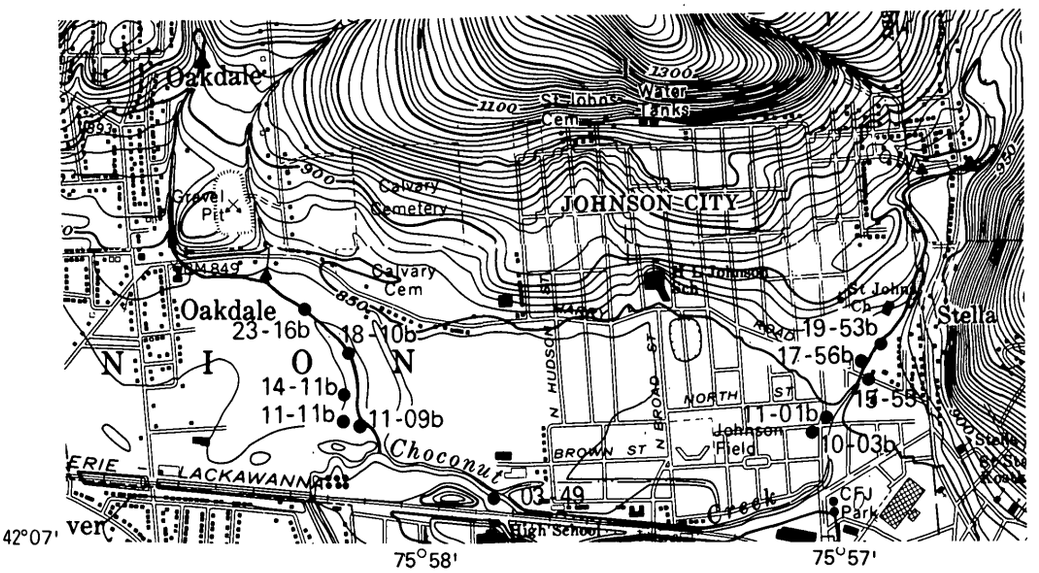

Base from U.S. Geological Survey
Castle Creek, N.Y., 1:24,000, 1968 and
Binghamton West, N.Y., 1:24,000, 1968

0 ¼ ½ KILOMETER

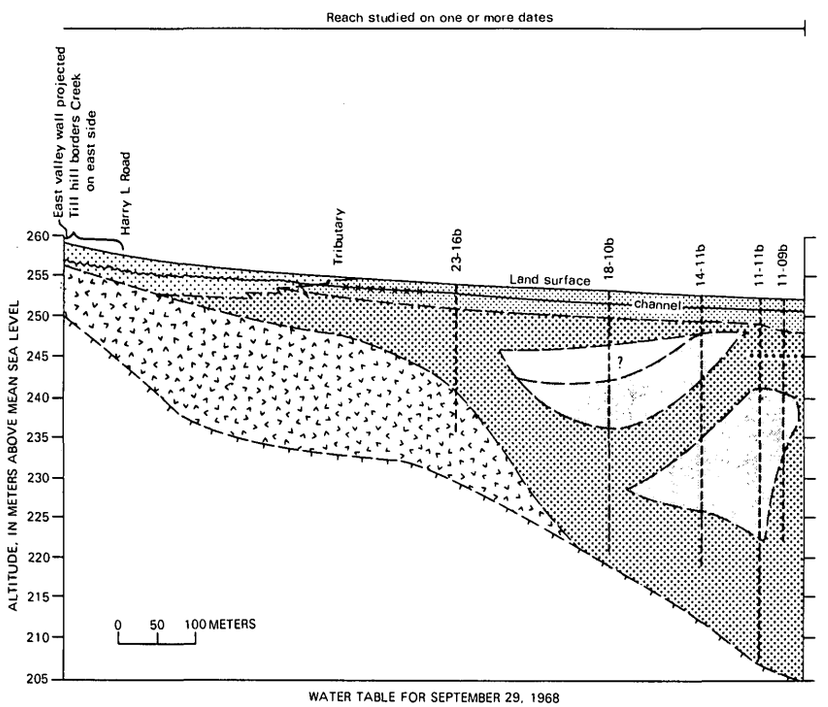

WATER TABLE FOR SEPTEMBER 29, 1968

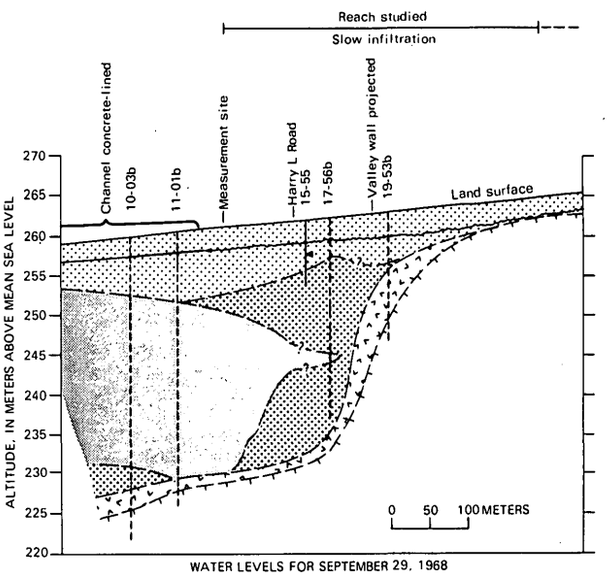

WATER LEVELS FOR SEPTEMBER 29, 1968

EXPLANATION

SYMBOLS ON MAPS

- Bedrock exposure
- Reach studied; dashed subreach is upstream from infiltration zone and not encompassed by some sets of measurements
- ▲ Partial or continuous-record station
- ▲ Alternate measurement site

} Points of streamflow measurement upstream from infiltration zone

- •28-08 Well and number
- •31-08b Test boring and number

} Numbers are seconds of latitude and longitude. Degrees and minutes are in map margin

FIGURE 1.—Geohydrologic features of stream reaches studied in detail. *A*, Mulholland Creek. *B*, Red Brook. *C*, Pumpelly Creek. *D*, Carter Creek. *E*, Thorn Hollow Creek. *F*, Finch Hollow Creek (left) and Little Choconut Creek (right).

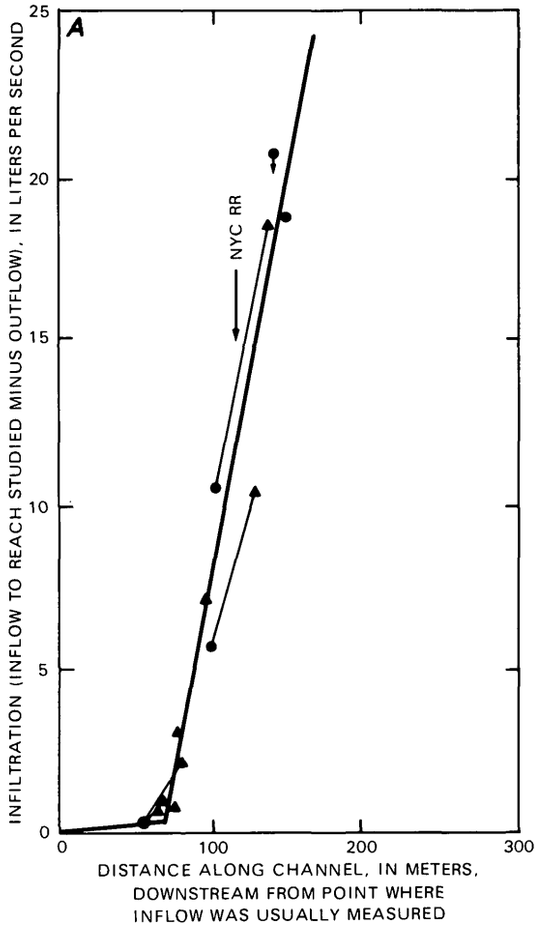

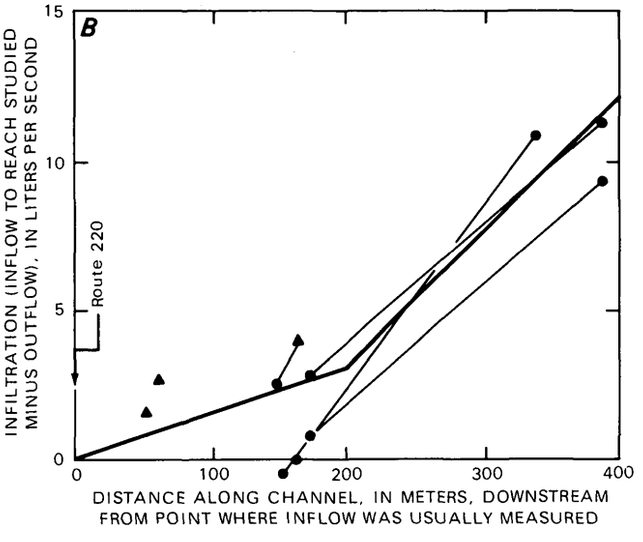

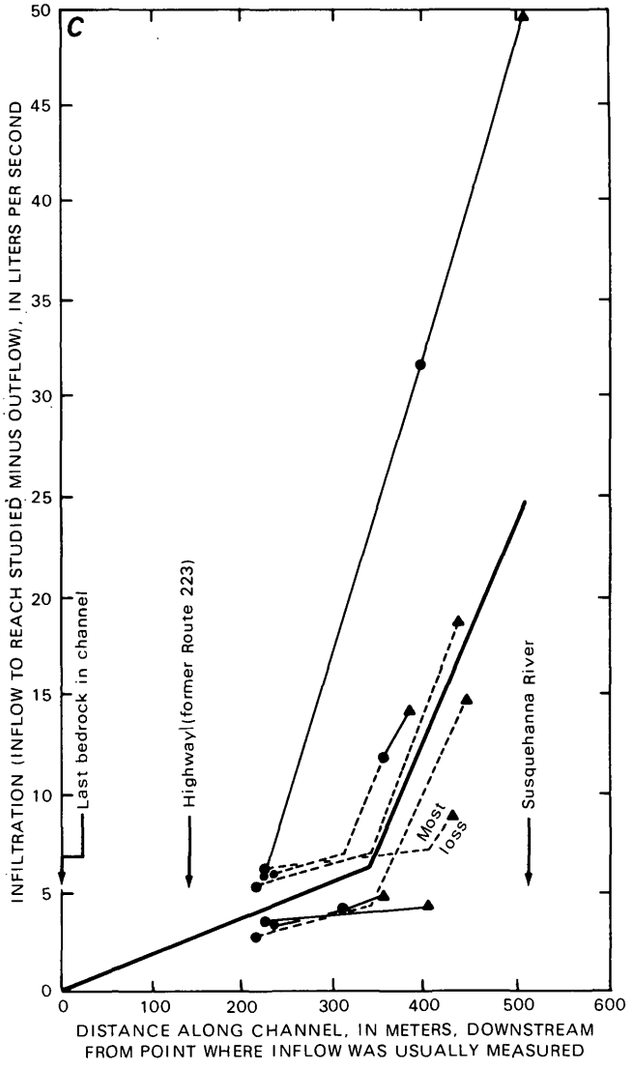

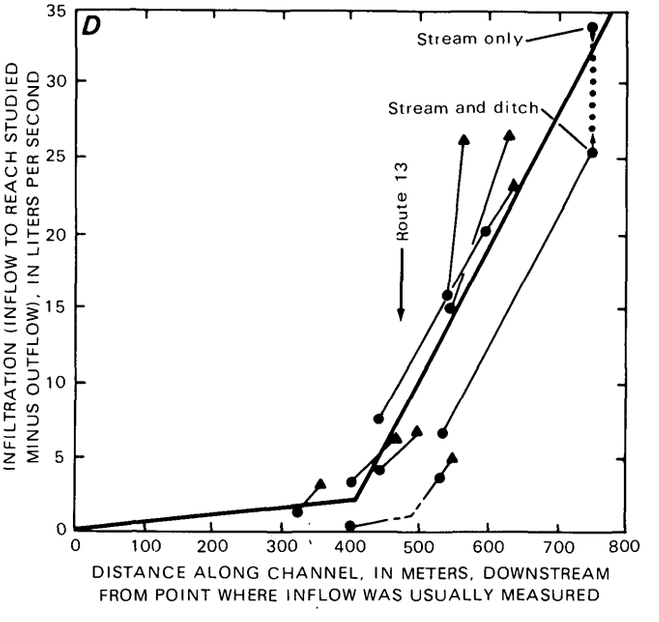

EXPLANATION

- ▲ Point at which stream went dry (infiltration equaled inflow)
- ● Point of flow measurement downstream from inflow measurement
- ●—▲ Measurements made on same date; line dashed where drawn to suggest change in infiltration rate
- ——— Trend line, estimated average infiltration rate

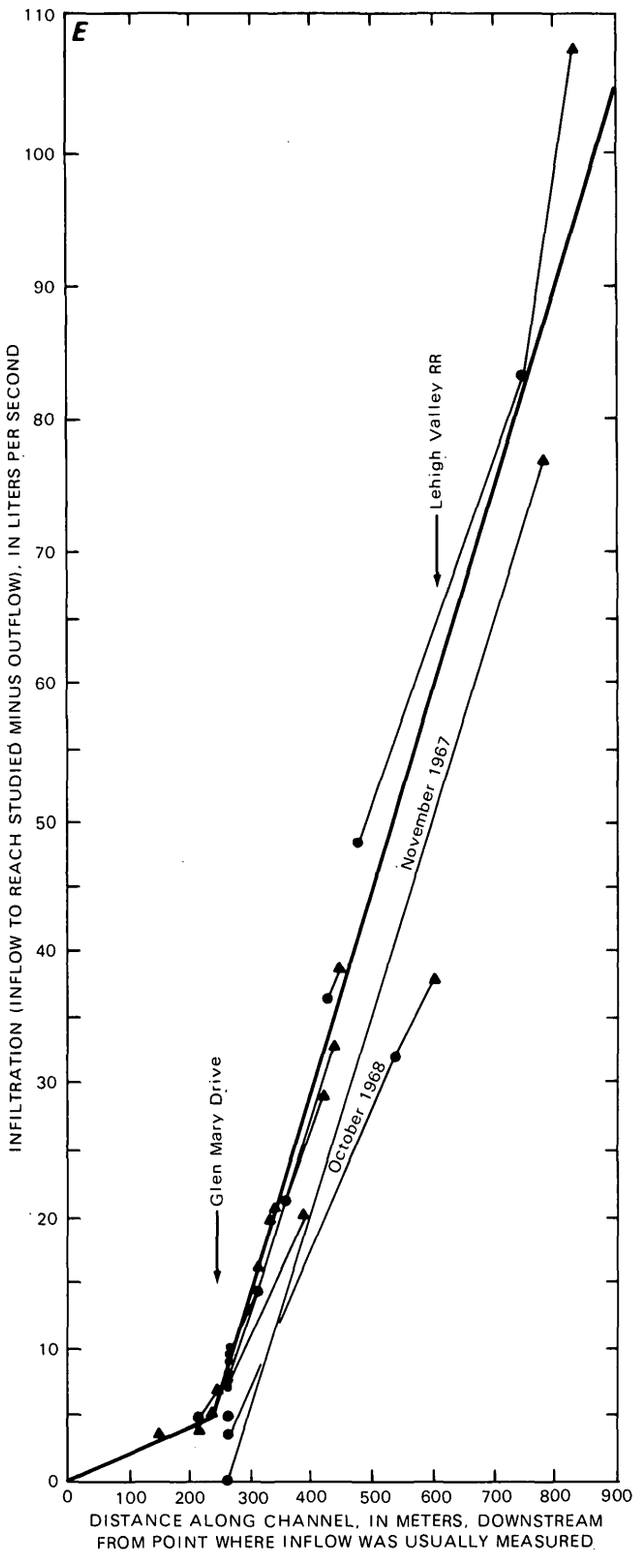

FIGURE 2.—Infiltration in relation to stream length. *A*, Mulholland Creek. *B*, Red Brook. *C*, Pumpelly Creek. *D*, Carter Creek. *E*, Thorn Hollow Creek.

3. Relation of the water table to the stream.
4. Hydraulic conductivity of the streambed and (or) underlying materials.
5. Presence of air in earth materials near the stream.
6. Chemical quality and suspended sediment in the water.
7. Velocity of streamflow (changes may favor deposition or erosion of sediment layers in the streambed).

The influence of the first five of these features on infiltration from tributary streams in the Susquehanna River basin may be evaluated from available field data.

Stream dimensions

Each stream studied began to lose water rapidly several hundred feet downstream from where it entered the major valley, or from the last known exposure of till or bedrock in its channel. Measured losses in this zone of rapid loss varied directly with stream length between measurement sites. That is, where the infiltration rate was most rapid, infiltration per unit length of channel was approximately constant (fig. 2*A*–*E*). By contrast, stream width and depth had little effect on infiltration. Plots of infiltration per unit length against width, and against the product of width and depth, showed no correlation.

Stream temperature

Measurements were made when stream temperatures were as low as 4.5° C and as high as 27° C, but adjusting measured losses to compensate for differences in viscosity of stream water did not reduce the scatter in loss per unit length of stream. Therefore, figure 2 is plotted without adjustment for stream temperature. Turbidity was negligible, and chemical quality was uniform during all measurements.

Water-table configuration

As shown in table 1, the stream reaches studied could generally be divided into an upstream subreach, in which the net infiltration rate was slow (0.6 to 2 L/s per 100 linear meters of channel), and a downstream subreach, in which infiltration was much more rapid (4.6 to 26 L/s per 100 m). Very small flows were entirely absorbed by infiltration within the upstream subreach. At somewhat larger flows that crossed the upstream subreach, infiltration loss increased; but at still larger flows, infiltration in the upstream subreach diminished rapidly, and a few measurements showed a net gain to the stream rather than a loss. This pattern is probably caused by bank storage; infiltration occurs at all stages when the stream is rising, but if

water cannot move away from the stream rapidly, some will return to the stream or at least block further infiltration during subsequent periods of rapidly declining flow. This pattern was not observed in the downstream subreach, which suggests that water there not only infiltrates the streambed more rapidly but also moves away from the stream more rapidly. Along some streams, the increase in infiltration rate that marks the start of the downstream subreach takes place near where the depth to till and bedrock increases (fig. 1*A* and *C*), perhaps because the water can move downward through glaciofluvial sand and gravel as well as laterally through the alluvium. However, along other streams till and bedrock seem to lie far below the channel more than 100 m upstream from where infiltration increases (fig. 1*D* and *E*). Furthermore, the point at which infiltration rates increase seems to shift from one date to another by as much as 100 m along some streams (fig. 2). These changes may be caused by changing water-table configuration within the alluvium—a function of prior infiltration and rainfall as well as of permeability distribution.

Hydraulic conductivity

Several papers dealing with infiltration from streams state or imply that the rate of infiltration is controlled by a thin streambed layer that is less permeable than the underlying sediment (Walton, 1963; Walton and others, 1967; Norris, 1970; Moore and Jenkins, 1966). This concept is supported by laboratory experiments in which fine suspended sediment in flowing water settled between the sand grains in a sandbed flume to form a cohesive mass (Martin, 1970). Furthermore, a few investigators (Moore and Jenkins, 1966; Burkham, 1970) studied grain-size distribution in streambeds from which infiltration losses were measured and reported that the upper several centimeters of sand and gravel was siltier and presumably less permeable than that below. Nevertheless, the following evidence suggests that infiltration from most tributary streams studied for this report is controlled by permeability distribution beyond the streambed rather than at the streambed:

1. The failure of infiltration to correlate with stream width, depth, and temperature could be explained if the rate of underground flow away from the stream were controlled by low permeability somewhere within the alluvium or underlying sediment where width through which flow occurs, hydraulic gradient, and temperature differ from that observed at the streambed.
2. The streams studied generally flow across loose gravel. Gravel penetrated by shallow holes dug in a few streambeds was not very silty—less silty than some alluvium penetrated by test wells near the streams at depths of 3 to 6 m.
3. Holes dug in streambeds a few meters away from the stream generally reached water only a few centimeters below stream level. A small ditch parallel to Carter Creek downstream from the highway (fig. 1*D*), about 9 m from the creek and incised only about 0.3 m deeper than the creekbed, carried flow whenever Carter Creek carried flow to the south side of the valley. These observations suggest that water flows away from a channel with modest head loss, that there is no unsaturated zone beneath the channel, and that the permeability of the materials at the streambed is therefore not a principal factor limiting the rate of infiltration.
4. On October 11, 1968, Thorn Hollow Creek did not carry flow beyond a point 46 m upstream from Glen Mary Drive (fig. 1*E*). Near Glen Mary Drive, depth to water was about 1 m below the dry channel; farther downstream, where the channel had been dry longer, depth to water was more than 4.5 m. In 1965, when the entire length of Thorn Hollow Creek shown in figure 1*E* was dry during a drought, water levels in wells 48–22, 49–16, and a nearby dug well were reportedly 6 m below the channel. By contrast, water levels in well 47–16 were nearly identical to creek level whenever the creek flowed past Glen Mary Drive, and water levels downstream in well 43–11 were within 1.5 m of creek level in May and June 1968 when the creek flowed past that well. These relationships indicate that storage in the alluvium is depleted only when streamflow ceases nearby for long periods—which means that near Glen Mary Drive, and probably downstream, water cannot drain away underground as fast as it can infiltrate into the alluvium through the streambed.

Although permeability beyond the streambed is important in limiting infiltration, the streambed itself may be the major limiting factor where it is very silty. Infiltration rates were low along Finch Hollow Creek (table 1) where the stream gradient was gentle, part of the channel was incised in massive silt, and part was choked with mud from nearby highway construction. Highway construction also contributed mud to a gentle reach of Pumpelly Creek where the streambed in summer consisted of silty gravel and wide silt-bottomed pools, and loss rates in that reach varied widely (figs. 1*C* and 2*C*). Larger infiltration losses

were observed on dates when Pumpelly Creek entered a steeper reach downstream that was not obviously silty and also once when the entire channel seemed to have been recently regraded.

Trapped air in earth materials

Heavy rains on October 19 and 24, 1968, caused flow of Thorn Hollow Creek to extend far beyond well 43–11. By October 29, water in well 43–11 had risen from the level shown in figure 1*E* to 3.5 m below creek level, and a continuous stream of air under pressure bubbled through the water and up the casing. The air presumably had been trapped between the rising water table and infiltrating rainfall and (or) streamflow and was forced 0.2 m downward through the water table to the top of the screen (fig. 3). Infiltration from Thorn Hollow Creek was less than average on October 29; perhaps pressure from the trapped air below helped to slow the flow of water away from the creek.

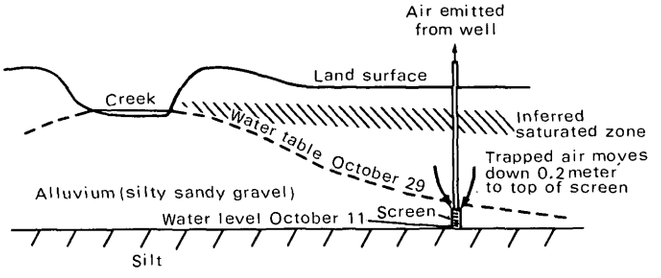

FIGURE 3.—Infiltration near Thorn Hollow Creek, October 29, 1968.

PERMEABILITY OF ALLUVIUM

Selection of model

Field data collected for this study may be used to compute the hydraulic conductivity of earth materials near the streams studied. However, because the values obtained depend in part on what model is used to manipulate the data, care should be given to selection of a suitable model. Several models from the literature are sketched in figure 4.

The fourth of these models is actually a set of general solutions for steady-state infiltration from canals or streams developed by Bouwer (1965) by use of a resistance-network analog. Bouwer's solutions closely reproduced several analytical solutions formulated by others for specific conditions or assumptions and were later republished (Bouwer, 1969) with more detailed comparison to specific analytical solutions. Bouwer

1.--Vertical saturated flow, unit gradient (Kantrowitz, 1970, p67; Randall and others, 1966, p88); $\Delta h/d \approx 1$

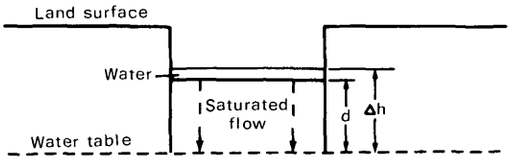

2.--Vertical unsaturated flow, thin poorly permeable layer at streambed (Walton, 1963; Walton and others, 1967; Bouwer, 1965, model C); $\Delta h/d \gg 1$

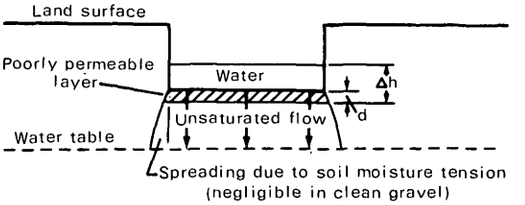

3.--Fully penetrating stream with lateral seepage (Ferris and others, 1962; Hall and Moench, 1972); $\Delta h/d$ normally $\ll 1$; may be modeled with poorly permeable streambank layer, $\Delta h/d > 1$

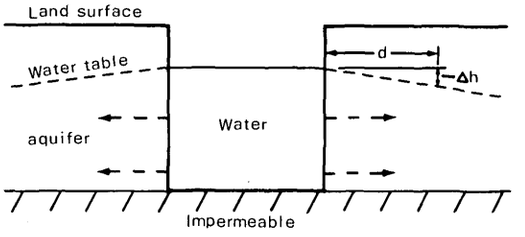

4.--Stream channel atop ground-water mound (Bouwer, 1965, models A and B)

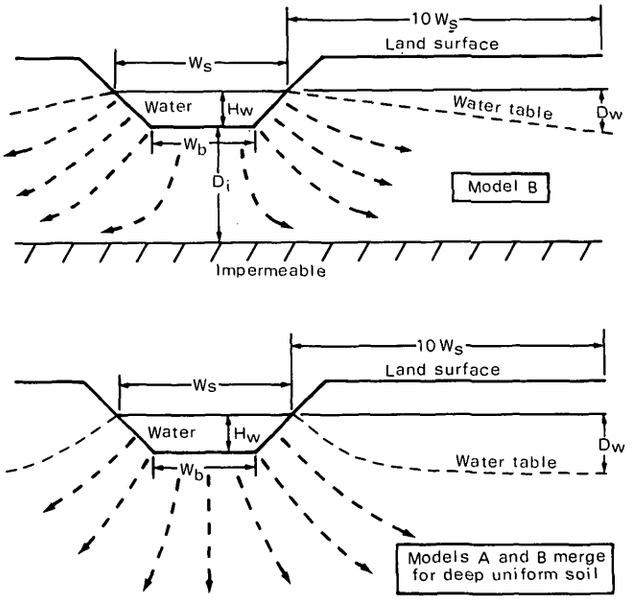

FIGURE 4.—Alternative models for stream-aquifer relationships. For sketches 1–3: Δh, loss in head during infiltration; d, sediment thickness through which head loss occurs. For sketch 4: W_s, stream surface width; H_w, stream depth; W_b, stream bottom width; D_w, depth to ground water below stream surface; and D_i, depth to assumed impermeable layer.

treats channels as incised in uniform soil that is underlain by material of much higher hydraulic conductivity (model A) or much lower hydraulic conductivity (model B) at known depth; models A and B merge if depth to the underlying material is more than five times stream width. Because of the generality of Bouwer's models and because they incorporate lateral and vertical flow from partially penetrating streams at gradients less than unity without a restrictive streambed layer, they seemed more representative of the streams studied than the other models in figure 4 and so were applied to compute average hydraulic conductivity of alluvium. However, the assumptions of steady-state flow and of isotropic hydraulic properties within the alluvium may be unrealistic, and extrapolation of the relationships presented by Bouwer was required to adapt them to the shallow streams studied.

More sophisticated models to better represent tributary streams in the Susquehanna River basin could be developed with analog or digital methods and would be particularly useful if water levels were available from piezometers at several depths and distances from streams in order to better evaluate anisotropy. Bouwer's analog models could be redesigned using smaller depth-to-width ratios for stream channels and allowing for variable anisotropy.

Computation of permeability

The models proposed by Bouwer (1965) were used, as follows, to estimate hydraulic conductivity (K) of earth materials near the tributary streams studied.

1. Determine, from a representative set of field measurements in each stream and from well logs, the factors that Bouwer used to describe infiltration: stream depth (H_w) and surface width (W_s); rate of fall of stream surface, or measured loss per unit area and time (I_s); depth to ground water below stream surface (D_w), measured at or adjusted to 10 stream widths from the stream; and depth to assumed impermeable layer (D_i) or permeable layer (D_p) below streambed.
2. Determine I_s/K from curves presented by Bouwer (1965, fig. 3 or 1969, fig. 7). Bouwer's curves represent trapezoidal channels having 1:1 side slopes and depth to bottom-width ratios of 0.75, 0.5, and 0.25. The natural channels studied in the Susquehanna River basin had depth to width ratios of 0.05 or less. Therefore, as suggested by Bouwer (1965, p. 44), three imaginary bottom widths (W_b) were computed for each stream, by starting with real surface width and assuming the shape and the three depth to width ratios used by Bouwer. Then a value of I_s/K for each depth to width ratio could be read from Bouwer's curves and extrapolated (fig. 5) to the ratio in the real stream.
3. Divide I_s by I_s/K to obtain hydraulic conductivity. Field data and estimated hydraulic conductivity for seven streams are listed in table 2. Earth materials beneath these streams generally resemble Bouwer's model B but may approximate

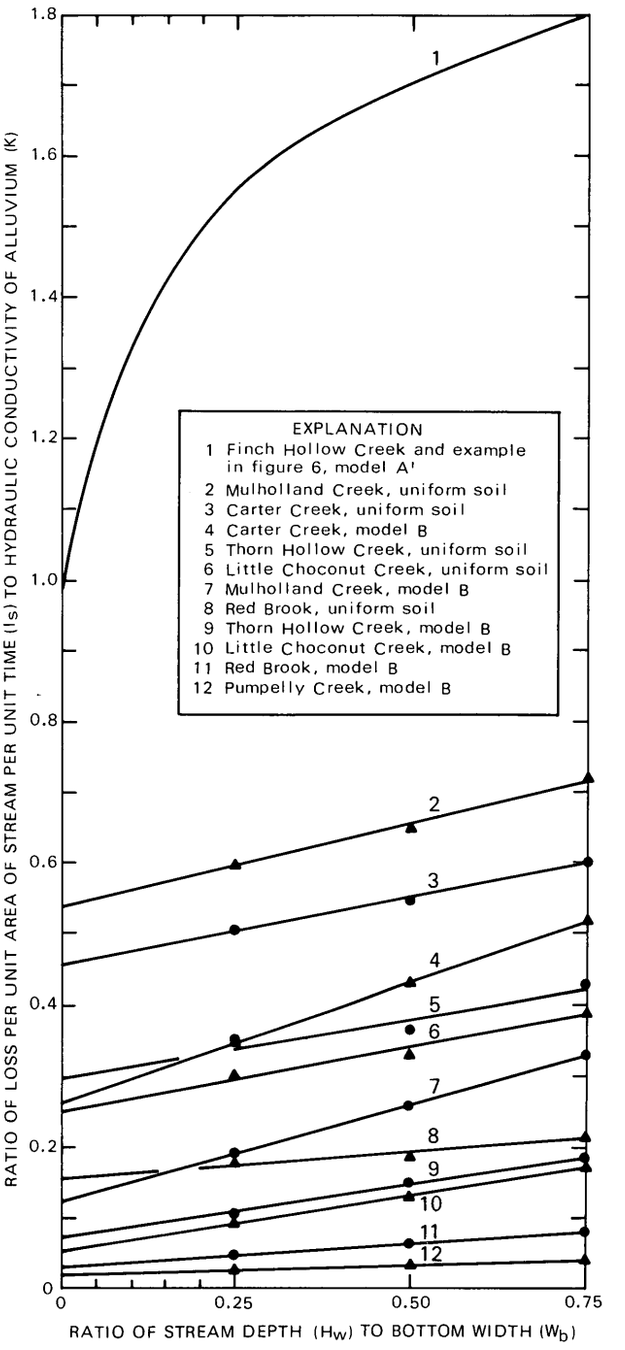

FIGURE 5.—Extrapolation of I_s/K ratios.

TABLE 2.—*Hydraulic conductivity of alluvium*

Stream name	Date of measurement[1]	In stream reach studied: Average Width (m)	Average Depth (cm)	Area (m^2)	Water loss (L/s)	At observation well: Distance from stream (m)	Depth to water below stream surface (m)	Depth to base of alluvium (m)	Hydraulic conductivity of alluvium[3]: Model chosen (Bouwer 1965)[2]	Value computed (m/d)	Estimated best value (m/d)
Carter Creek--	7-16-68	3	5	460	12.7	38	2.1	14	B AB	8.7 5.3	8
Thorn Hollow Creek-------	6-18 and 6-22-68	3.9	9	[4]2,000	[4]93.5	29	1.6	4	B AB	56 13	40
Mulholland Creek-------	5- 3-68	4.7	9	[5]370	18.7	78	3.7	9	B AB	33 8	20
Red Brook-----	10-18-68	3.2	14	680	8.5	37	.8	3.4	B AB	35 6.6	32
Pumpelly Cr.--	[6]9-23-67	3.4	9	890	6.2	52	.5	3.4	B	40	40
Little Choconut Creek---	[7]1968 avg	3	9	1,200	4.3	41	1.2	4.6	B AB	6 1.3	4
Finch Hollow Creek-------	[7]1968 avg	2.7	6	2,500	5.7	150	6.1	1.2	A'	.2	.2

[1] For measured flows and measurement site locations, see U.S. Geological Survey (1970).
[2] Bouwer (1965) referred to Model AB as "deep uniform soil" where models A and B merge. In model A', the water table is within a deep permeable layer.
[3] Alluvium is silty gravel in reaches studied (except for Finch Hollow Creek, where it is chiefly massive silt with possibly some silty gravel).
[4] Total for two successive reaches below Glen Mary Drive, measured on different dates.
[5] Area downstream from point of increase in loss rate (fig. 2A).
[6] Results imprecise because of small values of the ratio Is/K (see text) in computation.
[7] Stream width and depth estimated. Computation based on average infiltration and average depth to ground water from several pairs of measurements.

a "deep uniform soil" (model AB) where the alluvium overlies glaciofluvial gravel (fig. 1*A–F*). Therefore, hydraulic conductivity was computed for model B and also for model AB, and an intermediate value was selected as most probable. In adjusting D_w to a distance of 10 stream widths, a uniform water-table slope from stream to well was assumed for model B (Bouwer, 1965, fig. 4), and a nearly flat slope beyond 10 stream widths was assumed for model AB (Bouwer, 1965, fig. 2).

Factors that could cause the hydraulic conductivity values in table 2 to be in error include the following:

1. Errors in field measurement.
2. Imperfect judgment in selecting or weighting models A, AB, or B to arrive at the most probable value of hydraulic conductivity.
3. Adaptation of Bouwer's presentation to the streams studied. When depth to ground water is small, Bouwer's curves are difficult to read precisely. Also, Bouwer (1965, p. 41) recommends extrapolating results to observed H_w/W_b ratios but does not specify a method. In this study, straight-line extrapolation was used for model B or model AB. Bouwer (1964, p. 132) points out that "For essentially zero depth of innundation . . . streamlines are vertically downward" in soils with deep water tables or deep permeable layers—in which case I_s/K cannot exceed 1.0. Therefore, downward curvilinear extrapolation to $I_s/K=1.0$ at $D_w=0$ is required for model A and for deep water tables. For example, model A', a special case of model A in which the water table is within a deep permeable layer, may be extrapolated as shown in figure 5 (Bouwer, written commun., 1973).
4. Measurements not under steady-state conditions. As pointed out by Bouwer (1965, p. 39), steady-state infiltration is seldom achieved along a canal (or stream). Measurements near Thorn Hollow Creek in October 1968, described above, showed that storage in the alluvium is depleted during periods of no flow and takes some time to refill. If storage were still being refilled near an observation well during a set of measurements, computed K would be too small.
5. Anisotropy and partial penetration. Depth to the

water table (D_w) was determined by comparing the water level in a single observation well to stream stage exactly opposite the well. Observation wells were finished near the base of the alluvium, 3 to 8 m below streambed level, 8 to 16 stream widths away from the stream. Bouwer's analog model indicated (Bouwer, 1965, p. 40, fig. 4) that at these distances in an isotropic aquifer vertical flow components caused by infiltration would be insignificant. However, if the ratio of lateral to vertical hydraulic conductivity of the alluvium exceeds about 2, head at these distances would be lower at the base of the alluvium than at the water table. Consequently, computed K values would be smaller than if the observation well were fully penetrating.

Crude bedding, imbricate pebbles, and lack of silt lenses in small exposures suggest that the ratio of lateral to vertical hydraulic conductivity within the alluvium may be small, perhaps 10:1 or less. A trial calculation was made for each set of data in table 2, using the same computational procedure described above but assuming a ratio of vertical to lateral hydraulic conductivity of 10:1 and distorting coordinates accordingly. Lateral hydraulic conductivities thus computed averaged about 1.5 times the hydraulic conductivities computed assuming isotropic conditions. Such a difference is no greater than other possible sources of error, so hydraulic conductivity values such as those in table 2 could be applied to other situations in which flow is predominantly lateral.

Values of hydraulic conductivity for silty gravel alluvium selected as most probable (table 2) range from 4 to 41 m/d. A conservative average would be at least 13 m/d, which is equal to the hydraulic conductivity of well-sorted fine sand and is 10 to 20 percent of the average hydraulic conductivity in the only stratified-drift aquifer studied in detail during this investigation of the Susquehanna River basin. The preceding discussion of possible errors suggests that computed hydraulic conductivity values are more likely to be too small than too large. Nevertheless, even the smallest value exceeds infiltration rates calculated or quoted by Moore and Jenkins (1966) for reaches of small rivers in Colorado and Wisconsin where pumping had developed an unsaturated zone beneath the streambed. Where such an unsaturated zone exists, the infiltration rate should equal or slightly exceed vertical hydraulic conductivity of the streambed. Thus, tributary streams in the Susquehanna River basin may have relatively permeable alluvium.

Hydraulic conductivity is smaller near Finch Hollow Creek than near the other streams studied (table 2). The probable reason is that part or possibly all of the channel downstream from a tributary (fig. 1*F*) consisted of only a few inches of gravel atop massive silt or was choked with mud from highway construction. The silt must pinch out at some point upstream, above which at least a short reach of the channel probably rests on silty gravel, as with other streams; if so, much of the infiltration may occur there.

ESTIMATING INFILTRATION

Infiltration from tributary streams as they enter major valleys of the Susquehanna River basin is a significant source of aquifer recharge. Although infiltration varies with time and with position along the channel, under natural conditions a fairly uniform maximum rate per unit length of channel generally prevails over a hundred meters or more. Data in this article (table 1) suggest that the maximum rate for an average stream in the Susquehanna basin would be at least 10 L/s per 100 m. Infiltration from a tributary stream under natural conditions may be roughly estimated by applying that rate, for periods when streamflow is available, to the channel length underlain by alluvial gravel downstream from the bedrock wall of the major valley. The outer parts of some alluvial fans overlie lacustrine silt and clay or very thin sandy outwash, where infiltration can be recovered as ground water only by unusual arrangements of shallow wells or infiltration galleries; however, near the valley wall at least, the alluvium of most streams overlies glaciofluvial sand and gravel through which recharge to deeper aquifers can occur. Recharge available to these aquifers from infiltration under natural conditions could be estimated by considering only the channel length upstream from any lacustrine beds. Where these beds occur as close as 75 m from the subsurface valley wall, as seems common (figs. 1, 6; also Randall, 1972), recharge to deep aquifers would be about 7.5 L/s per stream when flow is available (10 L/s per 100 m, times 75 m).

If head in glaciofluvial aquifers underlying tributary streams were lowered many feet by large-scale ground-water development, infiltration might increase substantially. Prediction of potential infiltration under such conditions would require knowledge of aquifer and stream geometry and use of a model incorporating hydraulic conductivity, such as models presented by Bouwer (1965). As an example, consider the geometry in figure 6, assuming isotropic alluvium having an

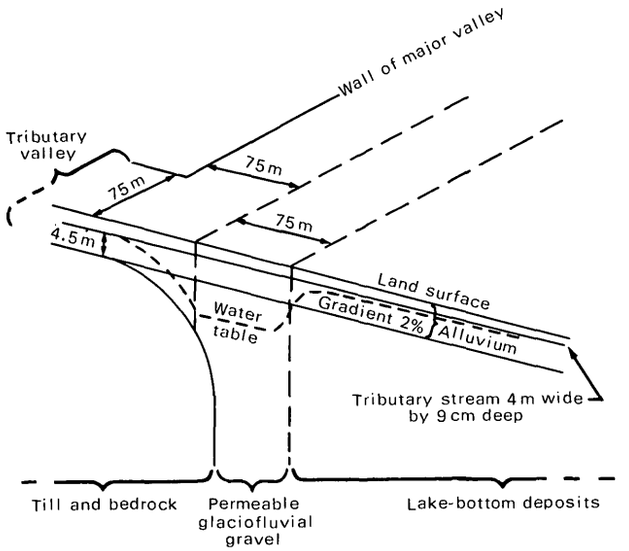

FIGURE 6.—Inferred geometry typical of some tributary streams in the Susquehanna River basin, with water table lowered as a result of ground-water development.

average hydraulic conductivity of 13 m/d, as estimated in this paper, and assuming lowered head in the glaciofluvial gravel, which is more permeable than the alluvium. If model A′ of Bouwer (1965) is applied to the reach in figure 6 where the alluvium overlies glaciofluvial gravel, infiltration from the stream may be estimated to be 50 L/s ($I_s/K=1.1$ for a stream depth of 9 cm; $K \times I_s/K \times$ stream area $= 13$ m/d $\times$ 1.1×75 m $\times 4$ m $= 4.3 \times 10^3$ m^3/d or 50 L/s). In the upstream reach underlain by till and bedrock, infiltration is limited to the rate at which underflow can move downstream through the alluvium toward the glaciofluvial gravel. Darcy's law may be applied to this reach and underflow thereby estimated to be 2 L/s ($K \times$ gradient $\times$ cross-sectional area $= 13$ m/d $\times$ $2/100 \times 150$ m $\times 4.5$ m $= 175$ m^3/d or 2 L/s). Thus, the predicted rate of recharge from stream infiltration to the deep glaciofluvial gravel in figure 6 would be 52 L/s when streamflow is available. If the alluvium were assumed to have a lateral K of 20 m/d and a 10:1 ratio of horizontal to vertical hydraulic conductivity (previous section), the same calculation predicts a potential infiltration rate of 31 L/s. Because very few measurements of water loss from tributary streams crossing developed aquifers have been made in or near the Susquehanna River basin in New York, there is presently no adequate basis for verifying such predictions. Flow of most tributary streams is likely to fall below the calculated infiltration rate for part of the year; thus flow duration would have to be estimated (Ku and others, 1975) to calculate annual infiltration for either natural or developed conditions.

REFERENCES CITED

Bouwer, Herman, 1964, Unsaturated flow in ground-water hydraulics: Am. Soc. Civil Engineers Proc., Jour. Hydraulics Div., v. 90, no. HY5, p. 121–243.

———1965, Theoretical aspects of seepage from open channels: Am. Soc. Civil Engineers Proc., Jour. Hydraulics Div., v. 91, no. HY3, p. 37–59.

———1969, Theory of seepage from open channels, *in* Chow, V. T., ed., 1969, Advances in hydroscience: New York City, Academic Press, 305 p.

Burkham, D. E., 1970, A method for relating infiltration rates to streamflow rates in perched streams: U.S. Geol. Survey Prof. Paper 700–D, p. D266–D271.

Crain, L. J., 1966, Ground-water resources of the Jamestown area, New York: New York State Conserv. Dept. Water Resources Comm. Bull. 58., 167 p.

Ferris, J. G., Knowles, D. B., Brown, R. H., and Stallman, R. W., 1962, Theory of aquifer tests: U.S. Geol. Survey Water-Supply Paper 1536–E, 174 p.

Hall, F. R., and Moench, A. F., 1972, Application of the convolution equation to stream-aquifer relationships: Water Resources Research, v. 8, no. 2, p. 847–493.

Hollyday, E. F., 1969, An appraisal of the ground-water resources of the Susquehanna River basin in New York: U.S. Geol. Survey open-file rept., 52 p.

Kantrowitz, I. H., 1970, Ground-water resources in the eastern Oswego River basin, New York: New York State Conserv. Dept. Basin Plan. Rept. ORB–2, 129 p.

Ku, Henry F. H., and others, 1975, Streamflow in the New York part of the Susquehanna River basin: New York State Dept. Environmental Conserv. Bull. 71, 130 p.

Martin, C. S., 1970, Effect of a porous sand bed on incipient sediment motion: Water Resources Research v. 6, no. 4, p. 1162–1174.

Moore, J. E., and Jenkins, C. T., 1966, An evaluation of the effect of ground-water pumpage on the infiltration rate of a semipervious streambed: Water Resources Research, v. 2, no. 4, p. 691–696.

Norris, S. E., 1970, The effect of stream discharge on streambed leakage to a glacial outwash aquifer: U.S. Geol. Survey Prof. Paper 700–D, p. D262–D265.

Randall, A. D., 1972, Records of wells and test borings in the Susquehanna River basin, New York: New York State Dept. Environmental Conserv. Bull. 69, 92 p.

Randall, A. D., Thomas, M. P., Thomas, C. E., and Baker, J. A., 1966, Water resources inventory of Connecticut, part 1, Quinebaug River basin: Connecticut Water Resources Bull. 8, 102 p.

U.S. Geological Survey, 1970, Water resources data for New York, 1969, part 1, Surface-water records: U.S. Geol. Survey open-file rept. 283 p.

Walton, W. C., 1963, Estimating the infiltration rate of a streambed by aquifer-test analysis: Berkeley, Internat. Assoc. Sci. Hydrology Pub. 63, p. 409–420.

Walton, W. C., Hills, D. L., and Grundeen, G. M., 1967, Recharge from induced streambed infiltration under varying ground-water-level and stream-stage conditions: Minneapolis, Minnesota Univ. Water Resources Research Center Bull. 6, 42 p.

Wetterhall, W. S., 1959, The ground-water resources of Chemung County: New York State Water Power and Control Comm. Bull. GW–40, 58 p.

Jour. Research U.S. Geol. Survey
Vol. 6, No. 3, May–June 1978, p. 299–305

RELATIONSHIP BETWEEN HYDROLOGY AND BOTTOMLAND VEGETATION IN THE OZARK MOUNTAINS OF MISSOURI

By E. J. HARVEY and JOHN SKELTON,
Rolla, Mo.

Work done in cooperation with Missouri Division of Geology and Land Survey

Abstract.—The identification of plants and plant assemblages that are common to stream reaches that gain water and those that do not is an important key in the study of limestone hydrology. In the Ozark Mountains of Missouri, a rapid change from a stream-channel growth of abundant willows (*Salix* spp.), touch-me-nots (*Impatiens capensis*), and sedges such as *Carex Frankii* and *Eleocharis* spp. to an abundant growth of bluestars (*Amsonia illustris*) indicates a rapid increase in depth to water. Vegetative indicators of hydrologic conditions are most helpful when used in conjunction with other information, but they are independently useful in pinpointing areas of abrupt hydrologic changes.

One aspect of a study of limestone hydrology in the Ozark Mountains of Missouri is an evaluation of methods that will lead to a better definition of losing streams and basins with relatively small volumes of runoff. This paper presents a preliminary evaluation of one facet of such an investigation—the identification of plants and plant assemblages that are common to stream reaches that gain water and those that do not. Because reaches of alluvial valleys that contain gaining streams are typified by shallow depths to water and losing reaches are typified by greater depths to water, the plant assemblage also is a clue to the depth to the water table. Thus, understanding the plant assemblage helps to evaluate a valley with respect to hydrologic problems that might be related to waste disposal, well location, or dam construction.

The importance of identifying lesser plants as well as trees and shrubs that are indicative of gaining and losing streams became apparent during a study of limestone hydrology in the Ozarks. Many flood plains, creek banks, and channels have been altered to such an extent by man's activities that the natural assemblage of trees and shrubs no longer exists or the populations have been severely depleted. For this reason, it is necessary to identify small plants when studying the relationship between vegetation and hydrology.

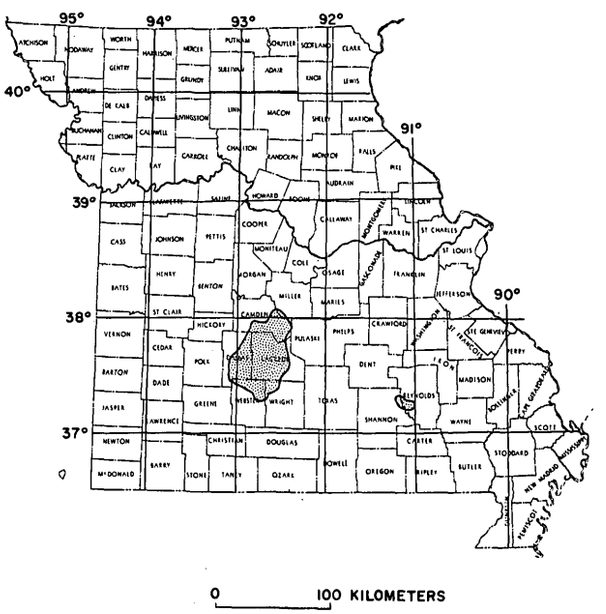

FIGURE 1.—Locations of areas in Missouri discussed in the report are indicated by stippled pattern; left is the Niangua-Osage Fork-Grandglaize area, and right is the Logan Creek area.

This study covers an area of about 5200 square kilometers (km²) and includes the Niangua River, Osage Fork of the Gasconade River, Bear Creek, Wet Glaize Creek and its tributary, Dry Auglaize Creek (fig. 1). The investigation was initiated after a thermal radiation study in 1971–74 of Logan Creek and its hydrologic relation to the Current River (Harvey and others, 1977). The vegetative patterns in the Logan Creek basin and their similarity to those observed in the present study will be mentioned later in this paper.

Acknowledgments.—In identifying plants and plant assemblages in various parts of the Missouri Ozarks,

the authors have relied heavily on the expertise of Leroy R. Korschgen, senior research biologist for the Missouri Department of Conservation. Mr. Korschgen accompanied the authors to the field to provide training in plant identification, furnished research materials and technical literature, and identified plant specimens that were brought to him by the authors. Without his assistance, these studies could not have been completed.

PLANT ASSOCIATIONS IN THE OZARKS

The Ozarks terrane in Missouri is made up mostly of fractured and faulted dolomite and sandstone that has extreme areal variation in its ability to store or transmit water. The water-bearing characteristics of the bedrock are important controls on the amount and distribution of water stored in the surface mantle in the uplands and in the alluvium in the valleys. Water in these unconsolidated deposits is, in turn, an important control on streamflow.

Many streams have perennial flow for long distances; others flow for only short distances before entering cavernous zones buried beneath the alluvial fill; still others have long dry reaches in the headwaters and perennial flow only in the lower reaches. The plant assemblages indicative of these diverse hydrologic conditions can be used in any season of the year (but not as readily in winter) to help determine perennial reaches of the streams and the existence of groundwater storage in the unconsolidated deposits.

Natural plant associations and succession in the Ozarks of Missouri were described by Steyermark (1940). He described five principal associations characteristic of different topographic and geologic environments of the Ozarks and listed descriptions, the dominant species, the plants of the understory, the ground cover, and the plant successions.

The five associations are: (1) sugar maple-bitternut hickory in the alluvial valleys, (2) sugar maple-white oak on slopes and limestone uplands, (3) oak-hickory on drier uplands with acid substratum, (4) oak-pine on acid soils derived from sandstone, chert, and igneous rocks, and (5) white oak-red maple which "commonly develops from drainages in acid soil areas such as slight draws in ravines, heads of tributaries of streams and upper slopes of hills and ravines." The five associations are not isolated from each other and plants in the sugar maple-white oak association may be mixed with the plants of the sugar maple-bitternut hickory association. The first association is of principal hydrologic interest because it occurs in alluvial valleys of streams having drainage areas of about 2 km^2 or greater.

In the sugar maple-bitternut hickory association are three to four stages of development depending on the area of the State (Steyermark, 1940, p. 365). Generally the first stage begins with Ward willow and sycamore, dominant species, often with witchhazel and common alder in the understory. A second stage may include silver maple, cottonwood, river birch, and black wil-

TABLE 1.—*Plants that are most useful in studying hydrologic conditions in the Niangua–Osage Fork–Grandglaize basins*

[Nomenclature after Steyermark, 1963]

Common name	Scientific name
Arrowhead	*Sagittaria rigida* Pursh
Bedstraw	*Galium Aparine* L.
Bitternut hickory	*Carya cordiformis* (Wang.) K. Koch
Blue cardinal flower	*Lobelia siphilitica* L.
Bluestar	*Amsonia illustris* Woodson
Blue phlox	*Phlox divaricata* L. var. *Laphamii* Wood
Box elder	*Acer Negundo* L.
Buttonbush	*Cephalanthus occidentalis* L.
Cardinal flower	*Lobelia Cardinalis* L.
Cattail	*Typha latifolia* L.
Common alder	*Alnus serrulata* (Ait.) Willd.
Common elderberry	*Sambucus canadensis* L.
Gray dogwood	*Cornus racemosa* Lam.
Grasses:	
Fowl meadowgrass	*Glyceria striata* (Lam.) Hitchc.
Spikegrass	*Uniola latifolia* Michx.
Great ironweed	*Vernonia crinita* Raf.
Lizardtail	*Saururus cernuus* L.
Maples:	
Silver	*Acer saccharum* Marsh
Sugar	*Acer saccharinum* L.
Ninebark	*Physocarpus opulifolius* (L.) Maxim.
Peppermint	*Mentha piperita* L.
River birch	*Betula nigra* L.
Rushes:	
Rush	*Juncus diffusissimus* Buckl.
Soft rush	*Juncus effusus* var. *solutus* Fern. and Wieg.
Scouring rush	*Equisetum hyemale* L.
Sedges:	
Bulrush	*Scirpus lineatus* Michx.
Chairmakers rush	*Scirpus americanus* Pers.
Common bulrush	*Scirpus atrovirens* Willd.
Fox sedge	*Carex vulpinoidea* Michx.
Franks sedge	*Carex Frankii* Kunth
Spikerush	*Eleocharis* spp.
Umbrella sedge	*Cyperus acuminatus* Torr. and Hook.
Umbrella sedge	*Cyperus strigosus* L.
Yellow nut grass	*Cyperus esculentus* L.
Small-flowered crowfoot	*Ranunculus abortivus* L.
Smartweed	*Polygonum* spp.
Swamp milkweed	*Asclepias incarnata* L.
Sycamore	*Platanus occidentalis* L.
Touch-me-not	*Impatiens* spp.
Watercress	*Nasturtium officinale* R. Br.
Waterplantain	*Alisma Plantago-aquatica* L.
Waterwillow	*Justicia americana* (L.) Vahl
Wild ageratum	*Eupatorium coelestinum* L.
Willows:	
Black	*Salix nigra* Marsh.
Sandbar	*Salix interior* Rowlee
Stiff	*Salix rigida* Muhl.
Ward	*Salix caroliniana* Michx.
Witchhazel	*Hamamelis vernalis* Sarg.

low. In the third and sometimes the fourth stage, American elm and green ash appear. Many species that appear as dominants in the earlier stages continue in varying numbers through the three or four stages.

A great variety of plants occurs on the flood plains, streambanks, gravel bars, and in slackwater pools along with the dominant trees and shrubs. Study of many sites by the authors resulted in the list of plants shown in table 1 that are useful in evaluating hydrologic conditions in the Niangua-Osage Fork-Grandglaize basins. The plants are easily recognized and many of them are indicative of a shallow water table.

All the plants are more distinctive at one season of the year than at another. For example, small-flowered crowfoot and bluestar are springtime plants. Cardinal flower and blue cardinal flower are late summer plants. Some plants flower for only a few weeks; others flower for months.

A change in types of plants from one site to another, especially if it occurs abruptly, may be interpreted as a marked change in the depth to the water table. Where abrupt changes in vegetation occur on the flood plain, detailed geologic mapping may reveal faults or other geologic structures that allow water to move to or from the alluvium and cause the vegetation change.

Many variations exist across the Ozarks. For example, in the Niangua-Osage Fork-Grandglaize area, birch, alder, cottonwood, and witchhazel are uncommon while in other parts of the Ozarks they may be abundant. The early stages of vegetation occur in the headwaters of the valley while the late stages develop downstream. The sequence in development is rather uniform.

PLANTS AS INDICATORS OF HYDROLOGIC CONDITIONS

Steyermark (1963) described about 2400 plant species occurring in Missouri of which about 300 species prefer bottomlands or wet places in the uplands of the project area. These 300 species are all a part of the sugar maple-bitternut hickory association.

Some of the plants described by Steyermark as bottomland species are not water lovers. Probably bluestar is the best example. It is found on gravel bars and banks of perennial streams, common to rare in distribution, but generally not present in the stream channel. However, bluestar is common or abundant in the channels of streams that have lost their flow to bedrock, and in June it may form a solid bank of blue flowers across the channel. Bluestar is one of the most significant vegetative indicators of hydrologic conditions that has been found, but when not flowering, its identification is difficult from a distance because it resembles young shoots of Ward willow.

The presence of water-loving plants does not always indicate a permanent shallow water table that is persistent throughout the valley. Plants that begin to grow early in the spring may be present while the supply of water is ample. When the supply of water is exhausted and a shallow water table is not present to sustain the plants, they will wilt. Spikerushes, waterwillow, stiff and sandbar willows, and other water-loving vegetation were observed at a site near Rolla, Mo., in early spring; in June these plants were brown and wilted while other plants less dependent on shallow moisture were thriving. If the site were visited early in the spring, a false impression about the permanence of the shallow water table might be obtained. Sites upstream and downstream from a point of interest should be investigated to determine if a local perched condition exists rather than a permanent shallow water table.

It has also been noted that sedges and bedstraw are extremely abundant in natural areas on flood plains underlain by a shallow water table. In natural fields under which the water table is deep, sedges and bedstraw may be present in scattered clumps, but the difference in the pervasiveness of the plants is striking.

In observing a perennial stream valley from its headwaters to its mouth, the authors noticed that a sequence in plant assemblages develops that generally follows Steyermark's observations. In the upper reaches of the basin, watercress, mint, touch-me-not, Ward and sandbar willows, sycamores, and various sedges and rushes are common to abundant. Topographic relief may be less, and broad open riffles and slackwater areas with less shading by dense tree cover promote growth of the small plants. Downstream many of these species become few or disappear; black willow appears and sycamore continues. Sugar and silver maples and box elder come into prominence and are practically continuous to the mouth.

Thus, vegetative patterns have developed along the stream valleys in response to the hydrology of the valleys. Niangua River and Osage Fork, both continuously flowing streams from headwaters to mouth, have similar patterns. The sandbar, Ward and stiff willows, sedges and rushes, watercress, and touch-me-not in the headwaters gradually disappear and are replaced by the tall black willows, maples, sycamores, ashes, and elms downstream. Dry Auglaize Creek, on the other hand, has only sporadic occurrences of the plants so prominent in the other two valleys. Groundwater levels are generally abnormally low throughout

the length of the valley, and this is reflected by both the vegetation and absence of flow in most reaches. Often, scattered clumps of some plant species normally found in abundance in a reach with a high water table occur in a channel or at the base of a bluff along a dry stream. In these instances, however, the variety and abundance of water-loving plants are lacking and a very local water-saturated condition seems to be indicated. No continuity in the pattern of the vegetation is apparent. It is not until Dry Auglaize Creek nears its junction with Wet Glaize Creek, a stream supported by springs, that any semblance of order is apparent.

Figure 2 shows the distribution of silver and sugar maples along Niangua River and tributaries, Osage

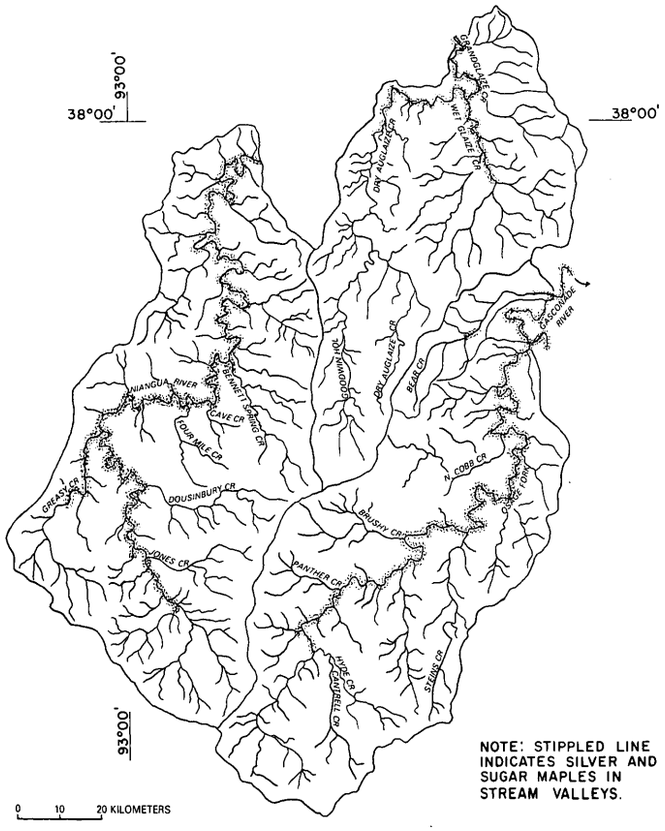

FIGURE 2.—Distribution of maples along major streams in Niangua–Osage Fork–Grandglaize area.

Fork, Wet Glaize, Dry Auglaize, and Bear Creeks, and a short reach of the Gasconade River. The distribution of maples along these streams is a good example of the relation between vegetation and perennial flow. Note the continuity of the pattern along major streams in the basins where perennial flow is present in contrast to the pattern shown in the Dry Auglaize and Bear Creek basins.

Steins Creek, an interrupted stream that is a tributary of the Osage Fork, can be used as an example of the correlation between vegetative assemblages, geology, ground-water levels, and streamflow (fig. 3). On July 2, 1976, during a period of low flow in the basin, streamflow and vegetative patterns were observed, and these data are tabulated in detail in table 2. The reach draining the upper two-thirds of the basin was dry, and according to local residents, this reach of the stream ceased to have surface flow shortly after a rain. The downstream reach from sites 4 to 6 was flowing to within 1 km (kilometer) of the mouth (site 7) and does so except during very severe drought.

Note in figure 3 that two normal faults cross the middle of the basin, forming a horst. Altitudes of water levels in wells along the divides and in the upland adjacent to Steins Creek indicate that the ground-water level stands below the bed of the channel in the reach across the horst and at least as far downstream as the north fault. In the uplands downstream from the horst, water levels in wells generally stand above the bed of the channel. Water levels measured in wells in the flood plain and adjacent bluffs showed that the water table declines to a maximum depth of 20 meters (m) below the flood plain about 13 km upstream from the mouth. The relationship between surface-water flow and ground-water levels in this basin is similar to that of the Logan Creek basin (discussed later in this paper) where detailed ground-water level data also are available near the stream.

At sites 1, 2, and 3, there was no surface flow. Bluestar was common at all three sites. Willows, sedges,

TABLE 2.—*Vegetative patterns and streamflow in Steins Creek basin, July 2, 1976*

[Flows at sites 4, 5, and 6 are 0.014 m^3/s, 0.028 m^3/s, and 0.006 m^3/s, respectively; flow at all other sites is zero. C, common; S, scattered]

Plants (common names)	Sites (see fig. 3)						
	1	2	3	4	5	6	7
Bluestar	C	C	C	S	S	S	C
Willow	---	---	---	C	C	C	---
Common bulrush	---	---	---	S	---	---	---
Franks sedge	---	---	---	S	C	---	---
Watercress	---	---	---	C	C	---	---
Smartweed	---	---	---	C	C	C	---
Fox sedge	---	---	---	---	S	---	---
Touch-me-not	---	---	---	---	C	C	---
Spike rush	---	---	---	---	C	---	---
Rushes	---	---	---	---	S	---	---
Waterwillow	---	---	---	---	C	---	---

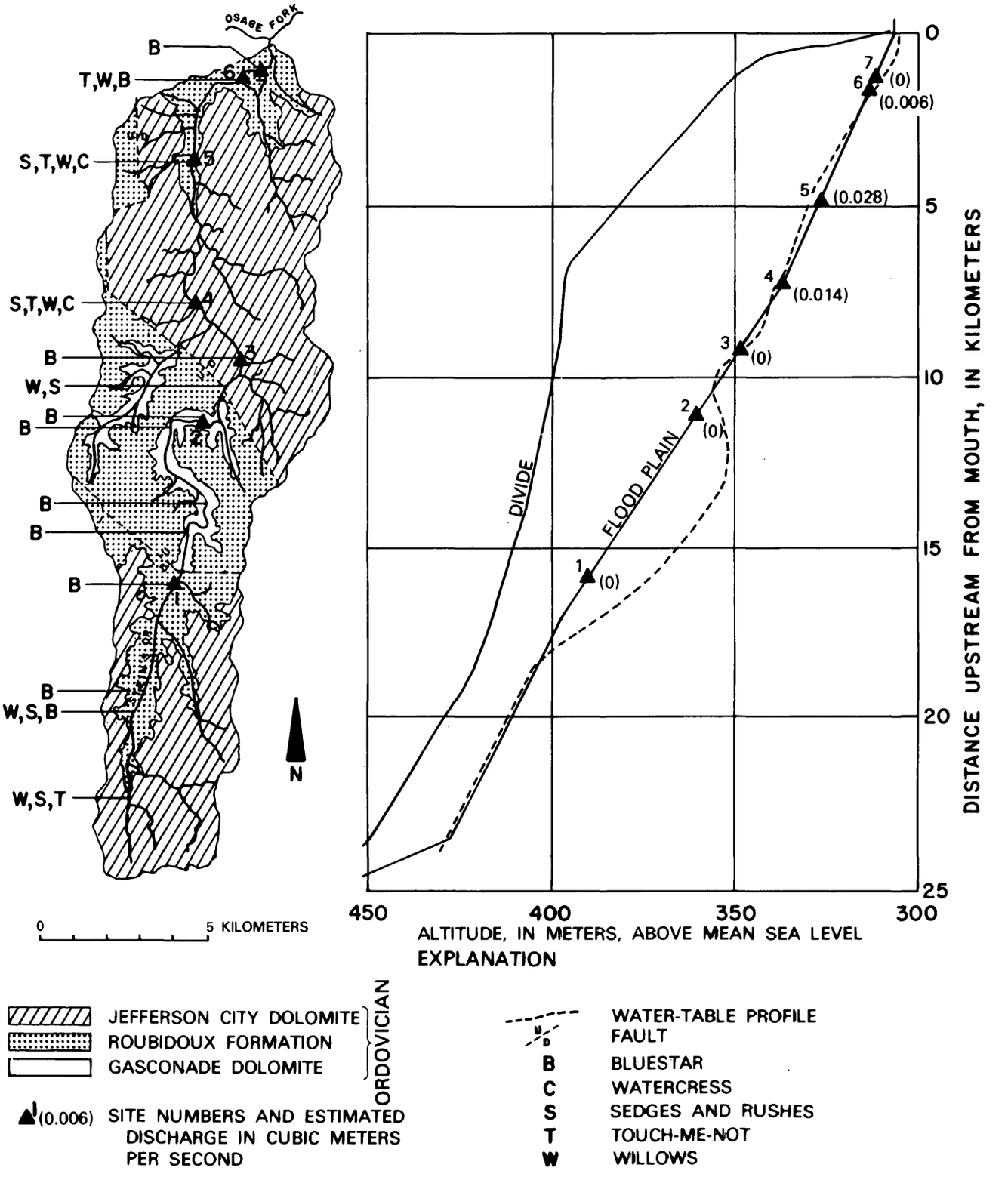

FIGURE 3.—Relationships between vegetation, streamflow, and geology in the Steins Creek basin. Geology by Missouri Division of Geology and Land Survey (written commun., 1976).

rushes, and other vegetation requiring ample moisture were absent. Three kinds of sedges were present, but rare, on the gravel bar at site 2, but the types of sedges normally occurring in perennial reaches, as shown at sites 4 and 5 in table 2, were absent.

At site 4 a flow of 0.014 cubic meters per second

(m^3/s) was estimated. Bluestar was present but scattered on the gravel bar. The sedge (*Carex Frankii*) and the common bulrush (*Scirpus atrovirens*), unobserved at the upstream sites, were present but scattered on the gravel bar and along the bank. Smartweeds were common across the gravel bar.

The suite of vegetation at site 5 was similar to that at site 4 except that watercress choked the broad stream channel upstream from the bridge. About 0.028 m^3/s of surface flow was estimated. Sedges, rushes, and waterwillows were common in the wide mud flats and broad, flat gravel bars. Rushes and sedges (*Scirpus atrovirens*, *Carex Frankii*, *C. vulpinoidea*, and *Eleocharis* sp.), characteristic of an abundant supply of water, were the types most frequently observed. The valley was broad and open at this site, and the general absence of shade was thought to be instrumental in the widespread development of the sedges. Touch-me-not was more abundant along the bank where it was shaded by trees downstream from the bridge. The vegetation seemed to be indicative of a shallow water table, although in extremely dry weather the surface flow may cease.

The changes in vegetation in the reach between sites 6 and 7 indicated a very rapid decline from a shallow to a deep water table. The stream was losing its flow, and only about 0.006 m^3/s was estimated to remain at site 6.

At site 6, bluestar was inconspicuous and the channel, gravel bars, and banks had a luxuriant willow growth. Touch-me-not was common at site 6 but disappeared about 100 m downstream. Sedges were virtually absent, perhaps due to the lack of a hospitable site for growth. The channel was on bedrock against a dolomite bluff on the right bank. Smartweed was tall and luxuriant.

Downstream toward site 7, willows decreased and bluestar increased markedly until the entire channel was given over to bluestar. Willows finally disappeared entirely while smartweed, which had a rank growth at site 6 and for a short distance downstream, became smaller and more scattered. The streambed was dry, and there were no pools. The sequence was from abundant willows and a few bluestars to a mixture of willows and bluestars, and finally to all bluestars.

As to the depth of the water table in the reach between sites 6 and 7, some estimates can be made on the basis of topographic map altitudes. If it is presumed that the water discharges into the Osage Fork, the water level below the bed of the channel cannot be more than 6.1 m, which is the difference in altitude between the area of loss on Steins Creek and the altitude of Osage Fork.

In the 1971–74 study of thermal radiation in the Logan Creek basin (see fig. 1), thermal imagery was obtained from two separate flights on the clear night of June 21, 1973, and showed that the flood plain of the upstream gaining reach of Logan Creek was cooler than the downstream losing reach (Harvey and others, 1977). The cooler nighttime temperatures were due to the abundance of water in the flood plain of the gaining reach. It had been determined earlier that flow in the upstream reach was diverted from the downstream reach through subterranean solution channels to the Current River (Feder and Barks, 1972). Ground-water levels in the gaining reach stand near the level of the flood plain. In the losing reach they are as much as 67 m below the level of the streambed (fig. 4).

The assemblage of plants in the upstream gaining reach of Logan Creek was typical of a shallow water table. In the downstream losing reach, the assemblage was entirely different. The dominant plants recognized in the two reaches are listed in table 3. Because of the shallow water table in the gaining reach, riparian vegetation was lush. In the losing reach, only large trees remained; the smaller growths of understory and ground cover were cleared by landowners to the bank of the stream, and sedges, rushes, and other water-loving vegetation were absent.

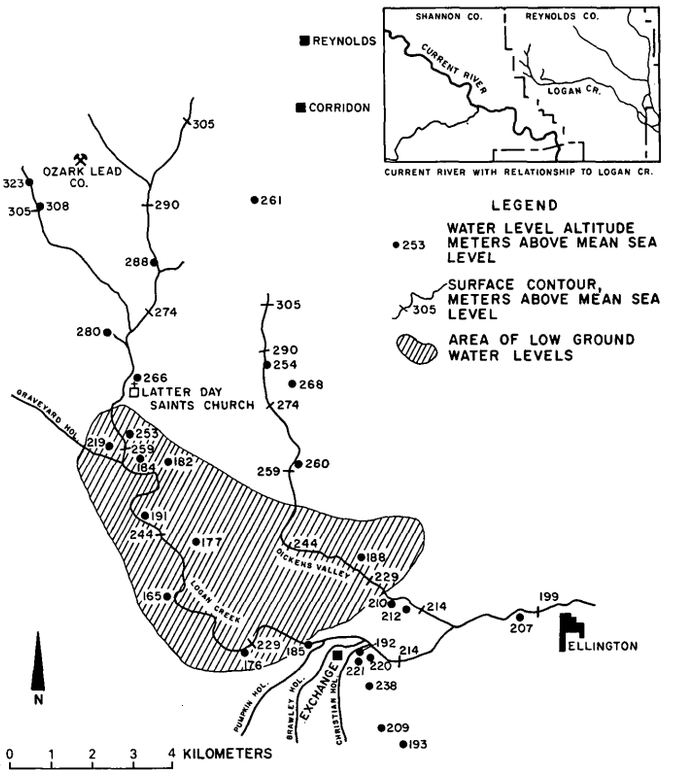

FIGURE 4.—Ground-water levels in Logan Creek basin. Modified from Harvey and others (1977).

TABLE 3.—*Partial list of plants on Logan Creek at sites in gaining and losing reaches (see fig. 4)*

[C, common; S, scattered; R, rare; N, not observed]

Common name	Upstream (gaining to Latter Day Saints Church)	Downstream (losing from Latter Day Saints Church to Exchange)
Cattails	C	N
Spikegrass	C	S
Witchhazel	S	C
Common bulrush	C	N
Fox sedge	C	N
Frank's sedge	C	N
Soft rush	C	N
Ward willow	C	R
Sandbar willow	C	R
Black willow	C	R
Stiff willow	C	R
Bitternut hickory	S	N
River birch	C	N
Watercress	C	N
Sycamore[1]	C	C
Maples	C	N
Touch-me-not	C	N
Dogwood	C	R
Bluestar[2]	N	N
Mint	C	N
Bedstraw	C	N
Buttonbush	C	N
Elderberry	C	N

[1] Sycamore is common downstream but more abundant and larger upstream.

[2] Bluestar, observed frequently in other stream valleys, is unreported from Reynolds County.

CONCLUSIONS

Plant assemblages can be identified that are indicative of gaining and losing conditions in the Ozarks stream valleys. Recognition of these plants is another key to appraising valleys in engineering-geologic problems concerning structural design and in the location of waste-disposal facilities.

A change from one plant assemblage to another in a stream valley not recently altered or cleared, especially if the change is abrupt, is suggestive of a marked change in the depth to the water table or saturated zone. For example, a rapid change from a channel growth of abundant willows, touch-me-nots, and sedges such as spike rush to an abundant channel growth of bluestars indicates a rapid increase in depth to water.

Plant assemblages existing under varying hydrologic conditions can be used in any season of the year (but not as readily in winter) to help evaluate low-flow characteristics of streams and ground-water–surface-water relationships. Vegetative indicators of hydrologic conditions are most helpful when used in conjunction with other information such as ground-water levels, geology, thermal imagery, and seepage runs; but they are independently useful in pinpointing areas of abrupt hydrologic changes. Where abrupt changes in vegetation occur on the flood plain, detailed geologic mapping may reveal faults or other geologic structures that allow water to move to or from the alluvium and cause the vegetation change.

To prevent erroneous conclusions about the permanence of a shallow water table at a stream site, reaches upstream and downstream should be examined. Further, vegetation at a site may appear to be indicative of a permanent shallow water table early in the spring, but a month or two later may show stress indicative of a temporary perched water table.

REFERENCES CITED

Feder, G. L., and Barks, J. H., 1972, A losing drainage basin in the Missouri Ozarks identified on side-looking radar imagery: U.S. Geol. Survey Prof. Paper 800–C, p. C249–C252.

Harvey, E. J., Williams, J. H., and Dinkel, T. E., 1977, Application of thermal imagery and aerial photography to hydrologic studies of karst terrane in Missouri: U.S. Geol. Survey Water-Resources Inv. 77–16.

Steyermark, J. A., 1940, Studies of vegetation of Missouri—I, Natural plant associations and succession in the Ozarks of Missouri: Chicago, Ill., Field Mus. of Nat. History, v. 9, no. 5, p. 349–475.

——— 1963, Flora of Missouri: Ames, Iowa State Univ. Press, 1728 p.

Jour. Research U.S. Geol. Survey
Vol. 6, No. 3, May–June 1978, p. 307–318

THREE-DIMENSIONAL FINITE-DIFFERENCE MODEL OF GROUND-WATER SYSTEM UNDERLYING THE MUSKEGON COUNTY WASTEWATER DISPOSAL SYSTEM, MICHIGAN

By WILLIAM B. FLECK and MICHAEL G. McDONALD, Lansing, Mich.

Prepared in cooperation with the Geological Survey Division, Michigan Department of Natural Resources

Abstract.—The spray irrigation system used by Muskegon County for wastewater treatment is the largest of its kind in the United States. It has 2200 hectares of irrigated farm land, 688 hectares of treatment lagoons, and 105 kilometers of drainage tile. The system has a design capacity of 1.8 cubic meters of wastewater per second. A three-dimensional finite-difference model was developed to study the effect of the disposal operation on ground-water conditions. Model calculations show that the water table at and adjacent to most of the wastewater site is lower as a result of the operation of the system to date. However, along the northwest boundary of the site, where irrigated land was not undertiled, the water table is 1 to 2 meters higher than it would be under natural conditions. Predictive simulations indicate that, even if the drainage tiles lost 75 percent of their effectiveness, the impact of disposal operations on ground-water levels would be negligible outside of the wastewater site.

Muskegon County, Mich., began construction of a 4047-ha wastewater system in 1971. By August 1974 the system was fully operative. This system, designed to use wastewater for spray irrigation of crops, is the first major regional system of its type constructed in the United States. It is located 16 km east of the city of Muskegon.

The purpose of this investigation was to develop a mathematical model of the ground-water flow system in and adjacent to the site so that this model could be used to estimate the effects of the wastewater facility on local ground-water conditions. Figure 1 shows the location and boundaries of the modeled area and the location of the wastewater facility.

The wastewater system has a design capacity of 1.8 m^3/s (Bauer Engineering, Inc., 1973). Five municipalities and two industries currently pipe 1.3 m^3/s to the site. Wastewater is aerated, chlorinated, and then used to irrigate corn. The treated water is sprayed on the land for 8 months; during the winter it is stored in two large lagoons, each having a surface area of 344 ha. The bottoms of the lagoons are about 3 m above the preconstruction altitude of the water table. Leakage from the lagoons is intercepted by ditches that surround about 90 percent of the perimeter of lagoon area. Water in these seepage ditches is either pumped back to the lagoons or to adjacent streams. From the lagoons, water is pumped to center pivot rigs capable of irrigating crops at a rate of 8 cm per week. There are 54 circles irrigating an area of 2200 ha (fig. 2). Most circles are drained by corrugated polyethylene tiles having diameters of 15–25 cm. The tile is perforated with 0.2 by 3.8-cm slots and is encased in a 0.45-mm-mesh fiberglass fabric. Drainage tile lines are generally set 1.5 to 2.5 m below land surface and are spaced at 150-m intervals. They are generally just below the water table except in the northwest corner of the site, where the tile lines are few and above the water table. The total length of the tile lines is 105 km. Drainage tiles are connected to concrete collector

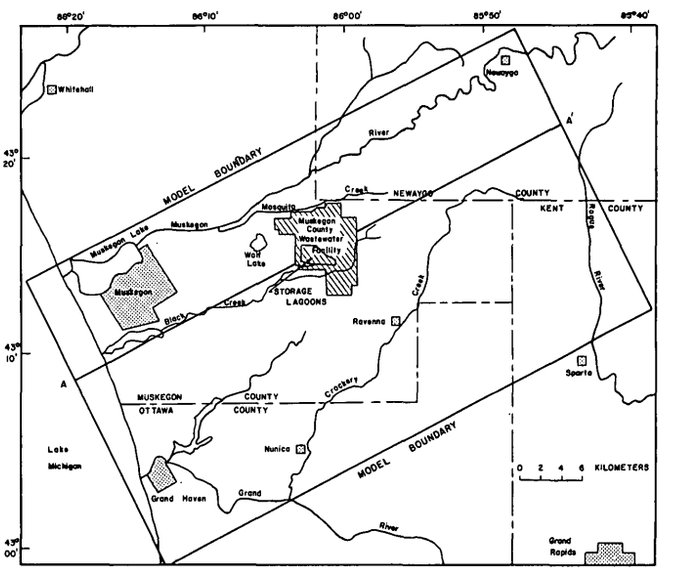

FIGURE 1.—Location of study area. Line A–A′ is trace of cross section shown in figure 3.

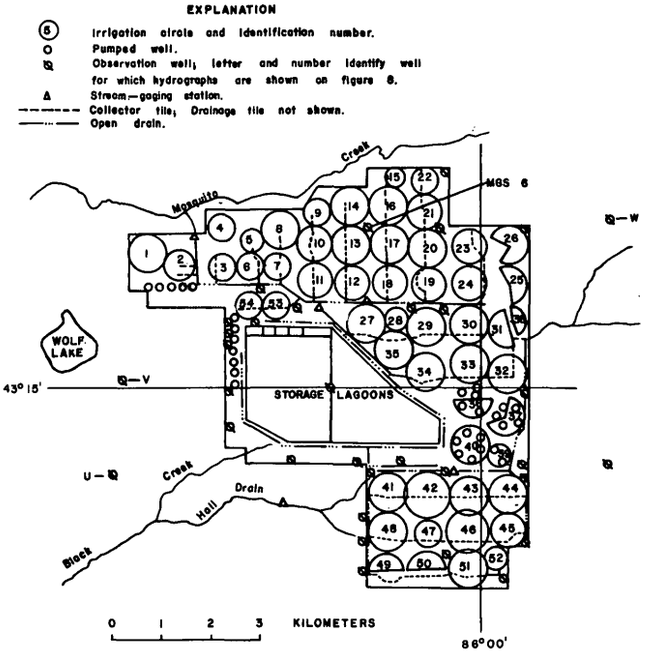

FIGURE 2.—Muskegon County wastewater system.

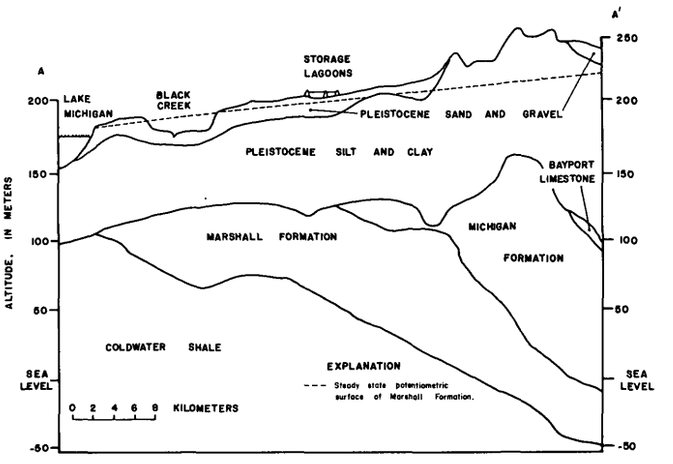

FIGURE 3.—Cross section of study area showing geologic formations. Location of section A–A' shown in figure 1.

tiles (fig. 2) that discharge to drainage ditches. In addition to tile, there are 30 wells (designated as pumped wells on fig. 2) that are used to control ground-water levels. Seven of the wells along the northwest edge of the lagoons are pumped to reduce ground-water mounding caused by lagoon leakage. The rest of the wells are used to control mounding caused by irrigation. This system of tiles, discharge wells, seepage ditches, and drainage ditches was designed to lower ground-water levels in the project area.

A mathematical model capable of simulating the hydrologic system of the wastewater site and its vicinity was developed. The model utilizes standard numerical techniques to solve the differential equation of three-dimensional ground-water flow; it includes routines for simulating the effects of rivers, lagoons, and drainage tiles on the ground-water system. Input to the model consisted primarily of available data. The only additional field data collected were water-level measurements of about 90 wells and streamflow information obtained at five locations in the vicinity of the wastewater site.

GEOLOGIC SETTING

Pleistocene deposits

The western half of the modeled area (fig. 1) is underlain by sediments deposited in Pleistocene lakes (fig. 3) (Martin, 1955). The composition of the sediments varies from tight clay to fine gravel. Generally, the upper 6 to 24 m is well-sorted stratified sand, interlayed with fine gravel and silt. Underlying the sand and gravel are beds of relatively impermeable silt and clay. Topography in the western half is flat and poorly drained; recharge to the ground-water body is high.

Most of the eastern part of the area is underlain by morainic sediments, poorly sorted silt and clay containing lenses of sand and gravel. Thin sand and gravel beds occur along some stream valleys. The thickness of the unconsolidated deposits ranges from 30 to 165 m. Under the wastewater site these deposits are approximately 85 m thick. Undulating topography, more extensive stream development, and low recharge to the ground-water body characterize the eastern part.

Consolidated deposits

Underlying the Pleistocene deposits are consolidated sedimentary rocks of Mississippian age (figs. 3, 4). They include the Bayport Limestone, Michigan Formation, Marshall Formation, and Coldwater Shale (Martin, 1936). The Bayport Limestone is predominantly limestone, sandstone, and shale. The Michigan Formation is composed of relatively impermeable shale, gypsum, dolomite, and limestone. These formations and the overlying silt and clay beds range in thickness from 24 m on the west to about 245 m on the east; they form a confining layer over the Marshall Formation. The Marshall Formation is composed of highly permeable gray, pink, and red sandstones (deWitt, 1960; Dorr and Eschman, 1970). This formation ranges from being absent in the western part of

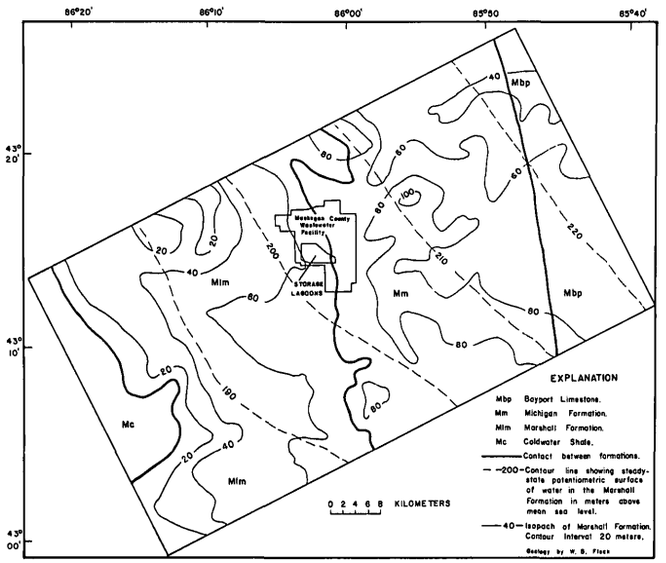

FIGURE 4.—Subcrop formations, thickness, and potentiometric surface of Marshall Formation.

the study area to as much as 100 m thick in the eastern part. The Coldwater Shale, a thick impermeable shale sequence, underlies and confines the Marshall Formation.

HYDROLOGIC SETTING

The region studied has an area of 1620 km^2. Logs of water wells drilled since 1969 and logs of exploratory oil and gas wells were used to determine the location, extent, and hydraulic properties of water-bearing materials and confining beds. Water-level measurements recorded on the well logs were used to estimate steady-state conditions.

The two principal aquifer systems are the water-table aquifer in the Pleistocene deposits and the artesian aquifer in the Marshall Formation (fig. 3). These aquifers are separated by thick confining beds of silt, clay, and shale.

Water-table aquifer

The water-table aquifer of the Pleistocene deposits is composed principally of sand containing some silt and gravel. The aquifer ranges from being absent where it pinches out against the morainic deposits in the eastern part to about 24 m thick in the west. Hydraulic conductivities of these materials were assigned on the basis of well-performance data within the study area and a general knowledge of the characteristics of glacial materials elsewhere. Initial estimates of transmissivity of the aquifer were determined from logs of wells by the relation

$$T = \sum_{i=1}^{n} K_i b_i, \qquad (1)$$

where K_i is the hydraulic conductivity,
b_i is the thickness of each lithologic unit, and
n is the number of units between the water table and the base of the Pleistocene aquifer.

Initial transmissivity values were later modified during model calibration. In the model, the water-table aquifer is represented by two layers; values contoured in figure 5 were consequently defined by the equation

$$T = K_2 b_2 + K_3 b_3, \qquad (2)$$

where K_2 and K_3 represent hydraulic conductivities and b_2 and b_3 represent the thickness of the two layers.

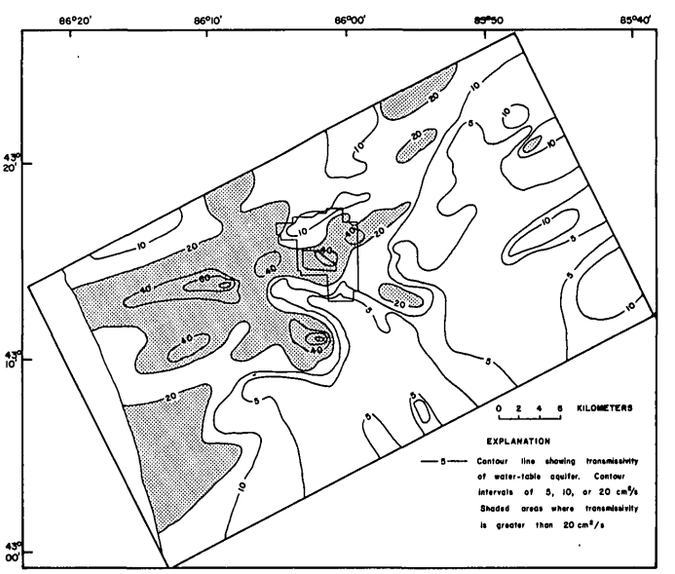

FIGURE 5.—Transmissivity of the water-table aquifer. (1 cm^2/s = 8.64 m^2/d.)

The regional gradient of the water table is toward Lake Michigan. Water levels range from 250 m above mean sea level on the east side of the study area to 177 m along the shore of Lake Michigan. Water discharges from the aquifer regionally to Lake Michigan and locally to streams. Along the north edge of the wastewater facility, the water table slopes downward about 15 m/km northward toward Mosquito Creek.

Recharge to the water-table aquifer was calculated to be 20 cm/yr, based on long-term precipitation,

streamflow, and ground-water levels. This value agrees well with those of Allen, Miller, and Wood (1972) and Walton (1970) for similar geohydrologic conditions in southwestern Michigan and Illinois. Precipitation at the wastewater site and recharge for 1974–75 are shown in table 1. Recharge rates were higher than average in 1974 and 1975 because of intensive storms.

TABLE 1.—*Monthly precipitation, ground-water discharge to streams, change in ground water in storage, and ground-water recharge, in centimeters, in the model area in 1974–1975.*

[Negative values of change in ground water in storage indicate declining water levels. Negative values of ground-water recharge result from losses due to evapotranspiration.]

	Precipitation [1]		Ground water					
			Discharge to streams [2]		Change in storage [3]		Recharge [4]	
	1974	1975	1974	1975	1974	1975	1974	1975
January	8.9	5.1	2.3	2.0	5.1	3.0	7.4	5.0
February	3.6	5.1	2.3	1.8	−1.3	3.0	1.0	4.8
March	10.9	5.6	3.6	2.8	2.0	2.5	5.6	5.3
April	6.9	5.1	4.1	3.0	3.0	0	7.1	3.0
May	14.7	5.1	3.8	2.3	−1.3	−4.8	2.5	−2.5
June	8.6	11.9	2.5	2.0	−6.4	−0.5	−3.9	1.5
July	2.8	4.1	1.5	1.5	−6.4	−5.6	−4.9	−4.1
August	9.1	23.6	1.3	1.3	−0.5	3.6	0.8	4.9
September	1.3	2.5	1.0	3.0	−2.0	3.0	−1.0	6.0
October	3.0	2.0	1.5	2.0	1.3	−0.5	2.8	1.5
November	6.6	9.1	1,8	2.5	3.8	1.8	5.6	4.3
December	3.3	6.4	1.8	3.6	0.5	2.8	2.3	6.4
Total	79.7	85.6	27.5	27.8	−2.2	8.3	25.3	36.1

[1] Data from rain gage at wastewater disposal site.
[2] Average values calculated from streamflow hydrographs of four gaging stations.
[3] Average from seven observation wells assuming specific yield of 0.2.
[4] Total of ground-water discharge and change in ground water in storage.

Artesian aquifer

The Marshall Formation is an artesian aquifer. Hydraulic conductivity values, determined from 7 pumping tests and 33 specific-capacity analyses (Brown and others, 1963; Walton, 1962), ranged from 8 to 800 m/d; the median value was approximately 80 m/d. The thickness of the Marshall Formation was determined from 750 oil and gas logs. In the eastern part of the study area, where the formation underlies the Michigan Formation, the thickness ranges from 18 to 100 m; the average thickness is about 73 m. In the western half, the thickness gradually decreases westward from about 70 m until the formation pinches out along the contact with the Coldwater Shale (fig. 3). Transmissivity of the Marshall Formation, determined by multiplying the formation thickness by the median hydraulic conductivity, ranges from 0 along the west border of the study area, where the Coldwater Shale is present, to 8000 m²/d just east of the wastewater site.

In most of the study area and to the east, the Marshall Formation is recharged by downward flow from the water-table aquifer. Water levels in the artesian aquifer are lower than the overlying water table; at the east edge of the study area, this difference is as much as 30 m. Flow within the Marshall Formation is to the west. The slope of the potentiometric surface is 0.8 to 1.9 m/km (fig. 4). At the shore of Lake Michigan, the head of the Marshall Formation is about 180 m above sea level, whereas the lake level is 177 m above sea level. The vertical flow pattern here changes from downward recharge to upward discharge toward the lake.

Confining unit

The confining beds of silt, clay, and shale that separate the water table and artesian aquifers range in thickness from 24 m in the west to about 245 m in the east. Vertical hydraulic conductivity of confining beds, 0.004 m/d, was estimated from previous investigations of similar materials in southern Michigan (Allen, Fleck, and Hanson, 1972) and in Ohio (Norris, 1963).

MODEL DESCRIPTION

A ground-water model is a mathematical description of the movement of water in a geologic environment. When converted to a form that permits computer solution of equations containing hydrologic and hydraulic parameters, the response of the ground-water system to stress may be predicted.

Basic ground-water flow model

The differential equation describing flow in a porous saturated medium is

$$\frac{\partial}{\partial x}\left(K_x \frac{\partial h}{\partial x}\right) + \frac{\partial}{\partial y}\left(K_y \frac{\partial h}{\partial y}\right) + \frac{\partial}{\partial z}\left(K_z \frac{\partial h}{\partial z}\right) = S_s \frac{\partial h}{\partial t} + W \quad (x,y,z,t), \qquad (3)$$

where h is the head at time t,
K_x, K_y, and K_z are principal components of the hydraulic conductivity tensor alined with the coordinate axes,
S_s is the specific storage, and
W is a source term for inflow or withdrawal per unit volume of an aquifer.

The terms K_x, K_y, S_s, W, $\frac{\partial h}{\partial x}$, $\frac{\partial h}{\partial y}$, and $\frac{\partial h}{\partial t}$ in equation 3 are assumed to be independent of z for the thickness z_1 to $z_1 + b$, and the equation can be integrated to give

$$\frac{\partial}{\partial x}\left(T_x \frac{\partial h}{\partial x}\right) + \frac{\partial}{\partial y}\left(T_y \frac{\partial h}{\partial y}\right) + \left(K_z \frac{\partial h}{\partial z}\right)_{z_1+b} - \left(K_z \frac{\partial h}{\partial z}\right)_{z_1} = S \frac{\partial h}{\partial t} + bW(x,y,z,t), \qquad (4)$$

where T_x and T_y are the principal components of the transmissivity tensor, and S is the storage coefficient, defined by $S = bS_s$.

In general, equation 4 cannot be solved analytically; however, it can be replaced with an approximating finite difference equation and thus solved numerically. The continuous entities of space and time are regarded as discrete cells, and flow is regarded as a change from one state of the system to the next in a stepwise fashion. The hydraulic properties of the material in each cell are assumed to be homogeneous, and the potentiometric head is calculated for a node at the center of each cell.

If the prism being modeled is divided into "I" rows, "J" columns, and "K" layers, then equation 4 is approximated by the set of N equations (N=I×J×K) as follows:

$$\begin{aligned}&T_{x(i,j+1/2,k)}\,(h_{i,j+1,k}-h_{i,j,k})/(\Delta x_{j+1/2}\Delta x_j)\\&-T_{x(i,j-1/2,k)}\,(h_{i,j,k}-h_{i,j-1,k})/(\Delta x_{i-1/2}\Delta x_j)\\&+T_{y(i+1/2,j,k)}(h_{i+1,j,k}-h_{i,j,k})/(\Delta y_{i+1/2}\Delta y_i)\\&-T_{y(i-1/2,j,k)}(h_{i,j,k}-h_{i-1,j,k})/(\Delta y_{i-1/2}\Delta y_i)\\&+K_{z(i,j,k+1/2)}(h_{i,j,k+1}-h_{i,j,k})/\Delta z_{k+1/2}\\&-K_{z(i,j,k+1/2)}(h_{i,j,k}-h_{i,j,k-1})/\Delta z_{k-1/2}\\&=[S'_{i,j,k}(h_{i,j,k}-\hat{h}_{i,j,k})/\Delta t]+b\,W_{i,j,k}\end{aligned}\qquad(5)$$

where $T_{x(i,j+1/2,k)}$ is the transmissivity along the x axis between node (i,j,k) and $(i,j+1k)$, and $T_{x(i,j-1/2,k)}$, $T_{y(i+1/2,j,k)}$, and $T_{y(i-1/2,j,k)}$ are similarly defined,

$K_{z(i,j,k+1/2)}$ is the hydraulic conductivity along the z axis between node (i,j,k) and node $(i,j,k+1)$, and $K_{z(i,j,k-1/2)}$ is similarly defined,

Δx_j, Δy_i, Δz_k are the widths of column j, row i, and layer k, respectively,

$W(i,j,k)$ is the source term for cell (i,j,k),

$\Delta x_{j+1/2}$, $\Delta y_{i+1/2}$, $\Delta z_{k+1/2}$ is the distance between node (i,j,k) and nodes $(i,j+1,k)$, $(i+1,j,k)$, and $(i,j,k+1)$, respectively,

$h_{(i+j+k)}$ is the potentiometric head at node (i,j,k) at the end of the time step,

$S'_{(i,j,k)}$ is the storage coefficient in cell (i,j,k), and

$\hat{h}_{(i,j,k)}$ is the potentiometric head at node (i,j,k) at the beginning of the time step.

Combining coefficients and bringing terms containing unknown head values to the left, equation 5 can be written in the form:

$$\begin{aligned}&A_0h_{i,j,k}+A_1h_{i,j+1,k}+A_2h_{i,j-1,k}+A_3h_{i+1,j,k}+A_4h_{i-1,j,k}\\&+A_5h_{i,j,k+1}+A_6h_{i,j,k-1}=q_0,\end{aligned}\qquad(6)$$

where $A_n(n=0,1,\ldots6)$ are constant with respect to time, and

$$q_0=b\,W_{i,j,k}-[S'_{(i,j,k)}\hat{h}(i,j,k)/\Delta t].$$

This system of N equations can be written in matrix form as

$$\bar{A}\bar{h}=\bar{Q}.\qquad(7)$$

Equation 7 is solved using the "Strongly Implicit Procedure" (SIP) developed by Stone (1968).

The computer program incorporating the techniques used to approximate a solution to equation 4 was developed by Trescott (1975). Modifications were made by Larson (written commun., March 1976) to simulate tile drainage and river leakage. A typical nonequilibrium simulation with this program will consist of several recharge periods, during each of which recharge to the top layer remains constant. The recharge periods are subdivided into time steps. The length of the time step (Δt in eq 5) affects the accuracy of the approximation to equation 3. As the time steps get shorter, the accuracy of approximation improves, but computation time increases. Similarly, as the cell dimensions become smaller, the accuracy of approximation improves, but again the computation time increases. Thus, the length of time step and size of the cells must be selected to give acceptable results in a reasonable processing time.

The hydraulic characteristics and the initial potentiometric heads for each cell are used at the beginning of simulation to calculate those elements of matrix $\bar{A}$ in equation 7 that remain constant throughout the simulation. The location and hydraulic characteristics of rivers and drainage tiles are used at the beginning of the simulation and stored for use throughout the simulation.

After the hydraulic constants have been calculated, recharge rates forming part of the W term in equation 4 are used with Δt to calculate the remaining entries of the matrices $\bar{A}$ and $\bar{Q}$ in equation 7. For each node, the SIP algorithm then iteratively calculates new heads that satisfy matrix equation 7. Similarly, heads are calculated for the remaining time steps and the process is repeated for the rest of the recharge periods.

Drainage analysis

A separate analysis was made to determine the effects of the drainage tiles. In this analysis, a cross-sectional model, based on simulation techniques described by Prickett and Lonnquist (1971), was utilized. The model simulated flow in a vertical plane perpendicular to a single drainage tile. The vertical depth of the cross section was assumed to be 10 m, which is representative of the thickness of the water-table aquifer; the width was taken as half the drain spacing or 75 m. To represent the drainage tile, a single node at one side of the mesh was held at a head equal to its elevation. This node was a square, 0.15 m on a side; inflow was permitted through one side and through the bottom. The simulation represented half of the flow field to a drain. The hydraulic conductivity of the drain node was reduced to a fraction of that elsewhere to represent the hydraulic resistance of the drain pipe and the surrounding fiberglass net. Also, modifications were made in the model to allow the water-table boundary to move.

During each simulation, the model was set to represent a fully saturated rectangular cross section, and recharge was applied to the uppermost node. A nonequilibrium simulation was conducted until steady-state conditions were achieved. As the nodes became dewatered during the simulation process, they were removed from the system by lowering the water-table boundary, and calculations were repeated to achieve a solution corresponding to the new boundary position. Except for the drain node and the recharge nodes, all boundaries were treated as zero-flow boundaries.

Model runs were made using values of lateral hydraulic conductivity that are in the range found at the Muskegon site. Also, several different ratios of lateral to vertical hydraulic conductivity were used. Results showed that the flow to both halves of a drainage tile could be expressed approximately as a function of hydraulic conductivity and average head above the drain by the relation

$$Q = K_L\ (h - V)G \text{ when } h > V, \qquad (8)$$

where Q is the flow into a unit length of drainage tile,
h is the average water-table elevation in the area drained by the tile,
V is the elevation of the tile,
K_L is the lateral hydraulic conductivity, and
G is a factor that varies with the anisotropy and with the hydraulic conductivity of the drain node.

When a vertical hydraulic conductivity equal to one-tenth the lateral hydraulic conductivity was used and when the conductivity in the drain node was set at one-tenth of the lateral conductivity elsewhere, G was found to be approximately 0.1. By varying the anisotropy and the conductivity of the drain node, values of G from 0.05 to 0.40 were obtained. These values were subsequently used in checking the sensitivity of the three-dimensional model under various drainage conditions.

Muskegon model

Applying the principles of modeling ground-water flow to the Muskegon wastewater disposal site entailed developing a grid and devising a method for simulating effects of lagoons, rivers, and drainage tiles. The area modeled was divided with a rectilinear grid into three water-bearing layers as shown in figure 6. Each layer has 44 rows and 48 columns. Layer 1, the lowermost layer, represents the Marshall Formation. Layer 2 represents all the water-table aquifer except the upper 6 m; layer 3 is the upper 6 m. The water-table aquifer was divided into two

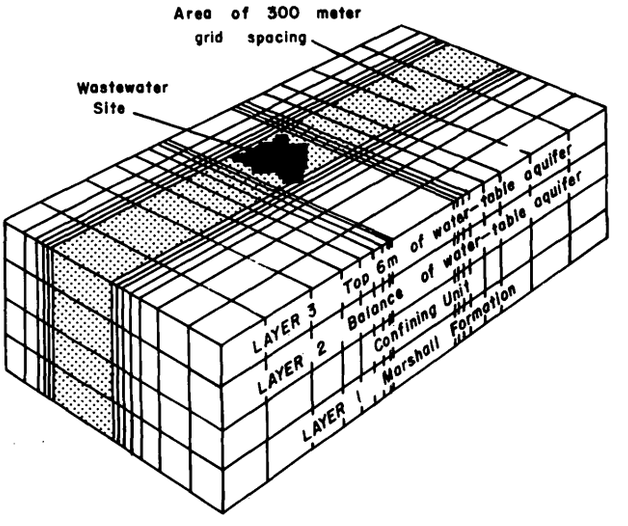

FIGURE 6.—Grid spacing used in finite-difference model. Horizontal spacing ranges from 300 m at wastewater site to 5000 m at edge of model.

layers, so that the drains and streams could be simulated in the uppermost layer as shallow features, rather than having their effect distributed through the full thickness of the aquifer. The confining unit between the Marshall Formation and the water-table aquifer was not treated as a separate layer; its effect was incorporated into the vertical hydraulic conductivities of layers 1 and 2.

The horizontal grid was designed so that the smallest cells (300 m on a side) were at the wastewater site (shaded area in figure 6). The grid spacing increased by a factor of 1.5 to the boundaries of the model area. Moving the boundaries far beyond the wastewater site greatly diminishes the sensitivity of the model at the site to the boundary conditions. All boundaries of the model area were treated as constant flow boundaries except the western boundary of the top layer, which was assumed to have a constant head equal to the elevation of Lake Michigan.

Storage effects were simulated only in the uppermost layer of the model. Compressive storage in the unconfined aquifer below the water table was not simulated, nor was artesian storage in the Marshall Sandstone. Compressive storage in the confining unit above the Marshall was also neglected. It was assumed that these compressive effects would be negligible in comparison to the water-table storage in the uppermost layer. Thus, the model grid below the uppermost layer was purely transmissive in character.

Flow to the drainage tiles was simulated using equation 8, with G equal to 0.1. In the model, this was done by adding the terms $(Gl_{i,j}\ K_{i,j}\ h_{i,j,k})$ and $(Gl_{i,j}$

$K_{i,j}$ $V_{i,j}$) to the left and right of equation 6, respectively, for each cell in layer 3 that contained drainage tiles, in each time step during which the head exceeded the tile elevation. In these expressions

$l_{i,j}$ is the length of tile in the cell,
$K_{i,j}$ is the hydraulic conductivity of the cell, and
$V_{i,j}$ is the average tile elevation in the cell.

During model calibration, values of G in the range 0.05 to 0.40 were used in equation 8. The response of the model was not particularly sensitive to variation in G within this range, and 0.1 was retained as giving the best results.

The effects of streams on the ground-water system were simulated using the method described by Prickett and Lonnquist (1971, p. 33). The method is based on assumptions that a streambed layer separates the stream from the aquifer and that seepage from the stream to the aquifer becomes constant when the water level in the aquifer falls below the bottom of the streambed. Under these assumptions, the rate of flow through the streambed is expressed by the equation

$$Q_r = K' A (M - y)/b \text{ when } h < y \quad (9)$$

and

$$Q_r = K' A (M - h)/b \text{ when } h \geq y, \quad (10)$$

where Q_r is the flow between the stream and the aquifer (it is positive when the flow is from the stream to the aquifer),
K' is the hydraulic conductivity,
b is the thickness of the streambed layer,
A is the area of streambed within the model cell,
M is the elevation of the stream surface,
y is the elevation of the bottom of the streambed layer, and
h is the head of a cell in layer 3 of the model.

In the Muskegon model, K' was taken as one-tenth of the local lateral hydraulic conductivity in layer 3 of the model, and b was taken as 1.5 m. Other values of these parameters were also tried during model calibration.

Recharge to the water-table aquifer from the lagoons was treated as an evenly distributed, constant seepage. In the initial model calibrations, the seepage rate through the bottom of the lagoons was assumed to be 0.58 m^3/s. This estimate was based upon pumpage records from the seepage ditches around the lagoons. Approximately 0.66 m^3/s is pumped from these ditches, and it was assumed that 80 percent of this, or 0.53 m^3/s, represents seepage from the lagoons. The balance represents drainage from other sources—that is, from surrounding irrigation circles or from regional ground-water flow. Also, because the seepage ditches do not completely enclose the lagoons, it was assumed that only 90 percent of the seepage from the lagoons was intercepted by the ditches. A total seepage of 0.58 m^3/s was, therefore, used.

If this estimate of lagoon seepage is accurate, it implies that the vertical hydraulic conductivity beneath the lagoons is considerably lower than that of the streambed or that of the water-table zone. This may reflect the effect of deposition of organic matter in the lagoons, even though the system has been operated only since 1974.

The seepage ditches around the lagoons were simulated as streams, by using equations 9 and 10, the streambed conductivity was assumed to be one-tenth of the local lateral hydraulic conductivity, and the streambed layer thickness was assumed to be 1.5 m. Seepage into the ditches in computer simulations was found to be in close agreement with field data.

Data base

Data required for model development included hydraulic properties of the hydrogeologic units, hydraulic properties of rivers and drainage tiles, and constant recharge and discharge sources. Heads and baseflow calculated by the model were compared with measured water levels and streamflow for purposes of calibration.

Initial estimates of the transmissivity of each cell in layers 1 and 2 and of horizontal hydraulic conductivity of each cell in layer 3 were made from lithologic data. Specific yield of layer 3 was set to 0.2. The storage coefficient for layers 1 and 2 was set to 0. The vertical hydraulic conductivity between the bottom two layers at each horizontal grid location was assumed to be equal to the vertical hydraulic conductivity of the confining unit divided by the thickness of the confining unit at the grid location. The vertical hydraulic conductivity between the top two layers at each grid location was initially assumed to be equal to one-tenth of the horizontal hydraulic conductivity of the cell in the top layer at that grid location.

Engineering blueprints were used to estimate length and average elevation of drainage tiles. For each cell, the length and average elevations of all tiles in the cell were used.

The width, length, and elevation of rivers in each cell of the upper layer were determined from topographic maps. Thickness of the streambed layer, as noted previously, was assumed to be 1.5 m. The vertical hydraulic conductivity of the streambed in each cell was initially assumed to be one-tenth of the horizontal hydraulic conductivity of the cell. A stream leakage factor was calculated independently of the

model program from width, length, hydraulic conductivity, and streambed thickness. The leakage factor and the stream elevation were used in model computations.

In calculating irrigation rates, the design capacities and number of hours of operating time of the irrigation rigs were considered. Total recharge for each cell in the model area was calculated from lagoon leakage, amount of irrigation, and natural recharge.

Water levels from two sources were available. A long-term average water-table map was derived from levels reported in driller's well records. Well hydrographs were drawn using water levels measured twice a month since 1970 in 90 observation wells.

Calibration

A model is calibrated by repetitively running the computer program using available hydraulic data. The results of each simulation are then used to refine estimates of hydraulic parameters for subsequent simulations. Development of the Muskegon model involved a steady-state calibration and a transient calibration. In each of these calibrations, it was observed that head differences between the upper and middle layers of the grid were negligible—that is, that heads in the upper 6 m of the water-table aquifer were essentially equal to those in the lower part of the aquifer. In presenting each simulation result, therefore, a single map of water-table aquifer head or changes in head has been utilized, rather than presenting separate maps for the two model layers representing the unconfined aquifer. Results are not shown for the artesian aquifer, inasmuch as changes in the potentiometric surface were small in all simulations.

During the steady-state calibration a specific yield of 0 was set in all cells of the uppermost layer, thereby eliminating the time dependence in equation 3. The purpose of steady-state calibration was to match the long-term average water table before construction of the wastewater facility with the water table calculated by the model. A uniform recharge of 20 cm/yr was used in computations.

A series of steady-state simulations was made to determine the sensitivity of the model to variations in the hydraulic parameters. The simulations indicated that the model was insensitive to changes in vertical hydraulic conductivity or stream leakage. The model, however, was very sensitive to changes in horizontal hydraulic conductivity and transmissivity. Best results were obtained when these parameters were reduced to half their initial values. The comparison between computed and measured water-table positions after steady-state calibration is shown in figure 7.

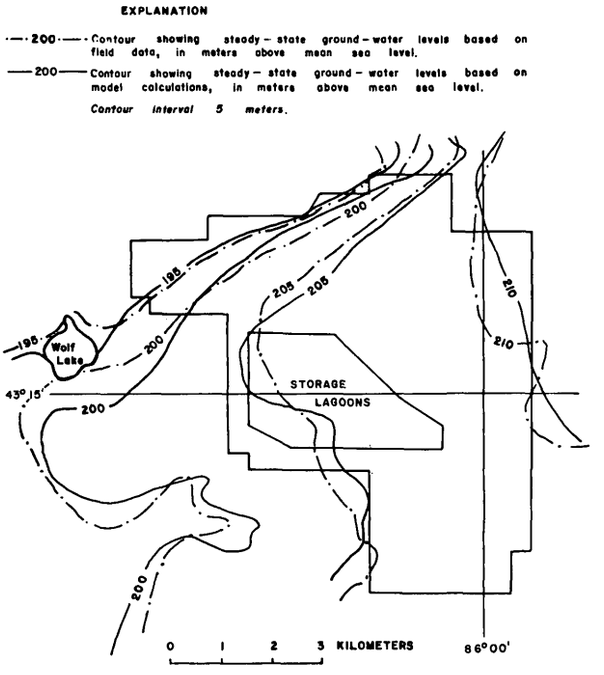

FIGURE 7.—Steady-state water table from field measurements and from model calculations.

Along the north edge of the area, step ground-water gradients caused difficulty in matching water levels.

Transient calibration was used to test assumptions regarding the specific yield and the hydraulic characteristics of the wastewater facility and to further refine other parameters. The period January 1974 to December 1975 was used for transient calibration. This period included the first growing season during which the facility operated at full capacity, as well as some earlier periods of operation at part capacity. Twenty-four monthly recharge periods were simulated. Initial heads used in the transient calibration were those calculated in the steady-state model.

Only minor changes were made in hydraulic conductivity and transmissivity during transient calibration. The model was not particularly sensitive to changes in specific yield, and the original value of 0.2 was ultimately retained because it gave the best results. Stream location and stream surface elevation proved to be important factors. For this reason an effort was made to include all streams regardless of size and to establish stream surface elevations as accurately as possible.

Figure 8 shows four representative hydrographs after transient calibration and illustrates the final match between computed and observed water-level trends. Figure 9 compares measured water levels in the water-table aquifer during July 1975 with those calculated by the model during transient calibration.

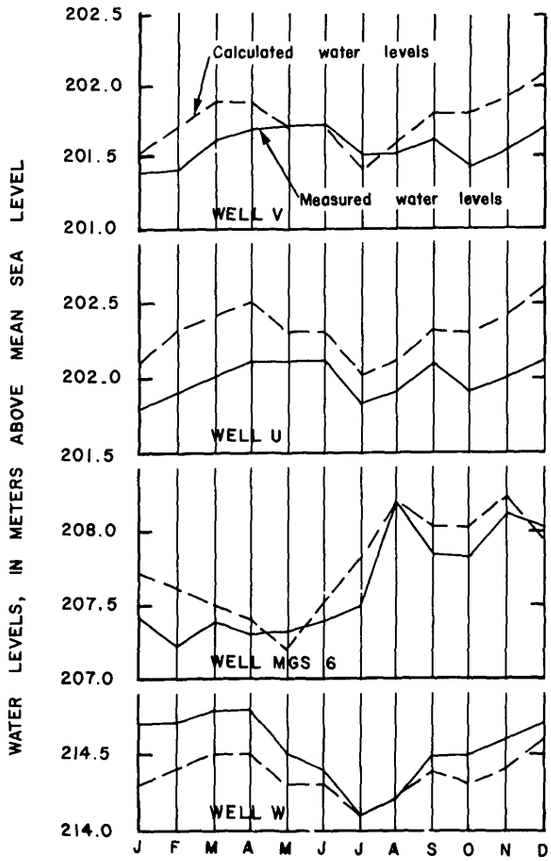

FIGURE 8.—Hydrographs of selected wells during 1975 from field measurements and from model calculations. Location of wells shown in figure 2.

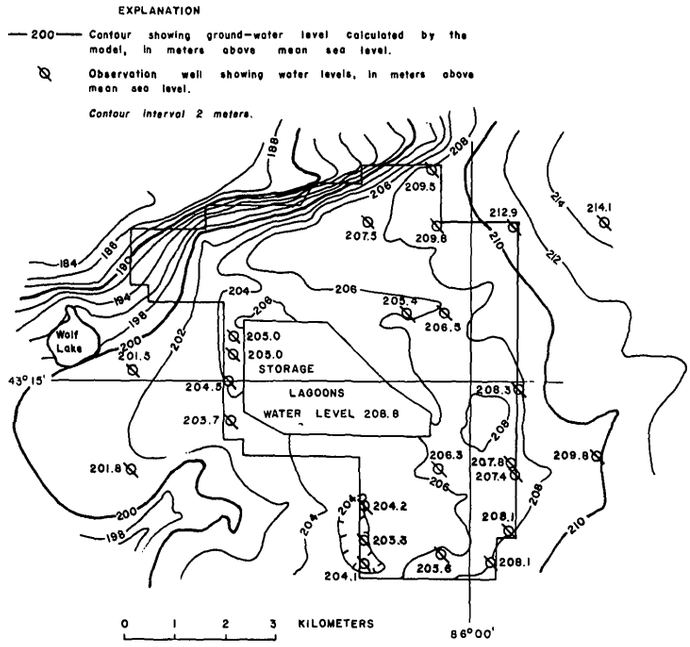

FIGURE 9.—Altitude of water table during July 1975 from field measurements and from model calculations.

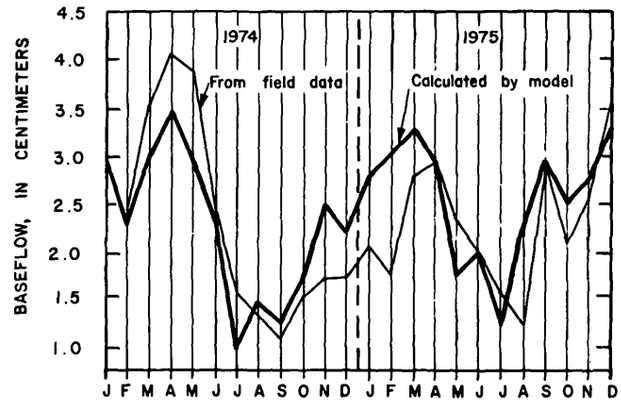

FIGURE 10.—Hydrographs of monthly baseflow from field measurements and from model calculations.

Figure 10 shows the comparison between the amount of observed and computed baseflow from the vicinity of the wastewater site during the period of transient calibration.

INITIAL MODEL APPLICATIONS

Effects of the system through 1975

The model was used to study the past effect of the operation of the wastewater system on regional ground-water levels. Water levels for 1975 were calculated as if the system had not been constructed. The impact the wastewater system has had on the regional water table was determined by subtracting the calculated water levels from the actual levels. Figure 11

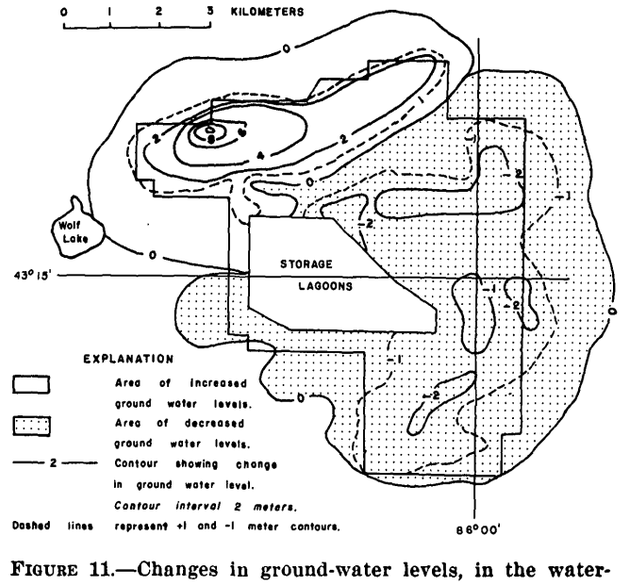

FIGURE 11.—Changes in ground-water levels, in the water-table aquifer, caused by operation of the wastewater system, July 1975.

shows this impact. In most of the site the effect of the facility has been to lower ground-water levels. However, water levels have risen in the northwestern part of the area where there are relatively few drains.

Predictive simulations

Several predictive simulations were made assuming a variety of operational conditions. In one simulation, it was assumed that irrigation would be maintained at a uniform rate of 4 cm per week (the average rate for 1975) in all irrigation circles, the lagoons would leak steadily at a rate of 0.58 m^3/s, and that drainage tile performance would again be described by equation 8, with G taken as 0.1. The December 1975 water-level configuration was used as the starting surface, and the simulation was carried to steady state. In this and in all subsequent predictive simulations, steady state was attained after 3 or 4 years of operation. The simulations were nevertheless carried for several additional years. The results for 10 years of operation are presented here for each simulation as the steady-state condition.

The results of the initial predictive simulation are

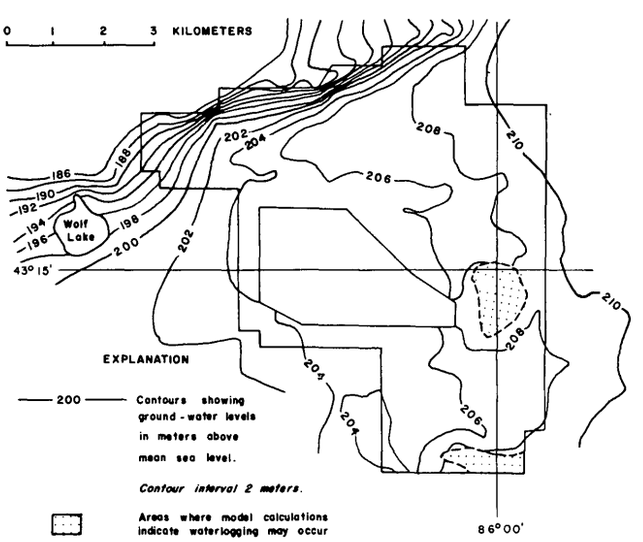

FIGURE 12.—Steady-state water table from model calculations with irrigation of 4 cm per week, normal lagoon leakage, and tile seepage.

shown in figure 12. The effects are primarily at the wastewater site. For a few areas within the site, the computed water levels are above land surface. These areas are shown on figure 12 as being waterlogged—that is, the water table in these areas would be approximately at land surface.

The results shown in figure 12 do not imply that waterlogging is a necessary consequence of the waste

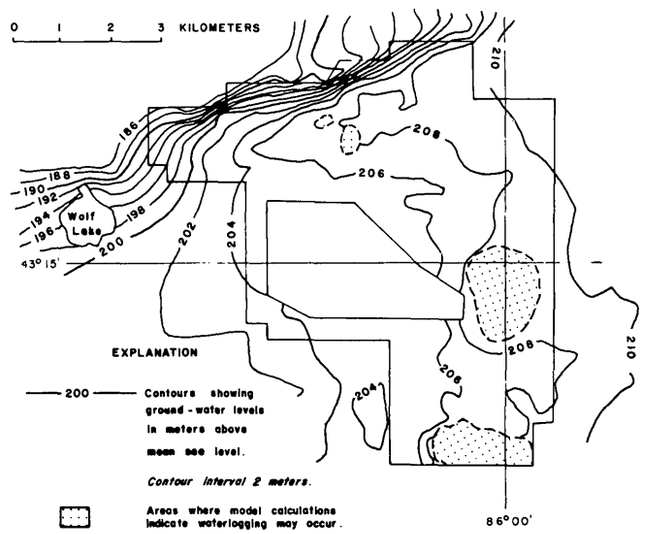

FIGURE 13.—Steady-state water table from model calculations with irrigation of 8 cm per week, normal lagoon leakage, and tile seepage.

disposal operation, but, rather, that irrigation at a rate of 4 cm per week over the entire area would probably cause such problems. In practice, irrigation rates will vary from one part of the system to another and will be managed so as to avoid waterlogging, or, alternatively, the number of drainage tiles could be increased to avoid waterlogging.

A second predictive simulation was made in which the irrigation rate was maintained at a uniform rate

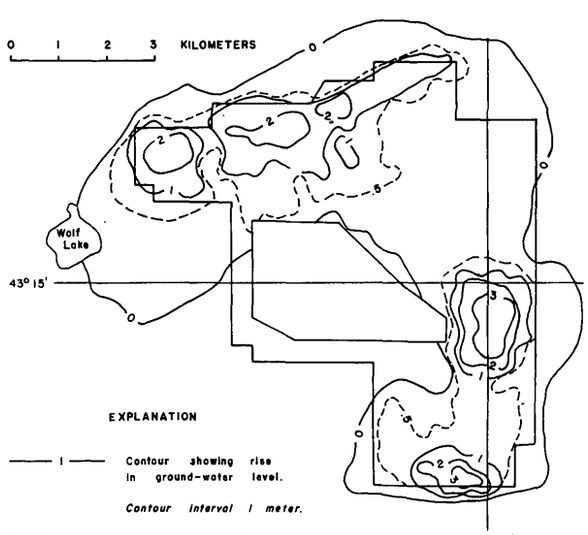

FIGURE 14.—Predicted rise in ground-water levels in the water-table aquifer, if irrigation is increased from 4 cm per week to 8 cm per week. In the southern part of the site, the increase of 4 cm per week in irrigation rate causes a rise of as much as 3 m.

of 8 cm per week (the design irrigation rate). Performance of drainage tiles and the lagoon seepage were the same as in the first predictive simulation. The 1975 water-level surface was again taken as the initial condition, and the simulation was continued to steady state. Figure 13 shows contours of the water-table elevation after steady state was reached. The increase in the irrigation rate from 4 to 8 cm per week caused the waterlogged area to increase from 150 ha to 400 ha. Figure 14 shows the rise in water level that may be expected with an increase in irrigation rate from 4 cm per week to 8 cm per week. The figure shows the difference between water-level elevations in figures 12 and 13.

A third predictive simulation assumed that the irrigation rate would be maintained at 8 cm per week, that lagoon leakage would continue at 0.58 m^3/s, but that the efficiency of the drainage tiles would be severely reduced by clogging. In the model, the factor G in equation 8 was reduced from 0.1 to 0.025, and thus the flow to the drains, for a given head differential, would be only 25 percent of that in earlier simulations. The 1975 water-table surface was again taken as the starting condition, and calculations were continued until steady state was achieved. Figure 15 shows contours

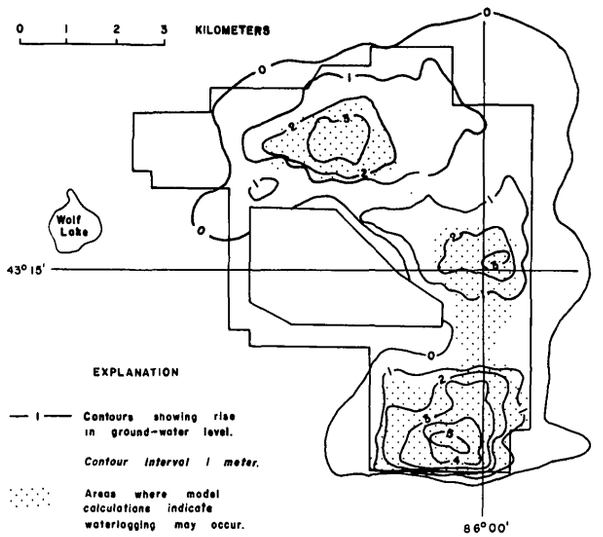

FIGURE 15.—Predicted rise in ground-water levels, in the water-table aquifer, when seepage into drainage tile is reduced by 75 percent.

of the change in water level that would result from clogging of the drains. The contours represent the rise in water level, above the levels shown in figure 13, that would result if drainage efficiency were reduced but other factors remained as in the previous simulation. Nearly half of the irrigated area becomes waterlogged. However, long before waterlogging became that extensive, irrigation practices or drainage tiles would be modified.

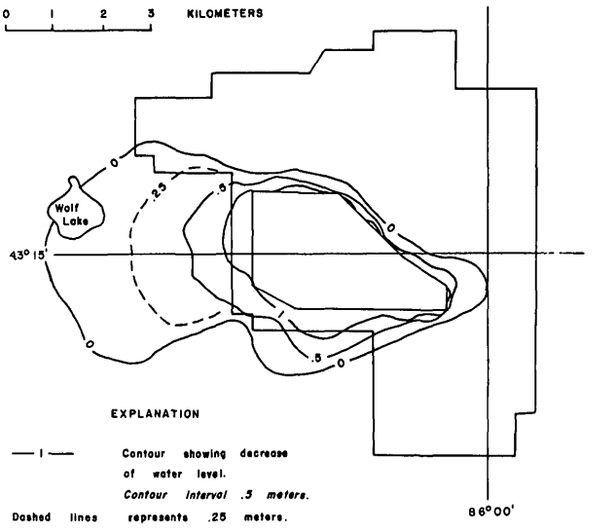

FIGURE 16.—Predicted decline in ground-water levels, in the water-table aquifer, if the bottoms of the storage lagoons become sealed.

In the final predictive simulation, seepage from the lagoons was reduced to zero while the other factors remained unchanged. The purpose of this simulation was to determine the effect on water levels if the bottoms of the lagoons became effectively sealed with organic matter. The 1975 water table was again taken as the starting condition, and the simulation was continued to steady state. Figure 16 shows contours of the changes in water level that would result from sealing the lagoons; that is, the changes caused by elimination of lagoon seepage while all other factors were maintained as in the second simulation. The changes in water level are relatively minor and are restricted to the immediate vicinity of the lagoons and a small area to the west that extends almost to Wolf Lake. There is virtually no reduction in the waterlogged areas from those in figure 13.

SUMMARY

The ground-water system in the vicinity of the Muskegon wastewater site was simulated using a three-dimensional finite difference model. During calibration of the model for steady-state conditions a constant recharge rate of 20 cm/year was used for simulated conditions before the wastewater disposal system was constructed. Irrigation systems, lagoons, and drainage tiles were incorporated in the model for calibration under transient flow conditions.

The calibrated model showed that except in the

northwest corner, where tile lines are few and are above the water table, ground-water levels are lower than they would be under natural conditions. Predictive simulations indicate that, even if the drainage tiles lose 75 percent of their effectiveness, the impact of disposal operations on ground-water levels outside of the wastewater site will be small.

REFERENCES CITED

Allen, W. B., Fleck, W. B., and Hanson, J. D., 1972, Geologic and hydrologic studies of three areas in southeast Michigan: U.S. Geol. Survey open-file rept., 31 p.

Allen, W. B., Miller, J. B., and Wood, W. W., 1972, Availability of water in Kalamazoo County, Southwestern Michigan: U.S. Geol. Survey Water-Supply Paper 1973, 129 p., 9 pls.

Bauer Engineering, Inc., 1973, Muskegon County, Michigan, wastewater management system No. 1: Bauer Engineering, Inc., 16 p.

Brown, R. H., Ferris, J. G., Jacob, C. E., Knowles, D. B., Meyer, R. R., Skibitzke H. E., and Theis, C. V., 1963, Methods of determining permeability, transmissibility, and drawdown: U.S. Geol. Survey Water-Supply Paper 1536–I, p. 243–341.

deWitt, Wallace, Jr., 1960, Geology of the Michigan basin with reference to subsurface disposal of radioactive wastes: U.S. Geol. Survey Trace Elements Inv. Rept. 771, 100 p.

Dorr, J. A., Jr., and Eschman, D. F., 1970, Geology of Michigan: Ann Arbor, The University of Michigan Press, 476 p.

Martin, H. M., compiler, 1936, The centennial geologic map of the southern peninsula of Michigan: Michigan Dept. Nat. Resources, Geol. Survey Div., Pub. 39, Geol. Ser. 33.

——— 1955, Map of the surface formations of the southern peninsula of Michigan: Michigan Dept. Nat. Resources, Geol. Survey Div. Pub. 49.

Norris, S. E., 1963, Permeability of glacial till: U.S. Geol. Survey Prof. Paper 450–E, p. 150–151.

Prickett, T. A., and Lonnquist, C. G., 1971, Selected digital computer techniques for ground-water resource evaluation: Illinois State Water Survey Bull. 55, 62 p.

Stone, H. L., 1968, Iterative solution of implicit approximations of multidimensional partial differential equations: Jour. Numerical Analysis, v. 5, no. 3, p. 530–557.

Trescott, P. C., 1975, Documentation of finite-difference model for simulation of three-dimensional ground-water flow: U.S. Geol. Survey Open-File Rept. 75–438, 103 p.

Walton, W. C., 1962, Selected analytical methods for well and aquifer evaluation: Illinois State Water Survey Bull. 49, 81 p.

——— 1970, Groundwater resource evaluation: New York, McGraw-Hill, 664 p.

Jour. Research U.S. Geol. Survey
Vol. 6, No. 3, May–June 1978, p. 319–324

IRON IN WATER NEAR WASTEWATER LAGOONS IN YELLOWSTONE NATIONAL PARK, WYOMING

By EDWARD R. COX, Cheyenne, Wyo.

Prepared in cooperation with the National Park Service

Abstract.—High dissolved-iron concentrations have been noted in water in wells used to monitor effluent that percolates from wastewater disposal lagoons near Old Faithful in Yellowstone National Park. The concentration of dissolved iron in water in a well increased from 80 μg/L (micrograms per liter) before a nearby lagoon was used for disposal of effluent to 17 000 μg/L after the lagoon was used. The effluent contained 180 μg/L of dissolved iron, and nearby Iron Spring Creek contained 30 μg/L or less of dissolved iron above and below the lagoons. Organic carbon, nitrogen, and sulfur in the effluent as methane, ammonia, and hydrogen sulfide are oxidized to carbon dioxide, nitrate, and sulfate, respectively, in the unsaturated zone and possibly in the saturated zone as ground water moves through sand and gravel toward Iron Spring Creek. This oxidation results in simultaneous reduction of iron in the sand and gravel from the insoluble ferric phase to the soluble ferrous phase. As ground water high in dissolved iron discharges at land surface near the stream, oxygen from the atmosphere oxidizes the iron back to the insoluble ferric phase, and ferric hydroxide precipitates. Ferric hydroxide also precipitates in some of the monitoring wells. Iron bacteria and other organisms are associated with the precipitates.

The U.S. Geological Survey is making a study for the National Park Service involving the monitoring of effluent that percolates from wastewater disposal lagoons at several sites in national parks in northwestern Wyoming. High dissolved-iron concentrations have been noted at times in water in some of the monitoring wells, particularly near the community of Old Faithful in southwestern Yellowstone National Park. The effluent and a nearby stream where the effluent probably discharges apparently do not have unusually high dissolved-iron concentrations. The purpose of this report is to explain the unusual dissolved-iron concentrations in water in the wells near Old Faithful.

GEOHYDROLOGIC SETTING

The Old Faithful wastewater lagoons are located about 1.6 kilometers west of the community of Old Faithful on kame-terrace deposits of obsidian and quartz sand and gravel. The terrace lies between hills and bluffs that were formed by rhyolite flows on the southwest and Iron Spring Creek on the northeast (fig. 1).

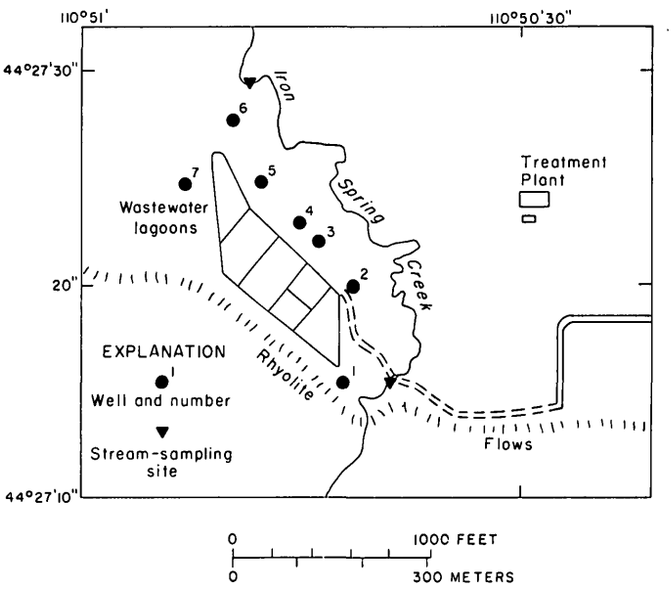

FIGURE 1.—Well locations and stream-sampling sites near the Old Faithful wastewater lagoons.

Effluent percolates from the lagoons to the water table, then moves laterally through the permeable sand and gravel toward Iron Spring Creek. The water table is about 7 to 9 meters below the terrace and slopes from the lagoons to the stream. Seeps are present along the stream and at the toe of a steep slope between the terrace and the stream.

CHEMICAL QUALITY OF WATER

Chemical analyses of water from wells, Iron Spring Creek, and the effluent near Old Faithful are shown

TABLE 1.—*Chemical analyses of water from wells, wastewater, effluent,*
[Analytical results in milligrams per liter (mg/L) or micrograms per liter

Source	Location (lat;long)	Date of collection	Temperature (°C)	Dissolved silica (SiO_2) (mg/L)	Dissolved iron (Fe) (µg/L)	Dissolved calcium (Ca) (mg/L)	Dissolved magnesium (Mg) (mg/L)	Dissolved sodium (Na) (mg/L)	Dissolved potassium (K) (mg/L)	Bicarbonate (HCO_3) (mg/L)	Carbonate (CO_3) (mg/L)
Well 1	442717;1105046	10- 8-74	15.0	89	80	5.5	1.3	15	2.6	42	0
Well 2	442720;1105041	8-27-74	19.0	58	80	4.0	1.1	25	6.6	6	0
		10-24-74	16.5	45	17,000	7.7	1.9	29	13	92	0
		8-24-76	18.5	42	200	1.8	.2	35	8.3	61	0
Well 3	442722;1105044	10-24-74	14.0	44	3,300	4.1	1.5	38	8.0	112	0
		6-23-75	12.0	37	260	4.6	.9	34	5.7	71	0
		8-25-76	16.0	43	1,700	2.8	.7	40	9.1	42	0
Well 4	442723;1105046	9-18-74	17.5	44	4,600	29	1.8	32	14	141	0
Well 5	442724;1105048	8-27-74	18.0	44	90	8.0	2.6	28	6.4	65	0
		6-23-75	15.0	59	970	11	2.3	67	7.3	18	0
		8-24-76	17.0	57	10	21	4.4	48	10	144	0
Well 6	442726;1105050	10-24-74	14.0	68	40	18	.8	35	11	63	0
Well 7	442723;1105052	9-18-74	15.0	59	2,100	11	2.2	50	13	131	0
		8-25-76	15.0	58	170	7.5	1.2	41	9.9	37	0
Effluent	442722;1105049	9- 8-75	24.0	45	180	4.8	1.3	43	11	189	0
Iron Spring Creek above lagoons.	442715;1105040	10-21-75	14.0	60	10	5.3	.5	17	3.7	45	0
		9-19-76	13.5	59	30	5.0	.6	17	3.6	41	0
Iron Spring Creek below lagoons.	442726;1105048	10-21-75	15.5	66	20	13	.6	25	4.4	61	0
		9-19-76	16.0	65	20	5.1	.6	25	4.4	42	0

in table 1. The wells, which have 32-millimeter-diameter plastic casing perforated below the water table, were sampled with a hand-operated bailer. The effluent was sampled at the discharge end of the pipe carrying effluent from the treatment plant to the lagoons. Specific conductance, temperature, and pH were determined in the field immediately after the samples were collected.

The individual lagoons are used alternately for disposal of effluent. Well 2 was sampled on August 27, 1974, before the nearby lagoon was used for disposal of effluent, and on October 24, 1974, after the lagoon was used. The concentration of dissolved iron increased from 80 to 17 000 µg/L during the period between the samples (table 1).

The effluent contained 180 µg/L of dissolved iron on September 8, 1975. Iron Spring Creek contained 30 µg/L or less of dissolved iron above and below the lagoons on October 21, 1975, and on September 19, 1976. These were the only samples from the effluent and the stream that have been collected during this study. Dissolved-iron concentration ranged from 0 to 340 µg/L in six samples collected from Iron Spring Creek about 0.8 kilometer northwest of the lagoons during 1969–70. The dissolved-iron concentration in Iron Spring Creek apparently is not appreciably different from that in other nearby streams (Cox, 1975, table 5).

EXPLANATION OF DISSOLVED-IRON CONCENTRATIONS

The effluent has relatively high concentrations of dissolved organic carbon and total nitrogen (table 1). Apparently, much of the carbon and nitrogen and presumably the sulfur as methane, ammonia, and hydrogen sulfide are oxidized to carbon dioxide, nitrate, and sulfate, respectively, as the effluent moves through the unsaturated zone to the water table and through the sand and gravel toward the stream. Such oxidations result in simultaneous reduction reactions. Iron can be affected by oxidation-reduction reactions (Hem, 1970, p. 28), is a common constituent in rocks and soils, and is undoubtedly present in the sand and gravel below the lagoons.

The following oxidation-reduction reactions probably occur as carbon, nitrogen, and sulfur are oxidized in the system. Although the system does not have standard conditions of 1 atmosphere of pressure and a temperature of 25°C, the standard potential ($E°$) in millivolts (mV) for each reaction was calculated using free-energy data from Latimer (1952).

and a stream near Old Faithful, Yellowstone National Park
(μg/L) except as indicated. Analyses by U.S. Geological Survey]

Dissolved sulfate (SO_4) (mg/L)	Dissolved chloride (Cl) (mg/L)	Dissolved fluoride (F) (mg/L)	Dissolved nitrite plus nitrate (N) (mg/L)	Total Kjeldahl nitrogen (N) (mg/L)	Total phosphorus (P) (mg/L)	Dissolved organic carbon (C) (mg/L)	Dissolved solids (Sum of constituents) (mg/L)	Hardness (Ca, Mg) (mg/L)	Specific conductance (μmho/cm at 25°C)	pH (units)	Eh (mV)
3.8	2.3	6.2	0.03	0.11	0.55	0.9	147	19	105	7.7	---
20	5.8	3.0	8.5	-----	1.0.	7.0	164	15	180	5.6	---
16	23	3.0	.09	4.5	11	7.4	201	27	290	6.9	100
10	36	2.8	.28	6.8	3.6	9.6	168	5	285	5.4	---
3.5	21	3.3	.61	10	3.6	5.8	185	16	290	6.7	120
2.1	21	3.2	.04	-----	2.4	7.0	144	15	215	5.5	---
9.4	37	3.7	6.6	6.5	1.0	6.9	197	10	350	5.8	---
13	21	3.9	.03	20	8.0	4.3	233	80	400	6.9	100
7.0	27	1.5	.23	-----	7.4	9.7	158	31	250	6.5	---
24	7.5	1.6	40	-----	.20	3.2	367	37	505	4.8	---
23	34	3.0	.11	5.6	7.7	21	272	71	475	6.3	---
11	47	.5	1.6	1.3	2.9	7.1	229	48	225	6.3	---
4.9	27	3.7	.06	10	9.9	10	238	37	420	6.9	100
6.0	30	2.7	11	4.4	2.7	9.7	223	24	310	5.6	---
9.8	28	2.4	.02	32	6.5	23	239	17	460	6.9	---
3.6	8.3	3.6	.00	.01	.01	.0	124	15	125	7.1	---
5.5	8.0	3.9	.08	.45	.00	.8	123	15	140	7.5	---
4.6	14	3.5	.00	.12	.02	2.3	161	35	170	7.2	---
6.2	16	4.3	.01	.45	.03	1.3	147	15	190	7.3	---

$$CH_4 + 2O_2 = CO_2 + 2H_2O \quad (E^\circ = 1025 \text{ mV}) \quad (1)$$

$$NH_4^+ + 2O_2 = NO_3^- + H_2O + 2H^+ \quad (E^\circ = 340 \text{ mV}) \quad (2)$$

$$H_2S + 2O_2 = SO_4^{-2} + 2H^+ \quad (E^\circ = 905 \text{ mV}) \quad (3)$$

$$CH_4 + 2H_2O + 8Fe^{+3} = CO_2 + 8H^+ + 8Fe^{+2} \quad (E^\circ = 577 \text{ mV}) \quad (4)$$

$$NH_4^+ + 3H_2O + 8\,Fe^{+3} = NO_3^- + 10H^+ + 8Fe^{+2} \quad (E^\circ = -108 \text{ mV}) \quad (5)$$

$$H_2S + 4H_2O + 8Fe^{+3} = SO_4^{-2} + 10H^+ + 8Fe^{+2} \quad (E^\circ = 457 \text{ mV}) \quad (6)$$

$$CH_4 + NO_3^- + 2H^+ = CO_2 + NH_4^+ + H_2O \quad (E^\circ = 686 \text{ mV}) \quad (7)$$

$$CH_4 + SO_4^{-2} + 2H^+ = H_2S + CO_2 + 2H_2O \quad (E^\circ = 120 \text{ mV}) \quad (8)$$

The positive values of E° for the carbon, nitrogen, and sulfur species in their reaction with oxygen (eqs 1–3) suggest their oxidation to carbon dioxide, nitrate, and sulfate could take place spontaneously in the unsaturated zone in this system. The reduction reactions (eqs 4–6) show that ferric iron can be reduced to the ferrous state. The negative value of E° in equation 5 suggests that the reaction may not be spontaneous, but energy from other reactions (such as eq 7) would be available to make the reaction possible.

The oxidation-reduction reactions can be used to explain the observed increases and decreases in constituents in the system. Selected constituents in the chemical analyses shown in table 1 are converted to millimoles per liter (mmol/L) in table 2. The differences between constituents in millimoles per liter in well 2 on August 27, 1974, before the nearby lagoon was used for disposal of effluent, and on October 24, 1974, after the lagoon was used, are as follows: Fe, +0.3031; Ca, +0.092; Mg, +0.033; Na, +0.17; K, +0.163; HCO_3, +1.410; SO_4, −0.041; Cl, +0.486; F, 0; and NO_2 plus NO_3, −0.601.

Using the reduction reactions (eqs 4–8) and the above data, the reduction of sulfate would generate 0.041 mmol of carbon dioxide, the reduction of nitrite plus nitrate would generate 0.601 mmol of carbon dioxide, and the reduction of iron would generate 0.3031/8 or 0.038 mmol of carbon dioxide. Total amount of carbon dioxide generated by these reactions is 0.680 mmol, or the equivalent of 0.680×61/44 or 0.943 mmole of bicarbonate. This does not account

TABLE 2.—*Concentration of selected constituents in millimoles per liter of water from wells, wastewater effluent, and a stream near Old Faithful, Yellowstone National Park*

Source	Location (lat;long)	Date of collection	Dissolved iron (Fe)	Dissolved calcium (Ca)	Dissolved magnesium (Mg)	Dissolved sodium (Na)	Dissolved potassium (K)	Bicarbonate (HCO_3)	Dissolved sulfate (SO_4)	Dissolved chloride (Cl)	Dissolved fluoride (F)	Dissolved nitrite plus nitrate (N)
Well 1	442717;1105046	10- 8-74	0.0014	0.137	0.053	0.65	0.066	0.688	0.040	0.065	0.326	0.002
Well 2	442720;1105041	8-27-74	.0014	.100	.045	1.09	.169	.098	.208	.164	.158	.607
		10-24-74	.3045	.192	.078	1.26	.332	1.508	.167	.650	.158	.006
		8-24-76	.0036	.045	.008	1.52	.212	1.000	.104	1.016	.147	.020
Well 3	442722;1105044	10-24-74	.0591	.102	.062	1.65	.205	1.836	.036	.592	.174	.044
		6-23-75	.0047	.115	.037	1.48	.146	1.164	.022	.592	.168	.003
		8-25-76	.0345	.070	.029	1.74	.233	.689	.098	1.044	.195	.472
Well 4	442723;1105046	9-18-74	.0824	.724	.074	1.39	.358	2.311	.135	.592	.205	.002
Well 5	442724;1105048	8-27-74	.0016	.200	.107	1.22	.164	1.065	.073	.762	.079	.016
		6-23-75	.0174	.274	.095	2.91	.187	.295	.250	.212	.084	2.856
		8-24-76	.0002	.524	.181	2.09	.256	2.361	.240	.960	.158	.008
Well 6	442726;1105050	10-24-74	.0007	.449	.033	1.52	.281	1.033	.115	1.326	.026	.114
Well 7	442723;1105052	9-18-74	.0376	.274	.090	2.18	.332	2.147	.051	.762	.195	.004
		8-25-76	.0030	.188	.050	1.78	.254	.607	.062	.847	.143	.786
Effluent	442722;1105049	9- 8-75	.0032	.120	.053	1.87	.281	3.100	.102	.790	.126	.001
Iron Spring Creek above lagoons.	442715;1105040	10-21-75	.0002	.132	.021	.74	.095	.738	.037	.234	.190	0
		9-19-76	.005	.125	.025	.74	.093	.672	.058	.226	.206	.006
Iron Spring Creek below lagoons.	442726;1105048	10-21-75	.0004	.324	.025	1.09	.113	1.000	.048	.395	.184	0
		9-19-76	.0004	.128	.025	1.09	.113	.689	.065	.452	.227	.001

completely for the difference of 1.410 mmole of bicarbonate. However, some of the carbon in the effluent could have been oxidized by the atmosphere before entering the system from the lagoon.

The oxidation potential (Eh) was calculated for four chemical analyses of water (wells 2, 3, 4, and 7, table 1) by using a method described by Hem (1960, p. 42–51). This method involves pH values and calculations and graphs to determine the ionic strength of the solution and the activities of iron and bicarbonate. These were the only analyses in table 1 with concentrations of iron high enough to fit the conditions of the calculations. Three of the four analyses have an Eh of 100 mV; the same three analyses have a pH of 6.9 (table 1).

An Eh of 100 mV and a pH of 6.9 are plotted on a stability-field diagram for aqueous ferric-ferrous solutions that commonly occur in natural waters (fig. 2). The plot of Eh and pH occurs in the area of Fe^{+2}, where the ferrous species dominates, and the iron is in solution as ferrous iron. If the Eh rose above about 250 mV and the pH remained 6.9, the $Fe(OH)_3$ (ferric hydroxide) species would dominate, and the iron would percipitate as the solid phase $Fe(OH)_3$.

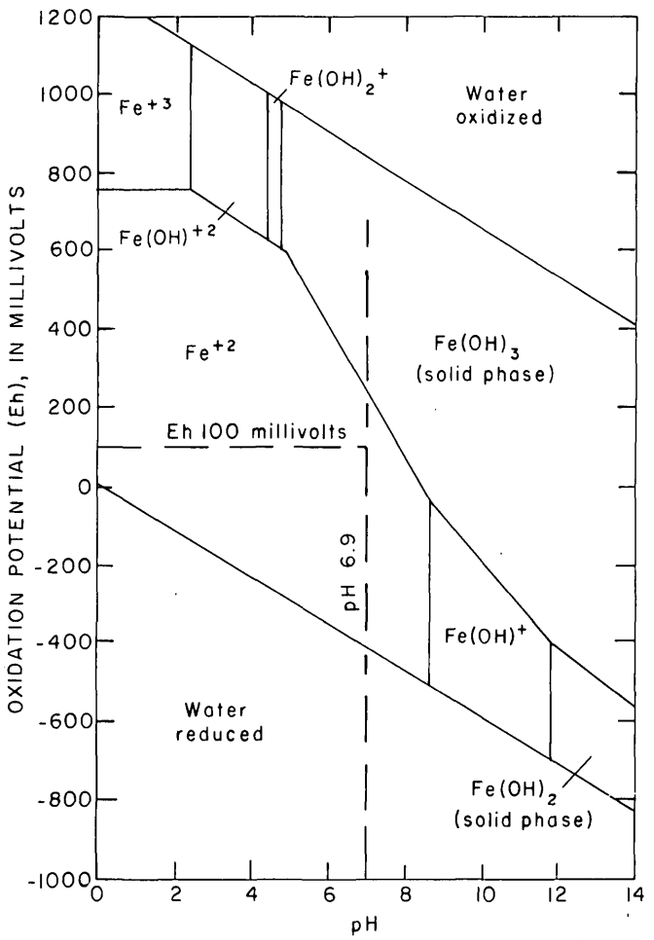

FIGURE 2.—Stability-field diagram for aqueous ferric-ferrous system. (Adapted from Hem and Cropper, 1959.)

In a study where many Eh values of ground water were measured and calculated, Back and Barnes (1965, p. C15) concluded that within the same aquifer the oxidation potential is higher near areas of recharge than it is near areas of discharge. Therefore, ground water at the wastewater lagoons near Old Faithful probably maintains an Eh low enough to transport dissolved iron as the ferrous species until it is oxygenated by the atmosphere at discharge areas. Then, as the Eh rises, ferric hydroxide precipitates.

Yellowish-brown precipitates have been noted at some of the seeps near Iron Spring Creek and occasionally at the water surface in some of the wells. The precipitates from the seeps and the wells appeared to be similar and were noted to contain organisms. These organisms were identified by B. W. Lium (written commun., 1976).

The precipitates had an abundance of the iron bacteria *Leptothrix* sp. This organism is common in slowly running freshwater containing iron. When growing under natural conditions in iron-rich water, *Leptothrix* sp. occurs with flocculent masses of hydrated ferric hydroxide containing many yellow-brown, smooth, relatively short, and empty sheaths. These organisms grow only at pH values of 6 and higher. Their temperature range is 10° to 35°C, with the optimum between 20° and 25°C (Mulder, 1974, p. 129–130).

Samples of the yellowish-brown precipitates also contained collembolas (springtails). These organisms occur in damp areas and on the surface of marshes, pools, and quiet backwaters of lakes and ponds (B. W. Lium, written commun., 1976). They were abundant in samples collected from the top of the water column in some of the wells.

Some samples of precipitates from the seeps and the wells turned to a dark color after a few days. Dark colored samples from a seep near Iron Spring Creek contained diatoms (*Pinnularia* sp. and *Nitzschia* sp.) and sulfate-reducing bacteria. Sulfate-reducing bacteria are common in environments of low dissolved oxygen in which hydrogen sulfide is produced (B. W. Lium, written commun., 1976). If hydrogen sulfide is present in the ground-water system near the seeps, the oxidation potential must be low, based on interpretation of an Eh-pH graph showing fields of dominance of sulfur species (Hem, 1970, p. 163).

Iron Spring Creek does not have high dissolved-iron concentration below the lagoons because the iron

is precipitated as the ground water containing effluent reaches the seeps or the stream. Under normal conditions, high dissolved-iron concentration would not be expected in a stream such as Iron Spring Creek because the iron would be stable in the ferric hydroxide phase, which is virtually insoluble in water except at a very low pH.

CONCLUSIONS

The high dissolved-iron concentrations in water in monitoring wells near the Old Faithful wastewater lagoons are a result of oxidation-reduction reactions. Organic carbon, nitrogen, and sulfur in the effluent percolating from the lagoons are oxidized in the unsaturated zone and possibly in the saturated zone as ground water moves through sand and gravel toward Iron Spring Creek. Iron in the sand and gravel below the lagoons simultaneously is reduced from the insoluble ferric phase to the soluble ferrous phase. As the ground water discharges at land surface near the stream, oxygen from the atmosphere oxidizes the iron back to the insoluble ferric phase, and the iron precipitates as yellowish-brown ferric hydroxide. Ferric hydroxide also precipitates in some of the monitoring wells. Bacteria and other organisms grow in the precipitates.

REFERENCES CITED

Back, William, and Barnes, Ivan, 1965, Relation of electrochemical potentials and iron content to ground-water flow patterns: U.S. Geol. Survey Prof. Paper 498–C, p. C1–C16.

Cox, E. R., 1975, Discharge measurements and chemical analyses of water in northwestern Wyoming: Wyoming Water Planning Program Rept. 14, 20 p.

Hem, J. D., 1960, Restraints on dissolved ferrous iron imposed by bicarbonate, redox potential, and pH: U.S. Geol. Survey Water-Supply Paper 1459–B, p. 32–55.

——— 1970, Study and interpretation of the chemical characteristics of natural water [2d ed]: U.S. Geol. Survey Water-Supply Paper 1473, 363 p.

Hem, J. D., and Cropper, W. H., 1959, Survey of ferrous-ferric chemical equilibria and redox potentials: U.S. Geol. Survey Water-Supply Paper 1459–A, p. 1–31.

Latimer, W. M., 1952, The oxidation states of the elements and their potentials in aqueous solutions [2d ed]: New York, Prentice-Hall, 392 p.

Mulder, E. G., 1974, Genus *Leptothrix*, *in* Buchanan, R. E. and Gibbons, N. E., coeditors, Bergey's manual of determinative bacteriology [8th ed]: Baltimore, The Williams and Wilkins Co., p. 129–133.

Jour. Research U.S. Geol. Survey
Vol. 6, No. 3, May–June 1978, p. 325–337

STUDIES OF HYDROXYALUMINUM COMPLEXES IN AQUEOUS SOLUTION

By J. L. BERSILLON,[1] D. W. BROWN, FRANÇOIS FIESSINGER,[2] and J. D. HEM,
Nancy, France, Menlo Park, Calif., Paris, France, Menlo Park, Calif.

Abstract.—The coagulating ability of partly neutralized $AlCl_3$ solutions used in water treatment depends on their basicity, expressed here as the ratio $NaOH/AlCl_3$. This work presents an identification of the aluminum species active in the coagulation process. The results give rise to an interpretative model which is consistent with those models proposed for high ionic strength by other investigators.

Aluminum salts are coagulants commonly used in water treatment for removing turbidity and a majority of the organic matter in river waters. Aluminum is used because of its hydrolyzing properties which cause precipitation of $Al(OH)_3$. These properties are also important in that adsorption by small amounts of the initial precipitate of the hydrolyzed species is thought to affect surface charge properties so as to induce coagulation even with small initial amounts of the resulting precipitate. Sludges which result from this kind of treatment are generally poorly organized and contain a great amount of water. These sludges have thixotropic properties which make their transfer and disposal difficult.

The study of the organization of precipitate involves aluminum chemistry in that the physicochemical properties of the coagulating solution will partly determine the physicochemical properties of the floc.

In trials made on natural and synthetic waters, coagulating ability seemed to depend on the amount of base which was added to the aluminum salt and on the quality and amount of colloids which were already present in those waters (J. L. Bersillon and others, unpub. data, 1976; Fiessinger, 1976). An industrial neutralization process was devised, allowing a wide range of coagulating solutions.

Highly concentrated solutions are used in this study to better approximate industrial considerations such as storage, quality of mixing, and water cost.

The final goal of this research is to determine the active species produced by such a process. With this in mind we modified a colorimetric method normally used for determining aluminum species in dilute solutions so that it could be used for concentrated solutions and chose a potentiometric back-titration method designed for aluminum solutions.

MINERALOGY OF ALUMINUM HYDROXIDES

The structures of three of the crystalline trihydroxides are well known. Bayerite, gibbsite and nordstrandite are bound by the same structural sheetlike unit in the plane defined by the *a* and *b* axes. This unit can be described by the coalescence of six-membered rings of hexacoordinated aluminum (Hem, 1968a, b; Hsu and Bates, 1964; P. H. Hsu, oral commun., 1975; Lippens, 1961), and these sheetlike units are stacked along the *c* axis (Hsu and Bates, 1964). For these three minerals there are two kinds of stacking, shown in figure 1, one of which can be generated from the other by a rotation about the *c* axis of one of the sheetlike units by 60°. Nordstrandite has two possible crystalline structures which are regular alternations of gibbsite and bayerite structures occurring as either one-on-one or two-on-two stacking (Lippens, 1961). Dimensions of structural unit cells for gibbsite, bayerite, and nordstrandite are given in angstroms in table 1.

With regard to less well-defined amorphous aluminum hydroxides, there are three kinds of gels which Lippens distinguishes: C_α gel, which is amorphous

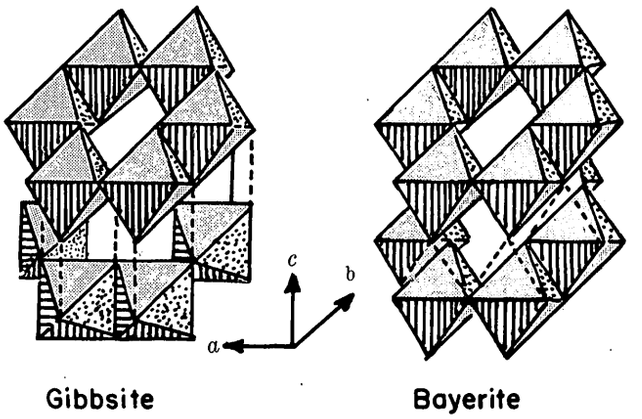

FIGURE 1.—Gibbsite and bayerite stacking. Dotted lines represent H-OH bonds between *a-b* OH-Al-OH layers.

[1] Institut National Polytechnique de Nancy, E.N.S.G., Nancy, France.
[2] Société Lyonnaise des Eaux Eclairage, Paris 16, France.

TABLE 1.—*Unit-cell parameters of crystalline aluminum trihydroxides given in Lippens (1961)*
[In angstroms; 1 angstrom = 0.1 nm]

	a	*b*	*c*
Gibbsite	8.673	5.068	9.716
Bayerite:			
hexagonal	8.741	5.047	4.730
monoclinic	8.674	5.061	4.713
Nordstrandite	8.63	5.01	19.12

to X-rays and is soluble in 0.03 molar HCl: C_β gel, which is similar to a gelatinous boehmite and is dispersed and slowly dissolved by dilute HCl; and C_γ gel, which could be a mixed product of crystalline trihydroxides and C_β gel. All these gels have $Al(OH)_3$ as a chemical formula. All the numerous authors (Fripiat and Pennequin, 1965; Fripiat and others, 1965; Herbillon and Gastuche, 1962a, b; Kerhof and others, 1975; Nail and others, 1975; Turner and Ross, 1970) who have investigated amorphous gels have found that this kind of product is highly hydrated and may include foreign anions. These gels can evolve into crystalline hydroxides with time, and the rate of this process can be affected by washing, dialysis, dilution, and heating. The transformation of gels into crystals was studied by either physical or chemical means, and it was generally found that foreign (particularly organic) ions included in amorphous gels halted the crystallization process.

Minerals which fall into the category of basic salts were found to be either partially substituted aluminum hydroxides where foreign anions (such as Cl^-) substitute for OH^- or specific structures including foreign anions such as SO_4^{2-}. Hsu (1973) and Turner and Ross (1970) have correlated the structures of these latter gels with their basicity (OH/Al ratios).

Thermodynamic data concerning free energy of formation of various aluminum hydroxides at 25°C are listed in table 2 in order of increasing stability.

ALUMINUM CHEMISTRY IN AQUEOUS SOLUTION

Monomeric hexacoordinated aluminum below pH 7 is distributed among the species Al^{3+}, $AlOH^{2+}$, and $Al(OH)_2^+$ because of the stepwise hydrolysis reactions

$$Al^{3+} + H_2O \rightleftarrows AlOH^{2+} + H^+$$

with equilibrium constant K_{11} and

$$AlOH^{2+} + H_2O \rightleftarrows Al(OH)_2^+ + H^+$$

with equilibrium constant K_{12}. In addition to these monomeric ions, polycations have been found by many workers, and it is now accepted that aluminum gives rise to polymers in mildly acidic solutions. The Al-Al bonding in such polycations and in sheetlike polymers is described in the literature as being due to double hydroxide bridging as shown in figure 2. The first step of polymerization of monomers into sheetlike structures should be formation of the dimer $Al_2(OH)_2(H_2O)_8^{4+}$ whose structure can be described as two Al octahedra sharing an edge. This species begins to predominate over the monomer $AlOH^{2+}$ as the total aluminum concentration begins to exceed about 10^{-3} molar. In the solutions studied here (C_{Al} = 0.1 molar) $Al_2(OH)_2^{4+}$ will be much more important than $AlOH^{2+}$.

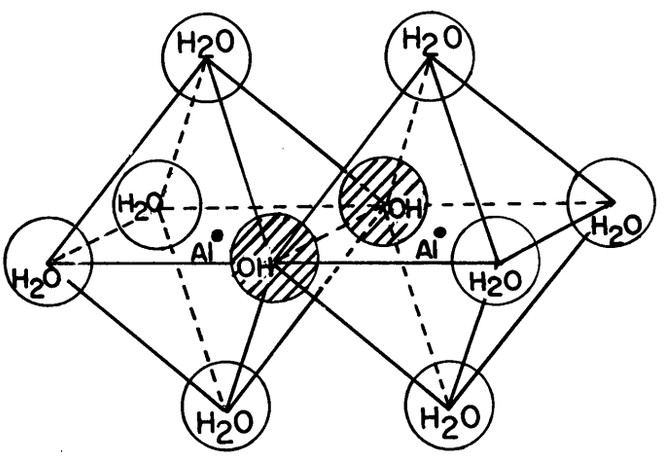

FIGURE 2.—Schematic representation of dimeric cation $Al_2(OH)_2(H_2O)_8^{4+}$, from Hem and Roberson (1967).

In the following polymerization steps additional aluminum octahedra are added to the $Al_2(OH)_2^{4+}$ dimer by hydroxide bridging, and the end product can be either chainlike polymers, the general formula of which is $Al_n(OH)_{2n-2}(H_2O)_{2n+2}^{+(n+2)}$, or sheetlike polymers, which are illustrated in figure 3. The latter polymer is cited by several workers (Brosset and others, 1954; Brown and Hem, 1975; Herbillon and Gastuche, 1962a, b; Hsu, 1973; Smith and Hem, 1972) and is the structurally most probable type of polymer. It is doubtful that some of the larger polymers illustrated in figure 3 have as high a charge as shown, but rather they exist as metastable ion pairs with temporarily attached nonstructural OH^- ions at the polymer edges. Studies on partly neutralized aluminum salts by Hsu (1963) and Hsu and Bates (1964) showed that crystalline trihydroxides are obtainable from aged solutions of these polymers. These hydroxides are obtained during the polymer growth in the *a* and *b* directions and are followed by stacking of the sheetlike units. The mechanism of this stack-

TABLE 2.—*Gibbs free energy of solid* $Al(OH)_3$

[1 kcal/mol = 4.184 kJ/mol]

Species	$^1\Delta G^\circ_{298}$ (kcal/mol)	$\log_{10}[Al^{3+}][H^+]^{-3}$	Reference
$Al(OH)_3$ amorphous	-271.9	10.39	Latimer (1952).
Microcrystalline gibbsite[2]	-272.3	10.09	Hem and Roberson (1967).
Pseudoboehmite	-272.7	9.80	Calculated from Rubin and Hayden (1973).
Gibbsite	-275.3±0.2	7.90	Parks (1972).
Bayerite	-274.6±0.1	8.41	Do.
Nordstrandite	-274.0	8.85	Hem, Roberson, Lind, and Polzer (1973).

[1] Calculated for the reaction $Al(OH)_{3c} + 3H^+ \rightleftharpoons Al^{3+} + 3H_2O(liq)$ at 25°C from free energy data using Parks' (1972) free energy of -116.0 kcal/mol for Al^{3+} and -56.69 kcal/mol for $H_2O(liq)$.

[2] The difference between ΔG°_{298} of regular and microcrystalline gibbsite is due to the particle-size effect.

ing is not well understood, being dependent on numerous physical conditions of neutralization and of aging, among them the final pH, ionic strength, and organics content.

Some authors ignore the hypothetical $Al(OH)_3^0$ species in equilibrum calculations. If it in fact exists, it should exist in molecular form, the structure of which is unknown. Presently it is hard to distinguish a large polymer such as $Al_{13}(OH)_{34}^{5+}$ or $Al_{96}(OH)_{264}^{24+}$ (OH/Al ratio = 2.61 and 2.75 respectively) from a species having $Al(OH)_3$ as the stoichiometric formula. Although colligative solution properties theoretically would distinguish between colloid-size polymers and molecular $Al(OH)_3^0$, this would be difficult in practice because of the wide size range of the polymers; there is no clear-cut boundary, in the solutions studied here, between dissolved and colloidal species. Furthermore, a form such as $Al(OH)_3^0$ is less likely to lead to a solid species as polymeric forms do. It was therefore assumed that monomeric species present in the pH range of interest are Al^{3+}, $AlOH^{2+}$, and $Al(OH)_2^+$. $Al(OH)_4^-$, in the experimental conditions used in our studies (pH 3 to 5), was assumed to be negligible. The polymeric species assumed to be present for the purpose of explaining the results were those in the set of sheetlike units described above and the dimer $Al_2(OH)_2(H_2O)_8^{4+}$. Thermodynamic data concerning monomeric and some polymeric species are summarized in table 3.

EXPERIMENTAL METHODS

Aliquots of 50 mL of a 0.50 molar $AlCl_3$ solution were neutralized by a volume in milliliters of 1.00

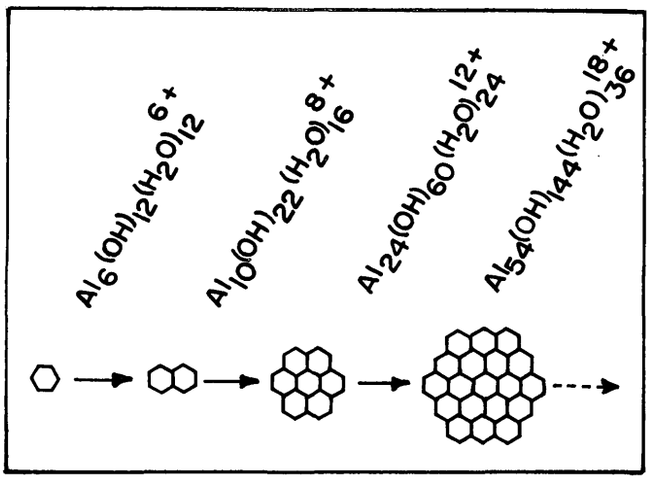

FIGURE 3.—Building of sheetlike units starting from the six-membered ring $Al_6(OH)_{12}(H_2O)_{12}^{6+}$. Hydroxides in formulas refer to bridging hydroxides only; species may contain nonbridging hydroxides and have lower positive charges. Modified from Smith and Hem (1972) and Hsu and Bates (1964).

TABLE 3.—*Thermodynamic data for soluble aluminum species, from Parks (1972) and Turner (1968a, 1975)*

[1 kcal/mol = 4.184 kJ/mol]

Species	ΔG°_{298} (kcal/mol)	log K_{mn} [1]
Al^{3+}	-116.0	---
$AlOH^{2+}$	-165.84	-5.01
$Al(OH)_2^+$	-217.5	-8.7
$Al(OH)_3^0$ aq	-265.3	-15.2
$Al(OH)_4^-$	-311	-23.3
$Al_2(OH)_2^{4+}$	---	-6.95
$Al_6(OH)_{15}^{3+}$	---	-47
$Al_7(OH)_{17}^{4+}$	---	-48.81
$Al_{13}(OH)_{34}^{5+}$	---	-97.6

[1] K_{mn} is the equilibrium constant for the reaction

$$mAl^{3+} + nH_2O \rightleftharpoons Al_m(OH)_n^{+3m-n} + nH^+.$$

normal NaOH solution equal to 25 r_n which was first diluted to 200 mL, where r_n is the desired NaOH/$AlCl_3$ ratio of the solution. This latter solution was added dropwise to the aliquot under vigorous magnetic stirring during 1 hour. The resulting solution was transferred into a polyethylene bottle and stored at room temperature (about 25°C). The aging time (t) of these solutions was set to 1, 5, and 24 hours, and the r_n values (NaOH/$AlCl_3$ ratios) used were 0.5, 1.0, 1.5, 1.8, 2.0, 2.2, 2.4, and 2.5. Each aluminum solution analysis is described by a title of the form *r-m-t* composed of the three parameters r (actually r_n), m, and t where r_n is the NaOH/$AlCl_3$ ratio of the solution, m is the molar concentration of total aluminum (always 0.10 molar), and t is the aging time in hours.

The method used here for differentiation between fast and slowly reacting hydroxides in acid media, represented by OH_f and OH_b, respectively, is that given by Hem and Roberson (1967). Aliquots of 10 mL were withdrawn from each *r-m-t* solution at t = 1, 5, and 24 hours and were placed in a titration vessel where the initial pH was measured and the solution was titrated with 0.102 molar HCl over several hours at a constant pH of 3.0 and at 25.0±0.1°C by using a pHstat.

The reverse ferron procedure, described previously by Smith (1969–1971) and used by Smith and Hem (1972), differentiates between three kinds of aluminum species:

1. Monomeric aluminum (Al_a) which reacts almost instantaneously with ferron at pH 5.
2. Polymeric aluminum of intermediate size containing up to 400 aluminum atoms per polymer (Al_b). These react slowly (first-order halftime, 15–20 minutes) with ferron at pH 5.
3. Al_c which does not react with ferron at pH 5. Some of this is probably solid material such as microcrystalline gibbsite of diameter about 0.1 μm (micrometer) or greater.

It differs from the standard ferron method for the determination of aluminum (Brown and others, 1970) in that the ferron (7-iodo-8-hydroxyquinoline-5-sulfonic acid) and sodium acetate reagents are first added to the sample (diluted to 25 mL), followed by immediate addition of 2 mL of the hydroxylamine hydrochloride reagent, from where the zero analysis time is taken.

In order to bring the aluminum concentrations within the analytical range, 1.0 mL aliquots of the *r-m-t* solutions were withdrawn at 1, 5, or 24 hours and diluted to 50 mL with a solution of 0.6 molar NaCl acidified with HCl to pH 4.5. No visibly large

particles were discernible, the largest particles being those of colloidal size and analyzed as Al_b and Al_c. The solutions were therefore not centrifuged or filtered prior to the analyses. One milliliter of this solution was then taken for the aluminum determination. This dilution procedure avoids any changes in the form of the hydroxide due to possible precipitation or dissolution caused by a shift in equilibrium resulting from dilution with a solution of higher pH.

According to Hem and Roberson (1967) and Hem (unpub. data, 1967), the dissolution of slowly reacting aluminum hydroxide (OH_b) by acid follows first-order kinetics, expressed

$$\frac{-d(OH_b)_t}{dt} = k(OH_b)_t,$$

where k is the first-order reaction rate constant. This can be rewritten as

$$\frac{d(OH_b)_t}{(OH_b)_t} = -k dt,$$

which integrates to give

$$\log_{10}(OH_b)_t = \log_{10}(OH_b)_0 - \frac{kt}{2.303},$$

where $(OH_b)_0$ is the initial concentration, at zero reaction time, of the slowly reacting hydroxide. After a relatively short time required for dissolution of the fast-reacting hydroxide (OH_f), also initially present, it no longer interferes, after which the logarithm of the concentration of hydroxide remaining in solution varies linearly with the time of titration. The intercept of the straight line defined by these latter points will be equal to the logarithm of the concentration of (OH_b) initially present. The use of this technique is shown in figure 4.

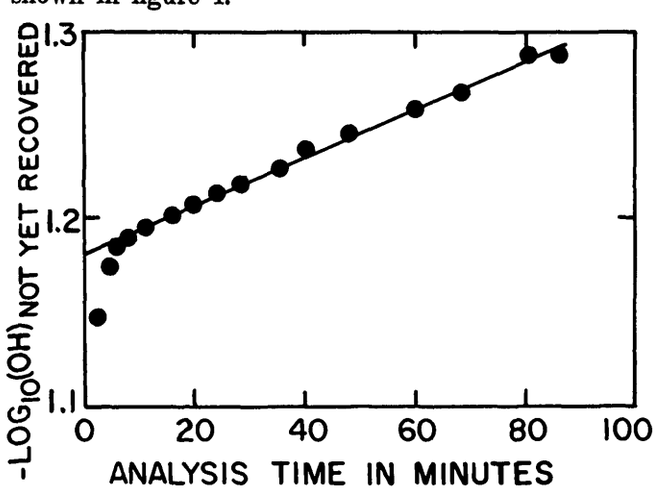

FIGURE 4.—Logarithm of hydroxide concentration not yet recovered from solution as a function of analysis time (analysis 1.0–0.1–1H). Intercept = $-\log_{10}(OH)_b$.

The amount of $Al_a + Al_b$ reacted at a given time is measured by absorbance of the solution at 370 nm (nanometers), the characteristic absorption wavelength for the ferron-aluminum complex. By plotting ($Al_a + Al_b$) recovered as a function of time, (Al_a) at reaction time zero should be equal to the intercept of the curve with the ($Al_a + Al_b$) recovered axis. Because of the high slope of this curve at low reaction times, however, this intercept is not graphically well defined.

Smith (1969) and Smith and Hem (1972) showed that the slowly reacting Al_b obeys first-order kinetics. Therefore, by plotting the logarithm of not yet recovered Al_b versus time reacted, a straight line is obtained defining an intercept with the $\log_{10}(Al_b)_{\text{not yet recovered}}$ axis, equal to $-\log_{10}(Al_b)$ at reaction time zero. The concentration of Al_b not yet recovered is calculated by subtracting the concentration of ($Al_a + Al_b$) recovered at a given time from the total ($Al_a + Al_b$) concentration recovered at the last point of the analysis (at 80–90 minutes). This latter quantity will very closely approximate the total ($Al_a + Al_b$) initially present. These quantities are all shown in figure 5 for representative analysis 1.0–0.1–1H. The logarithmic plot calculation was made using a computer program which calculated the slope and intercept of the straight line, graphically represented in figure 6;

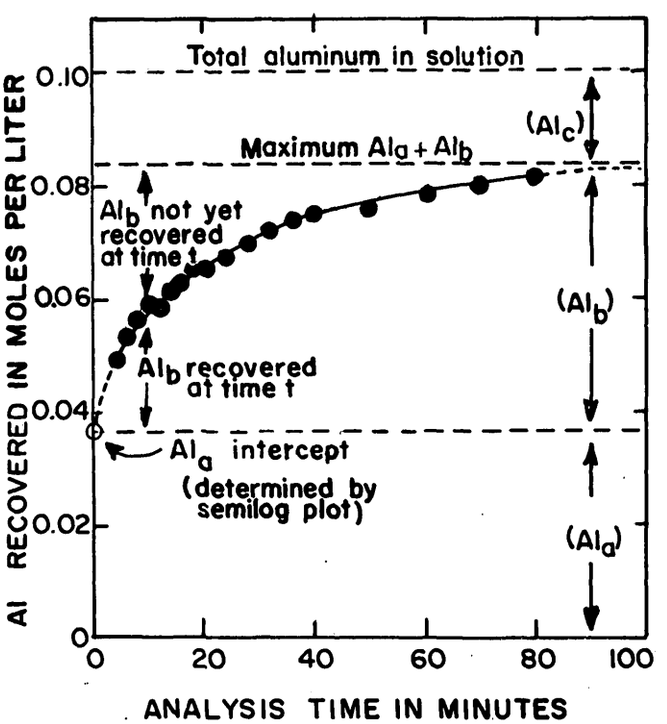

FIGURE 5.—Aluminum recovered as a function of analysis time using the reverse ferron method for analysis 1.0–0.1–1H. (See table 4 for data.)

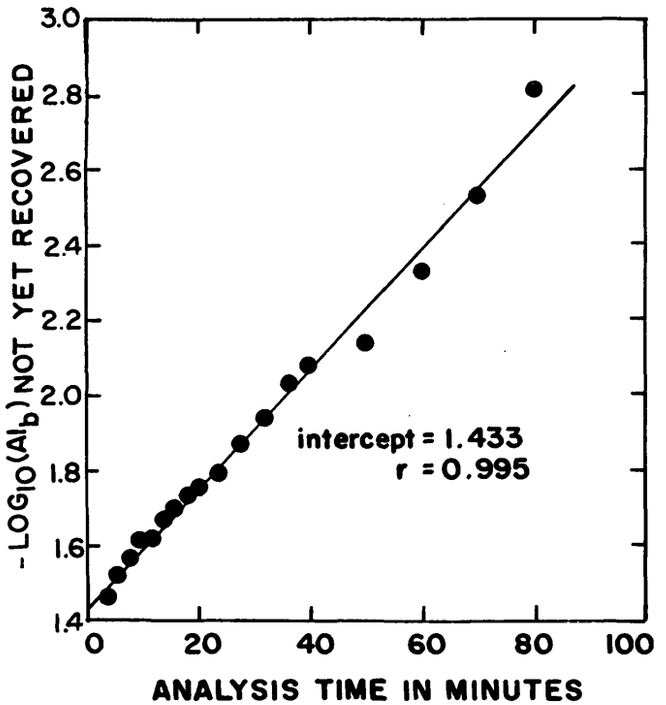

FIGURE 6.—Logarithm of (Al_b) not yet recovered as a function of analysis time for analysis 1.0–0.1–1H. (See table 4 for data.)

TABLE 4.—*Recovered* ($Al_a + Al_b$) *and*—$log_{10}(Al_b)$ *not yet recovered as a function of time for analysis 1.0–0.1–1H*

Analysis time (min.)	Absorbance	($Al_a + Al_b$) recovered (moles per liter)	$-\log_{10}(Al_b)_t$
4	0.247	0.0495	1.473
6	.267	.0537	1.531
8	.281	.0567	1.578
10	.292	.0590	1.618
12	.292	.0590	1.618
14	.305	.0618	1.671
16	.312	.0633	1.703
18	.320	.0651	1.743
20	.322	.0655	1.753
24	.330	.0672	1.798
28	.341	.0696	1.869
32	.351	.0718	1.946
36	.360	.0738	2.030
40	.365	.0749	2.089
50	.370	.0760	2.147
60	.381	.0784	2.329
70	.389	.0802	2.536
80	.395	.0816	2.804

data is given in table 4. The equation of the straight line can be expressed as follows:

$$\log_{10}(Al_b)_{\text{not yet recovered}} = \log_{10}(Al_b)_0 - \frac{kt}{2.303}.$$

Al_c is obtained by difference between ($Al_a + Al_b$) and the total aluminum concentration m.

EXPERIMENTAL RESULTS

Analyses of the solutions of various r_n values at 1, 5, and 24 hours are listed in table 5. The variations in concentrations of Al_a, Al_b, and Al_c with r_n and with aging time are shown graphically in figure 7. It appears that the region where r_n lies between 1.8 and 2.0 represents a sort of frontier between two fields. In this region, the soluble aluminum ($Al_a + Al_b$) reaches a maximum value as growth of Al_b ceases. It is past this region where Al_c begins to increase more rapidly with an increase in r_n. The decrease in the concentrations of Al_a as r_n increases is regular except for r_n about 2.4–2.5 at aging times of 1 and 24 hours. In addition, results at 5 hours' aging time where $r_n > 2$ seem to be unique in that the increase of Al_a with r_n is less than that at 1 and 24 hours and in that the minimum value of Al_a occurs at a value of r_n slightly lower than that for aging times of 1 and 24 hours. However, these results generally support previous data by J. L. Bersillon and François Fiessinger (unpub. data, 1976), which showed that the total ion concentration should reach a maximum at r_n of approximately 2.

The set of pH measurements shows a discontinuity of behavior for r_n between 1.5 and 2.0 in that the pH suddenly increases at a greater rate as r_n is increased. This effect is very pronounced at 1 hour, is smaller at 5 hours, and becomes nonexistent after 24 hours, as shown in figure 8.

As previously outlined in this paper, titrations of aliquots of these solutions at constant pH with hydrochloric acid yielded two kinds of hydroxides differentiable by their kinetics of reaction with H^+ at a constant pH of 3.0. Assuming that there are only two kinds of hydroxide, OH_f is obtained by the difference between the total hydroxide and OH_b concentrations; the validity of this assumption will be discussed later in this report. A second assumption concerning the character of OH_b has to be formulated. It is assumed here that OH_b and Al_b are measured concentrations of different ions of the same polymeric material. The average stoichiometric formula of the polymeric material can then be calculated by dividing OH_b concentrations by those of Al_b. These stoichiometric ratios, de-

TABLE 5—*Analyses of solutions of various r_n values at 1, 5, and 24 hours*

r_n	Hours aged	pH	Moles per liter Al_a	Al_b	Al_c	OH_b
0.5	1	3.75	0.0686	0.0293	0.0021	0.0174
	5	3.65	.0784	.0195	.0021	.0262
	24	3.64	.0626	.0244	.0130	.0285
1.0	1	3.81	.0478	.0359	.0168	.0661
	5	3.72	.0530	.0365	.0105	.0802
	24	3.74	.0473	.0433	.0094	.0863
1.5	1	3.85	.0416	.0479	.0105	.121
	5	3.83	.0416	.0536	.0048	.136
	24	3.81	.0305	.0552	.0143	.142
1.8	1	4.01	.0253	.0658	.0089	.141
	5	3.94	.0111	.0805	.0084	.166
	24	3.87	.0215	.0739	.0046	.173
2.0	1	4.02	.0190	.0743	.0068	.155
	5	3.97	.0130	.0783	.0084	.190
	24	3.94	.0145	.0806	.0049	.193
2.2	1	4.17	.0179	.0605	.0216	.160
	5	4.10	.0207	.0667	.0126	.195
	24	4.06	.0106	.0797	.0096	.213
2.4	1	4.37	.0126	.0501	.0373	.157
	5	4.32	.0133	.0671	.0196	.181
	24	4.28	.0062	.0701	.0237	.217
2.5	1	4.53	.0247	.0422	.0330	.131
	5	4.47	.0369	.0465	.0166	.133
	24	4.41	.0137	.0574	.0288	.136

noted by r_p, are tabulated in table 6 and plotted as functions of r_n, the overall OH/Al ratio in the solution at 1, 5, and 24 hours in figure 9.

DISCUSSION

In the low pH range of 3 to 5 used in these studies, the monomeric species are Al^{3+}, $AlOH^{2+}$, and $Al(OH)_2^+$, with negligible concentrations of $Al(OH)_4^-$.

For the purpose of calculating Al^{3+} activities for comparison with theoretical activities of Al^{3+} in equilibrium with a given form of aluminum hydroxide, the expression

$$[Al^{3+}] = \frac{(Al_a)}{\frac{1}{\gamma_{Al^{3+}}} + \frac{K_{11}}{[H^+]\gamma_{AlOH^{2+}}} + \frac{K_{11}K_{12}}{[H^+]^2\gamma_{Al(OH)_2^+}}}$$

may be used. Ion activity coefficients for the monomeric aluminum ions are represented by $\gamma_{Al^{3+}}$, $\gamma_{AlOH^{2+}}$, and $\gamma_{Al(OH)_2^+}$ and are calculable from Helgeson's extended Debye-Hückel equation (Truesdell and Jones, 1974, p. 241). K_{11} and K_{12} are the previously mentioned stepwise hydrolysis constants for formation of $AlOH^{2+}$ and $Al(OH)_2^+$, respectively. Hem and Roberson (1967) give K_{11} as $10^{-5.02}$ and $K_{11}K_{12}$ as

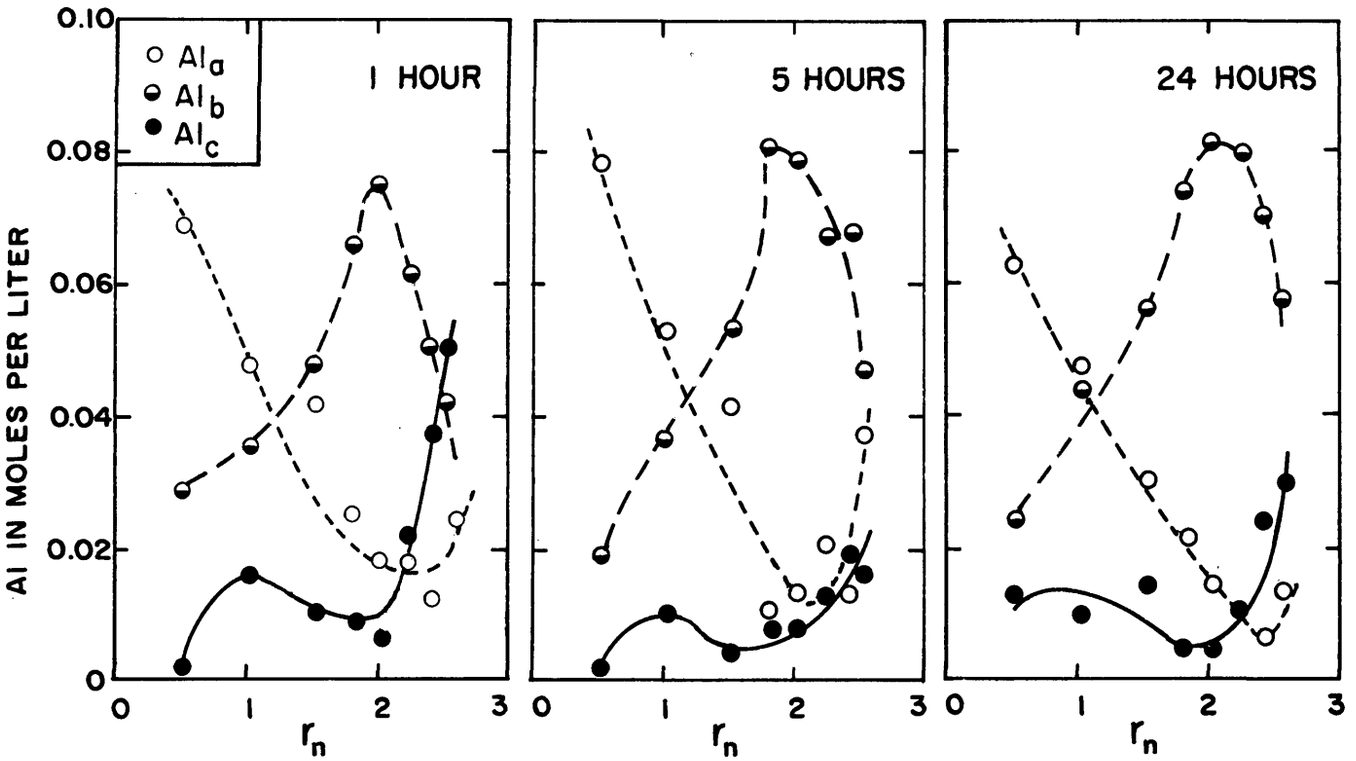

FIGURE 7.—Aluminum concentration as function of r_n at 1, 5, and 24 hours.

$10^{-8.56}$. The calculation of concentration, activity coefficients, and activities of each species involves an iterative calculation in which the ionic strength is calculated first by assuming that Al_a is in the Al^{3+} form. Ion activity coefficients which are used in the above expression are calculated from this ionic strength and are used to give the Al^{3+} activity, which can in turn be used in calculations of Al^{3+}, $AlOH^{2+}$, and $Al(OH)_2^+$ concentrations. These concentrations and those of Na^+ and Cl^- are used for recalculating the ionic strength.

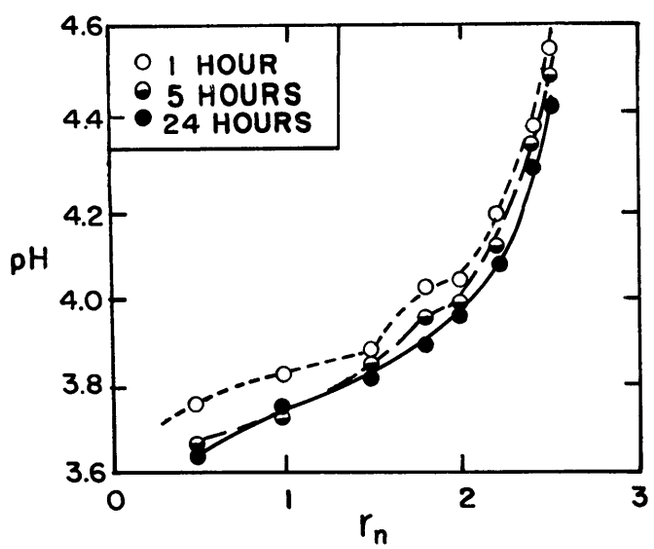

FIGURE 8.—pH as a function of r_n at 1, 5 ,and 24 hours.

Since there are many Al atoms per Al_b polymeric ion, the concentration expressed as the number of moles of ions per liter is very much smaller than the Al_b

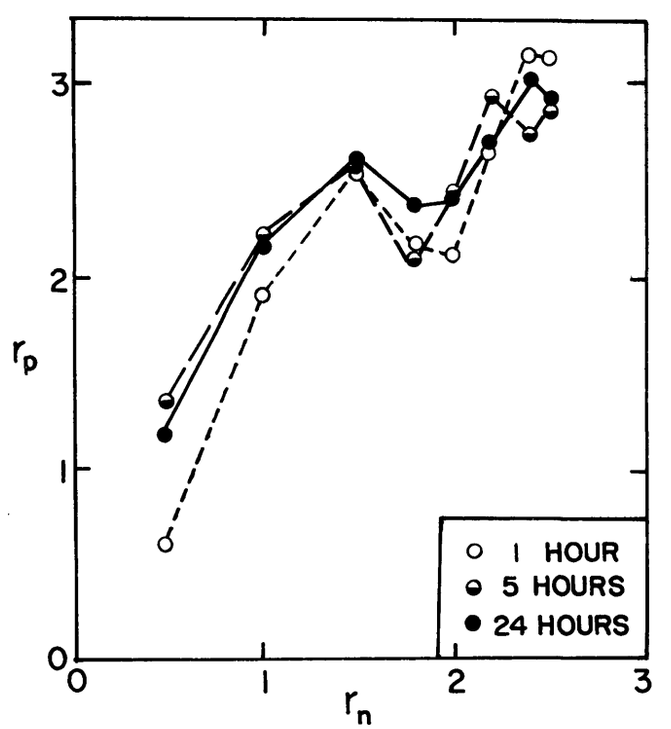

FIGURE 9.—OH_b/Al_b ratio (r_p) as a function of $NaOH/AlCl_3$ ratio (r_n) at 1, 5, and 24 hours.

TABLE 6.—OH_b/Al_b *ratios, ionic strengths, and* Al^{3+} *activities calculated from analytical data in table 5*

r_n	Hours aged	OH_b/Al_b	Ionic strength	$-\log_{10}[Al^{3+}]$
0.5	1	0.59	0.48	2.19
	5	1.34	.52	2.14
	24	1.17	.45	2.22
1.0	1	1.87	.41	2.32
	5	2.20	.43	2.28
	24	2.14	.41	2.33
1.5	1	2.53	.41	2.38
	5	2.59	.41	2.38
	24	2.58	.36	2.51
1.8	1	2.14	.35	2.59
	5	2.07	.29	2.91
	24	2.34	.33	2.64
2.0	1	2.08	.33	2.71
	5	2.42	.31	2.85
	24	2.40	.31	2.82
2.2	1	2.65	.33	2.76
	5	2.92	.35	2.69
	24	2.67	.30	2.96
2.4	1	3.14	.32	2.96
	5	2.70	.32	2.92
	24	3.01	.29	3.23
2.5	1	3.10	.35	2.78
	5	2.86	.40	2.57
	24	2.90	.32	2.95

concentration expressed in moles Al per liter in table 5. Consequently the Al_b contribution to ionic strength must be so small in comparison to the Al_a contribution as to be negligible, even if the Al_b concentration, expressed in moles of Al per liter, is larger than that of Al_a. The same can be said with regard to the Al_c concentration.

The above iterative calculation is carried through several times until there is no change in the calculated Al^{3+} activity. The ionic strengths and Al^{3+} activities calculated in this manner are given in table 6 along with the calculated OH_b/Al_b ratios. The hypothetical dissolution of an aluminum hydroxide in acid media may be written

$$Al(OH)_{3(c)} + 3H^+ \rightleftarrows Al^{3+} + 3H_2O.$$

The equilibrium constant should equal the activity product $[Al^{3+}][H^+]^{-3}$ at equilibrium. The stability boundary indicative of this fact may be represented by a straight line of slope -3 where $\log_{10}[Al^{3+}]$ is plotted versus pH as in figure 10. A point to the right of this boundary indicates supersaturation with respect to this mineral, and a point to the left represents undersaturation. The stability boundaries shown in figure 10 were calculated from equilibrium constants which were in turn calculated from the free energies also given in table 2 using Parks' (1972)

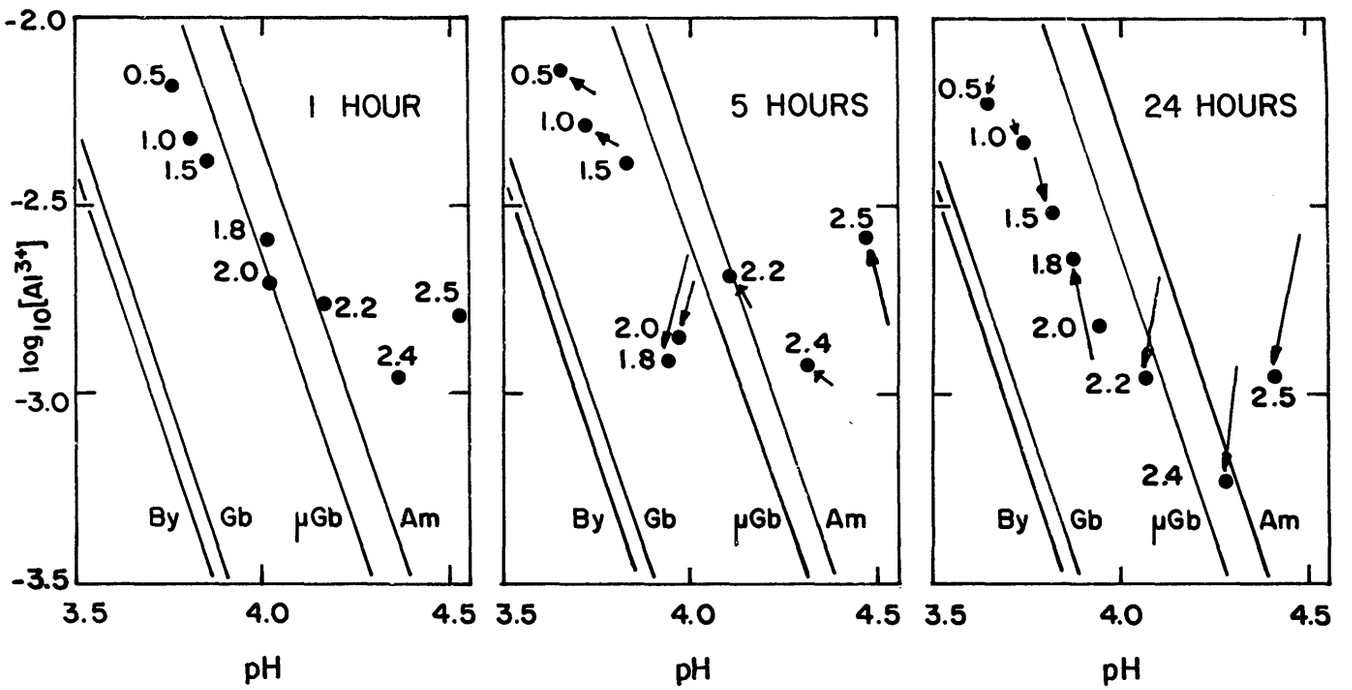

FIGURE 10.—Log_{10} $[Al^{3+}]$ in equilibrium with various $Al(OH)_3$ solids versus pH at 1, 5, and 24 hours. Am = amorphous, μGb = microcrystalline gibbsite, Gb = gibbsite, By = bayerite and nordstrandite. Figures next to large dots give r_n values, and arrows indicate motion of data point since previous measurement.

value of −116.0 kcal/mol for the free energy of Al^{3+}.

The data plotted in figure 10 indicate supersaturation at all values of r_n with respect to gibbsite and bayerite, whose stability fields are almost indistinguishable from one another. The points on this plot for r_n 2.0 or less lie between stability fields for gibbsite and microcrystalline gibbsite. This suggests that these solutions may contain gibbsite particles of some intermediate size. The positions of all the points tend to drift leftward toward the gibbsite stability boundary; this behavior is consistent with the growth of microcrystalline gibbsite particles over a 24-hour period. This does not, however, rule out the possibility of stacking of units in such a way that bayerite crystals are formed. Differentiation between gibbsite and bayerite on the basis of figure 10 alone is not possible.

It is apparent from figure 10 that solutions of r_n greater than 2.0 require more time to come to equilibrium with respect to bayerite or gibbsite because their initial compositions deviate further from equilibrium than do solutions of r_n less than 2.0. Given sufficient time these solutions would perhaps reach equilibrium with respect to gibbsite or a metastable equilibrium with respect to bayerite, depending on solution conditions.

However, solutions of r_n greater than 2.0 also should produce more precipitated solids for inspection than those of r_n less than 2.0. Solids removed from solutions of r_n 2.0 through 2.5 by filtration through millipore 0.1-μm-diameter filters at 24 hours aging gave no X-ray diffraction peaks, and no crystal structures could be identified by optical microscopic examination. Most of this material was probably amorphous, with perhaps a small amount of microcrystalline material also present, though not enough to identify. Although no definite crystal structures could be discerned by microscopic examination at this time, a few hexagonal gibbsite-like angles were noticed among the apparently amorphous material.

These solutions were stored again in a CO_2-free atmosphere for 20 days. Solids removed from these solutions after that time were again examined under a microscope, showing what appeared to be a mixture of amorphous (or microcrystalline below the resolution of the microscope) material, pyramidal and needle-like bayerite crystals of base length 2–3 μm, and rectangular nordstrandite crystals from 5 to 15 μm in length. No clearly defined gibbsite crystals could be discerned.

According to Turner (1968b), Turner and Ross (1970), and other workers, some substitution of Cl^- in structural positions of OH^- can occur in the precipi-

tate. This substitution is no doubt more probable at low pH, where the Cl^-/OH^- ratio is high, and may account for the low value of r_p at 1 hour's aging in the solution of 0.5 r_n. In this case, two kinds of polymers could be assumed to exist in the early stages of aging. These would be the "regular" polymers with all the bridging positions occupied by OH^- and also a much more unstable form with Cl^- substituted in some of the bridging positions. This latter species would undergo reorganization with time as these chlorides slowly exchanged with some solution hydroxides.

The anomalous decrease in r_p for r_n between 1.5 and 2.0 in figure 9 could be explained by the coexistence of polymers of different sizes. However, this should imply that smaller polymers could be formed even with an increase of r_n. As supersaturation in the preparation of the solution is attained more rapidly at higher r_n values, the crystal seeds are smaller, so that this is not impossible. A better explanation could be proposed by assuming that this behavior results from a "pyramidal stacking." Such large pyramidal units have a lower OH_b/Al_b ratio than if they were stacked in a normal manner. The existence of visible bayerite pyramidal and needlelike crystal structures after 20 days supports this hypothesis. This principle does not require the crystal growth to stop. It is supported by the fact that at lower values of r_n the monomeric species seem to tend to an equilibrium with bayerite or gibbsite. In addition, electron microscope studies by Schoen and Roberson (1970) showed bayerite crystals which looked like needles or pyramids with the c axis in the direction of elongation of the crystal.

There is some question as to whether the dimer $Al_2(OH)_2^{4+}$ is a metastable or a stable equilibrium species. The variation of $Al_2(OH)_2^{4+}$ concentration with ionic strength reported by Turner (1975) agrees so well with theory as to suggest the latter. Equilibrium concentrations for this dimer and for the monomeric species in a hypothetical solution 0.10 molar in noncolloidal aluminum were calculated using the formation constant K_{mn} given in table 3 and are plotted as a function of pH in figure 11. It can be inferred from this graph that the dimer may be the predominant form of noncolloidal aluminum above pH 4 ($r_n > 2.0$) in some of the solutions studied here. The Al^{3+} activities given in table 6 and plotted in figure 10 were calculated from analytical concentrations of Al_a from which dimers were presumed to have been excluded, having been included in Al_b. Turner (1975) used, for measuring dimer concentration, an analytical procedure which utilized the anomalously fast kinetics of the dimer in the first-order reaction of polymeric aluminum in the 8-quinolinate extraction technique; the species thought to be the dimer reacted at a much faster rate than did the remaining polymeric aluminum. This type of anomaly also occurred in our analytical procedure, as illustrated in figure 6, where the first four data points have a greater slope (thereby suggesting a greater initial reaction rate) than do the remaining points for the rest of the reaction. It appears as though our analytical technique for separating Al_a from Al_b did, like Turner's, properly place the dimer in the Al_b category. Our earlier equilibrium calculations of Al^{3+} activity from Al_a concentrations is therefore probably justified.

A model for the interpretation of these experiments can therefore be formulated; the solutions are probably best described by monomeric and dimeric species in equilibrium with bayerite or gibbsite. Supersaturation is made apparent when aluminum analyses include both Al_a and the dissolved polymeric species Al_b, which grows in a and b directions. The concentrations in terms of moles of Al per liter of these polymeric species increase with increasing r_n. If r_n is greater than 2.0, the polymeric species decrease in quantity but begin to grow in the c direction. The early stage of this process could be pyramidlike stacking of the sheetlike units.

The addition of sodium hydroxide during a 1-hour period for preparing a solution of r_n 1.8 to 2.0 is suf-

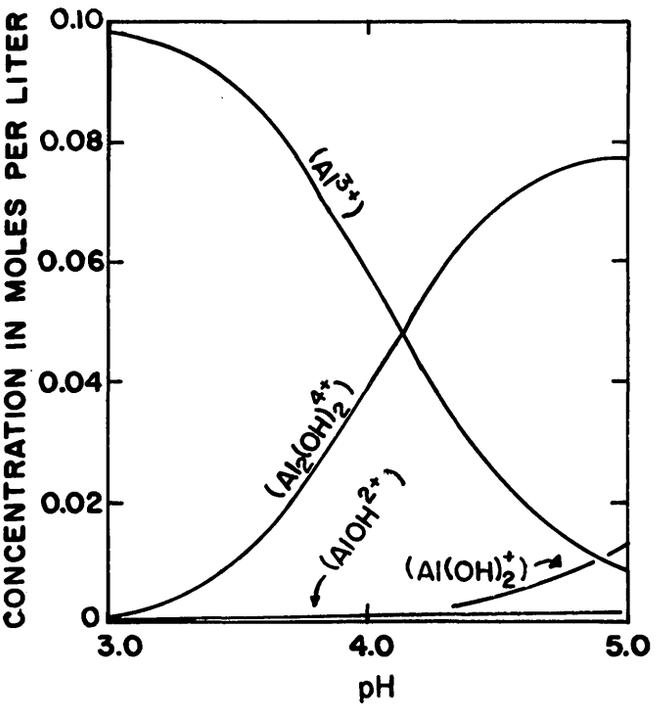

FIGURE 11.—Calculated equilibrium concentrations of aluminum in monomeric and dimeric forms in solutions 0.10 molar in $[(Al_a) + (Al_2(OH)_2^{4+})]$.

ficiently rapid to give to the solutions a true supersaturation of Al^{3+} with respect to gibbsite and bayerite. Because of the relatively rapid supersaturation, as a result of the required amount of NaOH being added during a 1-hour period, amorphous material with a stoichiometric formula $Al(OH)_{3-x}Cl_x$ may have been encountered so that measured Al_c may have included this type of "impurity" in addition to the true hydroxide polymers. Unfortunately, the solid product given by this partial neutralization was not present in sufficient amounts to be isolated and analyzed, but it is possible that basic aluminum chloride contributes to the measured Al_c as suggested by Turner (1968b). Attempts which were made to attribute fast-reacting OH_f to Al_a failed because most of the OH_f/Al_a ratios were greater than the theoretical ratio calculated from pH and ionic strength, perhaps because OH_f included some smaller Al_b polymers.

CONCLUSIONS

In the experimental conditions used here, the supersaturation with respect to gibbsite, bayerite, and amorphous $Al(OH)_3$ in neutralized aluminum chloride solutions at high ionic strength depends on the amount of hydroxide provided to the solutions. When only the monomeric Al_a species are considered, solutions of r_n between 0.5 and 2.5 are supersaturated with respect to gibbsite and bayerite, while solutions of r_n greater than 2.2 are also supersaturated with respect to amorphous $Al(OH)_3$ during the first hour. All these supersaturations decreased in magnitude over a period of 24-hours, after which their analyses gave activity products which lay between gibbsite and microcrystalline gibbsite stability fields, except for the r_n 2.4 and 2.5 solutions. These latter solutions were nearly saturated and supersaturated, respectively, but were probably still tending toward conditions of less saturation.

The polymeric material consists of sheetlike units such as those proposed by Hsu (1973). Growth of these units in size in the a and b directions results in units whose size at a given time depends on r_n; solutions of higher r_n give larger Al_b polymers. The supersaturation at 24 hours with respect to gibbsite and bayerite is always due to both monomeric and polymeric material; even when Al_a alone is considered, this supersaturation can be shown to exist. The polymeric material may possibly be described as pyramidal stacks of the defined sheetlike units. No conclusion can be proposed as to the exact character of the aluminum species analyzed as Al_c. This material may contain basic aluminum chloride (aluminum hydroxide partially substituted by chloride) in addition to the stacks of true aluminum hydroxide sheetlike units.

It would perhaps be interesting to make further investigations concerning chloride substitutions in the polymeric species. In this type of study, titrations of partly neutralized aluminum chloride solutions could be made with nitric instead of hydrochloric acid while simultaneously measuring H^+ and Cl^- activities by electrode during the titration. This kind of experiment could also provide some information about the meaning of OH_f. Ultracentrifugation should perhaps be investigated as a tool for the separation of Al_c from solution, after which the characteristics of its constituents could be investigated. Regular rates of addition of NaOH should be studied for the purpose of investigating the manner in which the solutions become supersaturated; such a study could show the relation between the rate of neutralization and the amount of base added and the effect of this relation on supersaturation by the monomeric species.

REFERENCES CITED

Brosset, Cyrill, Biedermann, George, and Sillen, L. G., 1954, Studies on the hydrolysis of metal ions XI. Aluminum, Al^{3+}: Acta Chem. Scandinavica, v. 8, no. 11, p. 1917–1926.

Brown, D. W., and Hem, J. D., 1975, Reactions of aqueous aluminum species at mineral surfaces: U.S. Geol. Survey Water-Supply Paper 1827–F, 48 p.

Brown, Eugene, Skougstad, M. W., and Fishman, M. J., 1970, Methods for collection and analysis of water samples for dissolved minerals and gases: U.S. Geol. Survey Techniques Water Resources Inv., book 5, chap. A1, p. 44–46.

Fiessinger, François, 1976, La coagulation: Errements anciens et connaissances novelles: Techniques et Sciences Municipales, v. 71, no. 4, p. 147–162; published by L'Association Générale des Hygiènistes et Techniciens Municipaux, France.

Fripiat, J. J., and Pennequin, Marc, 1965, Evolution de la composition et du poids moléculaire des hydroxydes d'aluminium et de fer purifiés par dialyse: Soc. Chim. France Bull., no. 6, p. 1655–1660.

Fripiat, J. J., van Cauwelaert, F., and Bosmans, H., 1965, Structure of aluminum cations in aqueous solutions: Jour. Phys. Chemistry, v. 69, no. 7, 2458–2461.

Hem, J. D. 1968a, Aluminum species in water, *in* Gould, R. F., ed., Trace inorganics in water: Washington, D.C., Am. Chem. Soc. Advances in Chemistry Ser., no. 73, p. 98–114.

———1968b, Graphical methods for studies of aqueous aluminum hydroxide, fluoride, and sulfate complexes: U.S. Geol. Survey Water-Supply Paper 1827–B, 33 p.

Hem, J. D., and Roberson, C. E., 1967, Form and stability of aluminum hydroxide complexes in dilute solution: U.S. Geol. Survey Water-Supply Paper 1827–A, 55 p.

Hem, J. D., Roberson, C. E., Lind, C. J., and Polzer, W. L., 1973, Chemical interactions of aluminum with aqueous silica at 25°C: U.S. Geol. Survey Water-Supply Paper 1827–E, 57 p.

Herbillon, Adrien, and Gastuche, M. C., 1962a, Synthèse et genèse de l'hydrargillite: Acad. Sci. Comptes Rendus, v. 254, no. 6, p. 1105–1107.

———1962b, Étude des complexes kaolinite-hydroxide d'aluminium. Synthèse et genèse des trihydrates cristallisés; [France] Centre Natl. Recherche Sci. Groupe Français Argiles Bull., v. 13, no. 8, p. 77–94.

Hsu, P. H. 1963, Effect of initial pH, phosphate, and silicate on the determination of aluminum with aluminon: Soil Sci., v. 96, no. 4, p. 230–238.

———1973, Effect of sulfate on the crystallization of aluminum hydroxide from aging hydroxyaluminum solutions, *in* J. Nicolas, ed., Travaux du comite International pour l'Etude des Bauxites de l'Alumine et d'Aluminium (ICSOBA): Internat. Cong., 3d, Internat. Comm. for Studies of Oxides, Bauxites, and Hydroxides of Aluminum, Nice, France, 1973, rept. 10, p. 613–620; published by Academie Yougoslave des Sciences et des Arts, Zagreb, Yugoslavia.

Hsu, P. H., and Bates, T. F., 1964, Formation of X-ray amorphous and crystalline aluminum hydroxides: Mineralog. Mag., v. 33, no. 264, p .749–768.

Kerkhof, N. J., White, J. L., and Hem, S. L., 1975, Effect of dilution on reactivity and structure of aluminum hydroxide gel: Jour. Pharm. Sci., v. 64, no. p. 940–942.

Lippens, B. C., 1961, Structure and texture of aluminas: Delft, Netherlands, Waltman, 179 p.

Nail, S. L., White, J. L., and Hem, S. L., 1975, Comparison of IR spectroscopic analysis and X-ray diffraction of aluminum hydroxide gel: Jour. Pharm. Sci., v. 64, no. 7, p. 1166–1169.

Parks, G. A., 1972, Free energies of formation and aqueous solubilities of aluminum hydroxides and oxide hydroxides at 25°C: Am. Mineralogist, v. 57, nos. 7–8, p. 1163–1189.

Rubin, A. J., and Hayden, P. L., 1973, Studies on the hydrolysis and precipitation of aluminum (III): Ohio State Univ., Water Resources Center Rept. 364X, 91 p.

Schoen, Robert, and Roberson, C. E., 1970, Structures of aluminum hydroxide and geochemical implications: Am. Mineralogist, v. 55, p. 43–77.

Smith, R. W., 1969, The state of Al(III) in aqueous solution and adsorption of hydrolysis products on αAl_2O_3: Stanford Univ., Stanford Calif., Ph. D. dissert.

Smith, R. W., 1971, Relations among equilibrium and nonequilibrium aqueous species of aluminum hydroxy complexes, *in* Gould, R. F., ed., Nonequilibrium systems in natural water chemistry: Washington, D.C., Am. Chem. Soc. Advances in Chemistry Ser., no. 106, p. 250–279.

Smith, R. W., and Hem, J. D., 1972, Effect of aging on aluminum hydroxide complexes in dilute aqueous solutions: U.S. Geol. Survey Water-Supply Paper 1827-D, 51 p.

Truesdell, A. H., and Jones, B. F., 1974, WATEQ, a computer program for calculating chemical equilibria of natural waters: U.S. Geol. Survey Jour. Research, v. 2, p. 233–248.

Turner, R. C., 1968a, Conditions in solution during the formation of gibbsite in dilute Al salt solutions: 1. Theoretical treatment of the effect of the formation of mono- and polynuclear hydroxyaluminum ions, precipitations, and crystallization on curves representing the titration of $AlCl_3$ with a base: Soil Sci., v. 106, no. 4, p. 291–296.

———1968b, Conditions in solution during the formation of gibbsite in dilute Al salt solutions: 2. Effect of length of time of reaction on the formation of polynuclear hydroxyaluminum cations, the substitution of other anions for OH– in amorphous $Al(OH)_3$ and the crystallization of gibbsite: Soil Sci., v. 106, no. 5, p. 338–344

———1975, The equilibrium constant for the formation of $Al_2(OH)_2^{+4}$ in aqueous solutions: Canadian Jour. Chemistry, v. 53, no. 19, p. 2811–2817.

Turner, R. C., and Ross, G. J., 1970, Conditions in solution during the formation of gibbsite in dilute Al salt solutions. 4. Effect of Cl conformation: Canadian Jour. Chemistry, v. 48, no. 5, p. 723–729.

Jour. Research U.S. Geol. Survey
Vol. 6, No. 3, May–June 1978, p. 339–346

AN EVALUATION OF ERRORS IN MAPPING LAND USE CHANGES FOR THE CENTRAL ATLANTIC REGIONAL ECOLOGICAL TEST SITE

By KATHERINE FITZPATRICK-LINS, Reston, Va.

Abstract.—Land use change maps prepared from high-resolution, high-altitude aerial photographs for the period 1970 to 1972 of the CARETS (Central Atlantic Regional Ecological Test Site) project were analyzed for accuracy. To test for errors of commission, all outlined areas (polygons) of land use change on five 1:100 000-scale maps were examined for accuracy. An estimate of the errors of omission was obtained by comparing the land use change polygons mapped for the Norfolk SMSA (Norfolk and Virginia Beach Standard Metropolitan Statistical Area) with the changes mapped in a more detailed study of the same area. The results of these studies showed that the largest number of errors was caused by misregistration of the land use change map to the 1970 land use map; however, only a very small percentage of the total land area of the land use change was affected by misregistration. In the Norfolk SMSA, which is an area of rapid urban growth, many of the land use changes had not been mapped. The conclusion is that quality control checks are necessary both during and after map compilation. The experience of the CARETS and other land use mapping experiments conducted in the early 1970's has resulted in the development of carefully designed quality-control procedures implemented in the nationwide mapping of land use and land cover currently being carried out by the U.S. Geological Survey.

The CARETS (Central Atlantic Regional Ecological Test Site) project, jointly sponsored by NASA (National Aeronautics and Space Administration) and the U.S. Geological Survey, was designed to evaluate Landsat images and high-altitude aircraft photographs as inputs to a regional land resources information system. The study area included the District of Columbia, 18 independent cities, and 74 counties in 5 States within the Chesapeake and Delaware Bay regions. Level II land use maps were compiled at a scale of 1:100 000 from 1970 high-resolution, high-altitude photographs by using a preliminary version of the land use classification scheme of Anderson and others (1976). Two years later, in 1972, similar aerial photographs were used to interpret land use change from 1970. These land use change maps were compiled so as to overlay directly the 1970 land use map.

Once the maps were compiled, they were made available to the public through open file at the Geological Survey. At that time it was considered necessary to evaluate the accuracy of the land use interpretations. The evaluation was completed in 1975 (Fitzpatrick, 1975). In that study, land use maps overlaid with the 1972 land use update were sampled using a stratified random sampling technique. One percent of the area was sampled. Although both the 1970 land use maps and the 1972 land use overlay were evaluated together, very few land use change data were included because almost no land use change polygons were found within the sampled areas. A separate accuracy evaluation of the land use change maps was therefore necessary to estimate their reliability.

STATEMENT OF THE PROBLEMS

The CARETS land use mapping project was an experimental mapping project to test the usability of high-altitude aerial photographs as a data source for a regional land information system. See figure 1 for an index of the CARETS map sheets. After the completion of the 1970 land use maps, the task of producing a complete set of 1972 land use updates for the entire CARETS test site was accomplished by the CARETS researchers in cooperation with two of the Geological Survey's Topographic Division Mapping Centers, the Rocky Mountain Mapping Center at the Federal Center in Denver and the Special Mapping Center in Reston.

The basic methodology of the update procedure was to use the 1970 land use map overlaid on the 1970 mosaic produced from NASA photographs as the mapping base. Areas 5- by 5-km square on the base map and on the corresponding 1972 high-altitude aerial photographs were systematically examined by a photointerpreter for land use changes. Where changes had occurred, the interpreter then drew polygons showing the extent of the changes on an overlay to the 1970 base map.

The exception to this procedure was made in areas where no 1970 NASA photographs existed and only the 1972 land use map had been produced. In these

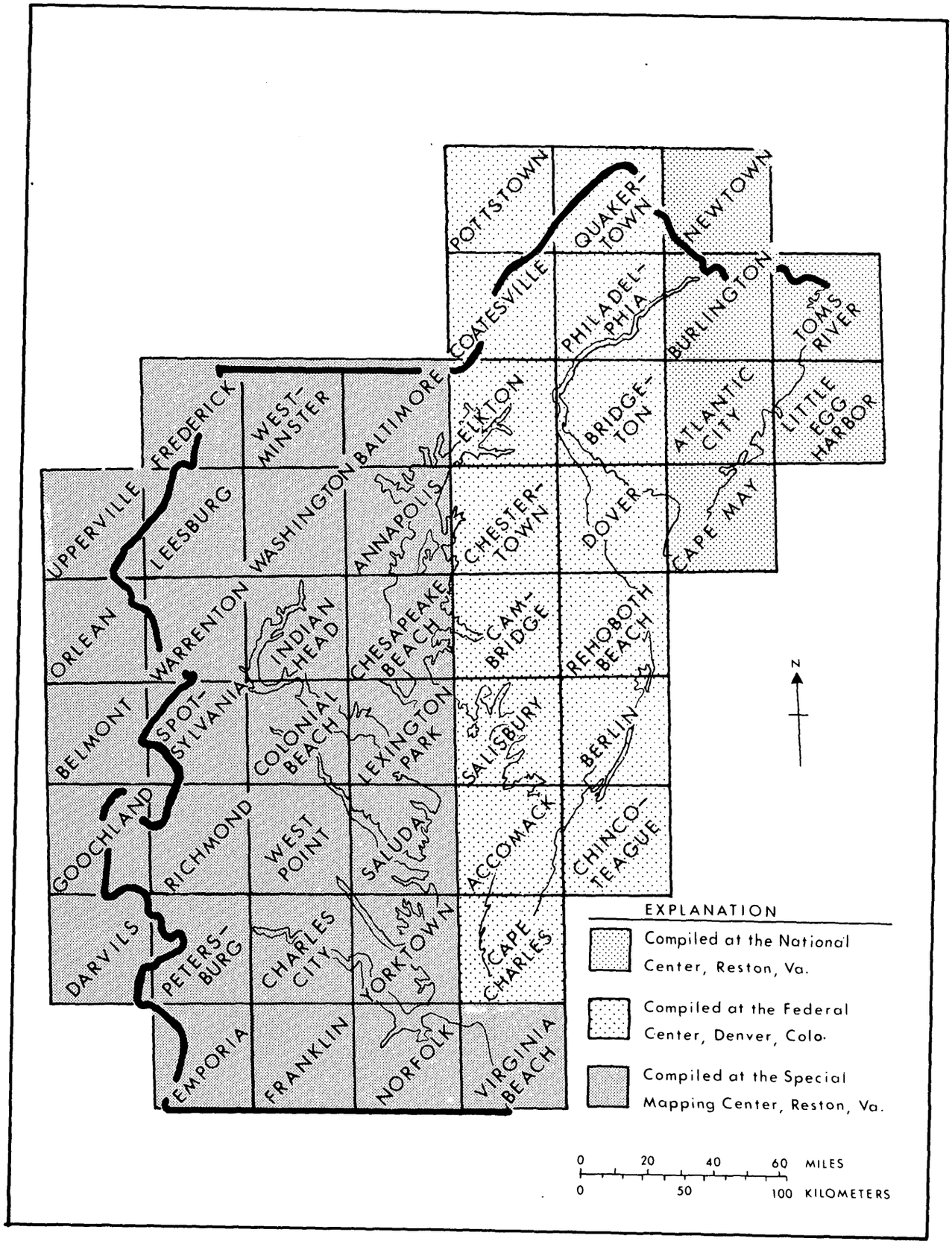

FIGURE 1.—Index to land use change maps compiled at the three Geological Survey centers.

areas, changes from 1970 to 1972 were mapped by comparing the 1972 map and mosaic base with existing 1970 USDA (U.S. Department of Agriculture) airphoto indexes. As in the former procedure, a separate land use change overlay was produced. This procedure was chosen to provide information on land use change uniformly over the entire CARETS area for the same 2-year period, rather than only between the two dates for which aerial photography happened to be available.

The major problems encountered in mapping the 1972 land use changes were as follows:

1. How to register the 1972 update accurately to the 1970 base.
2. How to indicate corrections to the original map that were not land use changes.
3. How to edit the maps to insure a uniform product.

These problems were addressed in a different manner by the interpreters at each region where the compilation was undertaken. Their resulting differences did not manifest themselves until the maps were completed.

An examination of the land use change maps revealed some mapping errors and inconsistencies which were then corrected. Later, other errors were noticed when the maps were processed for digitizing. Each of these errors could be ascribed to one of the following major error types:

Errors of commission:

1 Polygon boundaries on the 1972 map did not conform to the polygon boundaries on the 1970 map.
2 Two or more 1970 land uses had changed to a new land use but were recorded as a single 1970 land use on the 1972 land use update.
3 Corrections to the 1970 data base mapped as a land use change on the 1972 land use update.
4 Areas mapped as land use change that were smaller than the minimum recording unit.
5 Misinterpretation of 1972 land use.
6 Land use polygons drawn indicating change in areas where no change had occurred.
7 1970 land use codes misrecorded on the 1972 overlay.
8 The 1970 land use originally misinterpreted.
9 Transposed codes.

Errors of omission:

10 Land use change not mapped.

Almost every one of these errors could be related to one of the three major mapping problems stated earlier. It was therefore proposed that the frequency of occurrence of the errors resulting from these problems be evaluated and recommendations be made for future land use change mapping.

RESEARCH DESIGN AND RESULTS

The method for selecting map sheets used in this study had to include a significant portion of the land use change polygons even though they amounted to less than 1 percent of the total area of the map and were widely scattered. See the example of a land use change map in figure 2.

Errors of omission would be included as well as errors of commission. To check for errors of commission, only those polygons of land use change shown on published maps from each region were to be evaluated.

Identifying errors of omission would have involved rechecking land use change in the entire sample area a procedure requiring more expense and time than available. Selection of a 1-percent sample of the CARETS area, similar to the CARETS land use accuracy check (Fitzpatrick, 1975), would have included few land use change polygons. Selections of a larger area would have made it too difficult to check for errors of omission. For these reasons, the methodology chosen was a compromise of the above choices. The decision made was to evaluate the land use change as mapped and determine the reliability of the change polygons.

To approximate the number of errors of omission, the researcher compared the land use change for the Norfolk SMSA (Norfolk and Virginia Beach Standard Metropolitan Statistical Area) portion of the Norfolk and Virginia Beach sheets with a more precise land use change map of the same area. This more precise control map of land use change in the Norfolk SMSA was compiled as part of a detailed test of accuracy of land use information obtained from images of Landsat-1, formerly ERTS Earth Resources Technology Satellite). More interpreter time was spent compiling both land use and land use change maps for the Norfolk SMSA for this project than was spent in the standard land use change maps. In addition, each land use change appearing in the Norfolk SMSA was verified using 1972 high-resolution, high-altitude aerial photography. Therefore, the control map produced by these procedures was accepted as a standard against which land use change accuracy could be compared.

Five representative map sheets were selected for study of the errors of commission; two of these were also checked for errors of omission. The Washington sheet was selected as representative of the work of the Special Mapping Center in Reston, the Salisbury sheet as representative of the work by Rocky Mountain Mapping Center at the Federal Center in Denver, and the Toms River sheet as representative of the work of CARETS researchers at the National Center in Reston.

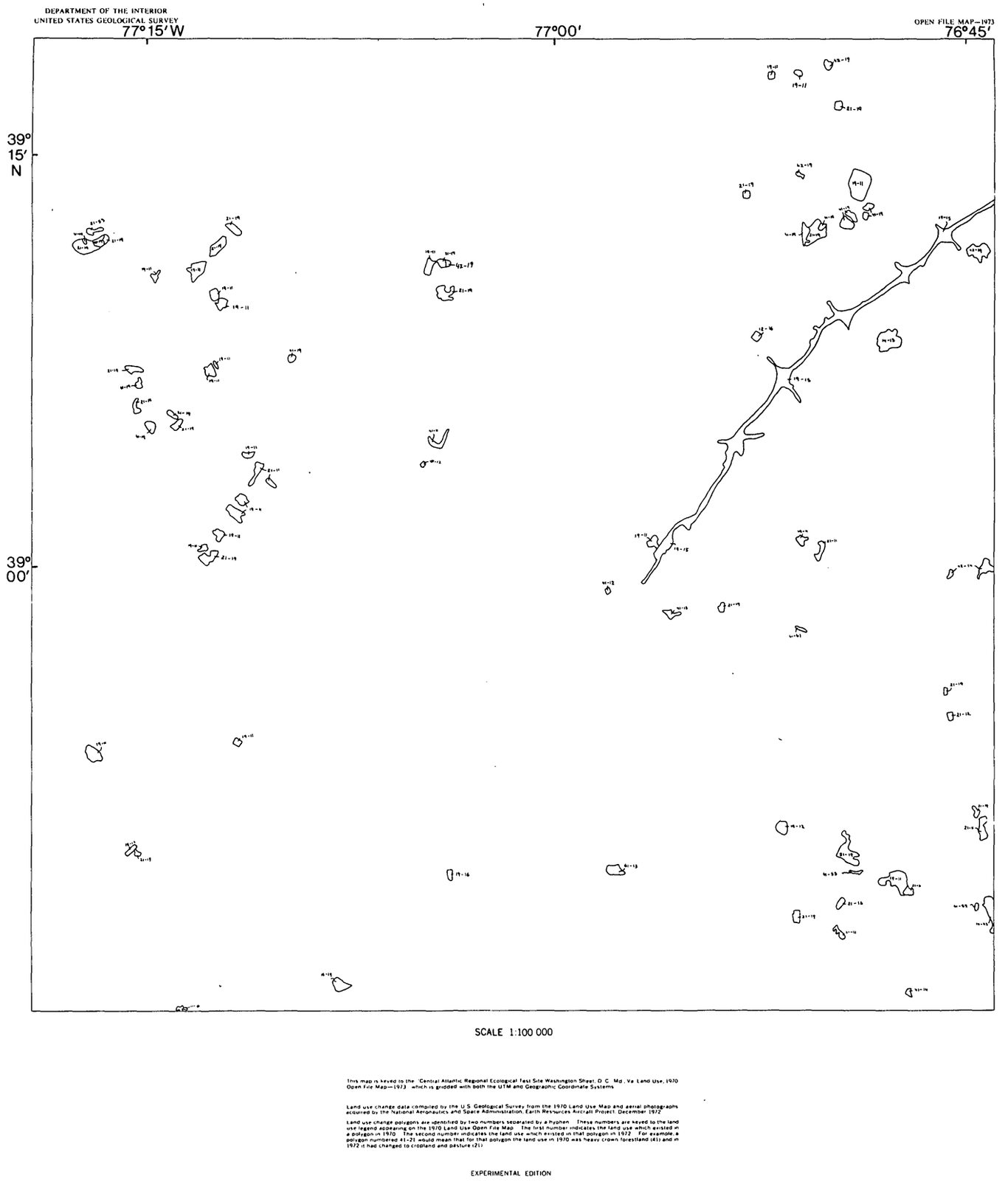

FIGURE 2.—An example of a land use change map prepared as an overlay for the land use map base.

See figure 1 for an index of the map sheets compiled. The Norfolk and Virginia Beach sheets were tested for both interpretation errors and errors of omission.

Errors of Commission

In order to detect errors of commission, a systematic procedure in checking the land use change polygons on each sheet was followed. For each sheet selected, the land use change polygons were assigned numbers arbitrarily from 1 to n. The land use change overlay was then registered to the 1970 land use map and mosaic. Each numbered polygon was checked against the 1970 photography and 1972 photography for evidence of change. In most sites a change mapped on the original land use change overlay had actually occurred; the change polygon then was checked to see if both the 1970 and 1972 interpretations were correct. If there were an error in interpretation, one or more of the nine codes listed earlier were assigned to describe the error.

Corrected land use change polygons were drawn on a separate overlay and the area was measured. Comparisons of these area measurements with the area measurements of the original land use change map were then possible.

Discussion of Errors of Commission

Boundary errors

The most significant cause of map inaccuracies was incorrect drawing of the polygon boundaries. Not enough care had been taken to insure that the boundaries of the land use change polygons matched those on the 1970 land use map. For 68 of the total 181 land use change polygons, the boundary was found to be incorrectly drawn. In some polygons the error was a major positional error; in others it was a slightly misdrawn boundary. The resulting difference in area was only 3 percent of the total area of the land use change polygons on the five map sheets inspected, a decrease from 1462 to 1412 ha (hectares). This is a negligible amount when compared to the 12 500 km^2 total area of the five complete map sheets.

No measure of the positional accuracy was made. It is recognized, however, that even a small positional error presents a major problem when the maps are digitized. Any attempt to digitally overlay the two maps would generate problem polygons where the boundaries did not match, thus creating the false impression of a greater or smaller land use change than actually occurred.

The ratio of the number of polygons found to have boundary errors to the number of land use change polygons per sheet was as follows:
40 of 84 on the Washington sheet,
1 of 14 on the Toms River sheet,
0 of 10 on the Salisbury sheet, and
27 of 73 on the Norfolk and Virginia Beach sheets.
For a synopsis of these and other errors see table 1.

Two or more land use polygons recorded as one

In many areas, where two or three land use types in 1970 changed to a single new land use type in 1972, the interpreters drew only one polygon to represent the change. Inaccuracies of this type, found in 24 of 181 polygons, were the second most frequent error. For the representative sheets, the numbers of polygons found with this error were as follows:
14 of 84 on the Washington sheet,
1 of 14 on the Toms River sheet,
3 of 10 on the Salisbury sheet, and
6 of 73 on the Norfolk and Virginia Beach sheets.

Correction to 1970 data base mistaken for land use change

The third most frequent form of error resulted when the change drawn was actually a correction to

TABLE 1.—*Number of polygons found with errors of commission on five land use change maps*

Sheet name	Total number	Number correct	Error type[1] 1	2	3	4	5	6	7	8	9
Washington	84	17	40	14	6	1	9	4	4	----	----
Toms River	14	8	1	1	----	----	----	----	3	1	----
Salisbury	10	5	----	3	1	1	1	1	----	----	----
Norfolk and Virginia Beach	73	7	27	6	15	17	4	7	1	----	----
Total	181	------	----	----	----	----	----	----	----	----	----

[1] Error types:

1. 1972 polygon boundary that did not conform to the 1970 boundaries.
2. Two or more land use polygons recorded as one.
3. Correction to the 1970 data base mapped as a land use change on the 1972 overlay.
4. Area smaller than the minimum recording unit mapped as land use change.
5. Misinterpretation of the 1972 land use.
6. Land use change polygon drawn where no change actually occurred.
7. 1970 land use misrecorded on the 1972 overlay.
8. 1970 land use originally misinterpreted.
9. Transposed codes.

the 1970 data base. Errors of this type were not interpretation errors but were mapped as changes rather than as corrections to the data base and therefore are misleading. Of the 181 change polygons, 22 were found to be corrections to the data base, rather than land use changes. On the Washington map sheet this error was found in 6 of the 84 polygons and on the Salisbury sheet was found in 1 of the 10 polygons. This kind of error was not found on the Toms River sheet. On the combined Norfolk and Virginia Beach sheets this error was found in 15 of the 73 polygons.

Areas mapped smaller than the minimum mapping size

Another common error resulted when areas smaller than the minimum mapping size were mapped as land use change polygons. These areas may have been identifiable as separate land uses in 1970 but were not mapped because they were below the minimum mapping size at a 1:100 000 scale. Interpreters mapping the 1972 land use change mapped these polygons as if change had occurred. According to specifications, mapping of these polygons is incorrect. Of the 181 land use change polygons 19 were found to be smaller than the minimum mapping size. On the Washington sheet this error accounted for only 1 of the 84 mapped polygons. On the Toms River sheet no polygons were found to be smaller than the minimum mapping size. On the Salisbury sheet, 1 polygon of the 10 land use change polygons was found to be smaller than the minimum mapping size. On the combined Norfolk and Virginia Beach sheets, 17 of 73 change polygons were found to be smaller than the minimum mapping size.

Additional error types

Other frequent error types listed in table 1 are error type 5, misinterpreting 1972 land use, and error type 6, interpreting land use where none had occurred. The 1972 land use was found to be in error in 9 of the 84 polygons on the Washington sheet and in 1 of the 10 polygons on the Salisbury sheet. No misinterpretations of the 1972 data were found on the Toms River sheet. On the combined Norfolk and Virginia Beach sheets, 1972 data were found to be misrecorded in 4 of 73 polygons. Of the polygons where change did not actually occur, 4 were found on the Washington sheet and 1 was found on the Salisbury sheet. On the combined Norfolk and Virginia Beach sheets, 7 polygons were found as change that did not occur.

For some polygons, more than one error applies, and so the sum of the error types and the number of correct polygons does not equal the total number of polygons.

Evaluation of the Five Map Sheets

Table 1 lists the five map sheets and the number of polygons found with errors of each type. According to this table the most accurate land use change maps examined are the Salisbury and Toms River sheets. Both of these sheets have 50 percent of the land use change polygons mapped correctly. Because very few boundary errors appear, the interpreters of these two sheets apparently adhered more closely to the boundaries drawn on the 1970 land use maps. The major error on the Salisbury sheet occurs where more than one land use changed to a single new land use and the interpreter mapped it as a single polygon. On the Toms River sheet, 3 of the 14 polygons were found with the 1970 land use misrecorded. This error did not occur as frequently on the other sheets examined and may have resulted from the complex mapping methods necessary for the Toms River sheet. The 1972 land use map and mosaic served as the base and the 1970 land use was interpreted afterwards from USDA airphoto indexes. For these areas a separate 1970 to 1972 change map was drawn from annotations on the new 1970 map. Some errors in recording the 1970 land use could easily have occurred.

The Washington sheet had a high ratio of incorrect to correct polygons. Of 84 land use change polygons only 17 were found without some error. The most frequent errors were in locating the boundary lines and in mapping areas of two or more land uses as a single polygon. These errors most likely occurred because some of the interpreters were not aware of the importance of registering the land use change overlay to the 1970 data base. To avoid this error in the future, the process of data overlays and the importance of registering the polygons to each other should be stressed.

Although the number of errors on any map sheet seems large, the actual area affected may be quite small. Table 2 shows the area of land use change before and

TABLE 2.—*Difference in area between original land use change interpretation and corrected interpretations on five maps*

Sheet name	Original map (ha)	Corrected maps (ha)	Difference	
			Hectares	Percent
Washington ----	2790	2742	48	2
Toms River ---	1042	1009	33	3
Salisbury ------	140	124	16	11
Norfolk and Virgina Beach	1843	1043	800	43

NOTE.—Only on the Norfolk and Virginia Beach sheets did polygons smaller than the minimum mapping size constitute a major portion of the total error. Even on these sheets, however, these polygons only amounted to a total of 57 ha. By removing these from the original map, an editor could only decrease the area in error from 800 ha to 743 ha and from 43 percent to 40 percent of the total.

after correction, and the percent difference as well as the area difference. On the Washington and Toms River sheets the area difference was as small as 2 and 3 percent.

The complexity of the maps is also a factor affecting the correctness of the interpretation. The most detailed sheets, the Washington sheet and the Norfolk and Virginia Beach sheets had errors in 80 to 90 percent of the polygons, 67 of 84 for the Washington sheet and 66 of 73 for the Norfolk and Virginia Beach sheets. In the two less detailed sheets, Salisbury and Toms River, 50 percent of the polygons were in error. The number of errors increases as the complexity of the data increases; however, this is not true of the actual area affected by the errors in mapping. The types of errors on each map sheet affect the area in error. The discrepancies in the proportion of error types between the map sheets listed in table 1 are the result of differences in interpreters and the use of nonstandard procedures at mapping centers.

Errors of Omission

To estimate the errors of omission on the land use change maps, the land use change of the Norfolk SMSA, mapped in the standard CARETS 1:100 000-scale map format, was compared with that mapped by CARETS researchers for a more comprehensive study. This second map, considered a control map, was compiled using both high-altitude photographs and Landsat-1 images. This mapping effort required twice the number of person hours, involved more polygons of land use change (Alexander and others, 1975), and was considered more accurate than the Norfolk and Virginia Beach land use change maps produced by less experienced compilers. Land use changes on the control map were outlined only if the changes were noticeable on the Landsat-1 images and verified by the high-altitude photography. Because interpreters could not detect all land use changes that occurred when using the Landsat-1 images, the resulting control map did not serve as an absolute measure of errors of omission. It did, however, serve as an estimate.

To compare the land use change maps (Norfolk and Virginia Beach) with the control map, they were registered to the control map and overlaid together on the 1970 mosaic. The 1970 and 1972 high-altitude photographs were then referenced. Each land use change polygon on the control map that did not appear on the standard Norfolk and Virginia Beach maps was verified against the 1970 and 1972 photographs. If the interpretation of the polygon was found to be correct on the control map, a new polygon of land use change was added to the Norfolk or Virginia Beach land use change map. The interpreter then measured the area of the new polygons on each sheet.

On the Norfolk sheet, within the Norfolk SMSA, an additional 660 ha of land use change were found using this method. On the Virginia Beach sheet 480 ha were found giving a total of 1140 ha not previously mapped in the Norfolk SMSA. In comparison, the area of land use change mapped originally on this SMSA portion of the Norfolk and Virginia Beach sheets was 1603 ha. Almost as much land use change was overlooked as was mapped on these two sheets by the original interpreters.

CONCLUSIONS

Many inaccuracies are present on the land use change maps. The errors made differ from mapping center to mapping center. It is not possible to separate the discrepancies due to differences in interpreters from those due to differences in mapping centers. The large discrepancies in the accuracy of the maps compiled at the three locations suggest that many errors could be due to the difference in the experience of the interpreters or to a difference in the instructions given. To avoid these errors in the futre, the same detailed instructions should be given at each center and interim checks on the work quality should be conducted in order to alter or correct the methodology. The land use update maps should be checked for registration to the land use base during compilation. All corrections must be made immediately. A final quality control check must be made both at the center where the work is performed and in the office originating the contract.

EPILOG

In the nationwide mapping of land use and land cover currently being carried out in the Geological Survey, carefully designed quality-control procedures have been developed as a result of the CARETS and other mapping experiments carried out in the early 1970's.

The CARETS maps may be used as an indication of land use that has changed between 1970 and 1972, but because of the large numbers of changes that were missed in the Norfolk-Virginia Beach area, it would be wise to assume that many other land use changes may also have been overlooked in similarly dynamic areas of CARETS. The major problem in using the land use change maps is in registering the polygons to the 1970 data base. A user may have to invest some time in additional cartographic work to insure perfect registration. This additional work would involve reference to the 1970 (pre-change) photographs or to the mosaic mapping base.

Problems of completely erroneous data are few. Once the registration problem is corrected the 1972 polygons can be entered on the 1970 data base for a more up to date land use map product, but the 1970–72 land use change map should not stand alone as a separate product.

REFERENCES CITED

Alexander, R. H., and others, 1975, Interpretation, compilation and field verification procedures in the CARETS project: NASA, Goddard Space Flight Center Type III final rept. for ERTS–1 inv., SR–125, v. 5, p. 177.

Anderson, J. R., Hardy, E. E., Roach, J. T., Witmer, R. E., 1976, A land use and land cover classification system for use with remote sensor data: U.S. Geol. Survey Prof. Paper 964, p. 28.

Fitzpatrick, K. A., 1975, Cost accuracy and consistency comparisons of land use maps made from high-altitude aircraft photography and ERTS imagery: NASA, Goddard Space Flight Center Type III final rept. for ERTS–1 inv., SR–125, v. 7, p. 57.

Jour. Research U.S. Geol. Survey
Vol. 6, No. 3, May–June 1978, p. 347–358

TRENCHES ACROSS THE 1906 TRACE OF THE SAN ANDREAS FAULT IN NORTHERN SAN MATEO COUNTY, CALIFORNIA

By M. G. BONILLA, J. N. ALT,[1] and L. D. HODGEN,
Menlo Park, Calif.

Work done in cooperation with U.S. Nuclear Regulatory Commission

Abstract.—Two trenches were excavated across the 1906 trace of the San Andreas fault near fences that were displaced by the 1906 faulting. About 18 displacements equal to the 1906 displacement would account for the offset of a stream adjacent to one of the trenches. Review of divergent reports on the amount of fault displacement in 1906 at 7 localities indicates that right slip ranged from about 2 m (meters) to about 3 m at the main trace and was about 0.6 m on a subsidiary trace near one of the trench sites. Materials exposed in the trenches included Franciscan bedrock, Merced(?) sandstone, alluvial deposits, and modern soils. Visibility of the evidence for faulting covered a wide range. Faulting was expressed in the trenches as conspicuous color differences, abrupt termination of geologic units, fractures, gouge, granulation of rock, streaked contacts, rounding of rock fragments, and slickensides. Irregularly shaped masses of gouge and other materials found in both trenches may also be a manifestation of faulting. Neither caving of the walls nor the inflow of ground water were reliable indicators of the locations of faults in these trenches. The features exposed in the trenches clearly indicated the presence of an important zone of faults with geologically young displacements, but they were inadequate to identify with certainty the 1906 break or the probable 1838 break. For example, evidence of the 1906 rupture could not be seen in a unit 200 mm (millimeters) thick that is believed to predate 1906. The approximate location in the trenches of the 1906 zone of ruptures could, however, be inferred from surface morphology, historic records, and evidence in the trenches. A moderately sharp and steep contact between two surface soils, in itself suggestive of very young faulting, did not have a fault below it. Brass monuments were installed at the trench sites so that future surface ruptures can be related to the faults and other structures mapped in the trenches.

As a basis for interpreting trench exposures across faults of unknown recency of displacement, two trenches, A and B, were excavated in the San Andreas fault zone where historic ruptures have occurred. Sites were chosen where the 1906 surface rupture could be crossed, where the amount of displacement in 1906 had been measured nearby, where bedded materials were likely to be found, and where datable materials might exist. The sites selected were about 20 km south of San Francisco on San Francisco Water Department land between San Andreas Dam and Crystal Springs Reservoir (fig. 1).

Trench A was excavated at the north edge of a fault sag, which was dry at the time (fig. 2) but which contains a pond most of the year. The west end of the trench was near the east base of a small northwest-trending fault-related ridge underlain by serpentinite. The rest of the trench was in the nearly flat ground at the edge of the pond and the lower end of a low alluvial fan that has its apex to the east. Judging by the float, the bedrock immediately east of the trench is chiefly sandstone and lesser amounts of chert and greenstone, all part of the Franciscan Formation, here of Jurassic and Cretaceous age. About 30 m south of trench A are the remains of a fence displaced by the 1906 faulting.

Trench B was excavated on a flat-topped spur between two offset streams and 130 m north of a fence displaced by the 1906 faulting (fig. 3). The west end of the trench began in a low outcrop of Franciscan greenstone. Just to the east is flat ground with a growth of *Juncus effusus* (identified by D. P. Adam, U.S. Geol. Survey), a plant common in moist areas that we hoped might indicate underlying organic deposits suitable for radiocarbon dating. Near the northeast end of the trench site, the surface gradually rises toward a broad ridge whose float suggests that the underlying bedrock consits of serpentinite and minor greenstone. The Merced(?) Formation (Pliocene and Pleistocene), which was encountered in the trench, was unexpected because it was not known to crop out in the vicinity (Brabb and Pampeyan, 1972).

The trenches were about 1 m wide, 3.5 m deep, and about 35 m long; each had a bearing of N. 56° E., perpendicular to the San Andreas fault. Excavation

[1] Presently with Woodward-Clyde Consultants, San Francisco, Calif.

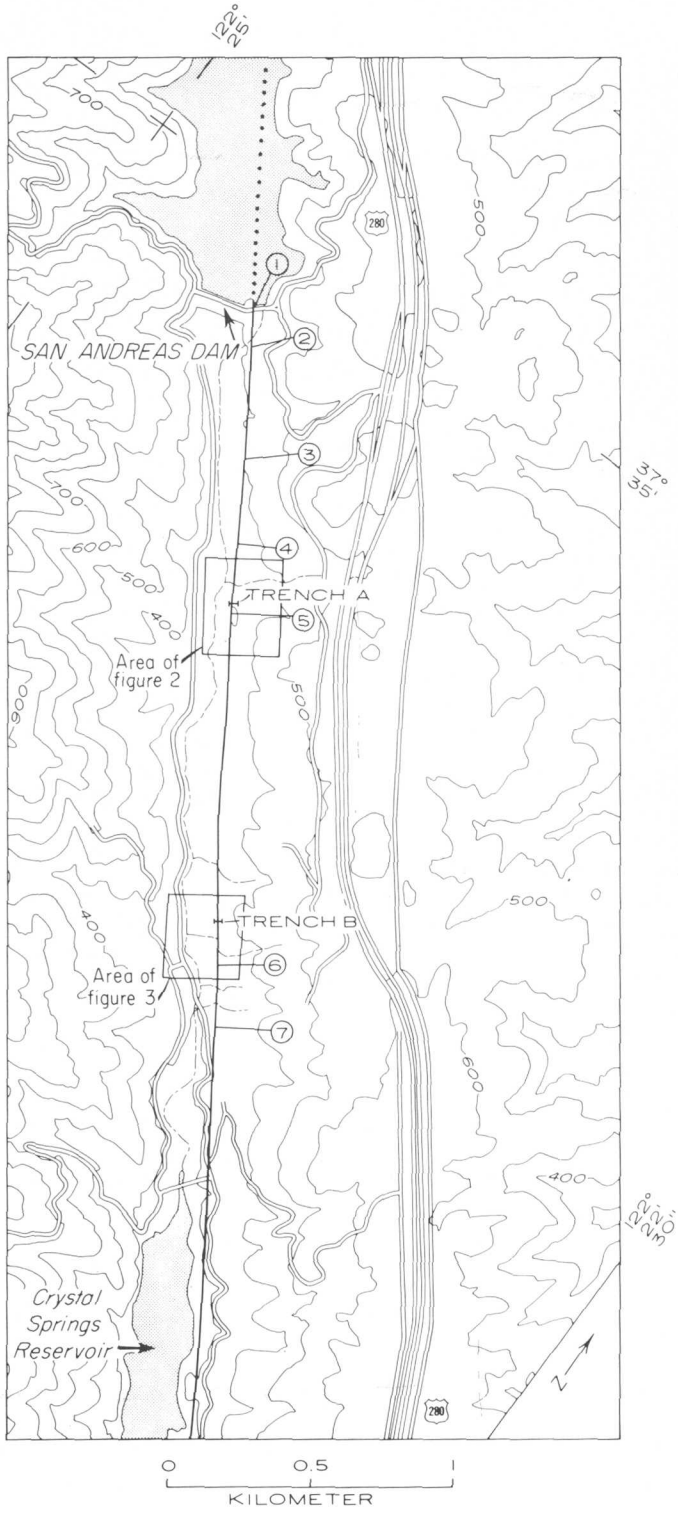

FIGURE 1.—Approximate location of 1906 trace of San Andreas fault (dotted where concealed by water), numbered localities of surface displacement in 1906, and offset streams near trench B. Base from U.S. Geological Survey 1:24 000, Montara Mountain quadrangle, 1969.

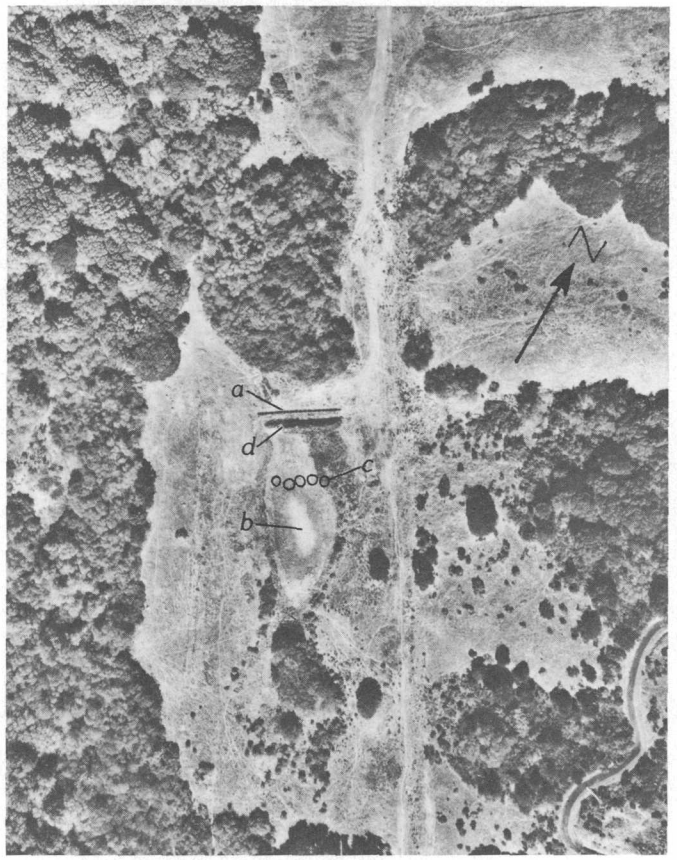

FIGURE 2.—Vertical aerial photograph showing (*a*) trench A, (*b*) adjacent fault sag, and (*c*) fence (loc. 5, fig. 1) displaced by faulting in 1906. Fence posts shown by circles. Trench (dark line) is 33 m long. Light-dark contrast in spoil pile (*d*) just southeast of trench indicates location of main strand of the fault.

was completed on September 15, mapping on November 1, and sampling, photography, and minor revisions of mapping on November 8, 1972. The mapping was interrupted by unusual early rains in mid-October as well as by work on other projects.

SAN ANDREAS FAULT

In this area the San Andreas fault is in a structurally controlled straight valley developed in rocks of the Franciscan Formation and serpentinite. Shears in the bedrock (Pampeyan, 1975), fault-related topography, and the trace of the 1906 faulting all indicate that the recently active strands are on the east side of the valley. Except for a sag pond, a few small scarps, and some rather poor examples of offset streams, the active trace of this segment of the San Andreas fault is not easy to identify, and much reliance must be placed on maps and photographs of the 1906 rupture. The 1906 trace can be closely located in relation to pre-

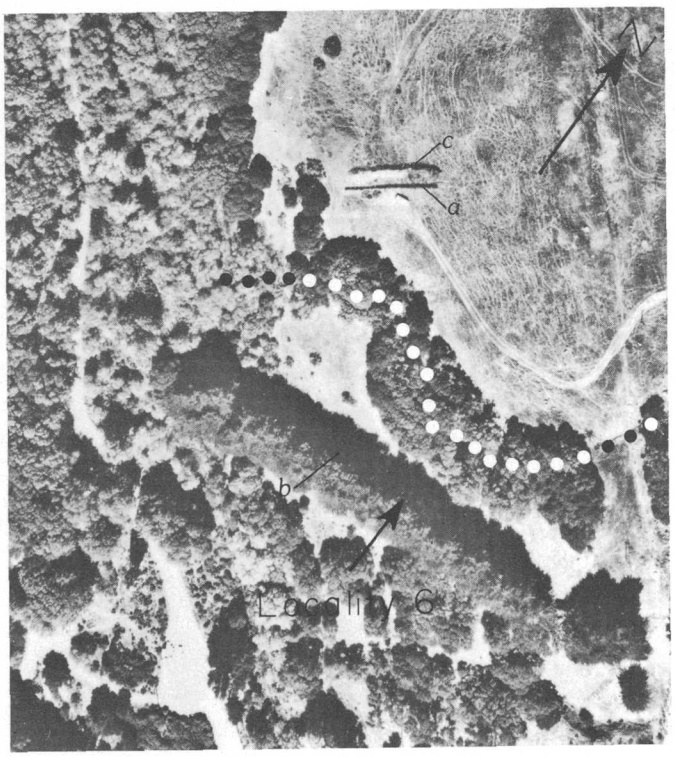

FIGURE 3.—Vertical aerial photograph showing (*a*) trench B, offset stream (indicated by series of dots), and (*b*) row of trees that conceal fence (loc. 6, fig. 1) offset by the San Andreas fault in 1906. Trench (dark line) is 37 m long. Light-dark contrast in spoil pile (*c*) immediately northwest of trench indicates location of main strand of the fault.

1906 structures that still exist, consisting of a culvert and tunnel near San Andreas Dam and fences and pipelines south of the dam. The 1906 trace trends about N. 34° W. and is slightly concave to the northeast.

Prehistoric faulting

Prehistoric surface displacements are suggested by at least four streams that turn northwestward as they approach the fault and locally flow in a direction opposite to the southeastward flow of the main stream. One of the four streams lies north of trench B, and the others lie south of it (fig. 1). Estimating the amount of offset of the streams is difficult because of the vegetational cover and because three of the streams curve gradually northward as they approach the 1906 trace. If one assumes that the gradual curve is the result of faulting distributed over a zone 40 to 70 m wide, the total offset of the streams can be estimated. The assumed width of distributed faulting is not excessive; in 1906 two fences north of the streams were distorted right-laterally over zones 75 to 200 m wide in addition to having sharp offsets at the main trace (Lawson and others, 1908, figs. 37 and 31). The estimated total fault offsets of the streams range from 60 to 80 m.

The first stream south of trench B makes a sharp bend as it approaches the 1906 trace of the fault. Assuming that the principal faulting was distributed over a zone 15 to 20 m wide, Wallace (1969, and subsequent written commun.) estimated an offset of 55 m for this stream. Horizontal displacements in 1906 were about 3 m in the vicinity of the stream. If the stream offset resulted from a series of displacements similar to 1906, about 18 shifts would be required to produce the offset.

Historic faulting

Surface faulting probably occurred in this area in 1838 as well as in 1906, but evidence of the 1838 faulting is very limited, chiefly because the San Francisco Peninsula in 1838 had very few residents who observed and recorded phenomena related to earthquakes and faulting. Nevertheless, after a careful study of the available data, Louderback (1947) could reasonably conclude that an earthquake comparable in intensity to the 1906 earthquake affected the area in 1838 and was accompanied by surface rupture on the San Andreas fault extending at least from near Santa Clara to near San Francisco.

Surface displacements that occurred on the San Andreas fault in 1906 were measured at seven localities within the area covered by figure 1. Right slip, measured at the San Andreas Dam, in a tunnel, and at pipelines and fences ranged from about 2 to 3 m at the main trace. Because inconsistent measurements of the 1906 displacements have been reported and because the report of Lawson and others (1908) shows, without explanation, more than one map of some of the displaced features, the measurements at the seven localities are discussed below from north to south.

At the San Andreas Dam (loc. 1, fig. 1) the displacement was 2.1 m, apparently measured across the zone of fractures, and 1.2 m at a point on the main break (Schussler, 1906, p. 79).

A brick tunnel (loc. 2, fig. 1) 120 m south of the dam was cut by the fault. The displacement was given as 2.1 m by Schussler, but Lawson and others (1908, p. 100) gave about 1.5 m, a figure that one also obtains by scaling on the drawing by Schussler (1906, p. 79). Although the tunnel has been repaired, a right-lateral bend is still clearly visible in it. A survey of the tunnel made in 1974 showed a misalinement of about 2.6 m between the original and repaired portions (E. H. Pampeyan, written commun., 1976); the indicated displacement resolved parallel to the fault was about 3 m distributed along some 25 m of the tunnel.

The fault intersected and displaced a fence (loc. 3, fig. 1) 515 m south of the dam. Part of this fence still exists, but the bend produced by the faulting either has been straightened or is concealed in dense brush. The report of Lawson and others (1908) contains two maps of the fence: figure 33, which is from Schussler (1906, p. 79, loc. L) and gives a strike-slip of 2.4 m, and the apparently more accurate figure 37, based on surveys by R. B. Symington, which shows 3.2 m of strike-slip distributed over a zone about 75 m wide. The strike-slip at the fault itself is about 2.7 m scaled from figure 37 of Lawson and others (1908).

About 300 m southeast of the fence the fault ruptured and telescoped the Pilarcitos pipeline (loc. 4, fig. 1). The displacement at the fault was only 0.5 m (Lawson and others, 1908, p. 100), but across a zone about 90 m wide the displacement was 2.1 m (Reid, 1910, p. 37).

The next fence (loc. 5, fig. 1) intersected by the fault is shown in both figure 34 and 38 of Lawson and others (1908). For recognition of this fact we are indebted to E. H. Pampeyan, who found the remnants of the fence and who recognized that the background of photograph 16 of Schussler (1906) is the same as the background of plate 60D of Lawson and others (1908). Those two figures, although derived from different sources, show two lines of rupture 27 m and 15 m apart, respectively, with a total displacement of about 4 m across the two strands. Figure 34 of Lawson and others, derived from a sketch by Schussler (1906, p. 79), suggests that the principal rupture was on the western strand, a conclusion seemingly reached by Lawson and others (1908, p. 100). However, figure 38, which is based on an accurate survey (Symington, 1911), clearly shows that the principal displacement was on the eastern strand. Scaling distances on figure 38 (an inexact procedure owing to the small scale and the use of two different scales in the figure) indicate that, exclusive of bends, the displacement was about 2.7 m on the eastern trace and about 0.6 m on the western trace. The scaled displacement of 2.7 m is probably more accurate than the 6 ft (1.8 m) given in the caption of plate 60D of Lawson and others. Five posts of the fence can still be found in the northern part of the sag pond immediately south of the site of trench A (fig. 2). If the straight line formed by the three easternmost posts is extended, the westernmost post is found to lie 0.74 m north of the line. This post (only a short segment of it remains) leans northward and is no doubt the same northward-leaning post whose top is visible in clear reproductions of Lawson's plate 60D. If the position of the base of the post and its inclination are taken into account, the displacement shown in plate 60D seems to be more than 1.8 m, and therefore the 2.7-m displacement mentioned above is favored.

About 1200 m farther south, the fault intersected another fence (loc. 6, fig. 1) bordered by rows of young cypress trees. The fence and the rows of trees were bent and displaced 2.7 m. A sketch of the offset fence is in Schussler (1906, p. 79) and in Lawson and others (1908, fig. 32). The latter report also shows a photograph (pl. 61B) of the fence and trees; the same photograph, but with a wider view, is shown by Taliaferro (1951, p. 148). The fence and the trees still exist 130 m south of the site of trench B (fig. 3). Although the fence has been modified somewhat since 1906, the 2.7 m of misalinement can still be measured.

About 210 m southeast of this fence, the fault encountered the Locks Creek pipeline (loc. 7, fig. 1), which was telescoped and shifted parallel to the fault. Schussler (1906, p. 79) stated that the movement was 2.4 m parallel to the fault; Robert Anderson (in Lawson and others, 1908, p. 101) concluded that the shift was about 3 m within 90 to 150 m of the fault, and Reid (1910, p. 37) calculated a shift 3.6 m parallel to the fault and distributed over a wide zone. Pipeline damage (such as at localities 4 and 7, fig. 1) is less reliable than fence damage as an indicator of width of the zone of faulting, because rigid pipe can transmit stresses over long distances.

DESCRIPTION OF UNITS MAPPED IN TRENCHES

After excavation by backhoe and shoring of the trench, the north wall was cleaned to get a fresh surface. The map units were then chosen, the contacts marked by nails, and the positions of the nails measured to the nearest 10 mm by using an x-y coordinate system. Mapping was generally done at a scale of 10 mm to 1 m with a plotting accuracy of about ± 25 mm, but larger mapping scales were used where greater detail was needed. In the following sections, reference to points in the trench diagrams (figs. 4 and 5) are given in meters for the x (horizontal) and y (vertical) coordinates, in that order, separated by a comma as in this example: (2.3,5.7). The mapping units are arbitrarily lettered, and the description generally proceeds from southwest to northeast in each trench.

Trench A

Unit	*Description*
A	Greenish-gray serpentinite; 95 percent consists of fractured and sheared matrix, and the remainder is subangular fragments of serpentinite up to 400 mm in diameter. Larger fragments of serpentinite protrude from soil west of trench.

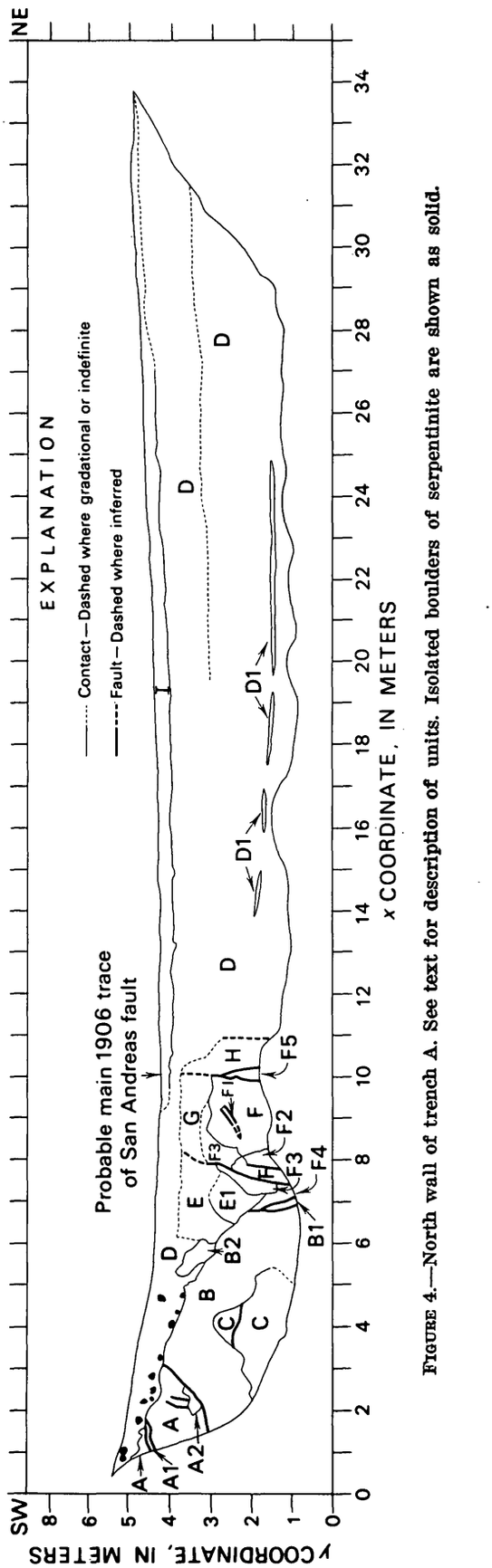

FIGURE 4.—North wall of trench A. See text for description of units. Isolated boulders of serpentinite are shown as solid.

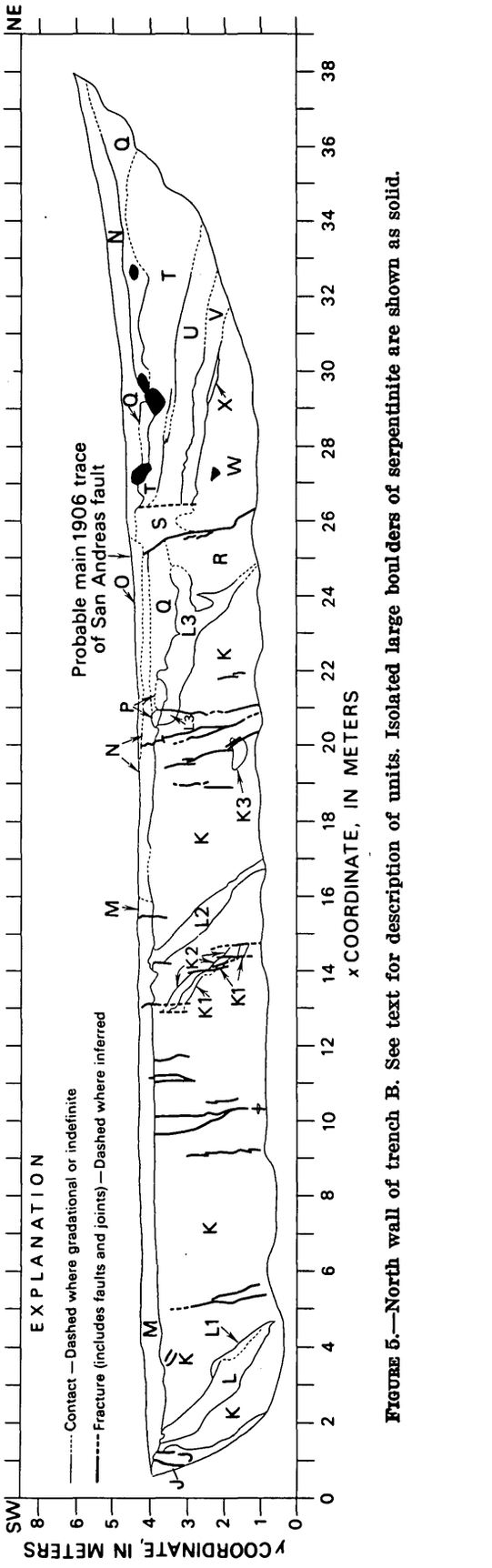

FIGURE 5.—North wall of trench B. See text for description of units. Isolated large boulders of serpentinite are shown as solid.

Unit	*Description*
A1	Green, brown, and black clay gouge, 80 to 130 mm thick.
A2	Brown, gray, and red clay. Contains scattered small (1 mm) rounded pieces of serpentinite.
B	Olive-gray greenstone, Franciscan Formation; ranges from granular to claylike consistency; largest intact fragments 300 mm in diameter; median size of visible fragments estimated to be 5–10 mm.
B1	Moderate olive brown plastic clay. Contains many small (2–3 mm) angular fragments of greenstone.
B2	Angular to subangular fragments of hard vesicular grayish-olive fine-grained volcanic rock, probably not Franciscan Formation, and rare subrounded serpentinite pieces, generally separated by dark-gray clayey silt and irregular large masses of light-olive-gray to dark-yellowish-orange clay. Rock fragments 50 to 150 mm in largest dimension.
C	Dark-greenish-gray fine-grained greenstone, Franciscan Formation; has curved parting surfaces with no obvious preferred orientation. Unit C is conspicuously more intact than unit B and is crossed by a 5- to 40-mm-thick zone of crushed sand- to clay-size greenstone striking N. 10° E. and dipping 10° E.
D	Medium-gray to grayish-black gravelly clayey silt. Gravel 40 percent (estimated), consists of Franciscan sandstone, red chert, greenstone, and serpentinite, listed in order of decreasing abundance within the whole unit. From about $x=6$ westward, serpentinite ranks second in abundance and ranges up to boulder size. No zonation, peds, or other soil structures were seen. Stratification is generally not apparent, but a difference in color was visible above (medium dark gray) and below (dark gray to grayish black) the dashed line shown on figure 4 extending eastward from $x=19.5$. The differences in color and composition noted above coupled with the variation in thickness suggest that this is a composite deposit, but further subdivision was not practical except for unit D1. All of unit D is probably older than 1906.
D1	Moderate-reddish-brown gravelly, clayey, moderately permeable sand. Pebbles are subangular, nearly all of Franciscan sandstone and a minor amount of chert. This unit, a discontinuous layer, constituted the most distinct stratification in unit D. Unit D1 was distinguishable from $x=14$ to about $x=25$. The trench walls caved below unit D1, a fact indicating that unit D is less cohesive or more sandy below D1 than above it.
E	Dark-gray silty clay. Contains angular fragments of Franciscan sandstone (some weathered and soft), red chert, greenstone, and serpentinite, listed in decreasing order of abundance. Median grain size of fragments estimated at 3 mm and maximum generally 15 mm; however, one rounded cobble 100 mm in diameter of hard fine-grained Franciscan(?) sandstone and one subangular cobble 150 mm in diameter of moderately weathered serpentinite were seen.
E1	Similar to unit E but less silty, more plastic, and contains very few rock fragments The lowest 400 mm to 500 mm is grayish black.
F	Mixture of dark-yellowish-orange clay and angular fragments of weathered Franciscan(?) sandstone. Proportion of sandstone ranges from 10 to 90 percent.
F1	Light-olive-gray sheared clay. Contains rock fragments less than 3 mm in diameter that seem to be Franciscan sandstone. Attitude obscure because outcrop is poor but is about N. 45° E., 35° NW. Pinches out to west; eastern termination concealed by timber supports.
F2	Mottled medium-gray and dusky-yellow plastic clay. Contains scattered subangular polished (by shearing) fragments as large as 15 mm diameter of rather soft very fine grained Franciscan(?) sandstone. West boundary zone (contact with unit F) has many nearly vertical polished surfaces.
F3	Medium-gray plastic clay. Contains small masses and streaks of dark-yellowish-orange weathered Franciscan(?) sandstone and a few rather fresh pieces of the same sandstone. Also contains a 5- to 8-mm-thick layer of grayish-black plastic clay, possibly derived from an overlying unit, whose attiude is N. 35° W., 45° SW. Black clay splays out upward at (7.9,2.8) and disappears.
F4	Medium-gray highly plastic clay. Contains scattered subangular fragments as much as 30 mm long of very fine grained Franciscan(?) siltstone.
F5	Dark-yellowish-brown silty sandy clay. Contains three angular fragments of serpentinite 90–150 mm in largest dimension and one subangular piece of dark-yellowish-orange fine-grained Franciscan (?) sandstone 80 mm in diameter.
G	Light-olive-gray to dark-gray clay. Contains a few subangular pieces (up to 70 mm) of serpentinite, a few angular to subangular pieces (up to 120 mm) of sandstone similar to that in unit F, and rare angular pieces of red chert. Contact with underlying unit F3 is very obscure east of $x=8.1$. Contact with unit H is obscure but seems to be a vertical fault.
H	Olive-gray silty clay. Contains scattered angular to subangular pieces (up to 40 mm) of serpentinite and rare pieces of very fine grained Franciscan(?) sandstone.
I	Friable gravelly silty sand, medium-light-gray (dry) to brownish-gray (damp). Contains abundant angular to subangular rock fragments whose median diameter is estimated to be 3 mm but whose maximum is as much as 25 mm. Fragments estimated to be 45 percent red chert; 45 percent Franciscan sandstone (slightly to highly weathered), siltstone, and shale; and 10 percent or less Franciscan greenstone and weathered serpentinite(?). Generally massive, but locally has indistinct nearly horizontal bedding. Generally has sharp contact with underlying unit. Near east end of trench, contains organic debris in various states of decay.

Trench B

Unit	*Description*
J	Moderate-yellowish-brown very firm to friable tuffaceous Franciscan greenstone. Consists of angular to subangular fragments (up to 150 mm) in a matrix of sand- to clay-size fragments.
K	Firm to friable closely jointed siltstone, very fine grained sandstone and mudstone, yellowish gray at top grading to medium gray at bottom of trench; contains poorly preserved mollusk shells and a few limestone nodules. Bedding not clearly defined, but strike is about N. 35° W. and dip ranges from about 35° to 50° NE. Merced(?) Formation.

Unit — *Description*

K1--Hard highly fractured grayish-orange sandstone. Merced(?) Formation.

K2--Friable moderately fractured light-gray noncalcareous sandstone. Merced(?) Formation.

K3--Hard fractured calcareous sandstone, mostly pale yellowish brown but grayish orange on joint faces. A small piece lies to the east (20.1,1.7), separated from the main block by mudstone of unit K that is bounded by fractures with no apparent slickensides. Merced(?) Formation.

L--Medium-dark-gray to yellowish-gray tough compact clay. Contains scattered angular to subangular pieces (up to 70 mm) of Franciscan(?) sandstone. Corners of some of the sandstone pieces are rounded by shearing.

L1--Same as L, but also contains scattered rounded pieces (up to 18 mm) of white very soft fine-grained calcareous sandstone or sandy limestone. Has laminations parallel to bedding in unit K immediately to east (N. 35° W., 50° NE.) and many approximately horizontal striations on slickensided surfaces with that attitude.

L2--Light-gray to black tough hard (dry) clay. Contains a few streamlined pieces (as long as 50 mm) of hard Franciscan(?) sandstone, scattered rounded pieces (as much as 10 mm in diameter) of calcareous friable white sandstone similar to the white sandstone in unit L1, and rare angular to subrounded pieces (as large as 100 mm) or irregular masses of white friable noncalcareous nontuffaceous sandstone. Attitude of top of unit is N. 47° W., 63° NE. at (16.2,2.0) and N. 25° W., 50° NE. at (15.3, 3.0).

L3--A varied unit consisting of gray to white sandstone, massive but randomly slickensided medium-gray clay, and clay that is generally dark gray to black but streaked with white. The streaked clay contains a few subangular pieces (up to 100 mm) of greenstone, apparently not tuffaceous, that have had their corners rounded by shearing. The streaks in the clay are generally inclined eastward approximately parallel to the base of the unit.

M--Surface soil. Dark-yellowish-brown silty clay. Has no conspicuous columns or other soil structure but locally is granular. Contains angular to subangular moderately fresh rock fragments, mostly Franciscan(?) sandstone but also some tuffaceous greenstone and rare chert.

N--Surface soil. Hard (dry) medium-dark-gray silty clay; moderately jointed (nearly vertical joints are about 50 mm apart and nearly horizontal irregular joints are 20–100 mm apart). Contains angular rock fragments as large as 80 mm, mostly of hard Franciscan sandstone, but a few are hard nontuffaceous greenstone. Contact with soil to west (unit M) is moderately sharp at grassroot level and less clear near base of soil. No fault found in fractured mudstone of unit K below this soil contact.

O--Artificial fill. Very similar in color and composition to unit N but has a subtle structure and jointing that are nearly horizontal except at east end where they turn abruptly upward parallel to basal contact. This fill is part of a road made in connection with construction of a pipeline in 1967. Part of this road is visible in figure 3 north of the trench.

P--Medium-greenish-gray plastic (damp) clay. Has many slickensided surfaces that seem to have a nearly random orientation—strikes range from north-south to east-west, dips range from 20° to 70° inclined in various directions; nearly all grooves and striae indicate dip-slip movement. The most prominent surfaces strike approximately parallel to the trench and dip toward it at about 45°; their prominence probably results from slight gravity movements and desiccation after excavation of the trench. Streaks of dark topsoil extend irregularly downward into this unit. One such dark zone coincides with an inconspicuous fault that seems to displace the bottom contact of the unit 30 mm, east side apparently up.

Q--Silty clay. Has an indefinite and gradational contact with unit N. Color grades from dark gray at top to light olive gray at base; gradation is by interfingering of streaks and zones of the two colors. No conspicuous jointing. Contains large boulders of serpentinite.

R--Moderate-yellowish-brown silty to sandy clay containing scattered rounded and polished grains of aphanitic rock as much as 3 mm in diameter. No bedding or other structures visible.

S--Grayish-black grading downward to dusky-brown very silty clay. Contains some subangular to angular pieces (as large as 50 mm) of serpentinite and rare pieces of yellow and green chert. Difficult to distinguish from unit N.

T--Medium-gray clay. Contains scattered subangular boulders of serpentinite. From about $x=26.5$ to $x=27.5$, black streaks extend downward into this unit from unit N.

U--Similar to unit T but dark gray; contains rare pieces of sheared shale as well as serpentinite boulders. Contact between units T and U is a sharp thin line in most places, possibly the base of a landslide or a shear surface within a landslide. To the east of $x=30.5$, unit U is lighter in color (medium dark gray) and less distinct from unit T, but the contact is marked by a streaked light-gray zone (apparently also clay) 5 to 15 mm thick.

V--Similar to unit T but without black streaks. The contact between unit S and units T, U, and V was obscured by timber supports on the north wall but is clearly nearly vertical. In the south wall, the apparent dip was 82° W., and serpentinite boulders seem to be more common at the contact than elsewhere in the unit.

W--Clay with scattered polished subangular to rounded rock fragments ranging in size from ½ mm to hundreds of millimeters. Clay is grayish black to dark gray and locally brownish black.

X--Medium-gray silty sandy clay. Contains small angular fragments of Franciscan(?) sandstone.

SUBSURFACE EXPRESSION OF FAULTING

The visibility in the trenches of evidence for faulting ranged from very high to very low. Most conspicuous was a color difference that appeared in each trench as excavation proceeded—a difference that was also evident in the spoil piles (see figs. 2 and 3). The color differences reflected lithologic variations. In trench A, the difference was between the dark alluvial

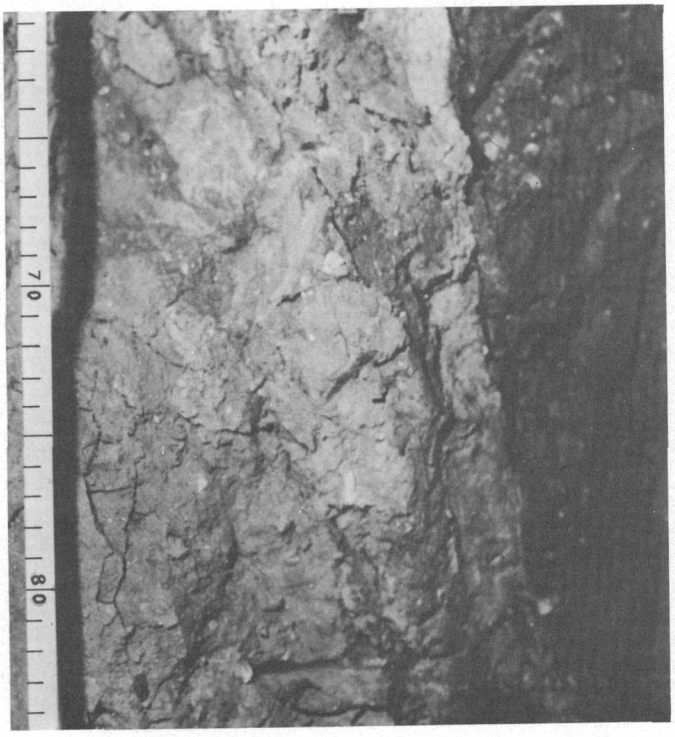

FIGURE 6.—Most conspicuous strand of the San Andreas fault visible in trench B and probably the principal locus of displacement in 1906. Note inclusions of the dark clay (unit W) in the light clay (unit R). Divisions on the tape, which is at x=25.5, are 10 mm apart. Center of photograph is at y=2.8.

deposits on the east and the lighter colored serpentinite, Franciscan rocks, and clay on the west. In trench B, the dark colluvial and landslide deposits on the east contrasted with the light-colored Merced(?) Formation and other materials on the west (fig. 6). The characteristics of the faults, probable faults, and joints that were seen in the two trenches are summarized in table 1.

The steepness of the contact between units D and E near (6.1,3.5) in trench A suggests a fault, but it probably is not because no fracture was found in unit B beneath it. However, a fault might not be visible in that unit because of its broken condition, or if the fault were highly irregular, it might pass east of unit B.

Evidence of shearing

Fault gouge and material resembling it occur as more or less tabular bodies whose attitudes are quite divergent. All the material here referred to as gouge consists predominantly of clay-size particles, but generally one could not tell whether it resulted from fault comminution of rock or merely from fault deformation of preexisting clays. Some of the gouge is in narrow zones along identifiable faults, and some is in comparatively thick irregular bodies. The serpentinite in trench A is traversed at (1.5,4.5) by a prominent zone of green, brown, and black gouge, 80–150 mm thick, oriented N. 70° E., 10° S. (unit A1). Unit A2 is probably gouge also, and the two short faults extending upward from unit A2 near (2.2,3.7) have a brown selvage, as much as 5 mm thick, that is assumed to be gouge. Unit B1, which strikes N. 45° W., is probably gouge; unit F1, oriented N. 45° E., 35° NW., and unit F5 are also believed to be fault gouge. The streaked contact zone near (25.7,2.7) in trench B, already described, probably contains both fault gouge and fault-deformed preexisting clay.

Granulation and crushing noted in the description of units B and C of trench A probably resulted from tectonic transport of those units along the San Andreas fault.

Rounding and polishing of pebbles and rock fragments have been mentioned in the descriptions of units A and F2 of trench A and units L, L2, L3, R, and W of trench B. These effects appear to have resulted from shearing, some of which is probably related to landsliding as well as faulting.

Slickensides were not common in the trenches but were noted in a few places. The contact zone between units F and F2, near x=7.8 in trench A, has numerous nearly vertical polished surfaces and is probably a fault. The other slickensides were all seen in trench B. Unit L1 has nearly horizontal striae on slickensided surfaces oriented about N. 35° W., 50° E., as does the basal contact of unit L. Unit P has slickensided surfaces with divergent orientations but, oddly, the grooves and striae all seem to be parallel to the dip direction of the surfaces. Some of the clay in unit L3 also has randomly oriented slickensides, but the trends of the striae were not recorded.

Caving and seepage

Neither caving of the trench walls nor seepage of ground water were reliable indicators of the location of faults. Caving occurred in the lower part of trench A from about x=7.5 to x=11, which includes the zone of prominent faulting, but it also extended eastward from there to x=17. In excavating trench B, the walls in the western 11 m of its length were left unsupported for a few hours. During this period, caving affected only the lower two-thirds of the south wall from about x=6 to x=9, a part of the trench that was unusually free of continuous joints and faults. Although the sag pond just south of trench A was completely dry at the surface, water began to appear about 10 minutes

TABLE 1.—*Faults and joints exposed in the trenches*

Coordinates of midpoint	Characteristics
Trench A	
1.4,4.6	Fault, upper contact of unit A1.
1.4,4.4	Fault, lower contact of unit A1.
2.1,3.8	Near-vertical fault; brown fault gouge as much as 5 mm thick along it.
2.3,3.7	Do.
2.5,3.5	Fault contact between units A and B; strike N.55° W., dip 25° W.
4.0,2.3	Zone 5-40 mm thick of crushed sand- to clay-size greenstone, strike N.10° E., dip 10° E., within unit C.
6.8,1.5	Fault, eastern boundary of unit B; strike about N.45° W.
6.9,1.3	Fault contact between units B1 and F4.
7.7,2.4	Fault offsets unit F3 and forms boundary between several units. In unit F3, marked by a 5-8mm-thick layer of grayish-black plastic clay that strikes N.35° W. and dips 45° SW. Above y=2.8, dark layer splays out into subparallel streaks. Forms indistinct contact between units E and G; not visible in unit D.
7.8,1.7	Probable fault with near-vertical polished surfaces forms part of contact between units F and F2.
8.9,2.5	Fault, upper contact of unit F1.
8.9,2.4	Fault, lower contact of unit F1.
10.0,2.9	Fault, upper part barely discernible; lower part, which bifurcates, clearly defined. Forms boundary between units.
10.9,2.2	Inferred fault forms near-vertical part of obscure contact between units H and D. No other evidence of faulting visible.
Trench B	
0.9,3.5	Fault in greenstone coincident with 50 mm step (lower on west) in surface of greenstone.
1.2,3.5	Fault in greenstone coincident with a step of about 80 mm (lower on east) in surface of greenstone; whether step formed before of after deposition of overlying sediments was not apparent.
3.7,3.3	Shear surface at bottom of fractured nodule of limestone; strike N.10° E., dip 20° E.
3.8,3.4	Shear surface at top of fractured nodule of limestone; strike N.-S., dip 30° E.
5.2,2.0	Fault or joint; no gouge or obvious slickensides. At one point strike is N.65° W., dip 75° N., but attitude varies from place to place.
5.4,1.6	Fault or joint; no gouge or obvious slickensides.
9.1,2.0	Set of nearly vertical fractures striking N.36° W. Has zone of alteration, perhaps partly fault gouge, 1-10 mm thick along walls; no slickensides found.
9.7,2.9	Fracture extends upward at least to base of unit M; joins another fracture downward.
10.1,2.2	Near-vertical fracture, strike N.30-55° W., crosses a flat-lying irregular concretion of calcium carbonate (10.3,1.0) without measurable separation of top or bottom. Lack of visible separation or difference in size across fracture indicates that neither strike-slip nor dip-slip of megascopic dimensions has occurred since formation of concretion. Walls of fracture have been altered, probably by weathering, to maximum depth of 5 mm; no slickensides were found. Extends at least to base of unit M.
10.5,2.0	Vertical fracture striking N.35° W. with wall alteration as much as 10 mm thick could not be traced vertically beyond limits shown on figure 5.
11.0,3.4	Fracture, no alteration or slickensides, dies out downward.
11.2,3.5	Fracture, no alteration or slickensides, dies out downward but extends short distance into modern soil, unit M.
11.6,3.5	Fracture, no alteration or slickensides, dies out downward.
12.8,3.3	Inferred fault; concealed by timber set.
13.1,3.5	Joint, open above y=3.5 and closed below that point.

TABLE 1.—*Faults and joints exposed in the trenches*—Continued

Coordinates of midpoint	Characteristics
Trench B (Cont.)	
14.0,2.4	Fault; displaces units K1 and K2; vertical separation 0.2-0.3 m.
14.2,3.7	Joint, dies out upward and downward.
14.3,1.7	Fault, dips eastward.
14.4,1.6	Fault, displaces units K1 and K2.
14.7,1.6	Fault, terminates units K1 and K2 on east.
15.5,4.0	Joint, strike N.15° E. (varies), near-vertical dip. Traced 0.8 m downward from ground surface.
18.9,2.2	Fracture, strike N.80° W., vertical. No alteration or slickensides visible.
19.0,2.8	Fracture, strike N.15° W., vertical. No alteration or slickensides visible.
19.8,2.3	Set of faults cuts and displaces unit K3. Faulting must have included a strike-slip component to account for different thicknesses of displaced parts of unit K3. At (19.9,2.0) strike is N.70° W., dip 87° N. In places as many as four parallel fractures occur in a width of 10 mm, but no slickensides were seen. Set of faults terminates upward a short distance below base of soil (unit N).
20.3,2.5	Joint or fault; strike N.53° W., dip 74° NE.
20.3,3.0	Joint or fault, joins fracture described above. Extends into soil (unit N) as a crack 5 mm wide but apparently does not displace base of soil.
20.9,2.4	Inconspicuous near-vertical fault; apparently produced a vertical separation of about 30 mm (east side higher) of base of unit P at (21.0,3.7). Because an equivalent separation of base of unit L3 is absent, displacement was probably primarily strike-slip.
21.9,1.8	Two small fractures with wall alteration about 10 mm thick. Could not be traced to bottom or top of trench.
25.7,2.7	Conspicuous fault forms contact between several units. Major part of contact is a zone in which contrasting colors of adjacent units are streaked and smeared together. At y=3.0, contact strikes N.50° W., dips 82° NE. Juxtaposes modern soil (unit N) and unit S at (25.2,4.2); base of unit N is higher east of fault than it is to the west.
26.5,3.5	Probable fault. Units T, U, and V terminate along this line and a small color difference in unit W (brownish black on west and dark gray on east) below the near-vertical eastern contact of unit S also suggests that a discontinuity extends downward into unit W.

after excavation of the western part of the trench. It came from the lower part of unit B and the other units from about x=5.5 to x=7.5. As trenching proceeded eastward, water seeped from unit H and the lower part of unit D east of x=10.9, and intermittent pumping was necessary for the rest of the time that the trench was open. In trench B, the ground was moist in the lower part of the east end, but no standing water accumulated. In summary, although caving in trench A occurred in the area of prominent faults, it also occurred in both trenches in areas that displayed no faults, and most of the ground-water seepage in trench A came from the unfaulted eastern part.

1906 trace

The principal displacement in 1906 at the site of trench A probably occurred on the fault that nearly reaches the surface at x=10. The eastern contacts of units F and F5 (near x=10) are faults. They separate units of different colors; in places the contacts are as

sharp as a knife edge and in other places they consist of a zone of streaked mixing of the contrasting colors approximately parallel to the contact. These faults join upward and could be seen in the trench wall as one clearly defined fault as far as the upper boundary of unit F (at 10.0,3.0), although this is not apparent in the photograph (fig. 7). Above that point, this fault

FIGURE 7.—North wall of trench A. The 1906 fault rupture was probably at $x=10$, near the white tape. Light-colored material is part of unit F. Tape is 6 mm wide.

was barely discernible as the contact between the closely similar units G and H. The fault was not seen in unit D, in unit I, or at the contact between them despite a long and careful search. The lower contact of unit D in that area is gradational and was very hard to identify, but the lower contact of unit I was clearly visible. Unit I, however, is probably related to the construction in 1967 of the pipeline, whose traces can be seen in figure 2, about 20 m east of the trench. In the eastern part of the trench, the unit contains organic matter in various states of decay, and the uneven ground surface indicates artificial grading. Unit I could not be positively identified in shallow test holes dug east of the trench, but 5 m east of the trench, a brown sand that may be its equivalent overlies 50 mm of gray clay that is probably fill, and artificial fill extends to a depth of at least 0.4 m from the surface at points 10 m and 14.4 m east of the trench. Unit I is interpreted as very young alluvium derived from the spoil pile and backfill of the pipeline that was constructed in 1967. Thus, despite the unfaulted condition of unit I, the principal displacement of 1906 is inferred to have occurred on the fault at $x=10$, because it is the most conspicuous in the trench, it could be traced as close to the surface as any other, and it is in the proper place in relation to the 1906 offset in the fence just south of the trench.

The principal displacement in 1906 at the site of trench B probably occurred on the fault that juxtaposes units N and S at (25.2,4.2). It was easily traced to the bottom of the trench because the moderate-yellowish-brown color of unit R contrasts well with the much darker colors of units S and W. The fault contact between unit R and the two units to the east was marked by a zone, 150 to 300 mm wide, in which the contrasting colors were streaked and smeared together (fig. 6) in the same way as the eastern contacts of units F and F5 in trench A. The attitude of the streaks at $y=3.0$ is N. 75° W., 77° N., and the attitude of the contact at the same elevation is N. 50° W., 82° NE. This attitude differs somewhat from the strike of the San Andreas fault in this vicinity (about N. 37° W.) inferred from geomorphic evidence. The principal displacement of 1906 is inferred to have occurred along the fault just described because it could be traced the full depth of the trench, it is the most conspicuous, has the greatest lithologic contrasts across it, and is the only one that displaced the base of the modern soil.

DISCUSSION

The evidence clearly indicates that an important zone of faults was crossed by the trenches and that some of the faults have had geologically recent displacement. Although no large fragments of wood suitable for radiocarbon dating were found, an age undoubtedly could have been determined from disseminated carbon in some of the deposits (such as unit N), but this was not attempted because of the known historic surface displacement on the fault. Even without radiocarbon dates or historic offset, one could infer recent fault movement because of the displacement of the surface soil in trench B and displacement of young alluvial deposits in both trenches.

The principal zone of displacement in 1906 was not identified as such solely from the evidence seen in the trenches but has been inferred on the basis of data from the trenches, from the surface morphology, and from the historical record. Presumably the 1838 faulting and some of the numerous displacements that have offset the streams in the vicinity occurred along the same faults that moved in 1906, but we have no proof of that.

The zone of young faults found in trench A is rather narrow; its width is commensurate with the 1906 faulting, except for the subsidiary rupture. The alluvial deposits east of $x=11$ do not seem to be traversed by faults. The steeply dipping faults, which are

the most likely to be related to recent movements on the San Andreas fault, were limited to the sector between $x=6.7$ and $x=11$, and within this group the two faults that can be traced to within 1 m of the surface are only 2 m apart. The width of the main rupture in 1906 at the trench site is not known, but judging from the published photograph (Lawson and others, 1908, pl. 60D) and its location with respect to the topography and the remnants of the offset fence, it was only a few meters wide. The subsidiary rupture with about 0.6 m of right slip that lay somewhere between 15 and 27 m west of the main rupture was too far west to be crossed by the trench.

The 1906 zone of surface rupture was apparently wider near trench B than it was near trench A. Neither the published map nor the photograph of the fence at locality 6 permits a quantitative measurement, but the photograph shows that the zone was wider than at locality 5. The present zone of misalinement of the fence and of offset of the stream north of it is about 20 m wide measured perpendicularly to the fault, but the 1906 rupture zone was probably narrower. The 1906 rupture very likely was centered on the fault at $x=25.7$ in trench B and may have extended to the probable fault at $x=26.5$. Small displacements also could have occurred near the ground surface in the vicinity of $x=20$ and perhaps $x=13$.

Four of the units in trench B (L, L1, L2, and L3) that resemble fault gouge are interpreted to have been emplaced as landslides during deposition of the Merced(?) Formation. These units are predominantly clay containing rock fragments apparently rounded to some extent by shearing. A landslide emplacement of material that was largely gouge is favored because the units and the laminations in them have a low dip, are oriented nearly parallel to bedding in the enclosing Merced(?) Formation (unit K), and at least two and perhaps three of them pinch out downdip within the Merced(?). The slickensides in unit L1 and at the base of unit L, as well as the thumblike eastward projection of unit L3, probably formed later as the result of stresses related to the San Andreas fault.

Other irregular masses occurred in addition to the "thumb" of unit L3. Examples are units R, S, B2, E1, and F1 through F5. Some of these units have already been classed as fault gouge, and the others probably represent materials that have been deformed to a lesser extent. The rock fragments in units F through F4 are of sandstone or siltstone inferred to be from the Franciscan Formation; the color of the units also resembles fresh to weathered Franciscan sedimentary rock. Units F through F4 probably were derived from a body of Franciscan rock (and perhaps a small amount of alluvium) that has been broken, sheared, and transported by faulting; some minor deformation under the force of gravity probably occurred also. The other iregular units besides units F through F4 may have had a similar origin.

The relative vertical movements suggested by the sag pond and serpentinite ridge near trench A can also be inferred from the sediments in the trench walls. The upward concavity of unit D1, which very likely was originally planar, suggests postdepositional downward movement slightly east of the lowest part of the present ground surface. It also suggests that the sag did not form by simple tilting or downdropping of a graben block but that folding played a role. Fragments of Franciscan sandstone and chert were found a short distance below the ground surface (near 1.7,4.65) in unit D. These rock types are not found in the serpentinite ridge west of the trench but are characteristic of the ridge east of the fault. The fragments were found as much as 0.4 m above the level of the ground surface that lies to the east. Considering that they were very likely transported from a source to the east, a relative vertical movement of at least 0.4 m between the serpentinite ridge and the fault sag to the east has probably occurred. What role was played by strike-slip in producing the relative vertical movement is unknown.

Some relations in the trenches indicate that care should be used in reaching conclusions about the age of most recent faulting. The last displacement on the faults at (8.2,3.7) and (10.0,3.7) in trench A might be inferred to be older than unit D, but such an inference is tenuous considering the invisibility of the 1906 rupture, which crossed unit D, probably at $x=10$. The moderately sharp and steep contact between two contrasting surface soils (units M and N, at 15.9,4.1) in trench B, if it were over a fault, would probably be considered evidence for very young displacement; however, no fault at all was found below that contact.

Assuming that another large displacement of the fault will occur in the not-too-distant future, monuments were installed at the trenches so that the future ruptures can be related to the faults and other structures mapped in the trenches. The monuments are brass disks, 97 mm in diameter, attached to galvanized steel pipes, 19 mm in diameter, driven into the ground. The words "U.S. Department of Interior Geological Survey National Center for Earthquake Research Menlo Park, Calif." are cast in the disks. One is stamped "Trench A" and the other "Trench B," and both are stamped "West End S.F.W.D." The monuments are on the trench centerlines; the one at trench A is set flush with the ground at $x=0.3\pm0.2$, and the one at trench B is about 150 mm below the ground surface at $x=0.1\pm0.2$.

REFERENCES CITED

Brabb, E. E., and Pampeyan, E. H., 1972, Preliminary geologic map of San Mateo County, California: U.S. Geol. Survey Misc. Field Studies Map MF–328, scale 1:62 500.

Lawson, A. C., and others, 1908, The California earthquake of April 18, 1906, Report of the State Earthquake Investigation Commission: Carnegie Inst. Washington Pub. 87, v. 1, 451 p.

Louderback, G. D., 1947, Central California earthquakes of the 1830's: Seismol. Soc. America Bull., v. 37, no. 1, p. 33–74.

Pampeyan, E. H., 1975, Geologic map of the San Andreas fault zone in San Andreas Lake, San Mateo County, California: U.S. Geol. Survey Misc. Field Studies Map MF–652, scale 1:6 000.

Reid, H. F., 1910, The mechanics of the earthquake, Volume 2 *of* The California earthquake of April 18, 1906, Report of the State Earthquake Investigation Commission: Carnegie Inst. Washington Pub. 87, v. 2, 192 p.

Schussler, Hermann, 1906, The water supply of San Francisco, California, before, during and after the earthquake of April 18th, 1906, and the subsequent conflagration: New York, Martin Brown Press, 103 p.

Symington, R. B., 1911, A boundary line deflection: Seismol. Soc. America Bull., v. 1, no. 2, p. 85, 1911.

Taliaferro, N. L., 1951, Geology of the San Francisco Bay counties: California Div. Mines Bull. 154, p. 117–150.

Wallace, R. E., 1969, Planning along active strands of the San Andreas fault: Assoc. Eng. Geologists Natl. Mtg., San Francisco, 1969, Field Trips [Guidebook], p. E5–E6.

Jour. Research U.S. Geol. Survey
Vol. 6, No. 3, May–June 1978, p. 359–367

STRUCTURAL CONTROL OF THE CUMBERLAND RIVER AND ITS ANCESTRAL CHANNELS AT FLAT LICK, KENTUCKY

By WAYNE L. NEWELL and DUDLEY D. RICE,
Reston, Va., Denver, Colo.

Prepared in cooperation with the Kentucky Geological Survey

Abstract.—Remnants of old alluvium on bedrock benches, as much as 76 m (250 ft) above the present course of the Cumberland River near Flat Lick, Ky., are associated with meander scars and broad valleys now occupied by underfit streams. The distribution of old alluvium and associated topographic features define two ancestral channels of the Cumberland River. The ancestral channels and the present river channel are superimposed on the crest and flanks of the Flat Lick anticline. All three channels trend westward, roughly parallel to the axis of the anticline. The oldest channel is on the north flank, the second oldest channel is superimposed on the crest, and the modern channel is entrenched in the south-dipping limb of the fold. The sequential pattern of channel downcutting and migration across the crest of the anticline can be explained in terms of structural and lithologic constraints upon fluvial processes without recourse to contemporaneous tectonism. The Flat Lick area apparently has not experienced major deformation during the erosional history interpreted from the surficial geology. Direct evidence for the age of the old alluvium has not been found. However, an estimate based on erosion rates suggests that the ancestral channels could have been established and abandoned as recently as one-half million years ago.

Extensive deposits of alluvium, from which past events in the evolution of drainage systems can be interpreted, are rare throughout the rugged terrain of eastern Kentucky. Rivers and creeks draining the Cumberland Plateau generally flow through sinuous ravines having narrow flood plains. Isolated gravel terraces capping benches as much as 100 m (300 ft) above modern river beds are all that remain of bygone valley bottoms. The scattered patches of old alluvium are so randomly preserved that any systematic study of drainage history is a discouraging prospect. However, some localities, such as the valley of the Cumberland River at Flat Lick, Ky., do contain abundant evidence of earlier river channels, facilitating at least a detailed study of fluvial processes and their history of interaction with the bedrock and former landscapes.

Regionally, the scant distribution of Cenozoic deposits inhibits attempts to evaluate the possibilities of Cenozoic deformation. In the Flat Lick area, extensive fluvial deposits are on the crest and flanks of the Flat Lick anticline, a locally significant producer of natural gas. What are the circumstances surrounding the coincidence of abundant alluvium and structure in a region characterized by scattered alluvium and flat-lying rocks? Possibly, uplift on the anticline influenced a sequence of old river courses. However, our analysis suggests that the distribution of old alluvium and meander-bend scars can be explained by processes other than contemporaneous tectonic activity. The area appears to have been tectonically stable during formation of the old channels.

REGIONAL SETTING

The headwaters of the Cumberland River above Pineville, Ky., drain the central part of the Cumberland overthrust block. Upper Mississippian and Lower Pennsylvanian strata of the Newman, Pennington, and Lee Formations are characterized by cherty limestone, limestone, shale, quartzose sandstone, and conglomerate and are extensively exposed along Pine Mountain at the faulted northern margin of the Cumberland overthrust block. Between Pineville and Williamsburg, the Cumberland River and its tributaries do not transect any of these rocks except a small exposure of Lee Formation along the White Mountain fault zone; instead, the river valley meanders through hills of shale, siltstone, sandstone, and coal of the Breathitt Formation (Lower and Middle Pennsylvanian). The index map (fig. 1) shows the location of these features.

STRATIGRAPHY AND STRUCTURE OF THE BEDROCK

Rock types of the lower part of the Breathitt Formation (Pennsylvanian) exposed in the Flat Lick area

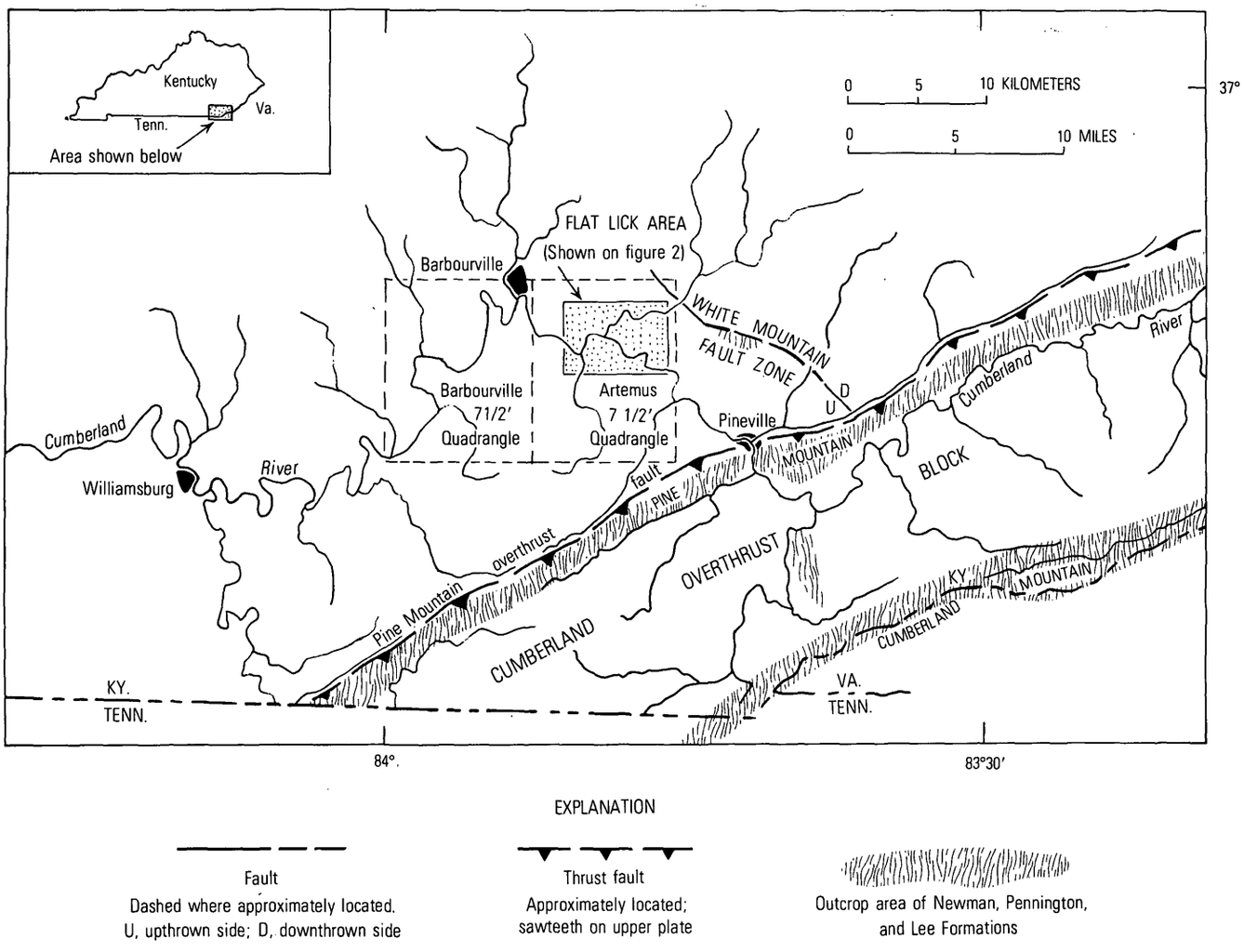

FIGURE 1.—Index map showing location of the upper portion of the Cumberland River, the Cumberland overthrust block, and the Flat Lick area.

include interbedded light-gray to yellowish-brown siltstone, olive-gray to black carbonaceous and sideritic shale, light-gray to yellowish-brown subgraywacke sandstone in beds as much as 12 m (40 ft) thick, and a few thin coal beds. These strata are exposed along the flanks of the Flat Lick anticline, a conspicuous elliptical dome having a roughly east-west axis of elongation (see fig. 2). The central part of the anticline is near Flat Lick, where the structural crest is about 120 m (400 ft) higher than adjacent shallow synclines. The anticline plunges westward into the eastern edge of the Barbourville 7.5-minute quadrangle. East of the crest, the plunging structure is terminated by the White Mountain fault zone (fig. 1). Two sandstone beds (shown in fig. 3) locally support dip slopes around the anticline.

Evidence to date the uplift of the Flat Lick anticline is inconclusive. All stratigraphic units from at least the Silurian to Middle Pennsylvanian decrease in thickness across the arch and increase in adjacent synclines. Thin Pennsylvanian marine limestone and fossiliferous shale beds are generally restricted to nearby synclinal basins and grade into thin discontinuous black shale on the flanks of the fold. The uplift of this structure was therefore probably of long duration. No evidence concerning post-Breathitt and pre-alluvium deformation exists, because no Upper Pennsylvanian to Upper Tertiary sedimentary record exists.

GEOMORPHOLOGY

The present river valley is characterized by a broadly meandering channel confined within bottomlands 0.8–1.6 km (0.5–1 mi) wide. Relief of the bottomland is

generally less than 30 m (100 ft). The entire valley meanders on an even broader scale among sharp ridges, steep slopes, and narrow ravines. Nearby hills rise as much as 365 m (1200 ft) above the river. Around the crest of the Flat Lick anticline, the topography is more subdued, as shown in figure 4.

In the bottomlands near Flat Lick, the river channel is incised 9–12 m (30–40 ft) below bedrock benches, which are generally above modern floods. The depth of incision of the modern channel below the bedrock benches appears to coincide with stage heights of floods in the 1.5- to 10-year recurrence interval as reported by McCabe (1962, p. 155–157). A lower terrace within the steep banks confining the channel corresponds to the bankfull stage of floods that, according to McCabe (1962, p. 155–157), have a recurrence interval of less than 1.5 years.

The bedrock benches are capped by as much as 4.5 m (15 ft) of older alluvium composed of sediments ranging in size from clay to boulders. Alluvium capping the benches and in the river channel contains local rock types and significant quantities of quartz, chert, conglomeratic sandstone, and limestone derived from sources outside the area. In contrast, the alluvium of all nearby tributaries is derived locally from rocks of the Breathitt Formation. The exotic gravels transported by the river are derived from the Newman, Pennington, and Lee Formations, which crop out largely in the Cumberland overthrust block.

Topographic form on the benches at places suggests old river channels whose natural levees and point bars have been modified by erosion and mass movement. Headward-eroding gullies and slopes covered by colluvium derived from alluvium and weathered bedrock are common.

Deeply weathered remnants of alluvium containing pebbles of quartz, chert, and conglomeratic sandstone have been found on isolated benches as much as 76 m (250 ft) above the modern channel of the river in the Artemus and Barbourville 7.5-minute quadrangles (Rice, 1974; Newell, 1975). Figure 5 illustrates typical exposures of old alluvium in these remnants.

Generally, ancient gravel deposits are too isolated to enable us to reconstruct earlier river courses. However, in the Flat Lick area, two ancient channel systems are defined by meander scars and patches of alluvium forming sinuous patterns at different levels (see figs. 2 and 4). The valley widths and the amplitudes and wavelengths of meanders of all channel systems, ancient and modern, are nearly identical. Deposits within the oldest system are highest, and those of the youngest system are lowest. Terrace deposits of the modern channel system are found between the present channel and about 18 m (60 ft) above it. Alluvial remnants of the two older systems also are found within intervals of about the same magnitude.

The highest and northernmost belt of old alluvium is designated as channel 1. Its course in general follows the lower reaches of Stinking Creek, a tributary to the Cumberland River. Bases of deposits in this belt are found between altitudes of 320 and 347 m 1050 and 1140+ ft). A central belt of alluvial remnants between altitudes of 314 and 330 m (1030 and 1080 ft) is designated as channel 2 and is found between Flat Lick and Himyar. The modern channel, channel 3, flows at altitudes between 298 and 290 m (979 and 950 ft).

Scattered patches of old alluvium above 347 m (1140 ft) in the area surrounding the crest of Flat Lick anticline indicate erosion and alluvial deposition by river courses that predate channel 1. However, the pattern formed by these patches is indistinct, and the trend and flow direction of older, higher level channels cannot be determined.

Channel 1 is the highest and earliest ancestral channel sufficiently well preserved to follow. Water in channel 1 flowed northward through Flat Lick, turned westward, and flowed through a gorge to Artemus. The channel eroded black shale and coal until it intersected a resistant sandstone bed (see fig. 3), which dips northward from the crest of the Flat Lick anticline. The sandstone impeded further downcutting by the river. Headward erosion of a tributary flowing through Himyar eventually breached the divide at Flat Lick and pirated the channel 1 segment of the ancient Cumberland River. Channel 2 provided a shorter steeper course across the crest of the anticline and entrenched its course to the level of another resistant sandstone bed, stratigraphically below the sandstone that had controlled channel 1. Downward cutting was again impeded. Continued headward erosion of local tributaries to the Cumberland River eventually intersected channel 2 south of Flat Lick. The river's discharge was pirated, and the course of the modern valley (channel 3) was established. During its early development, channel 3 was controlled by the same sandstone bed that had impeded downcutting of channel 2 (fig. 3). The channel first migrated down the dip slope of the sandstone bed and then cut through it and became entrenched in underlying shale because no possibilities existed for channel diversion through easily eroded rocks.

Each channel, ancestral and modern, was controlled by a resistant sandstone bed sandwiched between 3–9 m (10–30 ft) of easily eroded shale, siltstone, and coal. The ease of weathering and erosion of the less resistant

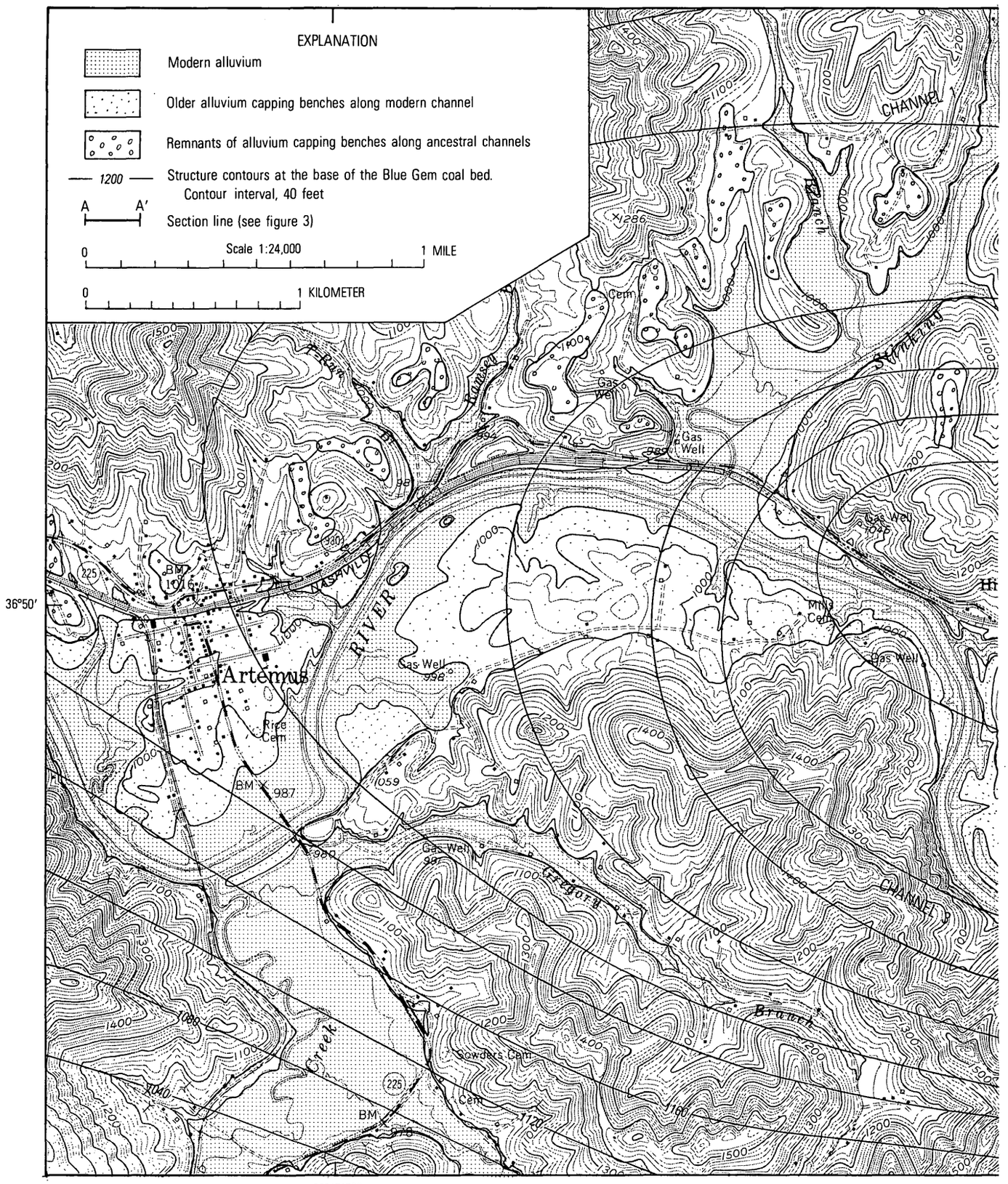

FIGURE 2.—Geologic map showing alluvial deposits, structure of the Flat Lick

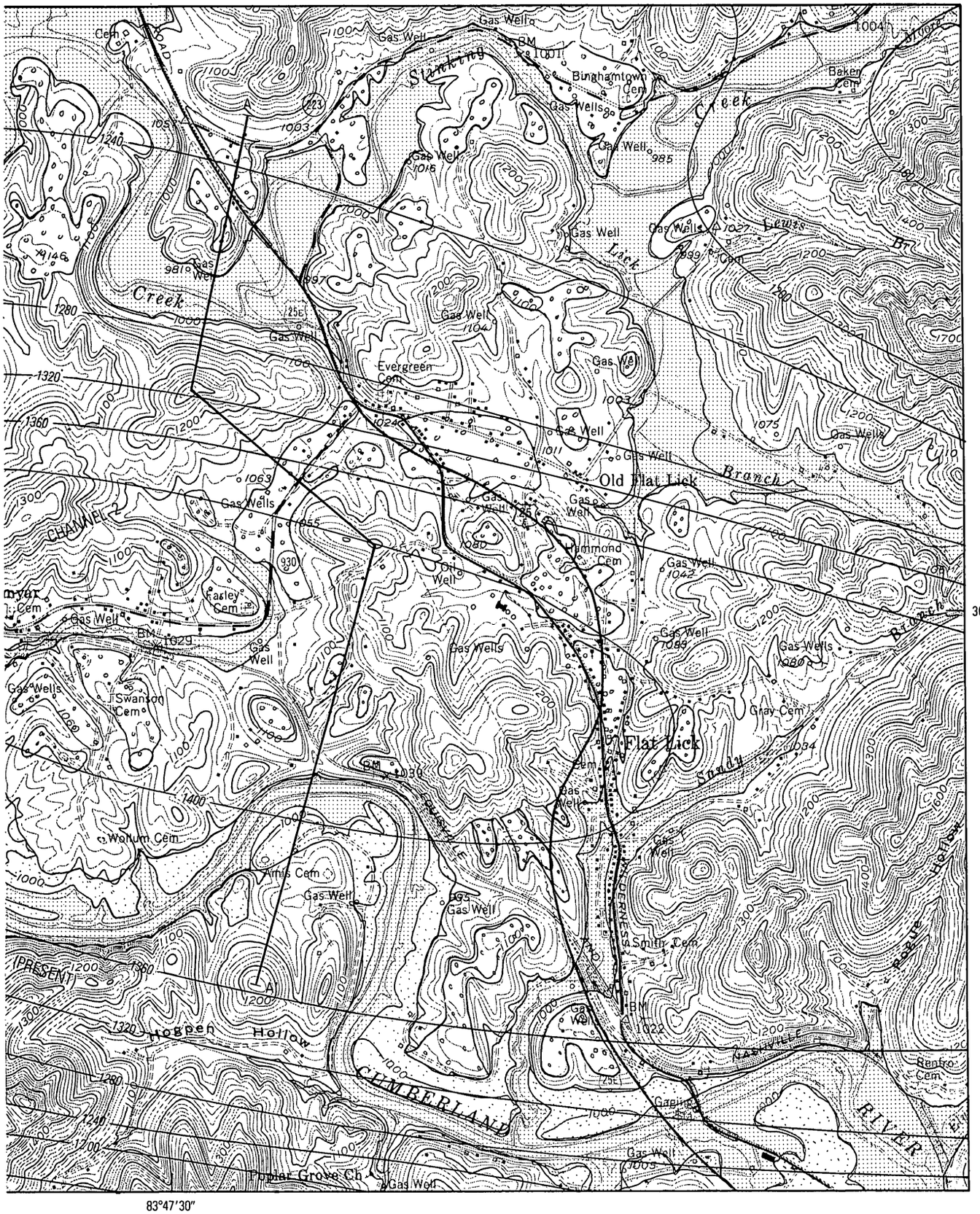

anticline, and location of A–A′ (see fig. 3). Channels numbered from oldest to youngest.

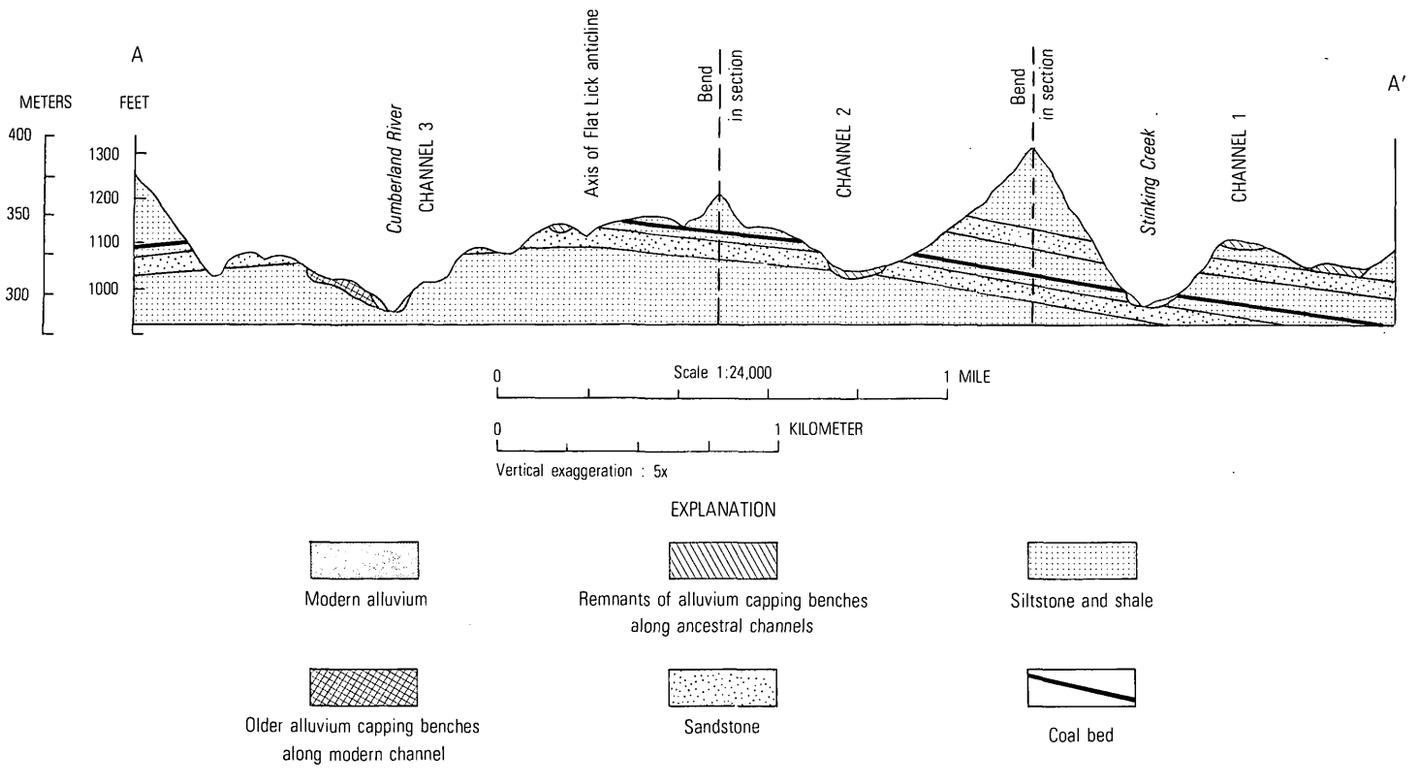

FIGURE 3.—Cross section along A–A′ (indexed in fig. 2) showing the Flat Lick anticline and structural and stratigraphic control of the ancestral and modern channels.

rocks facilitated lateral planation by the meandering river on top of the more resistant sandstone beds. As illustrated in figure 3, the remnants of channel 1 are perched on top of a sandstone on the north flank of the Flat Lick anticline. In adjusting to the gradient of the modern river, Stinking Creek, an underfit stream within channel 1, has produced a new set of small entrenched meanders superimposed on the older broader meander pattern of channel 1 and, as shown in figure 3, has cut down to the stratigraphically lower sandstone bed that impeded downcutting of channel 2 across the crest of the fold. Channel 2 has been well preserved because it is occupied by a small stream and has been little eroded; locally its remnants are underlain by or entrenched into the stratigraphically lower sandstone bed that crops out on the crest of the fold.

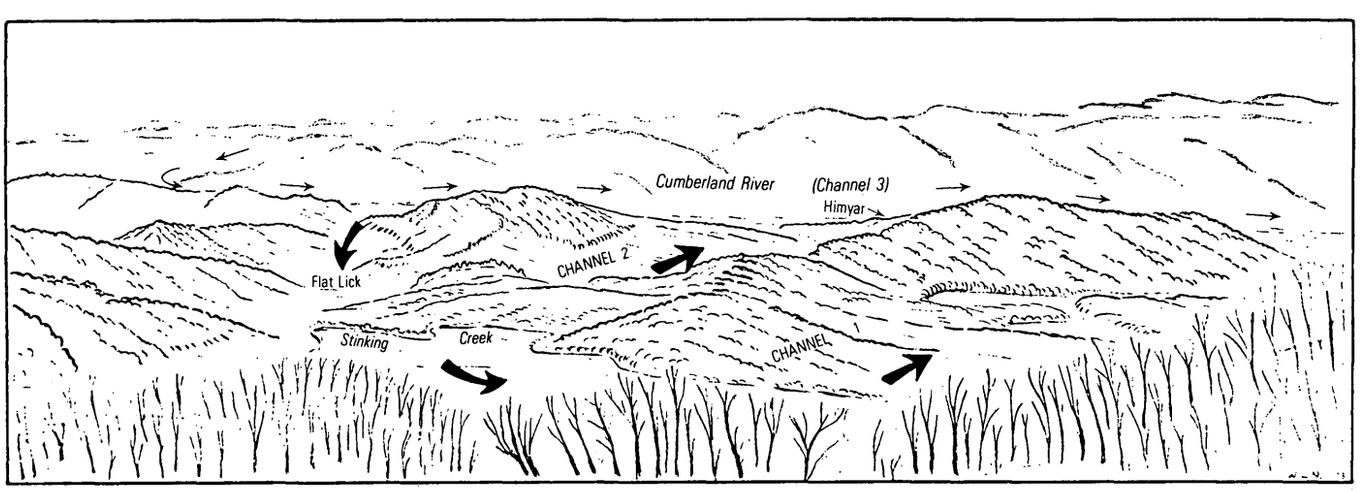

FIGURE 4.—Sketch of view looking south across the Flat Lick area. Foreground is subdued topography with ancestral river channels and underfit modern channel of Stinking Creek. Axis of Flat Lick anticline trends between Flat Lick and Himyar. The Cumberland River marks the edge of the rugged ridge and ravine topography in the background.

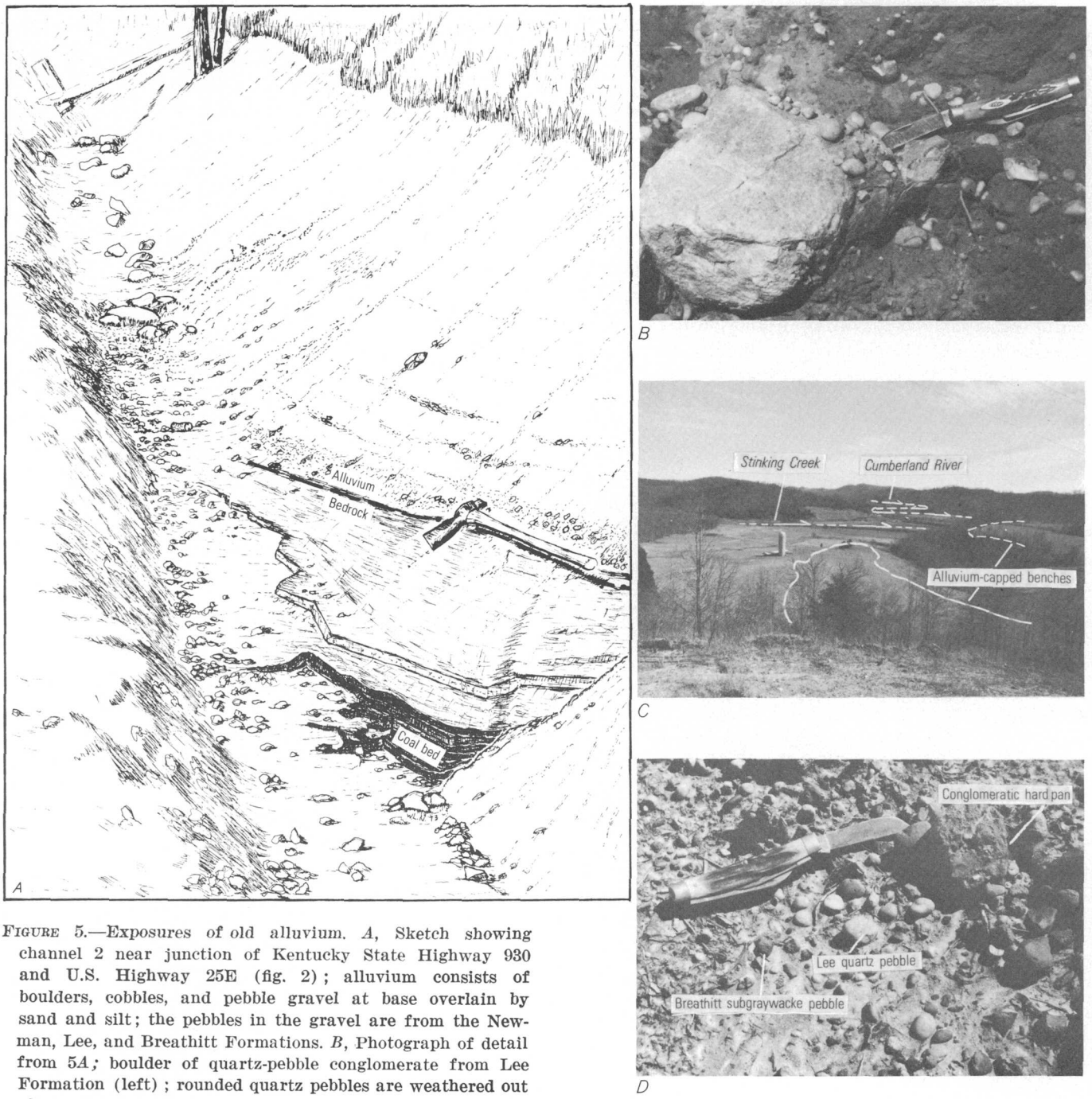

FIGURE 5.—Exposures of old alluvium. *A*, Sketch showing channel 2 near junction of Kentucky State Highway 930 and U.S. Highway 25E (fig. 2); alluvium consists of boulders, cobbles, and pebble gravel at base overlain by sand and silt; the pebbles in the gravel are from the Newman, Lee, and Breathitt Formations. *B*, Photograph of detail from 5*A*; boulder of quartz-pebble conglomerate from Lee Formation (left); rounded quartz pebbles are weathered out of similar conglomerate; angular chert pebble under knife blade is from Newman Limestone. *C*, Photograph of view looking south across the valley of Stinking Creek near its confluence with Cumberland River; bedrock benches in middleground are capped with old weathered gravel from the earliest recognizable channel (channel 1) of the Cumberland River. *D*, Photograph of gravel capping benches shown in 5*C*; gravel contains limonite-coated quartz pebbles from the Lee Formation and leached and oxidized Breathitt sandstone pebbles in a matrix of red oxidized sandy alluvial soil; at some localities limonite, precipitated from ground water, has cemented the pebbles into conglomeratic hardpans; a fragment of limonite-cemented conglomerate is in upper right of picture.

The modern Cumberland River channel, channel 3, originally was controlled by the lower sandstone and now is entrenched in shale on the south flank of the anticline.

AGE OF THE OLD CHANNELS

Direct evidence for the ages of the channel remnants was not found. However, duration of fluvial processes represented by the old channel gravels can be estimated from erosion rates. A denudation rate calculated from the sediment load of a large stream may be based on an average of the volume of sediment removed from a small intensively eroded area and the volume removed from a large slightly eroded area. Sites of intense erosion change from time to time, but the average erosion of a large drainage basin remains constant from year to year if other variables remain constant. If the river is in equilibruim with its watershed, the average lowering of its bed should reflect the average rate of erosion of the drainage area (Hack, 1965).

Valley width, amplitude and wavelength of valley meanders, and other channel variables are all related to the discharge of the river, a function of the drainage area and climate. The fact that these variables for all three Cumberland River channel systems have similar dimensions suggests that the drainage area and climate have not changed drastically since the formation of the earliest recognizable channel. Inspection of the area and runoff of the watershed supports this suggestion. The drainage area of about 2230 km^2 (900 mi^2) produces an average discharge of 46.7 m^3/s (1700 ft^3/s), equivalent to 55 L/s for each square kilometer of drainage area (1.9 ft^3/s for each square mile) (U.S. Geol. Survey, 1961, p. 14–19), a value representative of a large part of eastern Kentucky. The drainage area above Flat Lick is large enough so that the addition or deletion of small watersheds (less than 25 km^2 or 10 mi^2) because of piracy or diversion would not change its size and discharge by more than a few percent. Thus, little variation in the discharge and channel characteristics of the Cumberland River is reasonably certain from the time of deposition of the oldest recognizable alluvium until the present.

Our investigations of other abandoned meander bends in eastern Kentucky suggest that diversion from one channel to another is a very gradual process. Two channels can coexist for a period of time and be alternately affected by occasional perturbations such as landslides and sediment plugs at the mouths of local tributaries. Ultimately, structure, erodibility of bedrock, and gradient control the selection of one channel. As a result, sequences of terrace deposits have overlapping ranges of altitude along both the abandoned and occupied channels in the Flat Lick area.

An erosion rate for the Cumberland River can be calculated by converting the sediment load into an assumed uniform thickness of rock and soil that is eroded from the watershed on a yearly basis. This value is then compared with the thickness or volume of material eroded from a former topographic surface to yield an approximate duration of the erosion.

The sediment load of the Cumberland River in the area of study is undocumented. However, bedrock, soils, topography, climate, vegetation, and land use are similar throughout the Cumberland-Allegheny Plateau, and probably the sediment load of the Cumberland is similar to that of other Ohio River tributaries draining the area. Sediment loads reported (U.S. Geol. Survey, 1970) for streams in this region differ widely in magnitude, ranging from trace amounts for streams in forested watersheds to several metric tons per hectare (2.47 acres) per year for streams in watersheds where landslides, strip mining, or deforestation have taken place. Sediment loads of streams in watersheds as large as or larger than the Cumberland River watershed are more uniform than those of streams in smaller watersheds and are probably more consistent during longer periods. We estimate that the average volume of sediment contributed from this region is about 2.47 metric tons per hectare per year (1 ton per acre per year).

Judson and Ritter (1964) discussed the historical background and assumptions involved in estimating erosion rates from sediment-load data of major rivers. Inserting the value of 2.47 metric tons per hectare per year (= 247 metric tons per square kilometer per year = 640 tons per square mile per year) into their equation D(depth of denudation in inches per 1000 yr) = $(5.2 \times 10^{-3}) \times$ (tons per square mile per year) yields a denudation rate of 83.8 mm (3.3 in.) per 1000 years or about 305 mm (1 ft) per 4000 years (1 m/13 120 yr). This rate corresponds favorably with their denudation rates for broad regions. The rate is also of the same order of magnitude as the rate of 1 ft/7700 yr (1 m/25 256 yr) calculated by Hack (1965, p. 63) for the south fork of the Shenandoah River. The rates of Judson and Ritter (1964) and Hack (1965) are derived from both suspended and dissolved loads. Dissolved load is not incorporated in the calculation for the Cumberland River because carbonate minerals and other readily soluble minerals are uncommon and the dissolved load derived from them is thought to be of minor importance. If the dissolved load were included, the calculated rate would be slightly higher. If the erosion rate were 1 m/13 120 yr (1 ft/4000 yr), the modern channel could have been lowered 18 m (60 ft) below channel system 2 within 240 000 years. This approximation indicates that the Cumberland

River could easily produce the features observed along the valley bottom of the modern channel during the last quarter million years following piracy from ancestral channel 2. A quarter million years also would be ample time for the lowering of channel 2 below the earlier, higher channel 1 now occupied by Stinking Creek.

DISCUSSION AND CONCLUSIONS

On the basis of topographic forms and the low divide at Flat Lick, Jillson (in Jillson and Hodge, 1919, p. 9–11) recognized a probable ancient channel (channel 1 of this paper) along the course now occupied by Stinking Creek. He did not indicate that he recognized remnants of Cumberland River alluvium in channel 1, nor did he report morphological or alluvial evidence of channel 2 in the area between Himyar and Flat Lick. He attributed the diversion of the Cumberland River from ancient channel 1 into the lower present channel (channel 3) to uplift of the Flat Lick anticline. No evidence of warping or faulting of alluvium in the Artemus quadrangle has been found (Rice, 1974).

The manner in which streams are influenced by uplift is related to many factors, including discharge, gradient, topography, and lithology. Even sudden uplift across a high-discharge high-gradient stream flowing through weakly resistant rocks may not greatly affect the course of the stream. Hunt (1969) cited many examples on the Colorado Plateau of channels crossing areas of active doming. The channels maintained their course during uplift and eroded spectacular canyons through the uplifted areas.

At a locality of active doming, oversteepened gradients of old fluvial deposits are expected on the downstream side of the uplift; gradients on the upstream side would be flattened or reversed. The oldest channel deposits such as those in channel 1 would be deformed the most. The gradient of channel system 2 would be only slightly deformed, and the modern channel system would be unaffected. Gradients of the ancestral river courses cannot be precisely determined. However, on the basis of altitudes at the bedrock-terrace deposit contacts, gradients of both ancestral channels were determined to be approximately 1.23 m/km (4 ft/mi), about the same as that of the modern channel.

If uplift of the Flat Lick anticline had initiated the diversions of channels 1 and 2, the uplift would have created as much as 30 m (100 ft) of new structural relief. This is 25 percent of the apparent total structural relief on the anticline. It seems unreasonable to postulate this amount of uplift late in the history of the dome. Stratigraphic thinning across the fold suggests that most, if not all, of the uplift took place by the end of the Paleozoic Era.

All the surficial deposits and geomorphic features observed can be interpreted in terms of current processes and rates operating through the last half million years. The differing lithologies and the attitude of the Pennsylvanian strata through which the Cumberland River eroded are probably the principal controlling factors. Neither regional uplift nor continuing local deformation of the bedrock are needed to explain the history of the Cumberland River at Flat Lick. Moreover, because all fluvial features can be explained in terms of current processes, the old channels cannot be considered as evidence for recent uplift of the Flat Lick anticline.

The distribution of surficial deposits is unlikely to provide the evidence of vertical displacement of 1 meter or less (a few feet or less). An eroding landscape, such as the Flat Lick area, in which fluvial processes and slope processes are, for the most part, in equilibrium, cannot preserve evidence of small-scale faulting or folding for long time periods.

REFERENCES CITED

Hack, J. T., 1965, Geomorphology of the Shenandoah Valley, Virginia and West Virginia, and origin of the residual ore deposits: U.S. Geol. Survey Prof. Paper 484, 85 p.

Hunt, C. B., 1969, Geologic history of the Colorado River: U.S. Geol. Survey Prof. Paper 669–C, p. 59–130.

Jillson, W. R., and Hodge, J. M., 1919, The geology and coals of Stinking Creek (Knox County, Ky.): Kentucky Dept. Geology and Forestry, ser. 5, Bull. 3, 89 p.

Judson, Sheldon, and Ritter, D. F., 1964, Rates of regional denudation in the United States: Jour. Geophys. Research, v. 69, no. 16, p. 3395–3401.

McCabe, J. A., 1962, Floods in Kentucky—magnitude and frequency: Kentucky Geol. Survey, ser. 10, Inf. Circ. 9, 196 p.

Newell, W. L., 1975, Geologic map of the Barbourville quadrangle, Knox and Whitley Counties, Kentucky: U.S. Geol. Survey Geol. Quad. Map GQ–1254.

Rice, D. D., 1974, Geologic map of the Artemus quadrangle, Bell and Knox Counties, Kentucky: U.S. Geol. Survey Geol. Quad. Map GQ–1207.

U.S. Geological Survey, 1961, Surface water supply of the United States, 1960, Part 3–B, Cumberland and Tennessee River basins: U.S. Geol. Survey Water-Supply Paper 1706, 234 p.

———1970, Quality of surface waters of the United States, 1965, Parts 3 and 4, Ohio River basin and St. Lawrence River basin: U.S. Geol. Survey Water-Supply Paper 1962, 480 p.

Jour. Research U.S. Geol. Survey
Vol. 6, No. 3, May–June 1978, p. 369–381

DATING QUATERNARY FAULTS IN THE SOUTHWESTERN UNITED STATES BY USING BURIED CALCIC PALEOSOLS

By MICHAEL N. MACHETTE, Denver, Colo.

Abstract.—Calcareous soils are widespread on upper Pliocene to upper Pleistocene unconsolidated surficial deposits in semiarid portions of the southwestern United States. Where these soils are related to faults, the soils may provide a means for quantitatively estimating timing and amounts of Quaternary faulting. Soil age estimates are based on the amount of pedogenic $CaCO_3$ (g/cm^2-soil column) that has accumulated from soil processes, whereas rates of calcic-soil formation were calibrated by the K-Ar dating method, tephrochronology, vertebrate paleontology, and regional soil studies. The County Dump fault, west of Albuquerque, N. Mex. cuts a 500 000-year-old datum, the Llano de Albuquerque. The downdropped block of this fault contains a sequence of faulted younger deposits and intercalated calcic paleosols. Soil ages, and hence fault ages, can be calculated by measuring the total pedogenic calcium carbonate content in a section of buried paleosols and by using an independently established maximum soil formation rate of 0.35 g $CaCO_3 \cdot cm^{-2} \cdot 10^{-3}$ yr^{-1} for the Albuquerque area. This particular fault segment has had four discrete episodes of movement in the past 500 000 yr, the most recent of which occurred about 20 000 yr B.P. Recurrence intervals on the segment are 90 000–190 000 yr, but the composite recurrence interval for all fault movements in this area may be less by several orders of magnitude. This technique of quantifying soil properties and calculating ages of relict soils can be used to estimate ages of Quaternary deposits and associated surfaces, to correlate such features over broad regions, and to analyze regional trends in calcic-soil formation.

During the past decade, interest in Quaternary faulting has dramatically increased as a result of environmental concerns such as urban planning, seismic hazards, and especially the locating of nuclear powerplant sites. Contemporary surface faulting can be a major hazard at these sites, and thus it is currently a topic of intensive industrial and governmental research.

Various techniques are being used to determine the ages and amounts of Quaternary faulting. Datable material within faulted Quaternary deposits is sparse, and detailed fault histories have been reconstructed for only a few examples. More commonly, datable material provides a minimum or maximum age for faulting (Clark and Lajoie, 1974; Payne and Wilson, 1974). Unfortunately, the majority of datable material associated with many Quaternary faults is too old for the ^{14}C method and too young for either K-Ar or paleomagnetic methods.

Soils are common on unconsolidated surficial deposits related to faults and have been used to help establish the relative age of some faults. The use of soil stratigraphy in such studies was outlined by Shlemon (1975). Soil stratigraphy relies on the ability to recognize and correlate soils whose ages are usually known only in a relative sense (as Sangamon of the central United States or Bull Lake of the Rocky Mountains). Page and Walsh (1974) established criteria for evaluating the stratigraphic relations between soils and associated faults, and Douglas and others (1974) presented a case history in the use of soils to date faults at a particular site.

The potential use of soils to date episodes of normal faulting is particularly attractive. The downdropped block of a normal fault is often the site of sediment accumulation, and these sediments may bury previously developed soils. Hence, the downdropped block might often bear wedges of sediment containing buried soils; each soil represents a period of tectonic and geomorphic stability, whereas each sedimentary unit represents a period of landscape instability and subsequent adjustment that follows fault activity.

A site demonstrating this stratigraphic relationship is present just west of Albuquerque, N. Mex. (fig. 1). Detailed geologic and pedologic studies at this site, along with subsequent laboratory analyses of soil carbonate content and bulk density, provide a quantitative data base. The data base and an independently established soil formation rate, derived from regional pedologic and geologic studies and based on absolute age-

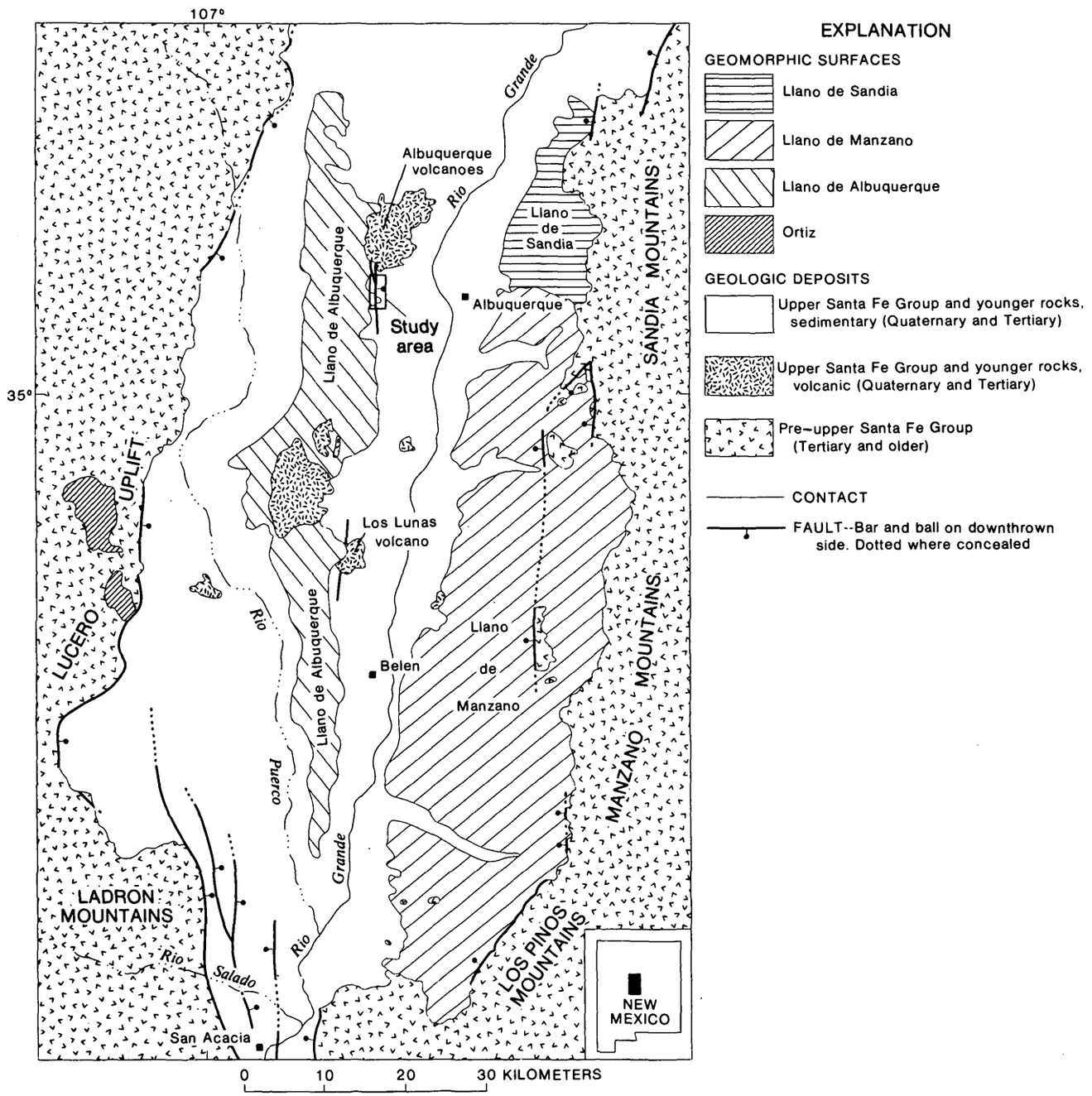

FIGURE 1.—Index and geologic sketch map of the Albuquerque-Belen basin, N. Mex.

dating of a geomorphic surface (Bachman and Machette, 1977), were used to estimate both the age and amounts of four episodes of recurrent faulting at the New Mexico site.

Acknowledgments.—This research is part of a study entitled "Methodology of dating Quaternary faulting, Continental Interior," undertaken by the U.S. Geological Survey on behalf of the Nuclear Regulatory Commission (Agreement NRC 49–25 1000).

I would like to thank George Bachman of the U.S. Geological Survey for supervision and guidance throughout the course of this project. Ned R. Timble (U.S. Geological Survey) helped measure soil sections, collect samples, and conduct a planetable survey.

Richard L. Koogle of Koogle and Pouls Engineering, Inc., Albuquerque, N. Mex., provided low-altitude airphoto coverage and vertical base control for the study area. P. W. Lambert (U.S. Geological Survey) and both John W. Hawley and Leland H. Gile of the Soil Conservation Service (U.S. Department of Agriculture) freely discussed the stratigraphic and pedologic aspects of Quaternary deposits in New Mexico. Additionally, Peter W. Birkeland (Colorado Univ.) provided valuable criticism and suggestions both in the field and during preparation of the manuscript.

CALCIC SOILS

As informally used here, calcic soils are those soils that have accumulations of pedogenic calcium carbonate (hereafter referred to as carbonate) as their principal horizon characteristic. These soils are more widely known to geologists as caliches, or calcretes, although these two terms commonly include marls, silcretes, ground-water carbonates, and terrestrial limestones (Goudie, 1971). A more restricted use of the term caliche is preferred here, inasmuch as the other above types of carbonate accumulations are not strictly pedogenic.

Well-developed calcic soils have zones of carbonate accumulation that represent master horizons; these horizons are the predominant feature of the soil. Gile, Peterson, and Grossman (1965, 1966) established criteria for distinguishing calcic-soil horizons based on structural morphology and recognized several stages of carbonate buildup (fig. 2).

The soil-horizon nomenclature used in this report is a modification of that used by the Soil Conservation Service (Soil Survey Staff, 1975) and follows closely the recommendations of Gile, Peterson, and Grossman (1965). Birkeland (1974) provides a useful discussion of soil nomenclature and taxonomy for the geologist's use.

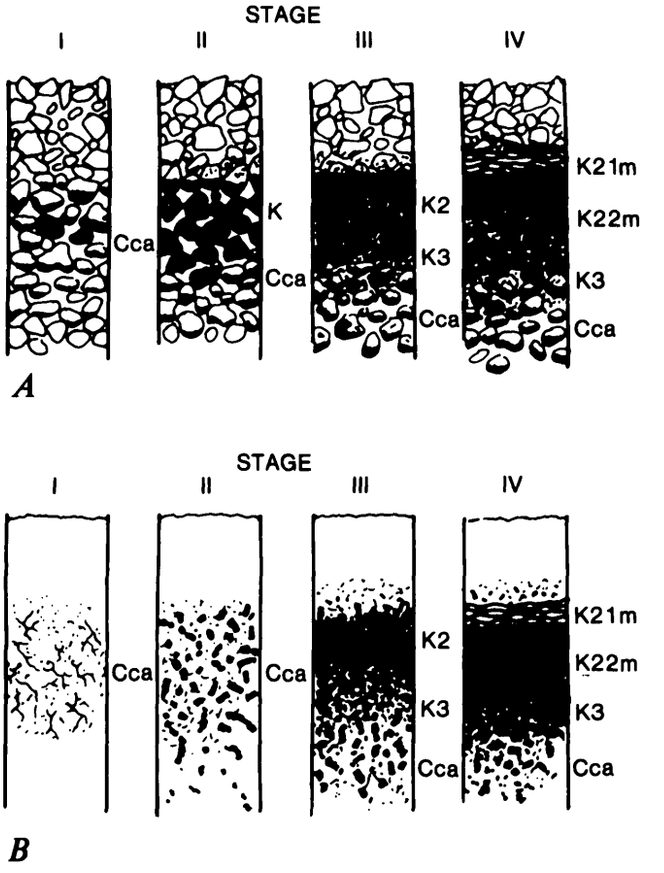

Stage	Gravelly parent material	Nongravelly parent material
I	Thin discontinuous pebble coatings	Few filaments or faint coatings on sand grains
II	Continuous pebble coating; matrix is calcareous but loose	Few to common nodules of varying hardness; matrix is commonly calcareous
III	All grains are coated with carbonate; best developed where voids are filled with carbonate	Internodular matrix grains are coated with carbonate; voids can be filled with carbonate
IV	Laminar horizon of nearly pure carbonate overlies horizon of stage III development	

FIGURE 2.—Sketches of carbonate buildup stages I, II, III, and IV for gravelly (*A*) and nongravelly (*B*) parent materials (from Gile, Peterson, and Grossman, 1966). Calcic-soil horizon nomenclature of Gile, Peterson, and Grossman (1965) is shown next to each soil profile. Black is carbonate.

GENESIS OF CALCIC SOILS

The genesis of calcic soils is briefly discussed here as background for the quantitative method and model developed later. For a more complete discussion of calcic-soil genesis see Gile, Hawley, and Grossman (1971), Gardner (1972), and Goudie (1973).

In the past, numerous processes have been attributed to the formation of carbonate in surficial deposits. These processes can be grouped into three categories (Gardner, 1972): (1) chemical or biochemical deposition in a lacustrine environment, (2) deposition from the capillary fringe of a shallow water table, and (3) pedogenic deposition from downward-infiltrating soil waters. Category 3 is now favored as the process by which calcic soils form in the southwestern United States, although this origin has not been widely accepted until the past decade.

Calcic soils are prominent geomorphic and pedologic

features on surficial deposits in semiarid portions of the southwestern United States. These soils range from the well-indurated pisolitic and laminated caprock of the Pliocene Ogallala Formation to weak accumulations of carbonate in the Fillmore Alluvium of Gile, Hawley, and Grossman (1971).

The pedogenic processes currently considered in the formation of calcic soils in semiarid portions of the southwestern United States are as follows:

1. A deposit may have primary (detrital) $CaCO_3$ in the parent material, and with repeated wetting and drying, calcium is transported in solution and reprecipitated as $CaCO_3$ at some depth beneath the surface. The depth is dictated mainly by the mean annual precipitation and the infiltration potential of the deposit (Arkley, 1963; Gile, 1977).
2. If little or no primary $CaCO_3$ is present, yet a Cca or K horizon has formed, three processes may have been responsible for $CaCO_3$ accumulation: (a) calcium-bearing minerals release Ca upon weathering (Goudie, 1973) and this combines with HCO_3^- to form $CaCO_3$ as H_2O is lost by evapotranspirative processes; (b) calcium, dissolved in rainwater (Junge and Werby, 1958), can enter the deposit and be precipitated as in 2(a) above; (c) solid $CaCO_3$, and $CaMg(CO_3)_2$ to a lesser extent, can be transported to a site as aerosolic dust- to eolian sand-size material (Gile and others, 1971) and be subsequently leached and reprecipitated as in 1 above.

Of the above-mentioned processes, a combination of 2(b) and 2(c) is currently favored as the predominant mode of calcic-soil formation in the southwestern United States (Gile and others, 1971; Gardner, 1972; Goudie, 1973).

The systematic development of calcic soils as a function of time has been recognized for years (Jenny, 1941a; Richmond, 1962; Scott, 1963), but quantitative data on this development have only recently become available. Arkley (1963), Gile, Hawley, and Grossman (1971), and Gardner (1972) have attempted to quantify the rate of pedogenic accumulation of carbonate in calcic soils; these attempts have been seriously hampered by a lack of reliable age determinations of the associated deposits. The data of Gile, Hawley, and Grossman (1971) and those of George Bachman and myself (1977) strongly suggest a progressive development in the percent $CaCO_3$, bulk density, structural morphology, overall thickness, and total carbonate content of calcic soils with time.

My estimates of soil ages are based on the amount of pedogenic $CaCO_3$ that has accumulated in a soil and on the assumption that the accumulation rate of pedogenic carbonate can be approximated by a linear function. If changes in the rate of carbonate accumulation occurred in the past and if these rate changes are cyclic (as in pluvial-interpluvial climates), the relative age error should be the largest for the least developed soils and smallest for the most developed soils since multiple-cycle variations in the rate would average out.

The factors that could affect the rate function are more complex than Jenny (1941b) suggested, inasmuch as much of the Ca in these calcic soils is derived from atmospheric and eolian sources. A further treatment of the factors affecting calcic-soil formation is not within the scope of this report. If and when a more accurately dated sequence of Quaternary deposits and calcic soils in the southwestern United States is available, additional refinement of a rate function would be possible.

ANALYSIS OF SOIL CARBONATE CONTENT

The estimate of soil age from the $CaCO_3$ content of a soil involves the measurement of horizon thicknesses, carbonate contents, and bulk densities. Using these three parameters, it is possible to compute the total amount of $CaCO_3$ in a 1-cm^2-soil column. The carbonate content of a sampled unit, Ct, consists of two separate components: Cs (secondary $CaCO_3$) and Cp (primary $CaCO_3$), where $Ct = Cs + Cp$, or $Cs = Ct - Cp$. Cs can be calculated in equation 1 using data in table 1.

$$Cs = (C_3P_3 - C_1P_1)\,d. \qquad \text{(eq 1)}$$

C_3 is the present $CaCO_3$ content (g $CaCO_3$/100 g soil),
C_1 is the original $CaCO_3$ content (g $CaCO_3$/100 g soil),
P_3 is the present oven-dry bulk density (g/cm^3),
P_1 is the original oven-dry bulk density (g/cm^3), and
d is the thickness, in centimeters, of the horizon or subhorizon sampled.

Therefore, Cs is expressed in g $CaCO_3$/cm^2-soil column. Finally, the sums of Cp, Cs, and Ct for all horizons are C_P (total primary $CaCO_3$), C_S (total secondary $CaCO_3$), and C_T (total $CaCO_3$ in the soil profile), respectively.

C_1 and P_1 generally have to be estimated for soil horizons because soil processes have masked the original (parent material) values. These two parameters can be measured in parent materials between paleosols and on presently overlying eolian sands.

TABLE 1.—*Sample numbers, soil horizons, and laboratory data used to calculate* $CaCO_3$ *values*

[Z, depth (m); d, thickness (cm); C_3, $CaCO_3$ content (g $CaCO_3$ /100 g soil); P_3, oven-dry bulk density (g/cm^3); Ct, total $CaCO_3$ (g $CaCO_3$/cm^2-soil column); C_1, estimated primary $CaCO_3$ content (g $CaCO_3$/100 g soil); P_1, estimated original oven-dry bulk density (g/cm^3); Cp, estimated primary $CaCO_3$ (g $CaCO_3$/cm^2-soil column); Cs, secondary $CaCO_3$ (g $CaCO_3$/cm^2-soil column); C_T, total of all Ct values; C_P, total of all Cp values; C_S, total of all Cs values; e, estimated value; var., variable]

Sample no.	Soil horizon	Z	d	C_3	P_3	Ct[1]	C_1	P_1	Cp[2]	Cs[3]	C_T[4]	C_P[5]	C_S[6]
6/3/74-3a	I Cn	0-0.42	42	0.030	1.7e	2.1	0.030	1.7	2.1	0.0	335.2	159.2	[7]176.0
10/12/74-2a, -2b	II C2ca	.42-.75	33	.115	1.61	6.1	.030	1.7	1.7	4.4	333.1	157.1	[7]175.8
10/12/74-2c	II C3ca	.75-.85	10	.094	1.80	1.7	.030	1.7	.5	1.2	327.0	155.4	171.6
-2d	II C3ca	.85-1.00	15	.066	1.75	1.7	.030	1.7	.8	.9	325.3	154.9	170.4
-2e	II C3ca	1.00-1.15	15	.045	.1.80	1.2	.030	1.7	.8	.4	323.6	154.1	169.5
-2f	II C3ca	1.15-1.25	10	.049	1.82	.9	.030	1.7	.5	.4	322.4	153.3	169.1
-2g	II Cn	1.25-1.40	15	.040	1.7e	1.0	.030	1.7	.8	.2	321.5	152.8	168.7
-2h	II Cn2	1.40-2.33	93	.030	1.7e	4.7	.030	1.7	4.7	0	320.5	152.0	168.5
9/13/75-17	III B2sca	2.33-2.63	30	.097	1.62	4.7	.030	1.7	1.5	3.2	315.8	147.3	[8]168.5
- 6	III B3sca	2.63-2.85	22	.046	1.81	1.8	.030	1.7	1.1	.7	311.1	145.8	165.3
- 5	III Cca	2.85-3.00	15	.088	1.94	2.6	.030	1.7	.8	1.8	309.3	144.7	164.6
- 1	III K21m	3.00-3.20	20	.331	1.69	11.2	.030	1.7	1.0	10.2	306.7	143.9	162.8
- 2	III K22m	3.20-3.42	22	.207	1.77	8.1	.030	1.7	1.1	7.0	295.5	142.9	152.6
- 3	III K3m	3.42-3.52	10	.125	1.82	2.3	.030	1.7	.5	1.8	287.4	141.8	145.6
- 4	III Cca2	3.52-3.75	23	.109	1.82	4.6	.030	1.7	1.2	3.4	285.1	141.3	143.8
-21	III Cca3	3.75-4.25	50	.056	1.65	4.6	.030	1.7	2.6	2.0	280.5	140.1	140.4
- 7	III Cn	4.25-5.00	75	.071	1.63	8.7	.030	1.7	3.8	4.9	275.9	137.5	138.4
-8, -18	IV Cn	5.00-6.10	110	.093	1.6e	16.4	.093	1.6	16.4	0	267.2	133.7	133.5
5/30/74-2	V K21m	6.10-6.40	30	.180	1.7e	9.2	.045	1.7	2.3	6.9	250.8	117.3	[9]133.5
-2a	V K22m	6.40-6.98	58	.183	1.73	18.4	.045	1.7	4.4	14.0	241.6	115.0	126.6
-2b	V K23m	6.98-7.28	30	.428	1.96	25.2	.045	1.7	2.3	22.9	223.2	110.6	112.6
-2c	V K3	7.28-7.80	58	.239	1.85	23.0	.045	1.7	4.0	19.0	198.0	108.3	89.7
-2d	V Cca	7.80-8.10	30	.061	1.73	3.2	.045	1.7	2.3	.9	175.0	104.3	70.7
-2e	V Cca2	8.10-8.60	50	.084	1.7e	7.1	.045	1.7	3.8	3.3	171.8	102.0	69.8
-2f	V Cn	8.60-10.20	160	.045	1.73	12.5	.045	1.7	12.2	.3	164.7	98.2	66.5
6/4/74-2a	VI C2ca	10.20-10.70	50	.154	1.7e	13.1	.040	1.7	3.4	9.7	152.2	86.0	[10]66.2
-2b	VI C3ca	10.70-11.45	75	.152	1.7e	19.4	.040	1.7	5.1	14.3	139.1	82.6	56.5
-2c	VI C4ca	11.45-12.80	135	.055	1.7e	12.6	.040	1.7	9.2	3.4	119.7	77.5	42.2
11/11/75-1a	VI Cn[11]	12.80+	var.	.011	1.7e	.019·d	.011	1.7	.019·d	0	107.1	68.3	38.8
-1b, -1c, -1d	VII Cca	0-1.80	180	.050	1.72	15.5	.040	1.7	12.2	3.3	107.1	68.3	38.8
-1e	VIII C11ca	1.80-1.90	10	.081	1.68	1.4	.100	1.7	1.7	-.3	91.6	56.1	[12]35.5
-1f	VIII C12ca	1.90-2.20	30	.142	1.7e	7.2	.100	1.7	5.1	2.1	90.2	54.4	35.8
-1g	VIII K21	2.20-2.60	40	.291	1.65	19.2	.100	1.7	6.8	12.4	83.0	49.3	33.7
-1h	VIII K22	2.60-2.90	30	.300	1.7e	15.3	.100	1.7	5.1	10.2	63.8	42.5	21.3
-1i	VIII K31	2.90-3.50	60	.172	1.7e	17.5	.100	1.7	10.2	7.3	48.5	37.4	11.1
-1j	VIII C32ca	3.50-4.30	80	.118	1.7e	16.0	.100	1.7	13.6	2.4	31.0	27.2	3.8
-1k	VIII C33ca	4.30-5.10	80	.110	1.7e	15.0	.100	1.7	13.6	1.4	15.0	13.6	1.4
-1l	VIII Cn	5.10+	([13])	.005	1.7e	.001·d	.005	1.7	.001·d	0	.001·d	.001·d	0

[1] $Ct = d \cdot C_3 \cdot P_3$.
[2] $Cp = d \cdot C_1 \cdot P_1$.
[3] Cs=Ct-Cp.
[4] Ct summed upwards from base.
[5] Cp summed upwards from base.
[6] Cs summed upwards from base.
[7] Top of soil U.
[8] Top of soil V.
[9] Top of soil X.
[10] Top of soil Y.
[11] Measured section offset. Thickness of unit VI variable; no evidence of pedogenic accumulation of $CaCO_3$; Cs=0, Ct=Cp.
[12] Top of soil Z.
[13] Bedrock, thickness unknown, perhaps several hundred m.

Methods of analysis

Samples were obtained throughout six measured and described partial sections containing the buried paleosols. Paleosols were described in detail where they are stratigraphically separated. A composite soil section (table 1) was then assembled. Each soil subhorizon was sampled one or more times, depending on thickness, for laboratory determination of both $CaCO_3$ content and bulk density. $CaCO_3$ content (C_3) was determined by the Chittick method, a gasometric $CaCO_3$ dissolution technique. The standard operating technique and analytical precision of the method were discussed by Dreimanis (1962). This method provides a quick, efficient, and inexpensive determination of carbonate contents of soils (Bachman and Machette, 1977).

Measurements of bulk density were made by two techniques. Channel samples of moderately to well-indurated horizons (Cca or K horizons) were oven dried and paraffin coated, and the bulk density was determined by the water-displacement method (American Society for Testing and Materials, 1974; Chleborad and others, 1975). In poorly indurated horizons, a calibrated sampling tube was driven into a prepared face of the soil; the resultant volume (100 cm^3 or 200 cm^3) was oven dried and weighed. Direct calculation of the oven-dry bulk density can then be made.

GEOLOGIC SETTING

Regional geology

The Albuquerque area contains a well-preserved sequence of Quaternary and upper Tertiary sediments and widespread interbedded volcanic rocks that were erupted during the last 5 million years (Bachman and Mehnert, 1978). The Rio Grande (fig. 1) occupies a central position in an active, 40- to 60-km-wide, structurally complex rift, topographically expressed as the Albuquerque-Belen basin. Geophysical and deep drill-hole data (Oliver and others, 1976; Kelley and others, 1976) suggest that the main rift is composed of smaller horsts and grabens that are obscured by Quaternary sediments. Our current understanding of the geologic history of the Albuquerque-Belen basin indicates that the basin was partially filled with bolson deposits in early Miocene to early Pliocene time and then by slowly aggrading piedmont-slope and axial-river deposits of the Rio Grande (fig. 3) during Pliocene to middle Pleistocene time (Chapin and Seager, 1975; Hawley and others, 1976; Machette, 1977; Bachman and Mehnert, 1978). Most of these deposits are extensively faulted, some of the oldest faults having thousands of meters of structural relief.

The framework of the Cenozoic geology of this area was laid by Bryan (1937) and Bryan and McCann (1937, 1938). Students of Bryan (Denny, 1940, 1941; Wright, 1946) contributed to a broader understanding of the geology of central New Mexico. Almost 30 yr later, Lambert (1968) completed the first detailed mapping of Cenozoic deposits in the Albuquerque-Belen basin. He recognized a sequence of eolian, alluvial flood-plain, terrace, and piedmont-slope deposits (fig. 3) of middle(?) Pleistocene to Holocene age, in part interbedded with upper Pleistocene volcanic flows (Bachman and others, 1975).

Some further refinement of this basic work may now be made through the recent availability of radiometric age dates. A major widespread geomorphic surface, the Ortiz (fig. 1), was recognized by Bryan (1937) and correlated with the Llano de Albuquerque, a lower, geographically isolated surface in the central part of the Albuquerque-Belen basin. The age of the Ortiz is about 3 m.y., inasmuch as numerous basalts overlying the surface have been dated using the K-Ar method at 2.5–2.8 m.y. (Bachman and Mehnert, 1978). The Llano de Albuquerque is now thought to be about 500 000 yr old, distinctly younger than the Ortiz. This age is based upon dated volcanic rocks that underlie and overlie the surface (Bachman and others, 1975), underlying volcanic ash, vertebrate paleontology, and

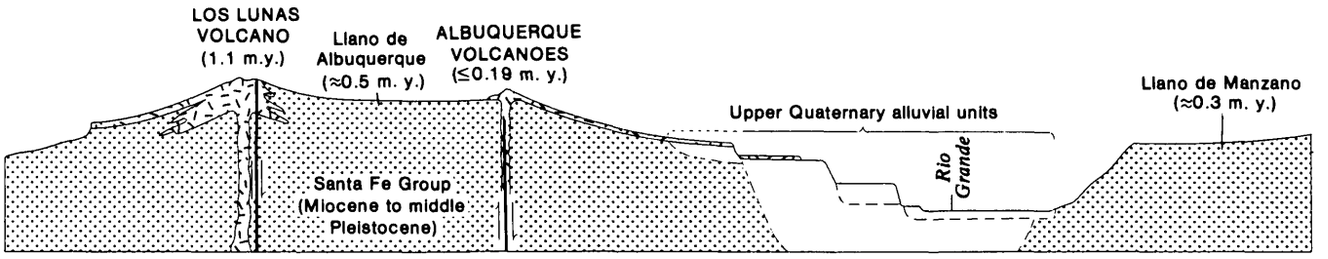

FIGURE 3.—Diagrammatic cross section of the Llano de Albuquerque, Llano de Manzano, and younger alluvial units in the vicinity of Albuquerque, N. Mex. Radiometric ages (Bachman and others, 1975) are by the K-Ar method. Dashed lines indicate base of upper Quaternary alluvial units. Arrows indicate relative direction of movement along faults.

regional geomorphic, geologic, and pedologic correlations (Hawley and others, 1976, Bachman and Machette, 1977). The Llano de Albuquerque represents in most places the culmination of basin-filling (Santa Fe Group) and predates the younger terrace and piedmont slope deposits of Lambert (1968). These data contradict the correlation of the Ortiz, Llano de Albuquerque, and Llano de Manzano (fig. 1) by Kelley and others (1976).

Geology of the study area

The study area lies just north of the Bernalillo County dump (fig. 4), located on the eastern edge of the Llano de Albuquerque. Here, the Llano slopes gently to the southeast, and about 2.5 km to the north it is overlain by the Albuquerque volcanoes, a string of eleven small volcanoes and spatter cones. Lava flows from the volcanoes spread easterly, over the eroded edge of the Llano, and down onto the two highest terraces of the Rio Grande (fig. 3). The oldest of the flows has been dated by the K-Ar method at 190 000±40 000 yr B. P. (Bachman and others, 1975). In my opinion the youngest flow may only be one-half as old, inasmuch as it is associated with the younger of the two terraces mentioned above.

A high-angle normal fault cuts the Llano de Albuquerque at the Bernalillo County dump (fig. 4). Lambert mapped this fault, recognized that it had had recurrent episodes of movement, and named it the County Dump fault. In the study area, the uppermost basin-fill deposit (bedrock) is the upper buff formation of the Santa Fe Group of Lambert (1968), previously the upper buff member of the Santa Fe Formation of Bryan (1937). The upper buff formation consists largely of well-sorted, well-rounded sand and gravel deposited by the Rio Grande.

Just north of the dump, the fault is well exposed in a natural outcrop (fig. 4); the fault dips 75°–80° E. and is clearly marked by a 30- to 50-cm-wide zone of reoriented gravel that resembles a clastic dike and by blocks of calcic soil that are sheared along the fault plane. No evidence suggests that this fault has been or is a source of $CaCO_3$ in the study area. The fault cuts the upper buff formation, and east of the fault a sequence of younger deposits and intercalated calcic paleosols are preserved in the downdropped block. The bulk of these deposits is fine to medium eolian sand, but minor amounts of pebbly colluvium and reworked soil are present, especially in the lower part of the section. These deposits are separated, markedly, by buried calcic paleosols (fig. 5). These soils are not considered to be features of past, more favorable soil-forming climates (as in soil-forming intervals) but

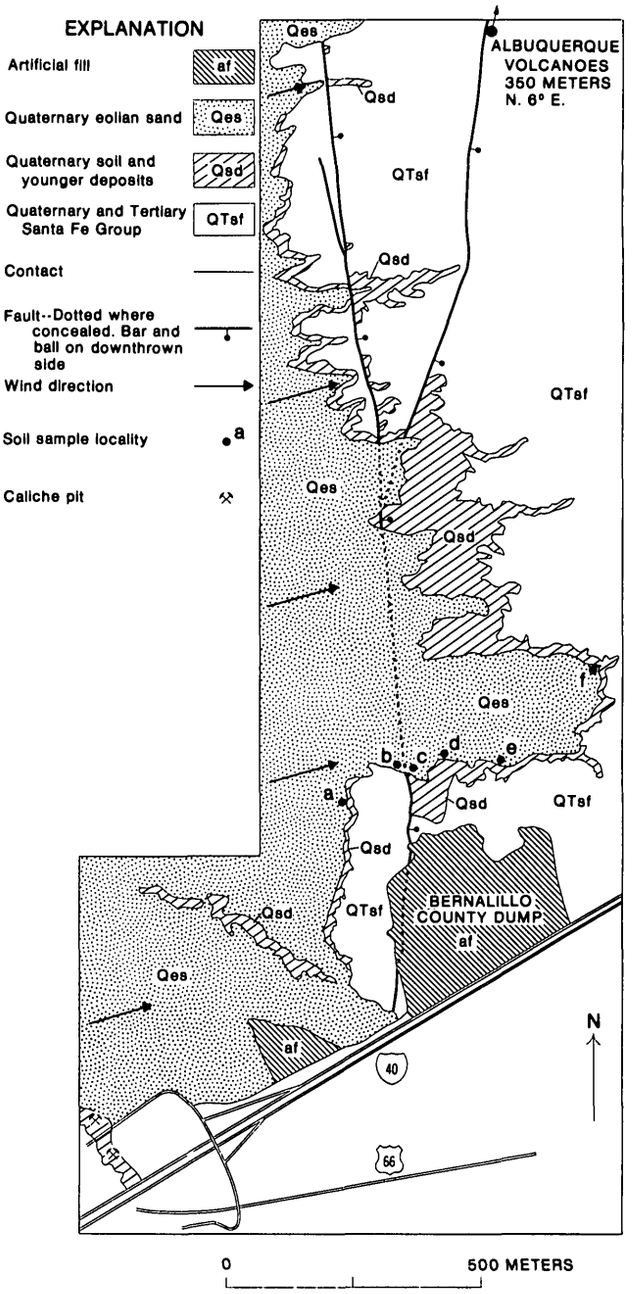

FIGURE 4.—Geologic map of the study area, Bernalillo County, N. Mex.

are the result of soil formation during periods of tectonic and geomorphic stability.

East of the fault, the younger deposits thin (fig. 6) and the buried paleosols (V, X, Y, and Z; fig. 5) converge (fig. 6, loc. f) to form a relict calcic soil (VX YZ) equivalent to that on the Llano de Albuquerque west of the fault (fig. 6, loc. a). Both relict soils are slightly eroded, but each is similar in total $CaCO_3$ content (C_T) to that of the composite buried paleosol

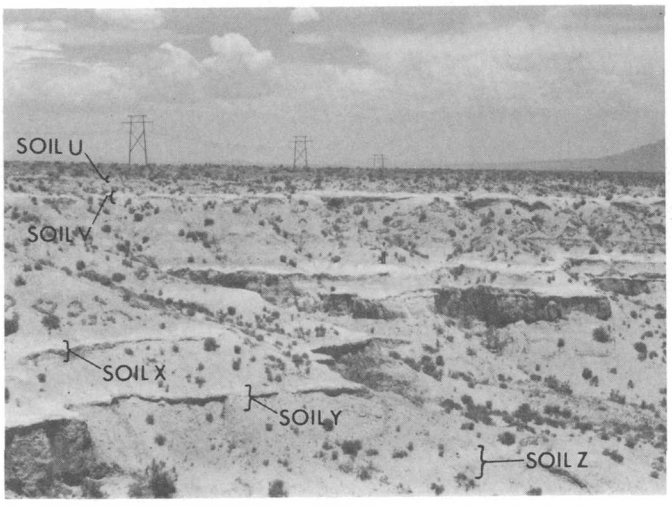

FIGURE 5.—Four buried paleosols (V, X, Y, and Z) and the modern surface soil (U). Photograph was taken from 6-m level, 100 m east of the County Dump fault; view is east, toward soil localities e and f (shown in fig. 6).

(fig. 7). Thus, these two relict soils help to establish the equivalence of the Llano de Albuquerque surface on each side of the fault. Additionally, the similar morphology, structural development, and total carbonate content of relict soils at numerous other locations on the Llano help to document the use of the Llano as a 500 000-yr datum.

SOILS DATA AND SOIL-AGE ESTIMATES

Using the descriptive soils and laboratory data (table 1), one may estimate the length of time that each paleosol remained at the surface. Likewise, the vertical separation between each buried soil at the fault represents the minimum movement during each episode of faulting.

Vertical sections containing soil profiles were described and sampled along the outcrop. These sections include soil profile horizonation, $CaCO_3$ content (C_3), and stratigraphic tie-lines (fig. 6). Soil profile locali-

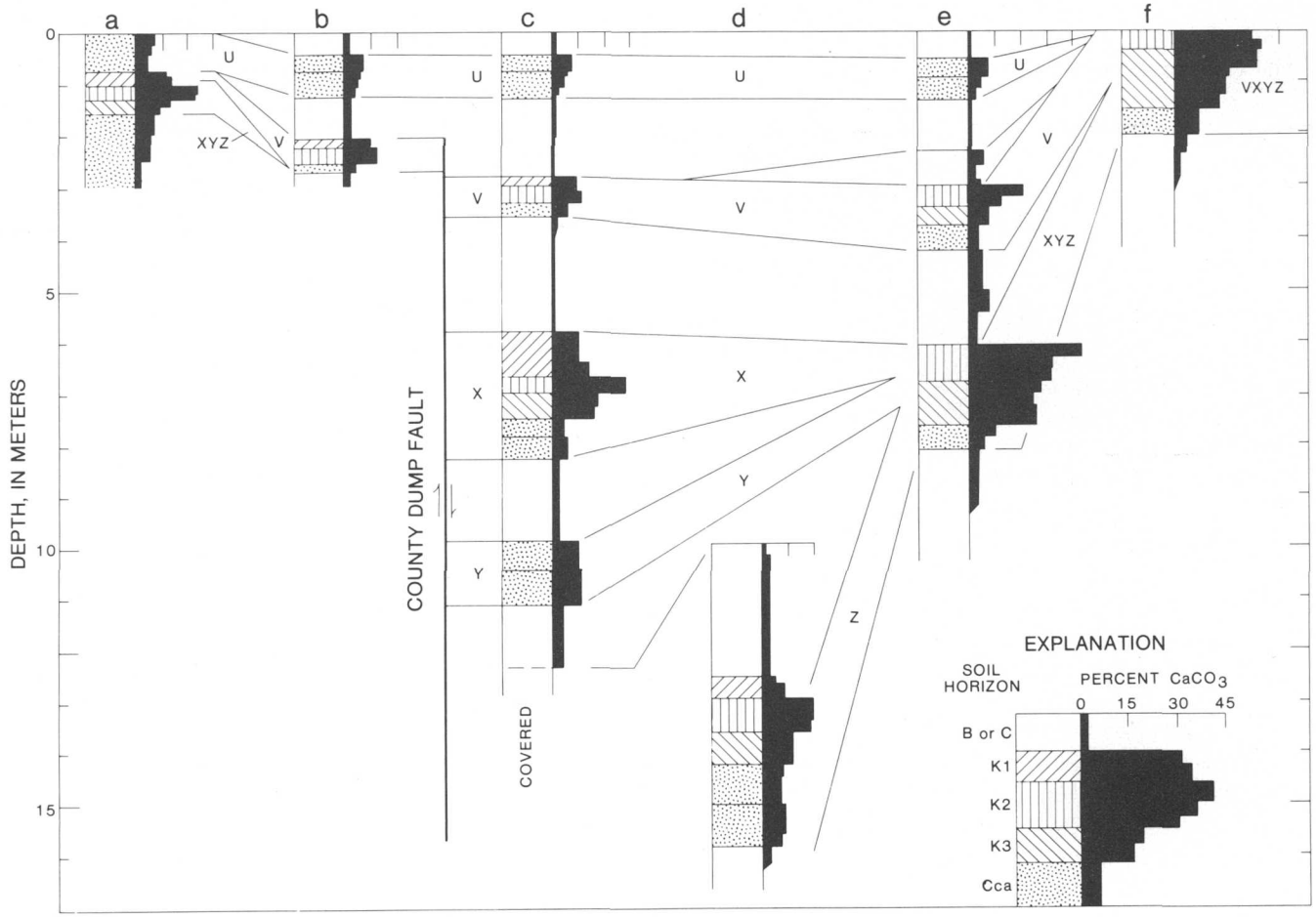

FIGURE 6.—Soil stratigraphy along a line perpendicular to the County Dump fault from soil sample localities a (west) to f (east). The columnar sections are based on detailed soil descriptions, laboratory data, and planetable survey.

ties b, c, d, and e were used to assemble a composite soil section (table 1) for calculation purposes. C_P, C_S, C_T, and the composite soil section are shown on the left side of figure 7. Sharp increases in C_S represent buried paleosols, whereas changes in slope for C_P represent slight differences in the primary $CaCO_3$ content of parent materials (table 1). The right side of figure 7 shows C_S only; each soil's contribution to the total C_S is shown by a hatched pattern.

Two assumptions are fundamental to the model developed here. The first assumption (previously discussed) is that of a constant rate of C_S accumulation. The second is that some amount of time is necessary for sedimentation and landscape stability to occur after faulting. Inasmuch as eolian sedimentation is an active and effective geomorphic agent in the study area, I have assumed that the time necessary for surface restabilization is negligible.

HISTORY OF FAULTING

The geologic history of the County Dump fault during the past 500 000 yr involves at least four discrete episodes of movement, deposition and surface restabilization of eolian and colluvial deposits on the downdropped block of the fault, and subsequent development of a calcic soil on each newly formed surface. Each buried soil represents a specific length of time during which it formed. The sum of C_S for the buried soils is about 1.25 times C_S in either of the adjacent relict soils. This discrepancy can be explained by (1) the erosion of adjacent relict soils (fig. 6, locs. a and f) with partial recycling of soil materials into the downdropped block, and (2) the effectiveness of the downdropped block in accumulating sediment; hence, the fault block acts as a $CaCO_3$ trap.

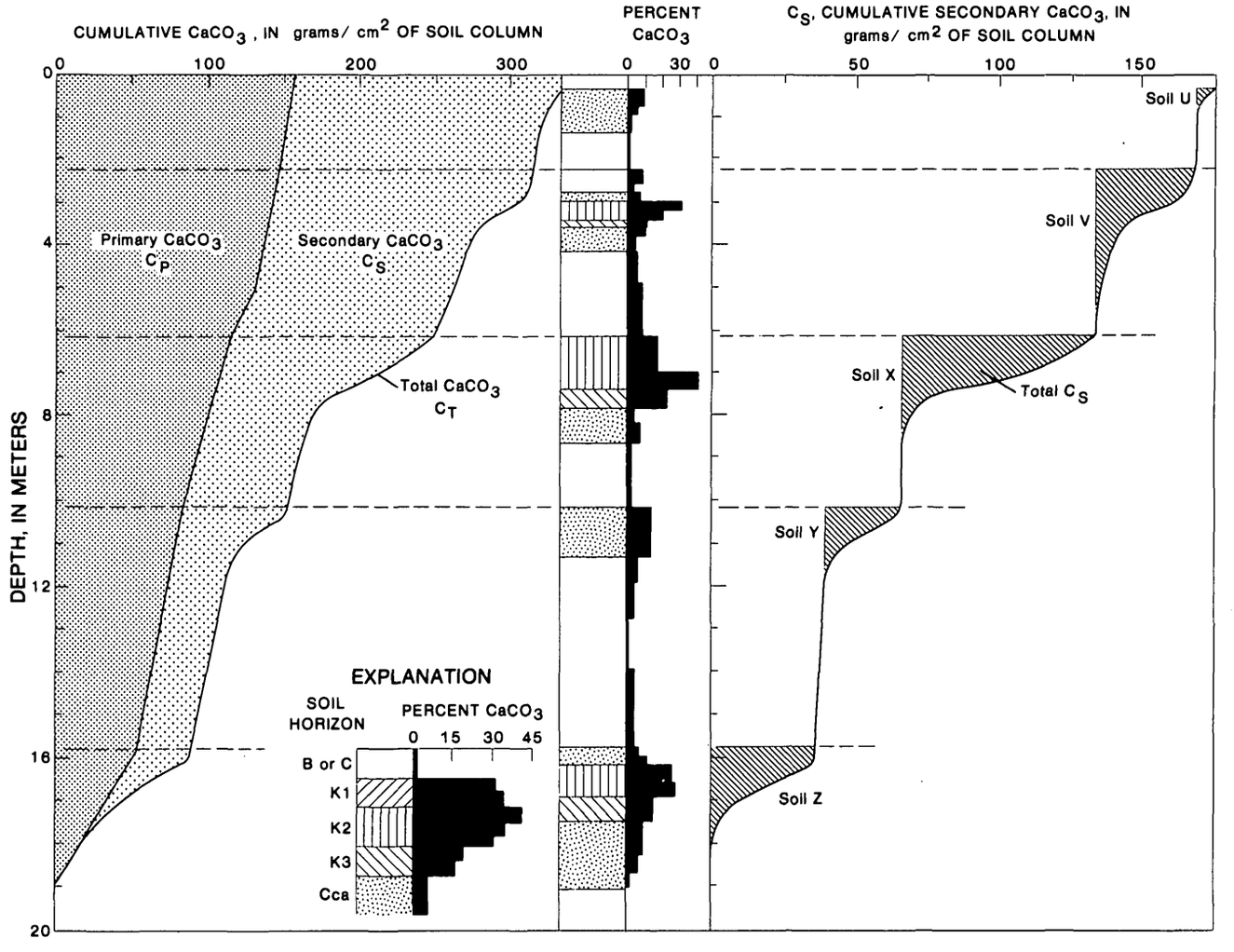

FIGURE 7.—Carbonate distribution in the composite soil section assembled from soil localities b, c, d, and e. Data for this figure are listed in table 1.

By plotting C_S for each soil of the composite soil section and considering that the Llano de Albuquerque formed 500 000 yr ago, I have been able to estimate ages for the individual buried soils (fig. 8). These ages represent the duration of soil formation; for example, soil Y formed from 400 000 yr B.P. to 310 000 yr B.P. The older age is the date of surface stabilization, after which a soil started to form, and the younger age is the date of the next episode of faulting, subsequent burial, and the end of that soil's development.

Using soil ages (fig. 8) and field relationships, the geologic history of the County Dump fault can be portrayed diagrammatically in a sequence of events (fig. 9). The first cross section shows the Llano de Albuquerque as it appeared just prior to 400 000 yr B.P.; a moderately developed soil (Z), which took about 100 000 yr to form, was present at the surface. At about 400 000 yr B.P., fault event 1 displaced the surface at least 7.8 m, down to the east. The displacement is expressed as a minimum because soil Z is covered at the fault and its upthrown equivalent has since been eroded.

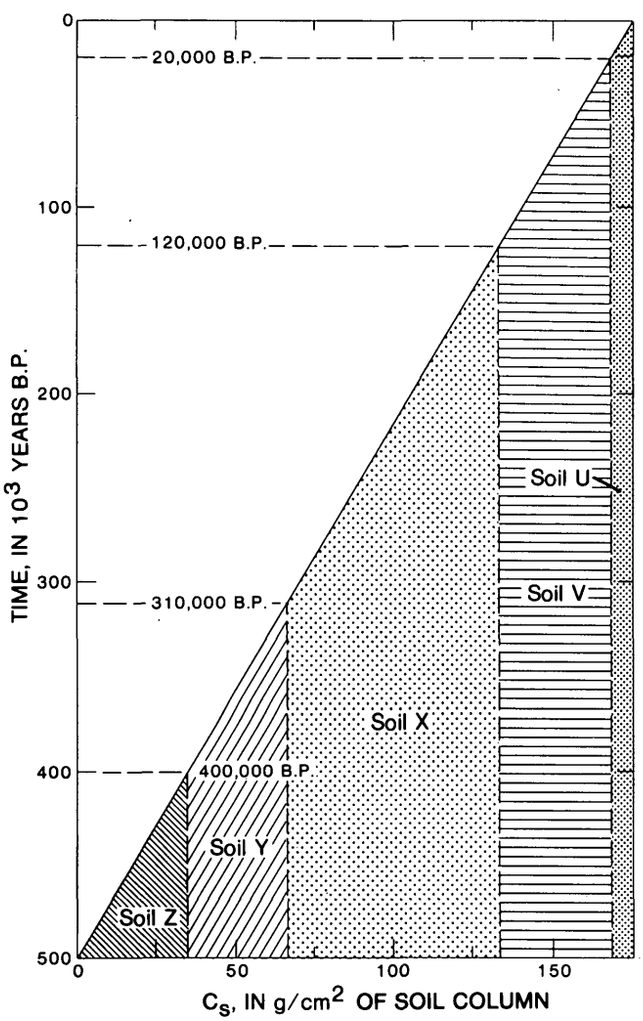

FIGURE 8.—Plot of C_S versus time. A total of 176 g $CaCO_3$/cm²-soil column has accumulated in the past 500 000 yr —an average rate of 0.35 g $CaCO_3 \cdot cm^{-2} \cdot 10^{-3}\ yr^{-1}$.

The remaining cross sections (2 through 5) illustrate how faulting continued to displace surface soils, which in turn became buried. During the past 400 000 yr, relict soils continued to form, both east and west of the fault, on stable surfaces. The uppermost soil (U) has formed in eolian sand (unit E) during the last 20 000 yr and is presently overlain, in places, by small coppice dunes. Soil U is not displaced by the fault; thus the last faulting occurred about 20 000 yr B.P. (cross section 5, fig. 9).

The ages of faulting, recurrence interval between faulting, and vertical-slip displacement for the County Dump fault are as follows:

Fault event	Age (yr B.P.)	Recurrence interval (yr)	Displacement (m)
1	400 000	------	>7.8
2	310 000	90 000	4.1
3	120 000	190 000	3.0
4	20 000	100 000	2.1

The history of the County Dump fault should not be interpreted as reflecting a 90 000- to 190 000-yr recurrence interval for movements on all the faults in the Rio Grande rift. The above example contains data from only one segment of a fault. If exposures were available on other segments, they could conceivably record a different history that might reflect fewer or greater numbers of events during the same time interval. Many other faults cut Quaternary deposits in the Albuquerque-Belen basin, and each has its own unique history of movements. The sum of all these events during a given time period might yield a composite recurrence interval several orders of magnitude less than that determined by studying only one fault or fault segment.

Other localities on the Llano de Albuquerque have similar evidence of recurrent faulting. The Sand Hills fault zone is located due west of the study area (fig. 1), on the west edge of the Llano de Albuquerque. Wright (1946) reported that 45 m of sediments on the eastern (downdropped) side of the Sand Hills fault zone contain 11 distinct zones of "calichified sand and gravel." George Bachman and I have measured and described a complete section at this site and have concluded that the Sand Hills fault zone has had a tectonic history much like that of the County Dump fault: recurrent faulting, periodic sedimentation, and subsequent soil formation. In addition, the Llano de Albuquerque has numerous broad north-south-trending swales. During 1975, Bachman and I drilled one

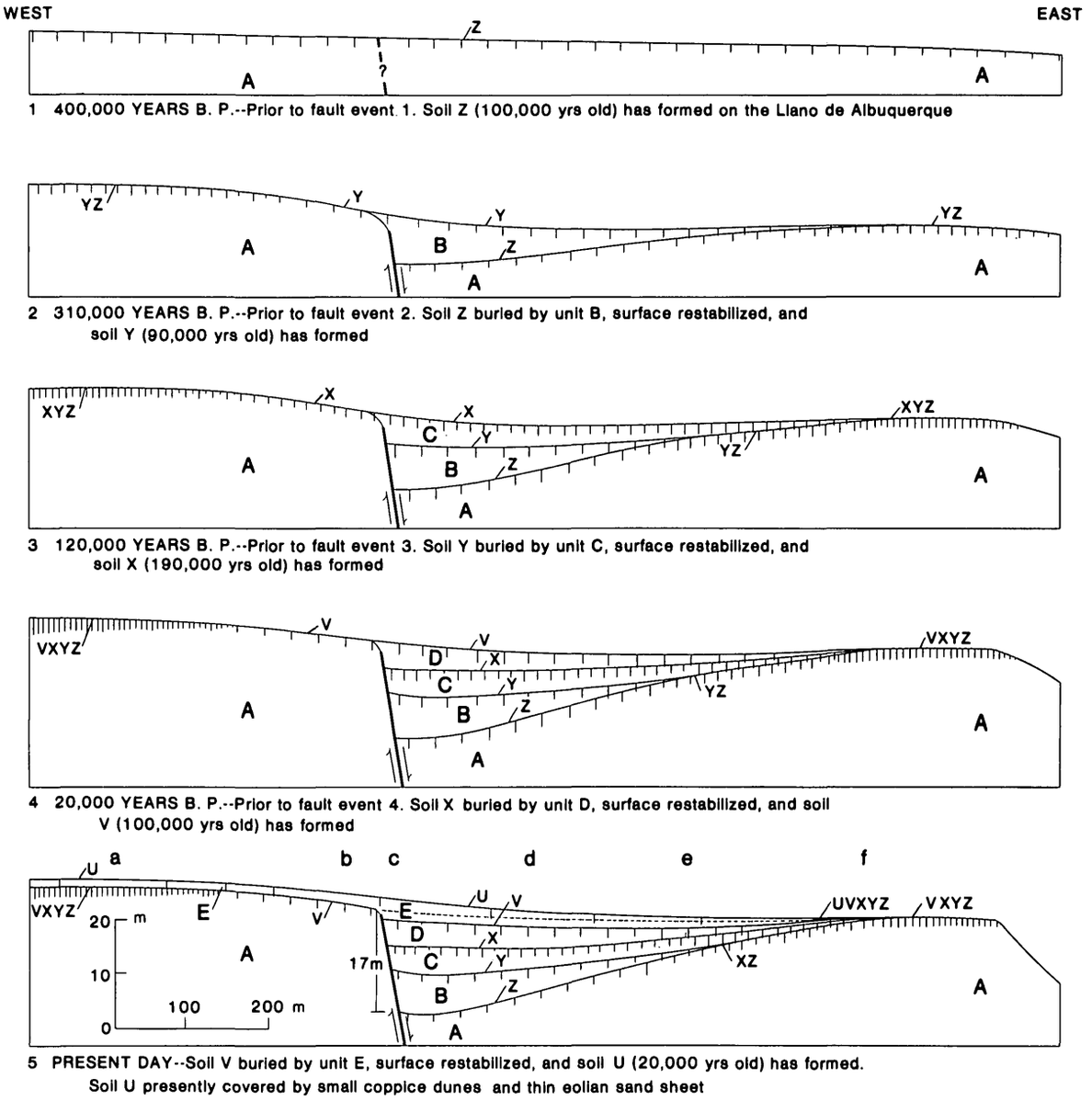

FIGURE 9.—Schematic cross sections showing sequence of events on the County Dump fault. Unit A is the upper buff formation of Lambert (1968); units B, C, D, and E are younger deposits. Soils U, V, X, Y, and Z (informal names) are shown by a vertical hachure pattern, the horizontal spacing of which is proportional to the duration of soil formation. Soil sample localities are shown by letters a, b, c, d, e, and f (figs. 4, 6).

such swale and found that it represented a buried fault scarp. I suggest that many of these swales may be buried fault scarps, some of which may have been recurrently active during late Pleistocene time. Deep trenching, drilling, and shallow geophysical surveys may help to substantiate this suggestion.

SUMMARY

The technique of quantifying calcic-soil properties and calculating ages of relict soils on the basis of $CaCO_3$ accumulation can also be used to estimate ages of Quaternary deposits and their associated surfaces, to correlate these features over broad regions, and to analyze regional trends in calcic-soil formation.

Advantages of the aforementioned approach to dating Quaternary faults are as follows:

1. The datable materials, calcic soils, are widespread in semiarid portions of the southwestern United

States and occur on stable geomorphic surfaces of late Pliocene to late Pleistocene age.

2. The method and analyses used are simple, easily attainable, and inexpensive (with the exception of absolute age dates).
3. The stratigraphic relations described at the study site are typical of recurrent Basin-and-Range faulting, and analogous sites are widespread in the western United States.
4. This approach yields ages, displacements, and recurrence intervals of faulting.

Finally, it should be emphasized that recurrence intervals calculated by this technique represent only specific fault segments. The composite recurrence interval for the whole fault, and moreover, all fault movements in an area, may be less by several orders of magnitude.

REFERENCES CITED

American Society for Testing and Materials, 1974, Standard method of test for specific gravity and absorption of coarse aggregate, *in* 1974 Annual Book of ASTM Standards, part 14: Am. Soc. Testing and Materials, p. 78–81.

Arkley, R. J., 1963, Calculation of carbonate and water movement in soil from climatic data: Soil Sci., v. 96, no. 4, p. 239–248.

Bachman, G. O., Marvin, R. F., Mehnert, H. H., and Merritt, Violet, 1975 K-Ar ages of the basalt flows at Los Lunas and Albuquerque, central New Mexico: Isochron/West, no. 13, p. 3–4.

Bachman, G. O., and Machette, M. N., 1977, Calcic soils and calcretes in the southwestern United States: U.S. Geol. Survey Open-File Rept. 77–794, 163 p.

Bachman, G. O., and Mehnert, H. H., 1978, Geologic significance of some recent K-Ar dates, central Rio Grande region, New Mexico: Geol. Soc. America Bull., v. 89, no. 2, p. 283–292.

Birkeland, P. W., 1974, Pedology, weathering and geomorphological research: New York, Oxford Univ. Press, 285 p.

Bryan, Kirk, 1937, Geology and ground-water conditions of the Rio Grande depression in Colorado and New Mexico, *in* U.S. National Resource Commission Planning Board, The Rio Grande joint investigation in the upper Rio Grande Basin, volume 1, part 2: Washington, U.S. Govt. Printing Office, p. 197–225.

Bryan, Kirk, and McCann, F. T., 1937, The Ceja del Rio Puerco, a border feature of the Basin and Range province in New Mexico: Jour. Geology, v. 45, no. 8, p. 801–828.

——— 1938, The Ceja del Rio Puerco, a border feature of the Basin and Range province in New Mexico, part 2, Geomorphology: Jour. Geology, v. 46, no. 1, p. 1–16.

Chapin, C. E., and Seager, W. R., 1975, Evolution of the Rio Grande Rift in the Socorro and Las Cruces areas, *in* New Mexico Geological Society Guidebook 26th Field Conference, Las Cruces County, 1975: p. 297–321.

Chleborad, A. F., Powers, P. S., and Farrow, R. A., 1975, A technique for measuring bulk volume of rock materials: Assoc. Eng. Geologists Bull., v. 12, no. 4, p. 317–322.

Clark, M. M., and Lajoie, K. R., 1974, Holocene behavior of the Garlock fault: Geol. Soc. America Abs. with Programs, v. 6, no. 3, p. 156.

Denny, C. S., 1940, Tertiary geology of the San Acacia area, New Mexico: Jour. Geology, v. 48, no. 1, p. 73–106.

——— 1941, Quaternary geology of the San Acacia area, New Mexico: Jour. Geology, v. 49, no. 3, p. 225–260.

Douglas, L. A., Ellwood, R. B., Fischer, J. A., Gates, T., Gibbons, J. F., Marks, J. H., McEldowney, R. C., McWhorter, J. G., and Robinson, C. M., Jr., 1974, Dating of fault movements—The approach at North Anna [Virginia]: Geol. Soc. America Abs. with Programs, v. 6, no. 7, p. 713.

Dreimanis, Aleksis, 1962, Quantitative determination of calcite and dolomite by using Chittick apparatus: Jour. Sed. Petrology, v. 32, no. 3, p. 520–529.

Gardner, L. R., 1972, Origin of the Mormon Mesa caliche, Clark County, Nevada: Geol. Soc. America Bull., v. 83, no. 1, p. 143–156.

Gile, L. H., 1977, Holocene soils and soil-geomorphic relations in a semiarid region of southern New Mexico: Quaternary Research, v. 7, no. 1, p. 112–132.

Gile, L. H., Peterson, F. F., and Grossman, R. B., 1965, The K-horizon; a master soil horizon of carbonate accumulation: Soil Sci., v. 99, no. 2, p. 74–82.

——— 1966, Morphological and genetic sequences of carbonate accumulation in desert soils: Soil Sci., v. 101, no. 5, p. 347–360.

Gile, L. H., Hawley, J. W., and Grossman, R. B., 1971, The identification, occurrence, and genesis of soils in an arid region of southern New Mexico, *in* Training bulletin, desert soil-geomorphology project, Dona Ana County, New Mexico: U.S. Dept. Agriculture, Soil Conserv. Service, Soil Survey Inv., 177 p.

Goudie, A. S., 1971, A regional bibliography of calcrete, *in* W. G. McGinnies, B. J. Goldman, and P. Paylore, eds., Food, fiber and the arid lands: Tucson, University of Arizona Press, p. 421–437.

——— 1973, Duricrusts in tropical and subtropical landscapes: London, Oxford University Press, 174 p.

Hawley, J. W., Bachman, G. O., and Manley, Kim, 1976, Quaternary stratigraphy in the Basin and Range and Great Plains provinces, New Mexico and Western Texas, *in* W. C. Mahaney, ed., Quaternary stratigraphy of North America: Stroudsburg, Pa., Dowden, Hutchinson, and Ross, Inc., p. 235–274.

Jenny, Hans, 1941a, Calcium in the soil, III—Pedogenic relations: Soil Sci. Soc. America Proc., v. 6, p. 27–35.

——— 1941b, Factors in soil development: New York, McGraw-Hill, 281 p.

Junge, C. E., and Werby, R. T., 1958, The concentration of chloride, sodium, potassium, calcium, and sulfate in rain water over the United States: Jour. Meteorology v. 15, no. 5, p. 417–425.

Kelley, V. C., Woodward, L. A., Kudo, A. M., and Callender, J. F., 1976, Guidebook to Albuquerque Basin of the Rio Grande Rift, New Mexico: New Mexico Bur. Mines and Mineral Resources Circ. 153, 31 p.

Lambert, P. W., 1968, Quaternary stratigraphy of the Albuquerque area, New Mexico: New Mexico Univ. Ph. D. thesis, 300 p.

Machette, M. N., 1977, Geology of the San Acacia quadrangle, Socorro County, New Mexico: U.S. Geol. Survey Geol. Quad. Map GQ–1415 [1978].

Oliver, Jack, Sanford, Allan, Chapin, Charles, and Kaufman, Sidney, 1976, Seismic reflection profiling of the deep basement—the Rio Grande Rift: Geol. Soc. America Abs. with Programs, v. 8, no. 6, p. 1035.

Page, W. D., and Walsh, J. P., 1974, The direct use of pedogenic soils to date fault movements: Geol. Soc. America Abs. with Programs, v. 6, no. 7, p. 902.

Payne, C. M., and Wilson, K. L., 1974, Age dating recent movement on the Raymond fault, Los Angeles County, California: Geol. Soc. America Abs. with Programs, v. 6, no. 3, p. 234.

Richmond, G. M., 1962, Quaternary stratigraphy of the La Sal Mountains, Utah: U.S. Geol. Survey Prof. Paper 324, 135 p.

Scott, G. R., 1963, Quaternary geology and geomorphic history of the Kassler quadrangle, Colorado: U.S. Geol. Survey Prof. Paper 421–A, p. 1–70.

Shlemon, R. J., 1975, Applications of soil stratigraphy for siting nuclear power plants: Geol. Soc. America Abs. with Programs, v. 7, no. 7, p. 1269.

Soil Survey Staff, 1975, Soil taxonomy—A basic system of soil classification for making and interpreting soil surveys: U.S. Dept. Agriculture, Agriculture Handb. no. 436, 754 p.

Wright, H. E., Jr., 1946, Tertiary and Quaternary geology of the lower Rio Puerco area, New Mexico: Geol. Soc. America Bull., v. 57, no. 5, p. 383–456.

Jour. Research U.S. Geol. Survey
Vol. 6, No. 3, May–June 1978, p. 383–390

PALEOMAGNETIC EVIDENCE FOR A LATE CRETACEOUS DEFORMATION OF THE GREAT VALLEY SEQUENCE, SACRAMENTO VALLEY, CALIFORNIA

by EDWARD A. MANKINEN, Menlo Park, Calif.

Abstract.—Paleomagnetic samples from five localities within the Great Valley sequence range in age from Late Jurassic to Late Cretaceous. All samples possess normal polarity, and alternating-field demagnetization experiments show that the remanence was acquired after the sequence was folded. A mean paleomagnetic pole position determined from 17 demagnetized samples is located at 72° N., 181° E., with the radius of the 95-percent circle of confidence equal to 5.4°. This pole position agrees very well with known Cretaceous poles from North America, a fact indicating that the deformation and remagnetization of the sequence must have occurred during the Late Cretaceous.

The Great Valley sequence of Bailey, Irwin, and Jones (1964) forms a thick north-trending belt of marine sedimentary rocks along the west margin of the Sacramento Valley. In general, the strata are homoclinical, with dips ranging from about 20° E. along Dry Creek near the north end of the sequence to as much as 70° E. along Putah Creek near the south end. The main rock types are mudstone, siltstone, sandstone, and conglomerate containing locally abundant fossils and representing a nearly continuous record of Late Jurassic to Late Cretaceous sedimentation. Detailed descriptions of the geology may be found in Bailey, Irwin, and Jones (1964), Ojakangas (1968), and Murphy, Rodda, and Morton (1969).

At the north end of the sequence, the strata unconformably overlie igneous and metamorphic rocks of the Klamath Mountains province (Irwin, 1960). Toward the west, they overlie mafic and ultramafic rocks of the Coast Range ophiolite (Bailey and others, 1970; Blake and Jones, 1977), and toward the east, the strata dip beneath upper Tertiary and Quaternary rocks.

Paleomagnetic samples were collected from five localities within the sequence (fig. 1). Samples from the Dry Creek–Budden Canyon section range in age from Hauterivian to early Coniacian (Murphy and others, 1969). Samples from the South Fork of Cottonwood Creek are of late Turonian through Coniacian age (Jones and Bailey, 1973). Samples from McCarty Creek are of Berriasian to early Hauterivian, and samples from Grindstone Creek are of mid-Tithonian to early Berriasian age (Jones and others, 1969; Imlay and Jones, 1970). The Venado Formation of Kirby (1943) sampled at Putah Creek is of Turonian age (Brown and Rich, 1960; Popenoe and others, 1960).

Acknowledgments.—Details of the geology and paleontology of the sequence, provided by D. L. Jones, were invaluable in the selection of sites for paleomagnetic sampling. C. S. Grommé contributed the samples from Putah Creek and many helpful discussions during the course of this study. Special thanks are also due A. H. Atkinson for assistance in the field and D. P. Elston for preliminary magnetic measurements of the collection.

METHODS USED

Samples were collected using a portable core drill and oriented using a magnetic compass. A total of 297 cores was collected, spanning a total stratigraphic thickness of approximately 15 000 m. Each core was cut into specimens 2.45 cm in diameter and 2.50 cm long, and one such specimen from each core was measured on a cryogenic magnetometer. Progressive AF (alternating-field) demagnetization experiments were performed using either a three-axis tumbler (Doell and Cox, 1976a) or a commercial 400-Hz (hertz) nontumbling demagnetizer. When the three-axis tumbler was used, the specimens were demagnetized twice at each increment of alternating field, and a vectorial method described by Grommé and Mankinen (1976) for eliminating the effects of rotational remanent magnetization was used to determine the true remanent magnetization at each step.

Weak-field susceptibilities were measured at 1000 Hz by using a commercial bridge. Saturation magnetizations were determined from magnetization curves obtained in fields from 0 to 9000 oersteds.

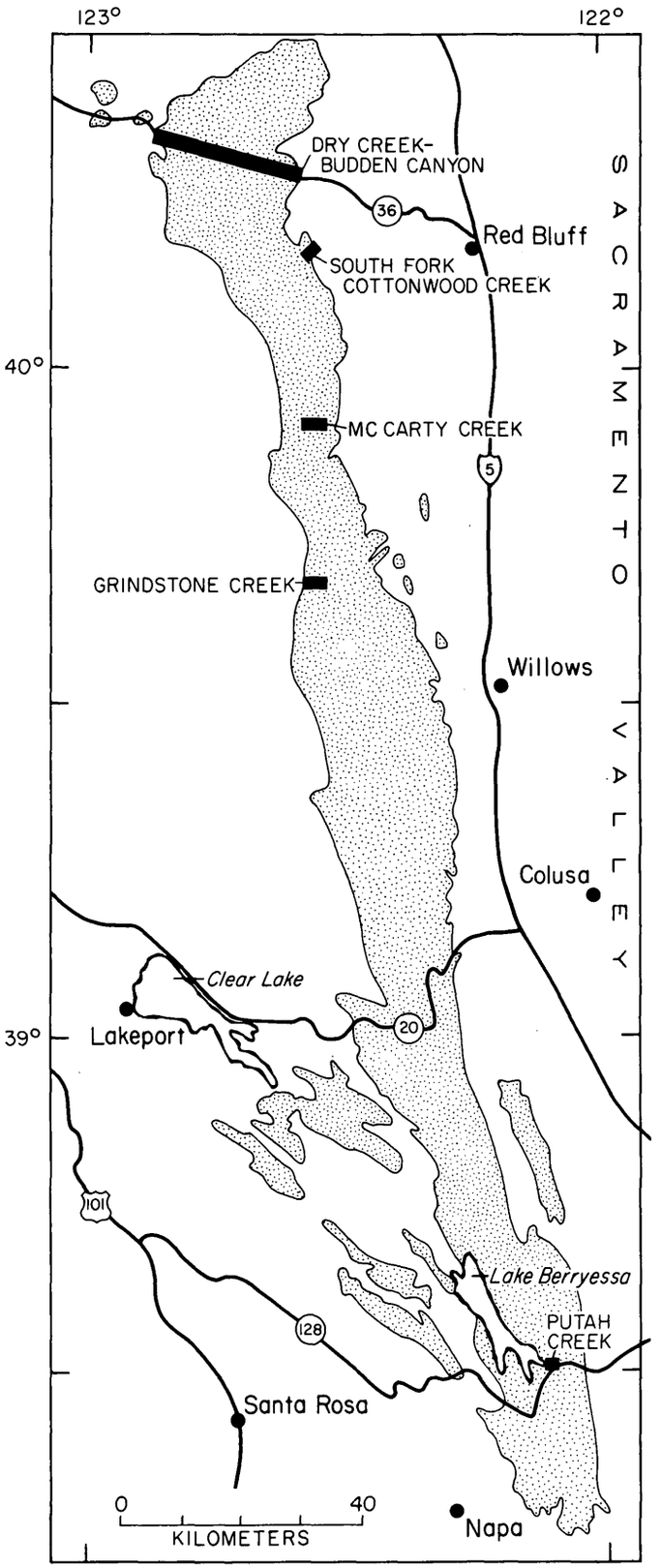

FIGURE 1.—Locations and informal names of sampled stratigraphic sections discussed in text. General distribution of Great Valley sequence (stippled) modified from Bailey, Irwin, and Jones (1964).

Saturation remanent magnetizations were induced in a field of 8000 Oe. Strong-field thermomagnetic curves were obtained using an automatic recording balance described by Doell and Cox (1967b). These experiments were made in air by using applied fields of 2500 to 4000 Oe at heating and cooling rates of 10°C/min.

REMANENCE MEASUREMENTS

NRM (natural remanent magnetization) measurements show only normal polarity for all samples. Average NRM directions and other magnetic properties were grouped by locality and are given in table 1. A mean direction of magnetization, calculated from the average for each locality, has a 95-percent-confidence circle (α_{95}) of 5° radius with an angular standard deviation to the mean of 5°. However, when all directions are corrected for the attitude of bedding, α_{95} increases to 16° and the angular standard deviation to 19°, demonstrating that the remanence was acquired after the sequence was folded.

In order to determine if the directions could be the result of VRM (viscous remanent magnetization) acquired in the present Earth's field, all samples except for those from Putah Creek were stored in the laboratory for 1 year before being remeasured. The average angular difference between measurements on any one sample was only 5°, a fact suggesting the absence of unstable components of NRM.

Progressive AF demagnetization experiments up to fields of 400 to 600 Oe were made on 19 samples from the four northern localities. These samples were selected from various stratigraphic levels throughout the sequence in order to get a representative sampling over a long period of time. When the logarithm of magnetization is plotted against the demagnetizing field, all the data fall on nearly straight lines, which again is an indication that significant components of anomalous magnetization are absent. The median demagnetizing field, the field at which the NRM intensity is reduced to half its initial value, ranged from 60 to 190 Oe with values most commonly between 100 and 150 Oe. All samples showed a systematic progression of direction along arcs of great circles, and the "best" direction for each was taken to be the last point that followed this systematic trend. The optimum demagnetizing field for all was between 150 and 350 Oe.

After demagnetization, all samples except two defined a group with a mean inclination of +65° and a declination of 339° (fig. 2). For these 17 samples, α_{95} was 4° and the precision parameter K of Fisher (1953) was 96. After the bedding correction was ap-

TABLE 1.—*Average NRM (natural remanent magnetization) directions and magnetic properties*

[N, number of samples; I, mean inclination of NRM, in degrees, positive downward; D, mean declination of NRM, in degrees east of north; u, uncorrected; c, corrected for attitude of bedding; J, geometric mean NRM intensity ($\times 10^{-5}$ emu/cm^3); X, geometric mean susceptibility ($\times 10^{-4}$); Q, geometric mean in-place ratio of remanent to induced magnetization (Koenigsberger ratio); SD_J, SD_X, SD_Q, range of one standard deviation of geometric means for J, X, and Q, respectively; K, precision parameter of Fisher (1953); α_{95}, 95-percent confidence circle about average direction; and s.d., angular standard deviation about average direction]

Locality	N	Average NRM directions				J	SD_J	X	SD_X	Q	SD_Q
		I_u	D_u	I_c	D_c						
Budden Canyon	28	+71	007	+59	052	0.46	{1.35 .16	0.32	{1.01 .10	0.27	{0.59 .13
Dry Creek	95	+68	017	+58	050	1.20	{5.24 .28	1.31	{5.30 .32	.17	{ .42 .07
South Fork Cottonwood Creek	10	+68	360	+35	034	1.97	{5.34 .73	1.27	{3.45 .46	.29	{ .36 .24
McCarty Creek	41	+69	345	+38	069	.30	{ .76 .12	.24	{ .48 .12	.24	{ .38 .15
Grindstone Creek	37	+68	337	+32	064	.43	{ .82 .22	.23	{ .32 .16	.36	{ .64 .20
Putah Creek	73	+70	353	+20	073	2.18	{5.08 .94	5.23	{14.9 1.84	.08	{ .14 .05
Average direction all localities	6	+69	356	+41	058						
Direction statistics		Uncorrected: $K = 218$, $\alpha_{95} = 5$, s.d. = 5		Corrected: $K = 18$, $\alpha_{95} = 16$, s.d. = 19							

plied, the mean inclination was +52° and the declination 46°, with $K = 18$ and $\alpha_{95} = 9°$. Clearly, even the stable magnetization recovered by AF demagnetization was acquired after the sequence was folded. Of the two samples that differed significantly from this group, one showed little change in direction during demagnetization, a fact indicating either that it became remagnetized at a later time than the other samples or that, because it was collected near a fault, some tectonic correction should have been applied. The second sample showed a progressive change toward a probable reversed direction, but no stable endpoint was reached before its magnetization became random. For this reason, it was not possible to determine whether the sample became remagnetized during a time when the Earth's field was reversed or whether some primary reversed magnetization was not completely destroyed during the postdeformation remagnetization.

Demagnetization curves for eight samples from Putah Creek also plot as straight lines, although the slopes are considerably steeper than those for the northern sections, a fact indicating that the NRM is softer at this locality. Median demagnetizing fields between 50 and 70 Oe and magnetic instability of most samples in fields as low as 100 to 150 Oe also suggest soft NRM. Changes in direction during demagnetization were much less systematic than in the other sections, and, as a result, the determination of the best direction for each sample tended to be more subjective. The mean direction of magnetization for these demagnetized samples, uncorrected for bedding attitude, has an inclination of +56° and a declination of 344° ($N = 8$, $K = 23$, $\alpha_{95} = 12°$), which is not statistically different from the mean calculated for the northern sections. Applying the tectonic correction gives an inclination of +26° and a declination of 58°, which corresponds to no known ancient field direction, again demonstrating remagnetization after deformation. The greater scatter in directions at this locality may simply be the result of the less stable magnetization, although more than one episode of remagnetization is certainly a possibility.

MAGNETIC PROPERTIES

The most obvious differences in magnetic properties between sections is that the Putah Creek samples have much higher susceptibilities and lower Koenigsberger ratios (table 1). Of the 73 samples from this locality, only 6 have susceptibilities in the 10^{-5} range with the remainder being 2×10^{-4} and higher. Of the samples from the northern sections, only 15 percent have susceptibilities approaching values as high as those from Putah Creek. Strong-field thermomagnetic curves were obtained from six samples taken from various

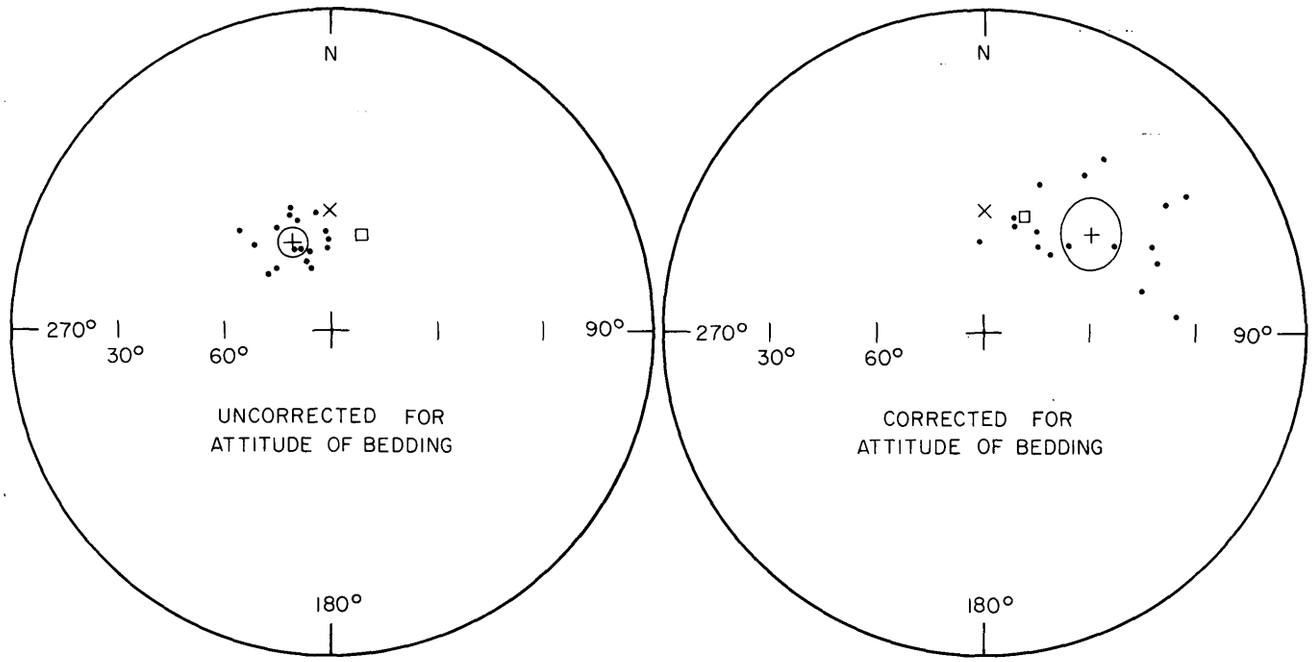

FIGURE 2.—Average remanent magnetization directions (dots) after magnetic cleaning. All directions on lower hemisphere of equal-area projection. Small cross, mean of all directions with its associated 95-percent-confidence circle; ×, ideal dipole field direction; small square, present field direction.

levels throughout the sequence and all have Curie temperatures between 575° and 580°C, facts showing that the main magnetic mineral present is magnetite.

Given identical mineralogy, both the susceptibility and the M_S (saturation magnetization) of a sample will vary with the volume fraction of magnetic minerals present, and the susceptibility will also vary with changes in grain size. Since both quantities increase with volume fraction, there should be a linear relation between saturation magnetization and susceptibility if this is the only variable. As shown in table 2 and figure 3*A*, the increase in both properties is not entirely linear, a fact suggesting some variation in grain size as well.

TABLE 2.—*Variation of magnetic properties with susceptibility*

[X, susceptibility ($\times 10^{-4}$); M_{RS}, saturation remanence ($\times 10^{-3}$ emu/g); M_S, saturation magnetization (emu/g); N.d., not determined]

	Putah Creek			Northern localities		
X	M_{RS}	M_S	M_{RS}/M_S	M_{RS}	M_S	M_{RS}/M_S
12.2	7.35	0.706	0.010			
7.95	3.60	.460	.008			
6.21	3.07	.368	.008			
5.65	4.60	.339	.014			
5.53				8.93	0.209	0.043
4.94	3.33	.237	.014			
4.34				5.18	.107	.048
3.47				8.53	.241	.035
.97				2.57	.051	.050
.53				1.50	.013	.115
.44	.88	.012	.073			
.33	.40	N.d.	N.d.			
.33				1.16	.009	.129
.33				1.13	.006	.188
.32				.81	N.d.	N.d.
.11				.25	N.d.	N.d.
.11				.59	.002	.295

The saturation remanence (M_{RS}) of a sample varies with volume fraction and also with the coercive force of the minerals, which is dependent on grain size. If the susceptibility differences seen are simply due to changes in concentration, then the saturation remanence at any given susceptibility should be the same if the coercive force is constant. Where there is an overlap in susceptibilities between sections (table 2), the saturation remanence of samples from Putah Creek is considerably lower, indicating a decrease in coercive force that must be due to an increase in grain size.

Since, for a constant volume fraction of magnetite, increase in grain size reduces the saturation remanence without changing the saturation magnetization, perhaps a more reliable indication of grain size variation would be the ratio of the two properties. This ratio in all samples is very small (table 2), indicating that the remanence is carried by multidomain grains; Stacey

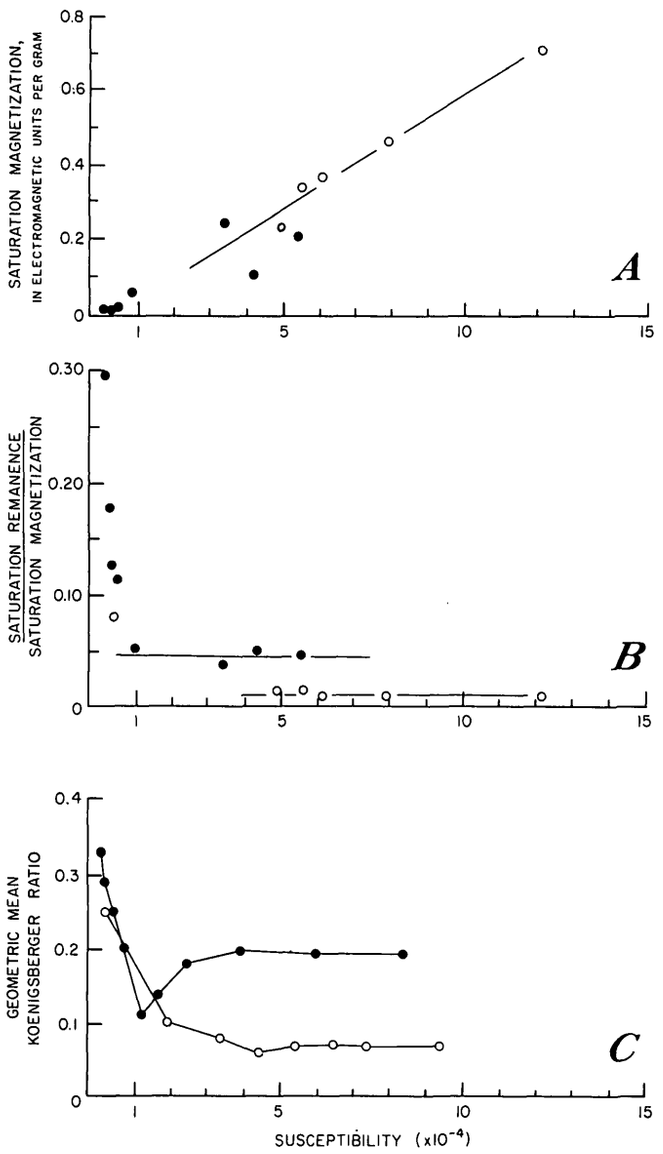

FIGURE 3.—Variation of magnetic properties with susceptibility. *A*, Saturation magnetization. *B*, Ratio of saturation remanence to saturation magnetization. *C*, Geometric mean Koenigsberger ratio. Circles, samples from Putah Creek; dots, samples from northern localities.

and Banerjee (1974) have shown that the saturation remanence should be about one-half of the saturation magnetization for single-domain grains. A plot of the ratio M_{RS}/M_S against susceptibility (fig. 3*B*) indicates a large variation in grain size throughout the sequence. With the exception of a few low-susceptibility samples that exhibited demagnetization behavior similar to those from the northern localities, the ratio for the Putah Creek samples is much lower, suggesting an appreciably larger grain size. This interpretation is substantiated in a general way by the lower Koenigsberger ratios for the Putah Creek samples (fig. 3*C*), because this ratio tends to increase with a decrease in grain size. These experiments all suggest that the remanence of the Putah Creek samples is carried by larger multidomain grains than are found in samples from the sections to the north. A larger grain size would be the most probable cause of the relatively unstable magnetization in the samples from Putah Creek.

DISCUSSION

A VGP (virtual geomagnetic pole) was calculated for each sample demagnetized (uncorrected for bedding attitude), except for those from Putah Creek, and the VGP's were then averaged to obtain a mean paleomagnetic pole located at 72° N., 181° E. (N=17, K = 44, α_{95}=5.4°). This pole is not significantly different from known reliable Cretaceous poles from North America (table 3 and fig. 4), a fact suggesting that the Great Valley sequence must have been folded and remagnetized during the Late Cretaceous. Pole positions omitted from the list of reliable Cretaceous poles in table 3 are those for the Dakota Sandstone (Runcorn, 1956) because of insufficient sampling and for the Bucks batholith and Guadaloupe Mountains (Grommé and others, 1967) because of their probable Late Jurassic age. Poles determined for the Boulder

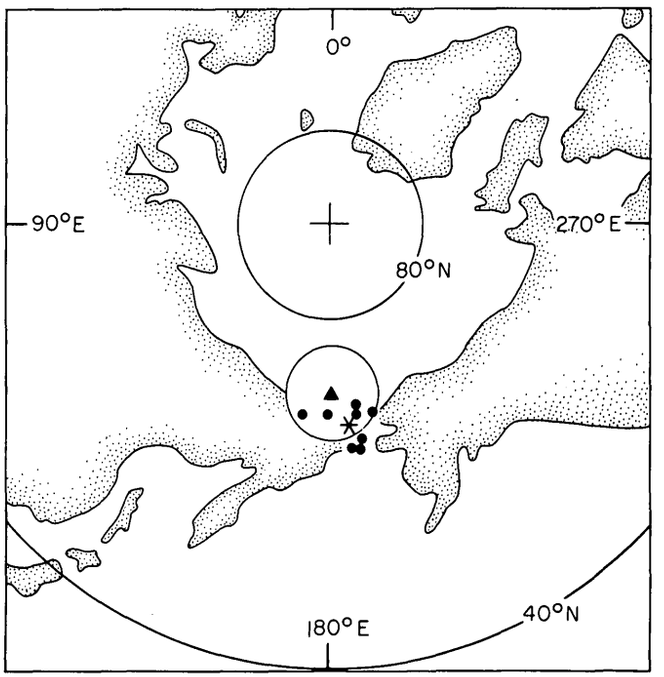

FIGURE 4.—Equal-area projection of part of northern hemisphere showing the pole position determined for the Great Valley sequence (triangle) and its associated 95-percent-confidence circle. Dots are Cretaceous pole positions listed in table 3; average of these poles shown as an asterisk.

TABLE 3.—*Cretaceous paleomagnetic pole positions for North America*

Rock unit	Locality	Pole position		Reference
Mt. Megantic intrusive	Quebec	69°N	172°E	Larochelle (1961)
Isachsen diabase	Canadian Arctic	69°N	180°E	Larochelle and Black (1963) Larochelle, Black and Wanlass (1965)
Sierra Nevada plutons	California	69°N	195°E	Grommé and Merrill (1965)
Mt. Ascutney intrusive	Vermont	65°N	186°E	Opdyke and Wensink (1966)
Elkhorn Mountains Volcanics	Montana	69°N	189°E	Hanna (1967)
Monteregian Hills intrusives	Quebec	70°N	189°E	Larochelle (1969)
Alkalic intrusives	Arkansas	65°N	187°E	Scharon and Hsu (1969)
Niobrara Formation	Colorado,Kansas	66°N	189°E	Shive and Frerichs (1974)
	Average:	68°N	186°E	

batholith (Hanna, 1973) and the Mesaverde Group (Kilbourne, 1969) were omitted because of their large error limits, and the pole for the Howe Sound plutons (Symons, 1973), because of its anomalous direction. Symons' high pole latitude (83° N.) for the Howe Sound plutons suggests that the plutons may have acquired their magnetization considerably later than the time of emplacement or, alternately, that some tectonic rotation has been involved, because they are located in the western cordillera, where anomalous directions have sometimes been observed (Beck, 1975). The pole for the Niobrara Formation was calculated from Shive and Frerichs' (1974) published data without the Kemmerer and Centennial Valley sites because of the large error limits for data from those localities.

NRM directions from Grindstone Creek and the lower 2500 m of the McCarty Creek section are tightly grouped, suggesting that the original remagnetization has not been much modified; therefore, a VGP was calculated for each section for comparison. The VGP for Grindstone Creek is located at 71° N., 189° E. ($N = 37$, $K = 29$, $\alpha_{95} = 4.5°$), and for McCarty Creek at 74° N., 196° E. ($N = 29$, $K = 56$, $\alpha_{95} = 3.6°$), neither of which is significantly different from the mean calculated for the demagnetized samples nor from the known Cretaceous poles.

Whereas the pole position determined from the Great Valley sequence is completely consistent with other poles determined for the Cretaceous Period, the possibility that the pole may have remained at the same location until some time during the Tertiary must be considered. Studies summarized by McElhinny (1973) have shown that the pole for the late Tertiary of North America is located near the geographic pole, but there are no reliable data for the early Tertiary. One method of determining an early Tertiary pole position would be to locate a well determined pole of the same age from Europe or Africa. The finite-rotation method of Pitman and Talwani (1972) could then be used to obtain the relative paleogeographic positions of the continents and the pole position relative to North America. A paleomagnetic pole ideal for this purpose is that given by Irving (1964) for the igneous complexes of the British Isles; recent age determinations (Duncan and others, 1972) show this pole to be Paleocene. By holding North America fixed and rotating Europe toward North America about Pitman and Talwani's (1972) 63-million-year

pole of rotation, a Paleocene paleomagnetic pole relative to North America would be located at 78° N., 170° E. This Paleocene pole is 11° away from the average Cretaceous pole (fig. 5) and on a very nearly direct path toward the Oligocene pole at 78° N., 146° E., reported by Grommé and McKee (1971), a fact strongly suggesting that the pole determined for the Great Valley sequence is indeed Cretaceous in age. This interpretation is in excellent agreement with suggestions by Irwin (1964), Blake, Irwin, and Coleman (1967), and Ernst (1970) that thrust faulting along the Great Valley province boundary occurred during the Late Cretaceous. However, this faulting may represent only the beginning of deformation in this region, because data presented by Hackel (1966) suggest that uplift of the sequence at the south end of the Sacramento Valley did not occur until after the early Eocene. Unfortunately, the error limits for the Putah Creek samples are too large for the data to be useful in proving or disproving this suggestion.

Considering the great sedimentary thicknesses involved, it is surprising that all samples seem to be of normal polarity. This suggests either that the remagnetization took place over a relatively short period of time or that the long Cretaceous normal polarity interval may have persisted until quite late in the Cretaceous. It is not now clear which alternative is the most likely. Studies of oceanic magnetic anomalies (Larson and Pitman, 1972) suggest that the Cretaceous normal polarity interval ended during the Coniacian Stage, and volcanic rocks having apparently the same age but mixed polarities (Hanna, 1967) tend to support this idea. However, other studies such as those by Pechersky and Khramov (1973), Shive and Frerichs (1974), and Keating, Helsley, and Pessagno (1975) show predominantly normal polarities at least until some time during the Maestrichtian.

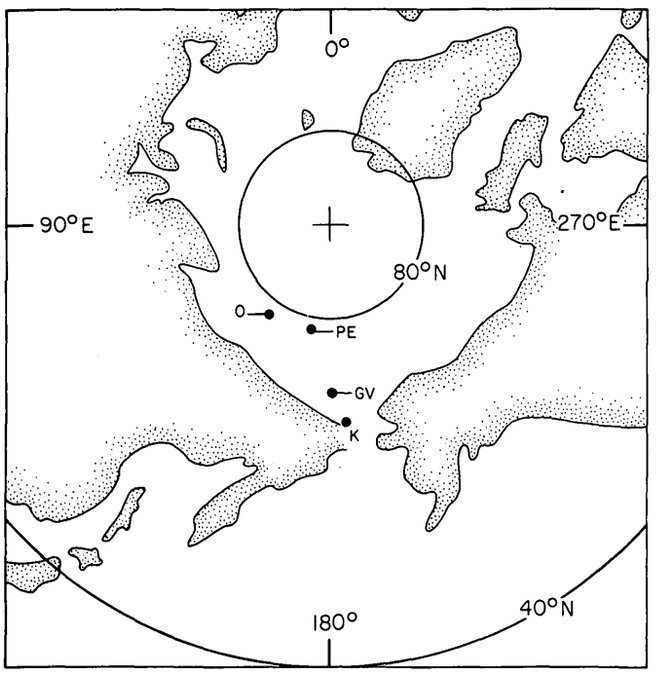

FIGURE 5.—Equal-area projection of part of the northern hemisphere showing the average Cretaceous pole (K) from table 3 and the poles for the Great Valley sequence (GV), the rotated European Paleocene (PE), and the Oligocene (O), from Grommé and McKee (1971).

The question of why these strata became remagnetized still remains to be answered. The deformation and remagnetization of the sequence are closely related in time, but it seems unlikely that the deformation itself could be the cause. The strata are only gently tilted throughout much of the sequence, and in none of the areas sampled are they penetratively deformed. Perhaps the remagnetization is due to the acquisition of a viscous PTRM (partial thermoremanence) similar to that described by Pullaiah, Irving, Buchan, and Dunlop (1975). If the strata were subjected to slightly elevated temperatures (100°C or more) for a long period of time, it is possible that some of the original NRM could be destroyed and a viscous PTRM produced, which would then become stabilized during cooling. To test this possibility, thermal demagnetization experiments were performed on 10 samples from the sequence. Changes in direction for two samples indicated that their primary magnetization may have been that of reversed polarity, but results from the other samples showed little or no improvement over those obtained by AF demagnetization. Both the thermal and AF demagnetization experiments suggest that the remagnetization of the sequence was very nearly complete and that neither technique is likely to provide results that are not ambiguous.

REFERENCES CITED

Bailey, E. H., Blake, M. C., Jr., and Jones, D. L., 1970, On-land Mesozoic oceanic crust in California Coast Ranges: U.S. Geol. Survey Prof. Paper 700–C, p. C70–C81.

Bailey, E. H., Irwin, W. P., and Jones, D. L., 1964. Franciscan and related rocks and their significance in the geology of western California: California Div. Mines and Geology Bull. 183, 177 p.

Beck, M. E., Jr., 1975, Remanent magnetism of the Twin Sisters dunite intrusion and implications for the tectonics of the western cordillera: Earth and Planetary Sci. Letters, v. 26, p. 263–268.

Blake, M. C., Jr., Irwin, W. P., and Coleman, R. G., 1967, Upside-down metamorphic zonation, blueschist facies, along a regional thrust in California and Oregon: U.S. Geol. Survey Prof. Paper 575–C, p. C1–C9.

Blake, M. C., Jr., and Jones, D. L., 1977, Plate tectonic history of the Yolla Bolly junction: Geol. Soc. America Guidebook, Cordilleran Sec. Mtg., Sacramento, Calif., 14 p.

Brown, R. D., Jr., and Rich, E. I., 1960, Early Cretaceous fossils in submarine slump deposits of late Cretaceous age, northern Sacramento Valley, California: U.S. Geol. Survey Prof. Paper 400–B, p. B318–B320.

Doell, R. R., and Cox, Allan, 1967a, Analysis of alternating field demagnetization equipment, *in* Collinson, D. W., Creer, K. M., and Runcorn, S. K., eds., Methods in paleomagnetism: Amsterdam, Elsevier, p. 241–253.

——— 1967b, Recording magnetic balance, *in* Collinson, D. W., Creer, K. M., and Runcorn, S. K., eds., Methods in paleomagnetism: Amsterdam, Elsevier, p. 440–444.

Duncan, R. A., Petersen, Nikolai, and Hargraves, R. B., 1972, Mantle plumes, movement of the European plate and polar wandering: Nature v. 239, p. 82–86.

Ernst, W. G., 1970, Tectonic contact between the Franciscan mélange and the Great Valley sequence—Crustal expression of a late Mesozoic Benioff zone: Jour. Geophys. Research, v. 70, p. 886–901.

Fisher, R. A., 1953, Dispersion on a sphere: Royal Soc. [London] Proc., Ser. A, v. 217, p. 295–305.

Grommé, C. S., and McKee, E. H., 1971, Mid-Tertiary paleomagnetic pole from volcanic rocks in the western United States: Am. Geophys. Union Trans., v. 52, p. 187.

Grommé, C. S., and Mankinen, E. A., 1976, Natural remanent magnetization, magnetic properties, and oxidation of titanomagnetite in basaltic rocks from DSDP Leg 34, *in* Yeats, R. S., Hart, S. R., and others, eds., Initial reports of the Deep Sea Drilling Project, v. 34: Washington, D.C., U.S. Govt. Printing Office, p. 485–494.

Grommé, C. S., and Merrill, R. T., 1965, Paleomagnetism of late Cretaceous plutons in the Sierra Nevada, California—Further results: Jour. Geophys. Research, v. 70, p. 3407–3420.

Grommé, C. S., Merrill, R. T., and Verhoogen, John, 1967, Paleomagnetism of Jurassic and Cretaceous plutonic rocks in the Sierra Nevada, California, and its significance for polar wandering and continental drift: Jour. Geophys. Research, v. 72, p. 5661–5684.

Hackel, Otto, 1966, Summary of the geology of the Great Valley, *in* Bailey, E. H., ed., Geology of Northern California: California Div. Mines and Geology Bull. 190, p. 217–238.

Hanna, W. F., 1967, Paleomagnetism of upper Cretaceous volcanic rocks of southwestern Montana: Jour. Geophys. Research, v. 72, p. 595–610.

——— 1973, Paleomagnetism of the late Cretaceous Boulder batholith, Montana: Am. Jour. Sci., v. 273, p. 778–802.

Imlay, R. W., and Jones, D. L., 1970, Ammonites from the *Buchia* zones in northwestern California and southwestern Oregon: U.S. Geol. Survey Prof. Paper 647–B, p. B1–B59.

Irving, E., 1964, Paleomagnetism and its application to geological and geophysical problems: New York, John Wiley and Sons, 399 p.

Irwin, W. P., 1960, Geologic reconnaissance of the northern Coast Ranges and Klamath Mountains, California, with a summary of the mineral resources: California Div. Mines Bull. 179, 80 p.

——— 1964, Late Mesozoic orogenies in the ultramafic belts of northwestern California and southwestern Oregon: U.S. Geol. Survey Prof. Paper 501–C, p. C1–C9.

Jones, D. L., and Bailey, E. H., 1973, Preliminary biostratigraphic map, Colyear Springs quadrangle, California: U.S. Geol. Survey Misc. Field Studies Map MF–517, scale 1:48,000.

Jones, D. L., Bailey, E. H., and Imlay, R. W., 1969, Structural and stratigraphic significance of the *Buchia* zones in the Colyear Springs-Paskenta area, California: U.S. Geol. Survey Prof. Paper 647–A, p. A1–A24.

Keating, B. H., Helsley, C. E., and Pessagno, E. A., Jr., 1975, Late Cretaceous reversal sequence: Geology, v. 3, p. 73–76.

Kilbourne, D. E., 1969, Paleomagnetism of some rocks from the Mesaverde Group, southwestern Wyoming and northeastern Utah: Geol. Soc. America Bull., v. 80, p. 2069–2074.

Kirby, J. M., 1943, Upper Cretaceous stratigraphy of the west side of Sacramento Valley south of Willows, Glen County, California: Am. Assoc. Petroleum Geologists Bull., v. 27, p. 279–305.

Larochelle, Andre, 1961, Application of paleomagnetism to geological correlations: Nature, v. 192, p. 37–39.

——— 1969, Paleomagnetism of the Monteregian Hills—Further new results: Jour. Geophys. Research, v. 74, p. 2570–2575.

Larochelle, Andre, and Black, R. F., 1963, An application of paleomagnetism in estimating the age of rocks: Nature, v. 198, p. 1260–1262.

Larochelle, Andre, Black, R. F., and Wanless, R. K., 1965, Paleomagnetism of the Isachsen diabasic rocks: Nature, v. 208, p. 179.

Larson, R. L., and Pitman, W. C., III, 1972, World-wide correlation of Mesozoic magnetic anomalies, and its implications: Geol. Soc. America Bull., v. 83, p. 3645–3662.

McElhinny, M. W., 1973, Paleomagnetism and plate tectonics: Cambridge, Cambridge Univ. Press, 358 p.

Murphy, M. A., Rodda, P. V., and Morton, D. M., 1969, Geology of the Ono quadrangle, Shasta and Tehama Counties, California: California Div. Mines and Geology Bull. 192, 28 p.

Ojakangas, R. W., 1968, Cretaceous sedimentation, Sacramento Valley, California: Geol. Soc. America Bull., v. 79, p. 973–1008.

Opdyke, N. D., and Wensink, Hans, 1966, Paleomagnetism of rocks from the White Mountain plutonic-volcanic series in New Hampshire and Vermont: Jour. Geophys. Research, v. 71, p. 3045–3051.

Pechersky, D. M., and Khramov, A. N., 1973, Mesozoic paleomagnetic scale of the USSR: Nature, v. 244, p. 499–501.

Pitman, W. C., III, and Talwani, Manik, 1972, Sea-floor spreading in the North Atlantic: Geol. Soc. America Bull., v. 83, p. 619–646.

Popenoe, W. P., Imlay, R. W., and Murphy, M. A., 1960, Correlation of the Cretaceous formations of the Pacific Coast (United States and northwestern Mexico): Geol. Soc. America Bull., v. 71, u. 1491–1540.

Pullaiah, G., Irving, E., Buchan, K. L., and Dunlop, D. J., 1975, Magnetization changes caused by burial and uplift: Earth and Planetary Sci. Letters, v. 28, p. 133–143.

Runcorn, S. K., 1956, Paleomagnetic survey in Arizona and Utah—Preliminary results: Geol. Soc. America Bull., v. 67, p. 301–316.

Scharon, LeRoy, and Hsu, I-Chi, 1969, Paleomagnetic investigation of some Arkansas alkalic igneous rocks: Jour. Geophys. Research, v. 74, p. 2774–2779.

Shive, P. N., and Frerichs, W. E., 1974, Paleomagnetism of the Niobrara Formation in Wyoming, Colorado, and Kansas: Jour. Geophys. Research, v. 79, p. 3001–3007.

Stacey, F. D., and Banerjee, S. K., 1974, The physical principles of rock magnetism: Amsterdam, Elsevier, 195 p.

Symons, D. T. A., 1973, Concordant Cretaceous paleolatitudes from felsic plutons in the Canadian Cordillera: Nature Phys. Sci., v. 241, p. 59–61.

Jour. Research U.S. Geol. Survey
Vol. 6, No. 3, May–June 1978, p. 391–394

TIME RELATION OF THE WATCHUNG BASALT FLOWS TO THE FAULTING IN THE NEWARK GRABEN

By GEORGE T. FAUST, Reston, Va.

Abstract.—In graben structures, volcanic eruptions and faulting are seldom simultaneous and often are not localized in the same place. Field studies in the Triassic basin of New Jersey have supplied evidence supporting the nonsimultaneity of volcanism and faulting in the Newark graben.

The Watchung Basalt flows are in the Triassic basin of northern New Jersey (fig. 1). The outcrop area is about 64 km long and about 16 km wide. The flows were extruded during three volcanic episodes. Each volcanic episode was a multiple event producing two flow units (fig. 2). A review and interpretation of the geologic setting of the Watchung Basalt flows of New Jersey has been published (Faust, 1975), and the reader is referred to it for details.

The time relation of volcanism to faulting or other crustal movements has long occupied the attention of geologists. Harker (1909, p. 13) had early noted that such relations must be based on careful investigations, and his comments, pertinent to this study, are as follows:

> Regarded more closely, the extrusion and intrusion of molten magmas have not always been strictly simultaneous with the main displacements of the solid crust, nor has igneous activity always been localized exactly on the principal lines of mechanical disturbance.

More recently, Rutten (1969, p. 436–437) in his review of the geology of Western Europe has reiterated this observation:

> An important fact, often too little stressed, is that the major volcanism does normally not occur within, or along the borders of the major graben. Apparently it is the fissures along which no larger movements took place that remained open and offered the best communication with the underlying magma, whereas the repeated movements along the major graben faults tended, on the other hand, to seal them off.

The hypothesis that the Triassic volcanism in the Newark graben was directly related to the faulting along the graben wall is attractive, but no unequivocal evidence has been forthcoming to support it. Widmer (1964, p. 72, 73, 77) has discussed this assumption. I have been disinclined to accept it and have sought field evidence to resolve the order of events and thus to discover the relations between the faulting and the fissure eruptions. Ratcliffe (1971, p. 136) has studied the Ramapo fault system in New York and New Jersey, and he suggests the following:

> The abundant igneous activity in the Newark Basin indicates the presence of a deep crustal fracture zone beneath the point where the igneous rocks were intruded or where they reached the surface. The relationship of the large intrusive Palisades phase to the east and the Watchung flows to the west of the basin suggests that the border fault at depth served as an avenue of magma ascent, although magma apparently never reached the surface along this fault.

The significance of the stratigraphic position of the Watchung Basalt flows relative to the fanglomerate beds along the fault wall in the Newark graben has not been previously recognized. Closely below the lower flow unit of each of the three Watchung Basalt episodes is a fanglomerate bed. The fanglomerate and lower flow unit are generally separated by only a very thin layer of shale, sand, or siltstone. The stratigraphy in First Watchung Mountain has been described by Darton (1890, p. 17), who found that for several miles north and south of Paterson, N.J., the lower flow unit of basalt lies above the fanglomerate (conglomerate) beds and is separated from them "by an inconsiderable thickness of sand and shale." During the 1973 field season, I found, near Oakland, N.J., a fanglomerate bed just under the lower flow unit of the second Watchung Basalt and separated from it by a thin layer of sediments. The contact was covered, but the thickness is less than 15 m. At Pompton Lakes, N.J., the third Watchung Basalt is also underlain by a fanglomerate and is separated from it by shales and sandstones. The presence of these fanglomerate beds throughout the Newark Group represents evidence for renewed uplift of the mountains that supplied the sediments to the Newark basin (Barrell, 1915, p. 28–29). Their almost periodic reappearance indicates recurrent movement along a fault wall.

It is thus obvious that the volcanic episodes that formed the Watchung Basalt flows each followed after a period of faulting in the graben which, in effect,

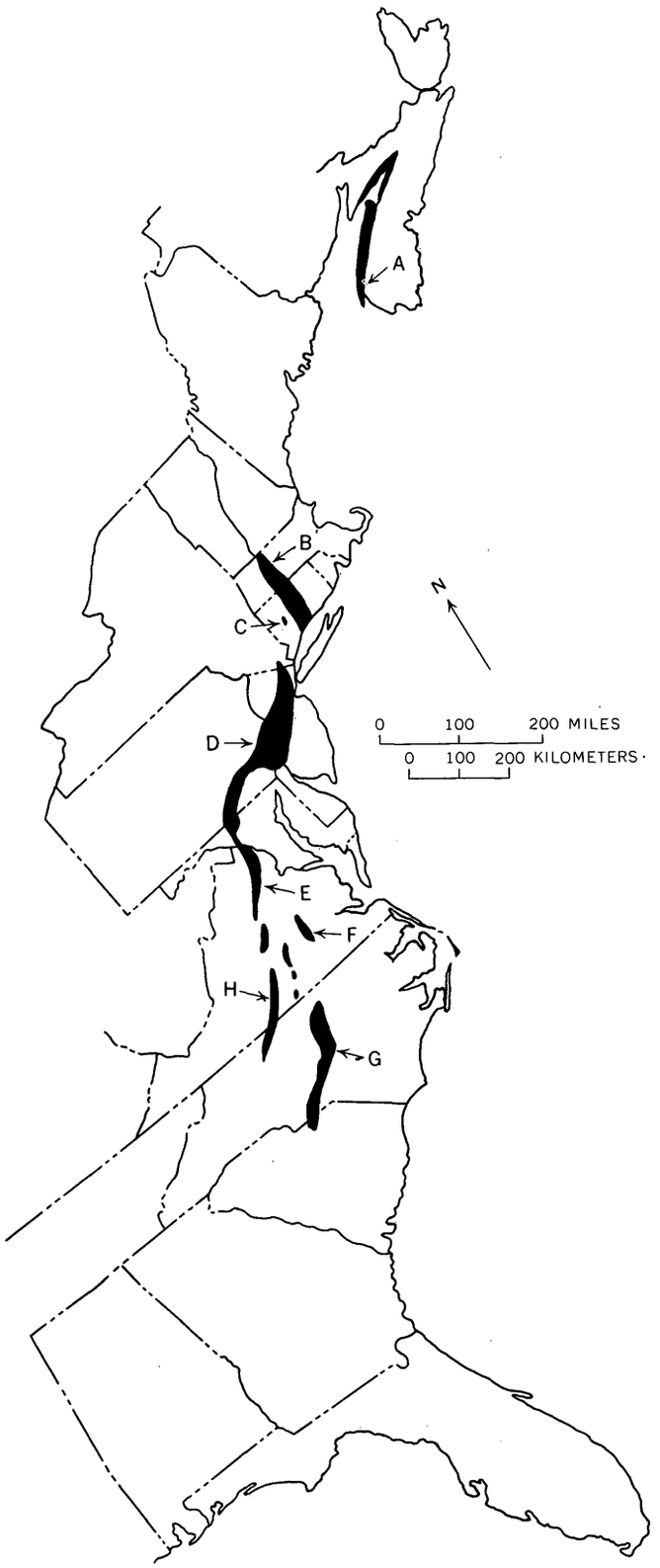

FIGURE 1.—Location of Triassic basins in Eastern United States. A, Nova Scotia basin. B, Connecticut basin (Connecticut and Massachusetts). C, Pomperaug Valley (the area is exaggerated). D, Newark-Gettysburg basin. E, Culpeper basin. F, Richmond basin. G, Deep River basin. H, Dan River basin.

elevated the horst to form highlands. The lava flows were not extruded at the same time that this faulting took place because the fanglomerate beds and the thin layer of separating sediments that underlie the lava flows represent the newly arrived detritus from the highland and indicate a time interval between faulting and the basalt outpourings. The apparent absence of fanglomerate beds immediately above the lava flows suggests that the highlands were not elevated during rifting and feeder-dike intrusion. It is very probable that the feeder dikes were more nearly in the center of the basin, 16, 24, or more kilometers away from the fault walls, and did not significantly affect the horst.

The feeder dike at West Orange, in First Mountain, is approximately 17 km distant from the border fault.

In Connecticut, the stratigraphic relations of the basalt sheets and the fanglomerates have been studied by several scientists. Russell (1922, p. 487, and fig. 2, 3, and 4) wrote as follows:

> The fanglomerate is found below the lower basalt flow, immediately below the main sheet, below the upper basalt flow, and above all the flows.

His figure 2 shows the fanglomerate immediately below the main sheet but not in the sediments above it. His figure 3 shows no fanglomerate above the main sheet; it shows extensive fanglomerate below the upper basalt flow. It also shows a thin layer of fanglomerate above a thin layer of sediments; this sequence is directly above the upper basalt flow. Russell (1922) recognized the fact that this fanglomerate that overlies the basalt flow contains huge angular basalt boulders close to the fault. He concluded the following (p. 492):

> It seems probable, therefore, that the bowlders were derived from portions of basalt that were lifted up by the faulting.

and on p. 491:

> They [basalt boulders] . . . may have been derived from basalt flows that had spread over on the east side of the fault, and then been uplifted.

These observations clearly suggest that faulting unrelated to the volcanism took place along the wall of the "Great Fault" sometime after the "upper basalt flow" was emplaced and had solidified.

Krynine (1950, p. 31–34, 36, 70) reexamined the stratigraphy of the Triassic rocks in the Connecticut basin. His tables and figures show fanglomerate below the "lower basalt flow," below the "main sheet," and below the "upper basalt flow." Regarding the extensive fanglomerate above the "upper basalt flow," he wrote (p. 70) as follows:

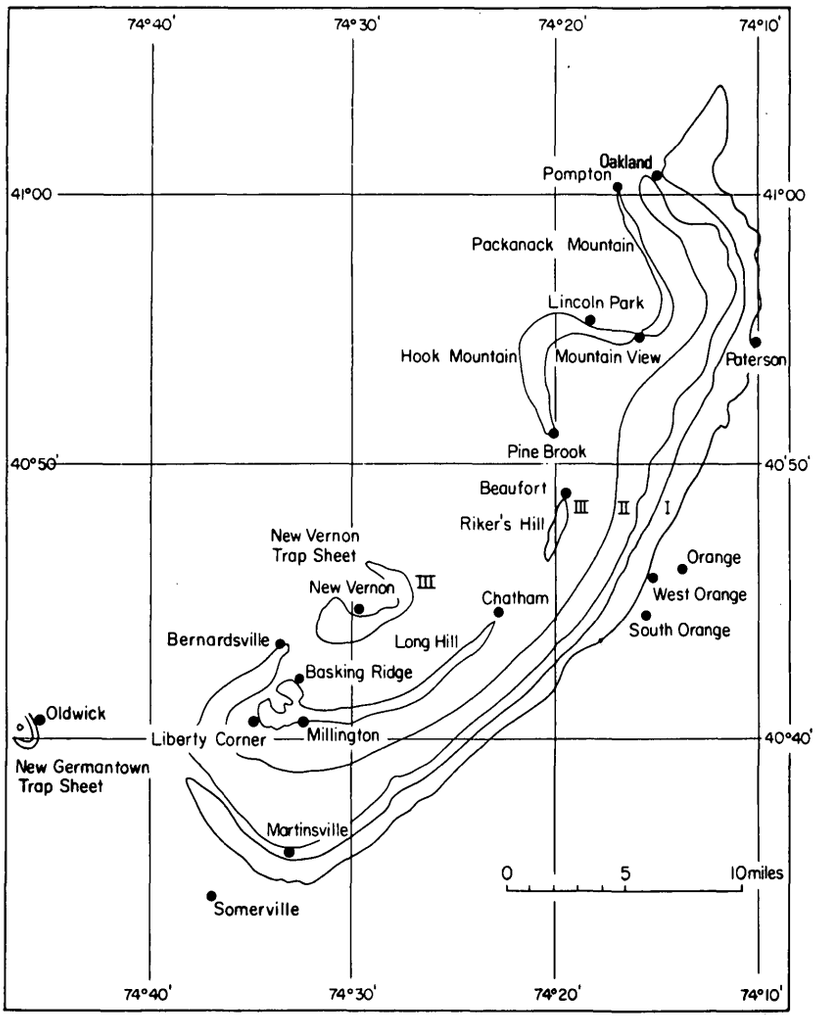

FIGURE 2.—Sketch map showing outline of the three Watchung Mountains and the New Germantown trap sheet (modified from Lewis, 1908, pl. 10). I, II, and III refer to First, Second, and Third Watchung Mountains. (1 mile = 1.609 kilometers.)

The lower Portland fanglomerates immediately above the upper lava flow contain at North Branford large basaltic boulders, thus indicating a certain extension of the upper lava flow east of the Great Fault.

He thus concurred with Russell (1922) in dating the origin of this fanglomerate above the "upper basalt flow" as after the emplacement and solidification of the basalt. The relations of the basalt to the fanglomerates in the Connecticut basin are the same as in the Newark basin, and they substantiate the interpretation proposed here of the nonsimultaneity of volcanism and faulting in the Triassic basins of eastern North America.

Faust (1975) suggested (1) that the periods of graben formation in the Newark basin reflected the state of tensional stress in the Continent Pangaea at that time, and (2) that the formation of the rift zone that permitted the outpouring of basaltic magma was directly related to the beginning of the breaking apart of the landmass composed of the present continents of North America, Europe, and Africa. These rift zones were deep and tapped basalt reservoirs in the lower crust or the upper mantle.

Acknowledgment.—I particularly thank Robert L. Smith for critical discussions regarding various facets of this problem.

REFERENCES CITED

Barrell, Joseph, 1915, Central Connecticut in the geologic past: Connecticut Geol. Survey Bull. 23, 44 p.

Darton, N. H., 1890, The relations of the traps of the Newark system in the New Jersey region: U.S. Geol. Survey Bull. 67, 82 p.

Faust, G. T., 1975, A review and interpretation of the geologic setting of the Watchung Basalt Flows, New Jersey: U.S. Geol. Survey Prof. Paper 864–A, 42 p.

Harker, Alfred, 1909, The natural history of igneous rocks: New York, Macmillan Company, 384 p.

Krynine, P. D., Petrology, stratigraphy, and origin of the Triassic sedimentary rocks of Connecticut: Connecticut Geol. and Nat. History Survey Bull. 73, 239 p.

Lewis, J. V., 1908, Petrography of the Newark igneous rocks of New Jersey: New Jersey Geol. Survey Ann. Rept. State Geologist for 1907, p. 97–167.

Ratcliffe, N. M., 1971, The Ramapo fault system in New York and adjacent northern New Jersey—A case of tectonic heredity: Geol. Soc. America Bull., v. 82, no. 1, p. 125–141.

Russell, W. L., 1922, The structural and stratigraphic relations of the great Triassic fault of southern Connecticut: Am. Jour. Sci., 5th ser., v. 4, p. 483–497.

Rutten, M. G., 1969, The geology of western Europe: Amsterdam, Elsevier Publ. Co., 520 p.

Widmer, Kemble, 1964, The geology and geography of New Jersey: Princeton, N.J., D. van Nostrand Co., Inc., 193 p.

Jour. Research U.S. Geol. Survey
Vol. 6, No. 3, May–June 1978, p. 395–408

PLEISTOCENE HISTORY OF VOLCANISM AND THE OWENS RIVER NEAR LITTLE LAKE, CALIFORNIA

By WENDELL A. DUFFIELD and GEORGE I. SMITH,
Menlo Park, Calif.

Abstract.—During pluvial periods of the Pleistocene and Holocene, a large river flowed south from Owens Lake to China Lake between the Sierra Nevada and the Coso Range. The most recent channel, dry during historic time, is clearly marked by cliffs and falls. An older, now-abandoned part of the channel beneath Pleistocene lavas east of the present course is inferred from a meander-shaped ridge in Mesozoic basement rocks and a strong positive magnetic anomaly, presumably produced by a wedge of canyon-filling basalt. Three cycles of eruption and stream erosion have occurred along the present course. The first resulted when water impounded by damming of the now-abandoned eastern course found its way along the west margin of a basalt flow at the base of the Sierra Nevada escarpment, eventually carving a canyon at least 150 meters deep. Subsequently, two cycles, each consisting of an intracanyon basalt flow followed by major stream erosion, modified this canyon to its present configuration. A potassium-argon age of about 440 000 years before present for the oldest of the three eroded lavas indicates that the river was not diverted from its easterly course until after that time. The age and character of lacustrine deposits in Searles Lake, a downstream part of the same drainage system, indicate that the greatest discharge of the river, and therefore, erosion of the two younger lavas since 440 000 years B.P., probably occurred between 130 000 and 10 000 years B.P. An estimate of the rate of erosion during this period of time together with loosely constrained potassium-argon ages for the basalt of intermediate age suggests that the youngest lava is probably a few tens of thousands of years old and the intermediate lava somewhat less than 100 000 years old. The youthfulness of the youngest basalt suggests that a fourth cycle of an intracanyon lava flow followed by stream erosion is a likely event for the near geologic future.

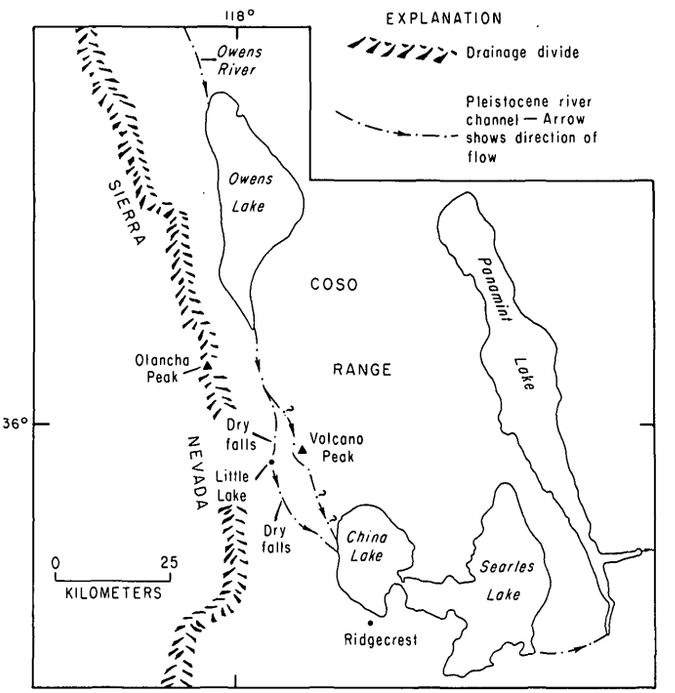

FIGURE 1.—System of Pleistocene lakes and interconnecting rivers in eastern California. Older Pleistocene river channel near Volcano Peak (queried where least certain) probably forced to westerly course near Little Lake by damming from intracanyon lava flow.

During part of Pleistocene time, much of the Western United States was dotted with systems of lakes and interconnecting rivers (Snyder and others, 1964). One such drainage system in eastern California included a river that flowed southward through a slot between the Sierra Nevada and the Coso Range, carrying the overflow from Owens Lake into China Lake intermittently during Pleistocene and Holocene time (fig. 1). Farther down drainage, water flowed from China Lake into Searles Lake, into Panamint Lake, and finally into Manly Lake, the sump of the drainage system in Death Valley. The channel, now dry, is the site of the 11-kilometer-long, manmade Haiwee Reservoir north of the mapped area, a naturally occurring shallow lake (Little Lake) near the village of Little Lake, two dry falls, and several kilometers of river-cut cliffs as high as 160 meters, mute reminders of considerable past flow of water through the area. (To avoid confusion between the village and the nearby body of water, the name Little Lake will refer to the village, except where otherwise noted.)

Discharge of the river, primarily a function of a fluctuating climate, has been deduced indirectly

through the study of lacustrine deposits in Searles Lake (Smith, 1968, 1976a, 1976b). Locally, the path followed by the discharge was repeatedly altered by intracanyon lava flows. Putnam (1955) was the first to note the presence of such lava flows. More recently, Duffield and Bacon (1977) showed that twice during Pleistocene time basaltic lavas entered the channel near Little Lake, presumably damming the river long enough to form ephemeral upstream lakes before overflow reestablished a channel along the margins of and over parts of the lava dams. Our present study suggests that during an earlier part of Pleistocene time, the river channel was about 5 km east of this course near Little Lake. At the site of this early channel, in a manner similar to the well-documented younger events, an intracanyon lava flow apparently dammed the river and forced it to the more westerly course, leaving behind a 3-km-long meander-cut escarpment in basement rocks and a thick prism of intracanyon basalt as evidence of the abandoned channel.

As the course and, to some degree, the discharge of the river have been affected by lava flows during the Pleistocene, a reasonably complete understanding of the history of the drainage system requires careful examination of local geology, especially late Cenozoic lava flows, in the Little Lake area.

Acknowledgments.—Richard J. Blakely helped with interpretation of the measured magnetic profiles and was largely responsible for computer modeling of the profiles.

DESCRIPTION OF THE ROCKS

The Little Lake area lies at the foot of a lofty fault-line escarpment that marks the boundary between the Basin and Range and the Sierra Nevada physiographic provinces. Present relief across the escarpment is about 1200 m, suggesting at least this much normal offset on the Sierra Nevada fault zone.

Basement rocks in the Sierra Nevada and the Coso Range constitute a Mesozoic crystalline complex dominated by plutons that range in composition from gabbroic through intermediate types to granitic. In the Coso Range, this basement complex is unconformably overlain by a patchy veneer of late Cenozoic sedimentary and volcanic rocks, many of which have been dated radiometrically by Lanphere, Dalrymple, and Smith (1975). The general volcanic sequence and its structural setting were summarized by Duffield (1975) and mapped by Duffield and Bacon (1977). Eruptive activity began about 4 million years ago and has occurred as recently as late Pleistocene. Some of the youngest Pleistocene lavas disrupted drainage in the Little Lake area.

Old gravels

The oldest post-Mesozoic deposits in the Little Lake area are alluvial gravels. These gravels apparently once formed a continuous apron of coalescing alluvial fans at the foot of the Sierra Nevada escarpment but are now represented by three isolated erosional remnants, one that overlies granitic rocks of the Sierra Nevada immediately northwest of Little Lake, another similar remnant about 8 km south of Little Lake, and a third that underlies basalt east of the present river channel south of Little Lake (figs. 2, 3). The beds in the remnants against the Sierra Nevada are graded to points east of the present channel and are being eroded by streams graded to the level of that channel, as much as 100 m below the present surface of the old gravels.

The gravels crop out best in roadcuts west of the present channel. Depositional units range in thickness from about 1 to several meters and consist of poorly sorted, moderately to well-rounded clasts ranging in size from silt to boulders as much as 3 m in diameter. All clasts are from the Mesozoic crystalline basement complex of the adjacent Sierra Nevada, and most are granitic. Some massive units contain abundant coarse fragments that are suspended in sand and silt, suggesting emplacement as mudflows. Other units are better sorted and stratified and appear to represent normal alluvial material.

Ten or more well-developed soil or weathering zones are exposed in the gravels west of the present channel, especially south of Little Lake, indicating an equal number of periods of nondeposition of sufficient duration for such soils to develop. These gravels are extensively weathered throughout; for example, both within and between soil zones, virtually all clasts that are relatively rich in biotite may be easily disaggregated to grus with a hammer or even by hand. Bulldozed roadcuts slice across large boulders of such rocks, exposing equally weathered material throughout. This degree of weathering is similar to that of biotite-rich boulders in Sherwin glacial deposits along the east side of the Sierra Nevada about 200 km north of Little Late, as described by Blackwelder (1931) and Sharp (1968).

The remnant of old gravels preserved beneath the cap of basalt along the east side of the present river channel is poorly exposed and crops out as loose granitic sand and cobbles admixed with basalt talus from the overlying lava. The gravels of this remnant are interpreted to represent the eastern extension of the alluvial fan derived from the adjacent Sierra Nevada, although they are now separated from the gravels to the west by a 1-km-wide stream channel and two intracanyon lava flows. Former continuity between the

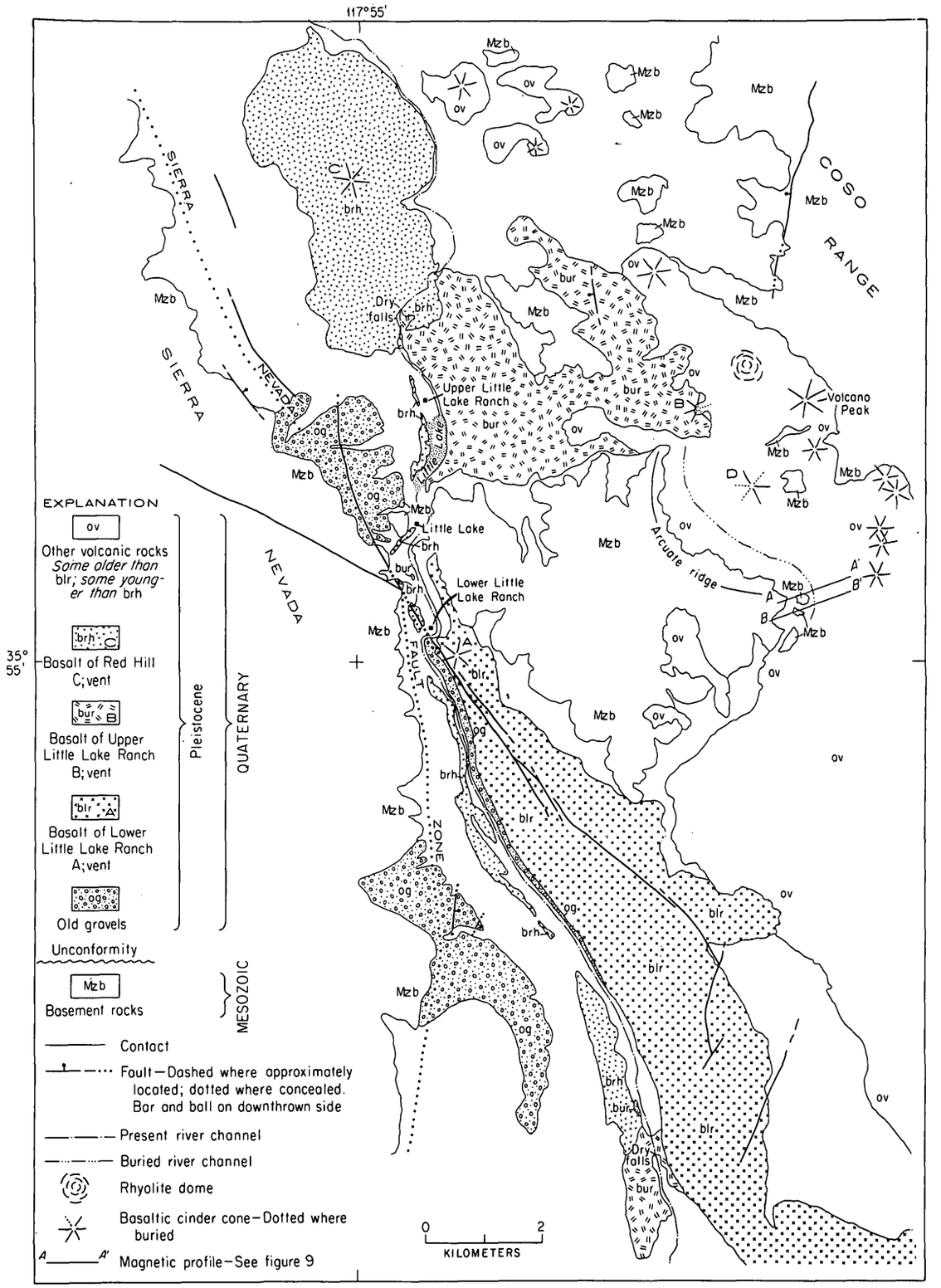

FIGURE 2.—Generalized geologic map of Little Lake area. Mostly buried basaltic cinder cone (D) may have fed an intracanyon flow, diverting river westward to Little Lake. Unlabeled areas include both Pliocene and (or) Pleistocene sedimentary rocks and Holocene deposits.

FIGURE 3.—Vertical aerial photograph of Little Lake area. Compare with figure 2. U.S. Geological Survey photograph USAF 744V022 taken by the U.S. Air Force in 1967.

eastern and western gravels is indicated by the facts that: (1) clasts are derived from the Mesozoic basement complex and are mostly granitic, (2) maximum clast size decreases away from the Sierra Nevada, and (3) the present upper surface of the western deposit (virtually parallel to bedding) shows alinement with the top of the eastern deposit when projected along strike across the intervening stream channel. Faulting within the Sierra Nevada fault zone that postdates deposition of the alluvial fan gravels must be considered in such a projection; two normal faults with offsets down to the east cut the western gravels (fig. 2), but demonstrable vertical displacement is only about 20 m, an amount that would not significantly alter the original profile of a continuous fan across the area. Moreover, the numerous soils and the pervasive

weathering in the western deposits suggest an age of hundreds of thousands of years, and the eastern gravels are overlain by 440 000-year-old basalt, consistent with such an age. It seems likely that the three remnants of old gravels do indeed represent parts of a single alluvial fan complex that grew eastward from the base of the Sierra Nevada escarpment several hundreds of thousands of years ago.

Contemporaneous gravel, derived from the adjacent Mesozoic terrane of the Coso Range (figs. 2, 3), probably interfingers from the east with the deposits from the Sierra Nevada, but direct evidence of such interfingering is lacking. Considering the relative sizes of the source areas, we suspect that gravel from the Coso Range would have been overwhelmed by the Sierra Nevada contribution to such an alluvial plain.

Basalt of Lower Little Lake Ranch

The oldest lava in the Little Lake area is informally called the basalt of Lower Little Lake Ranch (Duffield and Bacon, 1977). This lava was erupted from a vent now marked by a partly eroded cone of cinders and bombs at the rim of a 150-m-high, river-cut cliff about 2 km south-southeast of Little Lake, near the ranch from which its name is taken (figs. 2, 4). Two widespread flows were erupted from this vent, each about 3 to 5 m thick; the absence of an intervening soil or weathered zone indicates that the two were emplaced penecontemporaneously. Parts of the flows spread between 1 and 2 km north of the vent, lapping against Mesozoic basement rocks of the Coso Range and against gravels or basement rocks of the Sierra Nevada immediately south of Little Lake. Most of the lava, however, flowed south-southeastward, apparently spreading over the sloping surface of an alluvial plain composed of the old gravels. A unknown amount of lava may have ponded in the basin of China Lake. The present surface of the upper flow is moderately weathered, but much original rugged topography indicative of an aa-type flow is still preserved.

The rock is moderately porphyritic and contains 10 to 20 percent phenocrysts of plagioclase, olivine, and clinopyroxene, some as large as 3 millimeters. Plagioclase phenocrysts are most abundant, and most of the olivine is altered.

At some time after eruption of this basalt, overflow

FIGURE 4.—Present river channel as seen from Sierra Nevada escarpment near Little Lake. Part of granitic Sierra Nevada escarpment in foreground, erosional remnant of east-dipping old gravels (og) in far right background, cinder cone (A) of basalt of Lower Little Lake Ranch in left middle distance, and Lower Little Lake Ranch lava flows at top of canyon wall. Approximate base of lava flows shown by dashed line, queried where uncertain. U.S. Highway 395 crosses field of view. View to southeast.

from Owens Lake fed a major south-flowing stream that eroded a canyon at the foot of the Sierra Nevada escarpment in the Little Lake area. Because no erosional remnants of the basalt occur along the present frontal slope of the Sierra Nevada, we infer that this river first began to flow along the western edge of the lava where it lapped against the escarpment and that it subsequently eroded both vertically and laterally to the east until arriving at about its present position. The lofty river-cut cliff south-southeast of Little Lake (fig. 4) represents a little-altered remnant of the resulting canyon wall, whose present relief indicates a minimum of 160 m of downcutting. This relief probably was formed by washing out of the nearly unconsolidated older gravels while the overlying basalt cap retreated by progressive collapse as the river undercut it laterally, downslope away from the front of the Sierra Nevada (fig. 5).

Basalt of Upper Little Lake Ranch

Once established, the river channel at Little Lake has remained in nearly the same position to the present time and has alternately carried water and lava. The first lava flow to enter the channel, informally called the basalt of Upper Little Lake Ranch (Duffield and Bacon, 1977), was erupted from a vent now marked by a slightly eroded cinder cone partly covered by younger pyroclastic debris, about 5 km northeast of Little Lake (fig. 2). Only a single flow has been recognized from this vent; it spread north and west until it reached the river, then advanced downstream at least 15 km to where the most distant erosional remnant is exposed today. An unknown amount of this lava may have ponded in the basin of China Lake.

Judged by the exposed thickness of 70 m, lava may have completely filled the canyon where it entered the river channel above Little Lake. Downstream from Little Lake, however, the flow stayed well below

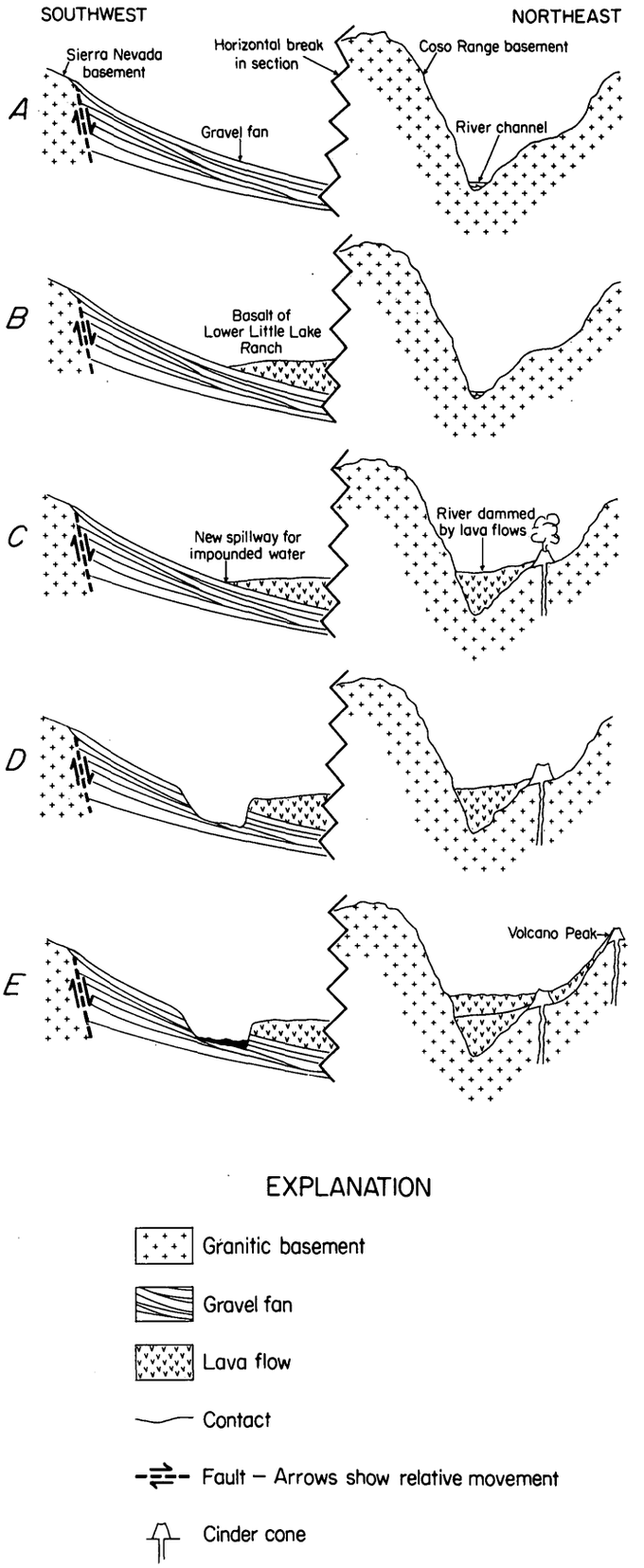

FIGURE 5.—Schematic cross sections about 8 km south of Little Lake. Elevation datum is constant across break in sections. Vertical exaggeration approximately ×7. *A*, Active river channel 5 km east of Little Lake and alluvial fan at foot of Sierra Nevada before eruption of basalt of Lower Little Lake Ranch. *B*, Basalt of Lower Little Lake Ranch laps onto Sierran fan and against granitic basement of Coso Range. *C*, Unnamed intracanyon lava dams channel, forcing water through new spillway at west margin of basalt of Lower Little Lake Ranch. *D*, Subsequent river erosion forms canyon in alluvial gravels, capped by basalt on east rim. *E*, Present configuration with canyon of *D* partly filled by basalts of Upper Little Lake Ranch and Red Hill and recent alluvium (all shaded).

the canyon rim, as indicated by the position of locally preserved marginal levees that mark the original maximum height of the flow at its edge.

This basalt is sparsely porphyritic, containing 1 to 2 percent phenocryst of olivine and plagioclase, about 1 to 2 mm in size, and is easily distinguished from the basalt of Lower Little Lake Ranch.

After emplacement of this lava, a river channel was reestablished through the area. Below Little Lake, where the prelava canyon had been only partly filled by the lava flow, the position of the new channel changed little, if any. Above Little Lake, however, the river was apparently diverted to the west margin of the new flow, where lava had lapped against the east-sloping wall of the canyon eroded earlier in the alluvial fan now represented by the remnant of old gravels there (fig. 2). Erosion along the contact cut vertically and laterally away from the Sierra Nevada escarpment as it had during the earlier canyon-cutting episode downstream in the basalt of Lower Little Lake Ranch. An impressive 70-m-high cliff was cut, exposing columnar basalt that now forms the backdrop for Little Lake (the lake) (fig. 6). Erosion of the basalt itself was probably facilitated by undercutting into the unconsolidated old gravels, although the base of the lava is not exposed in the present cliff behind the lake. Our interpretation of these events is shown in figure 7.

Basalt of Red Hill

After entrenchment of the river channel into the basalt of Upper Little Lake Ranch, an intracanyon lava flow, informally called the basalt of Red Hill (Duffield and Bacon, 1977), was erupted from a vent now marked by a little eroded, though greatly quarried, cinder cone about 5.5 km north-northwest of Little Lake (fig. 2). Lava ponded in an area of at least 2 km radius around the vent and fed a single flow that extended 16 km or more down the river channel. In the vent area, the river canyon was filled to overflowing; some lava lapped over the top of the preexisting river-cut cliff in the basalt of Upper Little Lake Ranch. At and below Little Lake (the lake), the

FIGURE 6.—Little Lake area as seen from Sierra Nevada escarpment. Note lake (L) in background, lofty erosional cliff cut into basalt of Upper Little Lake Ranch behind lake, exposures of Mezozoic basement rocks (Mzb), erosional remnants of old gravels (og) that underlie east-dipping surfaces in left middle distance, Red Hill cinder cone (C), and erosional remnants of basalt of Red Hill (brh) along west shore of lake and near railroad track in right middle distance. View to northeast.

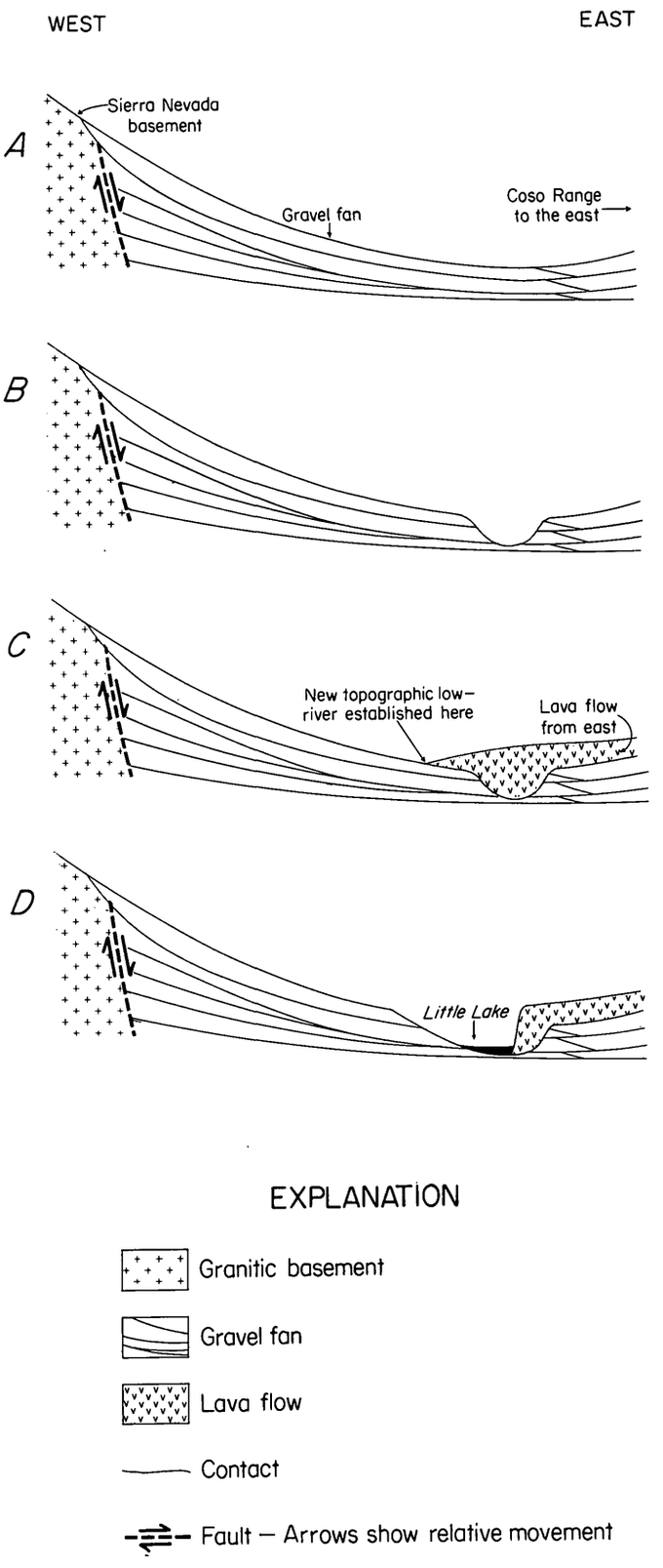

FIGURE 7.—Schematic cross sections 1.5 km north of Little Lake. Vertical exaggeration approximately ×7. *A*, Alluvial fan complex between Sierra Nevada and Coso Range before erosion of first channel (see fig. 5*A*). *B*, Stream erosion cuts channel in fan complex after downstream eruption of basalt of Lower Little Lake Ranch but before eruption of basalt of Upper Little Lake Ranch (see fig. 5*D*). *C*, Basalt of Upper Little Lake Ranch fills stream channel and laps upon east-dipping surface of old gravels to west. *D*, Subsequent erosion cuts into west margin of flow, forming channel later followed by basalt of Red Hill. Channel now partly filled with erosional remnants of basalt of Red Hill, lacustrine deposits of Little Lake (the lake), and recent alluvium (all shaded).

basalt of Red Hill stayed well below the rim of the preexisting canyon walls. In the downstream areas, the presently exposed rough upper surface on erosional remnants of the flow represent little altered original flow tops and commonly lie tens of meters below nearby canyon walls.

The basalt of Red Hill is moderately porphyritic, containing phenocrysts of plagioclase, olivine, and pyroxene as large as 3 mm. The general appearance is very similar to that of the basalt of Lower Little Lake Ranch, but the two lavas are easily distinguished in the field, as they differ in degree of weathering on flow surfaces and in geomorphic setting, one forming a rim-capping flow, the other, an intracanyon flow.

After emplacement of this basalt, the river connecting Owens and China Lakes again reestablished a channel in the Little Lake area. The course of the river was guided by newly formed topography around the east margin of the lava ponded near the vent, whereas downstream it apparently followed the earlier channel, only partly filled by the new lava flow. Ensuing erosion of the basalt of Red Hill destroyed or buried all but isolated remnants of its intracanyon flow, which can be traced 16 km downstream from the vent, and sculpted a 25-m-high waterfall about 2 km upstream from Little Lake (the lake).

Holocene deposits

The most recent geologic deposits in the area include (1) alluvium of the presently active fans that are encroaching from the west at the base of the Sierra Nevada escarpment and from the east from nearby parts of the Coso Range, (2) sand and gravel that partly fill the present stream channel and cover much of the two intracanyon lava flows, and (3) lacustrine beds that underlie Little Lake (the lake).

The lake appears to result from a natural dam, formed by alluvial fans coalescing from the west and the east near the narrowest part of the river canyon. During recent years, a rise in lake level of only 1 or 2 m would have resulted in overflow and perhaps erosion of a channel to drain the lake. Such an apparently

delicate balance between accumulation of the alluvial dam and water level in the lake may have resulted in repeated draining of the lake in the past. Mehringer and Sheppard (1977) cored 11.3 m of the lake beds and obtained a carbon-14 age of about 5000 years B.P. for the deepest material penetrated. Their interpretation of the sedimentary and fossil record of the core suggests alternating grassy meadow and marshy environments between 5000 and 3000 years B.P. and the presence of a shallow lake since 3000 years B.P. Out study suggests the possibility of two older sequences of lacustrine or fluvial deposits, one predating each of the two intracanyon flows. A deeper bore hole is needed to test this suggestion.

LOCATION OF RIVER CHANNEL BEFORE ERUPTION OF BASALT OF LOWER LITTLE LAKE RANCH

Field evidence suggests that there was no throughgoing north-south river channel at Little Lake when the basalt of Lower Little Lake Ranch was erupted. This lava flow spread more than 2 km laterally as it moved down a south-dipping alluvial slope toward China Lake basin; had a river channel existed, the flow probably would have been mostly restricted to that channel, in a manner similar to subsequent intracanyon flows of the basalts of Upper Little Lake Ranch and Red Hill. Moreover, at the time of this eruption, alluvial fan deposits, now represented by the erosional remnant of old gravels, apparently extended unbroken across the narrow slot between the Sierra Nevada and the Coso Range. We suspect that the narrowest part of the present canyon at Little Lake, which now separates steeply rising exposures of Mesozoic bedrock by only about 350 m was the site of a bedrock-cored saddle between north- and south-sloping alluvial plains when the basalt of Lower Little Lake Ranch was erupted. Where was the throughgoing river channel then?

Taking present topography on the Mesozoic basement rocks as a reasonable approximation to basement topography during Pleistocene time, the only other possible gap through which water might have flowed southward in the general area between the Sierra Nevada and the Coso Range is about 5 km nearly due east of Little Lake (Duffield and Bacon, 1977; figs. 2, 3). This gap is now flooded with an unknown thickness of Pleistocene basalt flows and minor rhyolite tuff from as many as 10 nearby vents, burying any river canyon that might be carved in underlying rocks. Geomorphic and geophysical data argue strongly that such a buried canyon does in fact exist. The lava-flooded area is flanked by ridges of Mesozoic basement rocks as high as 300 m. To the east, the basement rocks are mostly covered by Pleistocene volcanic rocks, but apparently they form two en echelon north-northeast-trending ridges capped by cinder deposits (Duffield and Bacon, 1977). To the west, in contrast, the basement rocks form a smoothly arcuate ridge that traces a 90° arc before plunging beneath Pleistocene basalt flows (figs. 3, 8). This shape suggests a river-cut meander, an origin that we favor.

Because contrasting magnetization between basalt and underlying granitic rocks should yield a positive magnetic anomaly over a wedge of canyon-filling basalt, to test our hypothesis of a buried river channel, we measured two parallel magnetic profiles at right angles to the path the river would have followed. Both profiles show a high-amplitude anomaly above the hypothesized canyon (fig. 9).

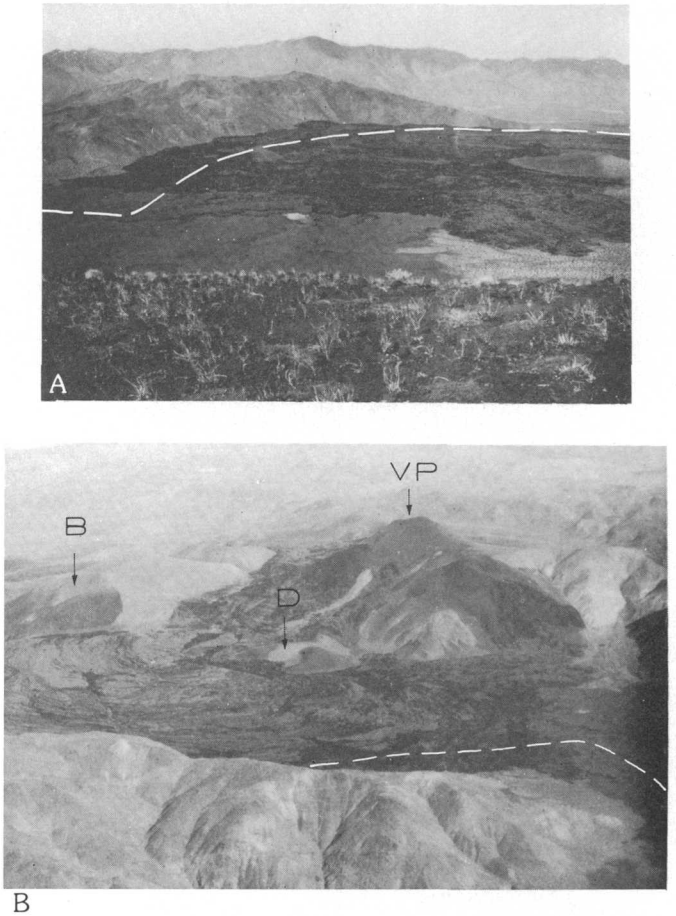

FIGURE 8.—Meander-shaped arcuate ridge in Mesozoic basement rocks and flat-lying Pleistocene lavas that may bury a river channel. *A*, Approximate location of hypothesized channel shown by dashed line. Sierra Nevada in background. View to west. *B*, Approximate location of hypothesized channel shown by dashed line. B = cinder cone at vent of basalt of Upper Little Lake Ranch. D = basalt cinder cone that may have fed flow that filled channel and diverted river to Little Lake area. VP = Volcano Peak, vent area for darkest and youngest flow covering hypothesized river channel. Oblique aerial view to north.

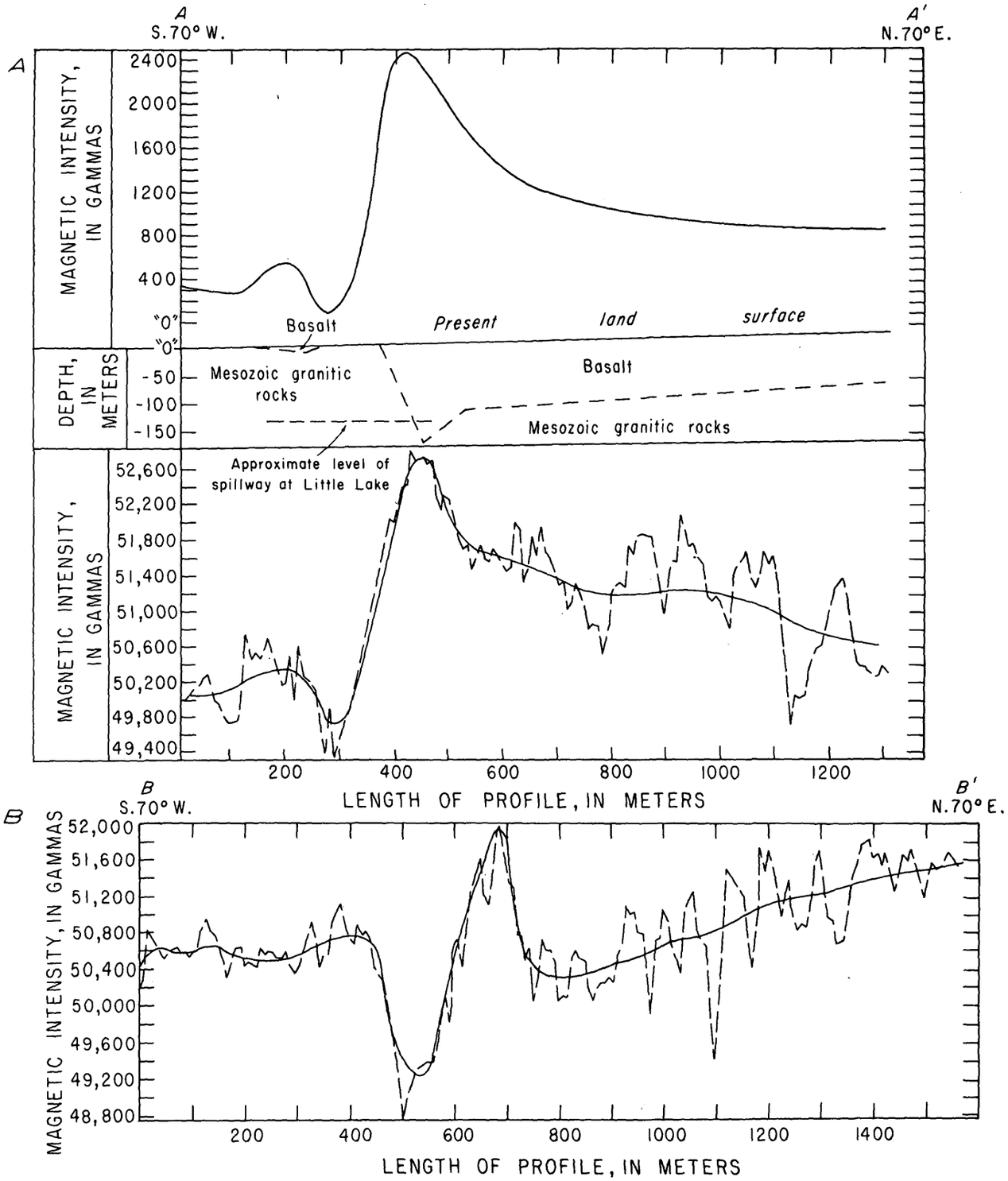

FIGURE 9.—Magnetic profiles across hypothesized river canyon near Volcano Peak (see fig. 2 for locations). *A*, Lower graph shows plot of field data and visually smoothed curve of profile *A–A'*. Note prominent magnetic high, suggestive of a buried river channel near southwest end of section. Upper graph was computed with reference to a geologic cross section, as explained in text. Assumed contrast in magnetizations between canyon-filling basalt and underlying granite is 0.009, a reasonable figure for such rocks. *B*, Graph of field data and visually smoothed curve along profile *B–B'* about 240 *m* south of *A–A'*. Shape of curve is similar to *A* except at northeast end, where magnetic intensity increases, consistent with surface geology that indicates deepening granitic basement and thickening basalt there. Magnetic measurements made with Geometrics proton precision magnetometer at 8-m spacing.

Profiles constructed directly from the field data show changes in field strength of several hundred gammas between adjacent stations, 8 m apart, probably reflecting effects such as lightning strikes, irregular surface topography on the traversed basaltic lava flows, and variation in abundance and texture of ferromagnetic minerals. Nonetheless, a major anomaly over the hypothesized canyon is of much greater wavelength and magnitude and is clearly seen through the shorter wavelength noise. A visually smoothed profile (fig. 9), made to average out the short wavelength fluctuations, enhances the major anomaly and provides some control for geophysical modeling.

For the modeling study, a geologic cross section was constructed on the assumption that a river channel in granitic rocks of uniform magnetization is filled with basalt flows of uniform but higher magnetization. The number of flows that fill such a channel is unknown, but they must all be younger than the basalt of Lower Little Lake Ranch, which was erupted about 440 000 years B.P., well within the present period of normal magnetic polarity (Cox, 1969). Accordingly, we assume that remanent magnetism of the canyon-filling flows parallels the present magnetic field; the bulk magnetization, then, consists of the added effects of parallel remanent and induced components and gives rise to the observed anomaly.

Surface geology and an estimate of a reasonable shape for a buried channel provide some control on the configuration of the cross section. The approximate minimum thickness of channel-filling basalt can be computed as the elevation difference between the line of the magnetometer profile and the upper surface of the basalt of Lower Little Lake Ranch near Little Lake, the inferred alternate spillway for impounded water. From the resulting cross section (fig. 9*A*), a magnetic profile was computed, using a program written by R. J. Blakely (unpub. data, 1977). The computed profile and the visually smoothed version of the measured profile are similar enough to suggest that the constructed geologic cross section is a close approximation of the actual section. Closer agreement between the measured and computed magnetic profiles could be achieved through changes in the assumed configuration of the buried Mesozoic basement rocks and in the magnetic properties of the rocks, but such manipulations would not significantly alter the interpretation. The critical discovery is the existence of the magnetic anomaly where hypothesized on purely geologic evidence. Presumably, anomalies associated with additional magnetometer profiles to the north and south would trace the upstream and downstream path of the river.

CORRELATION OF ERUPTIONS AND EROSION WITH SIERRA NEVADA GLACIAL HISTORY AND SEARLES LAKE LACUSTRINE DEPOSITS

Field determinations with a portable flux-gate magnetometer show that the three Pleistocene eruptions in the Little Lake area occurred during a time of normal magnetic polarity and are, therefore, presumably younger than about 700 000 years B.P. (Cox, 1969). Potassium-argon radiometric dates are consistent with this interpretation and provide enough constraints on timing of eruptive and erosional events to permit tentative correlations with periods of glaciation in the Sierra Nevada, the principal source of water flowing through the Little Lake area, and changing water levels of Searles Lake, a downstream part of the same drainage system.

Two superimposed flows of the basalt of Lower Little Lake Ranch yield potassium-argon ages of 399 000±45 000 and 486 000±108 000 years B.P. (table 1), the upper flow giving the younger age. For our purposes, the two flows can be assumed to have been erupted about 440 000 years ago, the average of the potassium-argon ages. At that time, the river presumably was following its now abandoned and buried course 5 km east of Little Lake. Prior to that time, runoff associated with the Sherwin Glaciation (>710 000 years B.P.; see Sheridan, 1971), and possibly earlier glaciations in the Sierra Nevada, might account for erosion of the buried channel.

In any event, some time after 440 000 years B.P., the course of the river shifted to the foot of the Sierra Nevada escarpment at Little Lake. Why the eastern channel was abandoned is not well documented, but intracanyon lava or a fault scarp may have diverted the river. At least one basaltic cinder cone that may have fed such a flow barely protrudes through the younger surface lavas in the area of the meander (figs. 2, 8*B*), and other lavas of appropriate age occur there. The possibility of blockage by a fault scarp is more speculative. There are no scarps cutting the present surface lavas in the area of the meander, but late Cenozoic faulting is common elsewhere in the Coso Range (Duffield and Bacon, 1977). Moreover, the river may have been originally channeled through the area of the present meander-shaped ridge along a west-northwest-trending zone of faults that cut across the south part of the Coso Range and beyond and have been locally active as recently as late Cenozoic time (Duffield and Bacon, 1977) and apparently as early as Mesozoic time (von Huene, 1960). However, the amount of "instantaneous" relief resulting from a fault displacement seems less likely to have provided a sufficiently high dam to cause diversion of the river than

TABLE 1.—*Erosion and probable ages of Pleistocene basalt near Little Lake*

Channel-cutting episode	Youngest basalt affected	Erosional feature formed	Rock type eroded	Probable age of youngest basalt affected
Youngest	Basalt of Red Hill.	25-m drop at dry falls, 3.3 km north of Little Lake.	Basalt	22,000 years B.P.[1]
Intermediate	Basalt of Upper Little Lake Ranch.	70-m scarp behind Little Lake (the lake).	Basalt and underlying alluvial gravel.	55,000 years B.P.[1] 140,000±89,000 years B.P.[2] >77,000±8,000 years B.P.[3]
Oldest	Basalt of Lower Little Lake Ranch.	160-m scarp south-southeast of Little Lake.	Basalt and underlying alluvial gravel.	399,000±45,000 years B.P.[2] (Upper flow). 486,000±108,000 years B.P.[2] (Lower flow).

[1]Calculated on the basis of a constant rate of canyon downcutting between 10,000 years B.P. and 130,000 years B.P. See text for discussion.

[2]Potassium-argon age (Duffield and Bacon, 1977).

[3]Potassium-argon age (Lanphere and others, 1975). Pyroclastic debris associated with their sample no. 1 overlies basalt of Upper Little Lake Ranch.

ponding of lava. Accordingly, we believe that blockage by lava tipped the balance in favor of the present location of the channel at Little Lake.

The ages of the basalts of Upper Little Lake Ranch and Red Hill are difficult to establish. The basalt of Upper Little Lake Ranch has yielded a potassium-argon age of 140 000 years, but so little radiogenic argon was recovered from the rock that the uncertainty is nearly ±64 percent of this age (table 1). Lanphere, Dalrymple, and Smith (1975) reported a potassium-argon age of 77 000 ±8000 years for a rhyolite dome whose pyroclastic debris partly blankets the cinder cone at the vent of the basalt of Upper Little Lake Ranch; this provides a reasonably well established minimum age for that basalt unit. Repeated attempts to date basalt of Red Hill have proved futile because no radiogenic argon has been recovered (G. Brent Dalrymple, oral commun., 1976). The glacial events in the Sierra Nevada and related lacustrine deposits in Searles Lake provide some contraints on possible ages of the basalts.

Smith's studies (1962; 1968, fig. 4; 1976b) of lacustrine deposits in Searles Lake indicate that the most recent large-scale flow of water that might account for erosion of the lavas and gravels near Little Lake ended about 10 000 years ago. Some water probably passed through the channel in the Little Lake area en route to Searles Lake during parts of Holocene time, the youngest flow ceasing about 2000 years ago (Smith, 1976a), but the volumes apparently were not large. The Searles lacustrine deposits indicate that the first significant flow of water into Searles Lake through the Little Lake area in post-Sherwin time, that is, since about 710 000 years ago, began about 130 000 years ago. Between 10 000 and 130 000 years ago, the water in Searles Lake generally remained high, at times overflowing into Panamint, the next lake in the chain (Smith, 1962; 1968, fig. 4; 1976b). Accordingly, the eruption and subsequent erosion of the basalts of Upper Little Lake Ranch and Red Hill most likely occurred between 130 000 and 10 000 years ago. With this time constraint, estimated ages of the eruptions may be calculated by assuming a constant rate of erosion. We recognize that erosion probably was episodic, but the record of sedimentation in Searles Lake suggests considerable flow past Little Lake during much of the 120 000-year interval, with few extended, possibly dry periods.

The amount of vertical channel erosion during the 120 000-year period of interest may be estimated from

present topography. This procedure somewhat underestimates actual erosion, because a basal, though probably small, part of the erosional scarps is buried by younger deposits. Nonetheless, as a first approximation, we have reconstructed three sequential episodes of canyon downcutting (table 1) with reference to the cycles of eruption and erosion as explained in preceding sections. The two older episodes were apparently characterized by removal of nearly unconsolidated alluvial gravel and thereby represent directly comparable modes of erosion. The youngest episode was apparently characterized by streambed plucking and abrasion within basalt, a contrasting mode of erosion that almost certainly proceeded more slowly than earlier canyon downcutting. The effect of this slower mode of erosion on our assumption of a constant rate would be to make our calculated ages too young; this effect may be at least partly offset by deepening of the channel since 10 000 years ago.

Total downcutting for the three episodes of erosion, that is, for the entire 120 000-year period, is 255 m, yielding an average rate of 2.125 millimeter per year between 10 000 and 130 000 years ago. At this rate, the scarp in the basalt of Lower Little Lake Ranch and underlying rocks could have formed in about 75 000 years, that in the basalt of Upper Little Lake Ranch in about 33 000 years, implying ages of 55 000 and 22 000 years B.P. for the basalts of Upper Little Ranch and Red Hill, respectively (table 1). An age of 55 000 years B.P. for basalt of Upper Little Lake Ranch is inconsistent with the potassium-argon age of 77 000 ±8000 years for overlying rhyolite (Lanphere and others, 1975). The independently determined potassium argon age of 140 000 ±89 000 years is consistent with both estimates, but only because it is not closely constrained.

In summary, the age of the basalt of Lower Little Lake Ranch seems reasonably well fixed by potassium-argon dates alone. The ages of the younger two basalts are problematic because the possible errors associated with the methods used to date them may be about as great as the true ages of the rocks. Nonetheless, considering all lines of evidence, we suggest that the basalt of Red Hill is probably no more than a few tens of thousands of years old, the basalt of Upper Little Lake Ranch probably somewhat less than 100 000 years old, and the basalt of Lower Little Lake Ranch about 440 000 years old. These ages are generally consistent with available evidence and provide guidelines for possible future dating by more accurate techniques.

CLOSING REMARKS

The Pleistocene history of the Little Lake area primarily reflects a struggle between the fairly steady force of stream erosion and the less frequent, but more powerful, eruptions of intracanyon lava flows. The decipherable parts of the story indicate that each has prevailed at different times, with an apparent lull in the struggle at the present time. The abundance of nearby volcanic rocks that are only a few tens of thousands of years or less in age suggests the likelihood of future eruption to set the stage for yet another cycle of eruption and erosion.

An understanding of the Quaternary geologic record at Little Lake is critical to an understanding of other parts of the drainage system that passes through that area. For example, we have little idea of how long each intracanyon lava dammed outflow from Owens Lake, but blockage may have lasted long enough to affect the nature of deposits in downstream basins such as China and Searles Lakes, where evaporation to form a salt layer could have occurred in less than a century. During blockage, one or more new lakes must have formed in Rose Valley, immediately upstream of Little Lake; presumably, buried evidence of their former existence still remains. Moreover, the older buried channel east of Little Lake may now provide a major conduit for groundwater to help recharge the heavily pumped subsurface waters of China Lake basin. Continuing studies will better establish the sequence of late Quaternary events in the Little Lake area.

REFERENCES CITED

Blackwelder, Eliot, 1931, Pleistocene glaciation in the Sierra Nevada and Basin Ranges: Geol. Soc. America Bull., v. 42, p. 865–922.

Cox, Allan, 1969, Geomagnetic reversals: Science, v. 163, p. 237–245.

Duffield, W. A., 1975, Late Cenozoic ring faulting and volcanism in the Coso Range area of California: Geology, v. 3, p. 335–338.

Duffield, W. A., and Bacon, C. R., 1977, Preliminary geologic map of the Coso volcanic field and adjacent areas, Inyo County, California, *with a table of* New K/Ar dates by G. B. Dalrymple: U.S. Geol. Survey Open-File Rept. 77–311, scale 1:50 000.

Lanphere, M. A., Dalrymple, G. B., and Smith, R. L., 1975, K-Ar ages of Pleistocene rhyolitic volcanism in the Coso Mountains, California: Geology, v. 3, p. 339–341.

Mehringer, P. J., and Sheppard, J. C., 1977, Holocene history of Little Lake, Mojave Desert, California, *in* The Ancient Californias: Los Angeles County Mus. Nat. History Quart. [In press.]

Putnam, W. C., 1955, Pleistocene overflow channels at Little Lake California [abs]: Geol. Soc. America Bull., v. 66, no. 12, pt. 2, p. 1607.

Sharp, R. P., 1968, Sherwin till-Bishop tuff geologic relationships, Sierra Nevada, California: Geol. Soc. America Bull., v. 79, p. 351–364.

Sheridan, M. F., 1971, Guidebook to the Quaternary geology of the east-central Sierra Nevada: Phoenix, Lebeau Printing Co., 60 p.

Smith, G. I., 1962, Subsurface stratigraphy of late Quaternary deposits, Searles Lake, California—A summary: U.S. Geol. Survey Prof. Paper 450–C, p. C65–C69.

Smith, G. I., 1968, Late Quaternary geologic and climatic history of Searles Lake, southeastern California, *in* Means of correlation of Quaternary succession: Internat. Assoc. Quaternary Research Cong., 7th, Denver 1965, Proc., v. 8, p. 293–310.

Smith, G. I., 1976a, Origin of lithium and other components in the Searles Lake evaporites, California, *in* Vine, J. D., ed., Lithium resources and requirements by the year 2000: U.S. Geol. Survey Prof. Paper 1003, p. 92–103.

——— 1976b, Paleoclimate record in the upper Quaternary sediments or Searles Lake, California, U.S.A., *in* Paleolimnology of Lake Biwa and the Japanese Pleistocene, Shoji Horie, ed.: Kyoto, Kyoto Univ., v. 4, p. 577–605.

Snyder, C. T., Hardman, G., and Zdenek, F. F., 1964, Pleistocene lakes in the great basin: U.S. Geol. Survey Misc. Geol. Inv. Map I–416, scale 1:1 000 000.

von Huene, R. E., 1960, Structural geology and gravimetry of Indian Wells Valley, southeastern California: Los Angeles, California Univ., Ph.D. thesis, 138 p.

Jour. Research U.S. Geol. Survey
Vol. 6, No. 3, May–June 1978, p. 409–424

CHEMISTRY OF TERTIARY VOLCANIC ROCKS IN THE ELDORADO MOUNTAINS, CLARK COUNTY, NEVADA, AND COMPARISONS WITH ROCKS FROM SOME NEARBY AREAS

By R. ERNEST ANDERSON, Denver, Colo.

Abstract.—Chemical variations of 27 rocks that erupted from in and near the Eldorado Mountains, southern Nevada, show (1) fair to good correlation suggestive of a cogenetic suite, (2) a range of uncorrected silica values from about 48 to 74 weight percent with no strong tendency toward bimodality, (3) a calc-alkaline characteristic, and (4) a shift from early eruptions having an anomalously low level of iron enrichment to later eruptions having a more normal level of iron enrichment. Analyses of rocks not known to have been erupted from the Eldorado Mountains (for example, five analyses of the tuff of Bridge Spring and two analyses of the Fortification Basalt Member of the Muddy Creek Formation) are not anomalous when compared with the other rocks, except that iron concentration in the Fortification Basalt Member may be higher than normal. Extensive K-Ar age data provide a clear time framework for the chemical changes as well as for the structural history of the area. The inception of intense extensional tectonism about 15 million years ago was marked by an abrupt shift to more iron-rich and more typically calc-alkalic volcanic products (Mount Davis Volcanics) than those erupted earlier (Patsy Mine Volcanics), but no corresponding shift in K_2O or total alkali contents or ratios is recognized nor is there any obvious shift toward bimodality in rocks younger than 15 million years. These data, together with data from the Oatman district of Arizona, 100 kilometers to the south-southeast, indicate that the northern part of the lower Colorado River area does not fit into the published Cenozoic patterns of volcanic and tectonic evolution of the western United States. A brief review of nearby areas indicates that they may not fit well either.

The Eldorado Mountains are a north-trending group of ridges and low mountains located south of Hoover Dam between the canyon of the Colorado River on the east and the Eldorado Valley on the west (fig. 1). Bedrock consists of Precambrian metamorphic rocks mantled by a thick pile of upper Tertiary volcanic rocks that are extensively intruded by numerous upper Tertiary plutons.

Discovery of ore in the Eldorado Mountains was made by soldiers stationed at Fort Mohave, Ariz., in 1857 (Hansen, 1962). Early geologic investigations in the Eldorado mining district were reported by Spurr (1903) and Ransome (1907). Vanderburg (1937, p. 26–34) described the general geologic setting of the Eldorado district and reported on the nature and extent of the ore deposits. Hansen (1962) made a thorough investigation of the geology and abandoned mines. He mapped the district at a scale of approximately 1:35 900. The Eldorado Mountains form part of an area between Lake Mead and Davis Dam mapped and described by Longwell (1963). A report by Anderson (1971a) included special consideration of the structural geology of the Eldorado Mountains; a report by Anderson and others (1972) included data on the ages of the Tertiary rocks exposed there.

Longwell (1963) was the first to publish chemical data on the Tertiary volcanic rocks in the Eldorado Mountains, although the same data were reported and discussed earlier by Hansen (1962). The analyzed rocks are siliceous glassy volcanic flows, perlites, or vitrophyres that are interlayered between the more typical mafic to intermediate rocks of the area. The analyses (Longwell, 1963) do not represent the most volumetrically significant rock types in any given area, and they are of glassy rocks in which alkalis may have been disturbed during hydration and (or) ground-water alteration (Noble, 1965, 1967; Lipman, 1965; Lipman and others, 1969). Nevertheless, they are useful in evaluating the general chemical characteristics of the volcanic pile. Of thirteen reported analyses (Longwell, 1963), five are from the Eldorado Mountains. Of the five, one is from the Mount Davis Volcanics (L207, table 1) and four are from the middle rhyolitic part of the Patsy Mine Volcanics, as determined from unpublished mapping by the writer. One of the four Patsy Mine analyses is spurious as a result of rock alteration, so only three are considered (L311, L345, L350, table 1).

In the course of mapping in the Eldorado Mountains in 1970, the writer measured a composite west-east stratigraphic section across the steeply east-tilted volcanic pile north of Nelson, Nev. (Anderson, 1971a, fig. 1). Samples representing the main units were collected and analyzed in the laboratories of the U.S. Geological Survey, as were selected samples from nearby sites. In all, 34 rocks were analyzed, of which

TABLE 1.—*Chemical analyses and norms of volcanic rocks that are known or can be inferred to have erupted from the Eldorado Mountains*

[Analyses arranged from oldest rocks on left to youngest on right. Plotting symbols are those used in figure 4. Sample locality, description, stratigraphic position, and, where known, isotopic age are published separately (Anderson, 1977). Analysis of field Nos. TP4, 7, 8, 12, 14, 15, 19, 23, 25, 26, 66, 41, 44, 47, 52, 57, BC355 and 356 performed in the U.S. Geological Survey rapid rock analysis laboratory under Leonard Shapiro; analysts: P. L. D. Elmore, G. W. Chloe, J. Kelsey, S. D. Botts, H. Smith, Lowell Artis, J. L. Glenn. Analysis of Nos. TP21, 35, BC409B, TP46, and BC411 performed in the U.S. Geological Survey laboratory under Claude Huffman, Jr.: SiO_2, Al_2O_3, Fe_2O_3, P_2O_5 by X-ray fluorescence (values for Fe_2O_3 are total Fe expressed as Fe_2O_3) by J. S. Wahlberg; MgO, CaO, Na_2O, K_2O by atomic absorption by R. L. Rahill; TiO_2 by colorimetric method by R. L. Rahill; F by specific ion method by W. D. Goss and D. R. Norton. For Nos. L311, 345, 350, and 207, analysis from Longwell (1963, table 2), Rock Analysis Laboratory, University of Minnesota, Eileen Oslund, analyst. Leaders, ---, indicate no data; tr, trace]

	Patsy Mine Volcanics														
	Lower											Middle			Upper
Plotting symbol	A	C	B	D	E	F	G	H	II	I	J	K	X	ϕ	L
Field no.	TP4	TP7	TP8	TP12	TP14	TP15	TP19	TP21	TP23	TP25	TP26	L311	L345	L350	TP35
Laboratory no.	384	386	387	W170 388	389	390	391	D160 393	W170 392	W170 393	W170 394	R1543	R1544	R1545	D160 392
Mineral	Chemical analyses (in weight percent)														
SiO_2	50.0	64.5	51.1	58.6	55.1	55.1	56.0	52.9	68.2	70.0	49.2	72.21	72.91	73.65	62.9
Al_2O_3	16.8	14.7	15.4	15.1	15.9	14.1	14.0	14.1	14.6	14.6	14.3	12.34	12.53	12.87	14.4
Fe_2O_3	6.5	2.9	6.0	3.4	5.4	4.7	4.6	8.5	2.2	2.0	4.6	.59	.43	.78	5.3
FeO	.60	1.2	1.3	2.3	1.0	.84	.96	---	.06	.24	3.8	.18	.30	.09	---
MgO	3.8	2.6	5.7	4.7	5.2	5.7	5.8	7.12	.70	.84	7.5	.12	.13	.19	3.72
CaO	6.6	3.0	8.4	6.2	6.1	6.7	6.6	6.59	3.0	1.8	8.4	.97	.69	.79	4.63
Na_2O	3.1	3.4	2.7	3.0	3.4	3.0	2.8	2.98	3.4	2.9	3.5	3.33	3.67	3.49	4.00
K_2O	5.2	3.3	4.0	1.8	2.5	3.6	4.4	3.15	4.7	5.7	2.8	4.16	4.52	4.58	2.38
H_2O-	.73	.42	.67	1.1	1.9	1.6	1.4	---	2.0	.31	.62	4.75	3.99	2.96	---
H_2O+	2.0	2.0	1.6	2.3	1.7	2.0	1.4	---	.76	.59	2.5	1.00	.24	.20	---
TiO_2	1.1	.66	1.1	.92	1.1	.86	.99	1.25	.41	.40	1.6	.12	.13	.11	.63
P_2O_5	1.5	.27	1.0	.44	.56	.63	.88	.93	.14	.12	1.0	.01	.01	.01	.40
MnO	.8	.06	.10	.08	.06	.10	.07	---	.06	.07	.14	.05	.04	.05	---
CO_2	2.0	.72	.15	<.05	.05	.59	.10	---	.78	.05	.10	---	---	---	---
F	---	---	---	---	---	---	---	.15	---	---	---	---	---	---	.08
Total	100	100	99	100	100	100	100	98	99	100	100	100	100	100	98
Normative minerals	Norms (in percent)														
Q	---	23.3	0.1	17.0	8.1	6.3	5.8	3.9	24.7	26.9	---	36.9	34.2	35.1	17.8
C	---	.8	---	---	---	---	---	---	---	.7	---	.7	.4	.7	---
OR	32.3	20.2	24.4	11.0	15.3	22.3	26.8	19.1	28.5	34.1	17.1	26.1	28.0	28.0	14.3
AB	27.5	29.8	23.6	26.3	29.9	26.6	24.4	25.8	29.5	24.9	29.1	30.0	32.6	30.6	34.4
AN	17.4	13.6	18.7	23.2	21.5	15.1	13.0	16.2	11.0	8.3	15.5	5.0	3.5	4.0	14.5
NE	---	---	---	---	---	---	---	---	---	---	.8	---	---	---	---
WO	2.3	---	7.4	2.4	2.5	6.5	6.2	2.6	1.0	---	8.7	---	---	---	1.5
EN	2.5	6.7	14.7	12.1	13.4	14.9	14.9	18.2	1.8	2.1	7.3	.3	.3	.5	9.4
FS	---	---	---	---	---	---	---	---	---	---	.3	---	.1	---	---
FO	5.2	---	---	---	---	---	---	---	---	---	8.4	---	---	---	---
FA	---	---	---	---	---	---	---	---	---	---	.4	---	---	---	---
MT	---	2.2	1.4	5.1	.2	.6	.5	---	---	---	6.9	.4	.7	.1	---
HM	6.8	1.5	5.3	---	5.4	4.5	4.4	8.7	2.3	2.0	---	.3	---	.7	5.4
IL	1.5	1.3	2.2	1.8	2.2	1.7	1.9	---	.3	.7	3.1	.2	.3	.2	---
TN	0.9	---	---	---	---	---	---	3.1	.7	---	---	---	---	---	1.6
RU	---	---	---	---	---	---	---	---	---	.1	---	---	---	---	---
AP	3.7	.7	2.4	1.1	1.4	1.6	2.1	2.3	.3	.3	2.4	tr	tr	tr	1.0
FR	---	---	---	---	---	---	---	.1	---	---	---	---	---	---	.1

4 are not reported herein. Two of those not reported are from altered lavas in the voluminous lower part of the volcanic pile and are chemically spurious; another is a silicified rhyolite having 85 percent silica; and the fourth is a slightly altered equivalent of an unaltered lava from which a more reliable analysis is reported. The analytical data for the remaining 30 samples are presented in tables 1 and 2. With the exception of the lower part of the volcanic pile, which is difficult to interpret in terms of original chemical composition owing to pervasive though locally mild alteration, these previously unpublished analyses together with those published by Longwell (1963) represent all of the volumetrically significant volcanic rocks in the area. Therefore, the analyses are adequate for an appraisal of the major-element chemical char-

TABLE 1.—*Chemical analyses and norms of volcanic rocks that are known or can be inferred to have erupted from the Eldorado Mountains*—Continued

	Mount Davis Volcanics											
	Lower			Middle				Upper				
Plotting symbol ----	T	M	N	P	O	Q	R	≤	S	U	V	W
Field no.----	BC409B	TP66	TP41	TP44	TP46	TP47	TP52	L207	TP57	BC411	BC355	BC356
Laboratory no.	D160 390	W170 401	W170 397	W170 398	D160 391	W170 402	W170 403	R1539	W170 404	D160 389	W170 408	W170 409
Mineral	Chemical analyses (in weight percent)											
SiO_2 ----	52.0	53.0	53.7	65.3	57.9	58.5	58.5	66.85	54.2	54.3	47.8	55.2
Al_2O_3 ----	14.9	16.5	16.2	15.2	15.1	16.9	17.0	15.25	16.0	15.2	15.9	16.9
Fe_2O_3 ----	10.1	7.2	5.7	2.2	7.2	4.0	4.2	1.26	4.9	9.2	8.1	2.7
FeO ----	---	.92	2.1	.64	---	1.1	1.1	.57	2.6	---	.76	4.6
MgO ----	7.31	4.4	4.7	1.1	3.36	2.9	2.6	.46	5.0	6.06	8.1	5.7
CaO ----	7.95	6.9	7.0	5.2	5.70	5.8	6.7	1.38	7.6	6.83	7.2	6.7
Na_2O ----	3.34	3.4	3.2	3.4	3.89	3.8	3.8	3.90	3.4	3.73	2.7	3.5
K_2O ----	1.62	3.1	3.0	4.3	3.77	3.5	3.2	5.74	2.0	2.31	2.0	1.8
H_2O- ----	---	1.2	.69	.40	---	.62	.29	.18	1.1	---	2.2	.23
H_2O+ ----	---	.90	1.2	.90	---	1.1	.63	3.53	1.2	---	2.8	.97
TiO_2 ----	1.23	1.3	1.3	.46	1.17	.94	.87	.41	1.2	1.39	1.4	1.1
P_2O_5 ----	.79	.88	.63	.20	.75	.63	.86	.07	.40	.74	.56	.42
MnO ----	---	.09	.13	.06	---	.10	.11	.06	.12	---	.14	.12
CO_2 ----	---	.05	.09	.08	---	<.05	.08	---	.10	---	.16	<.05
F ----	.10	---	---	---	.14	---	---	---	---	.08	---	---
Total ----	99	100	100	99	99	100	100	100	100	100	100	100
Normative minerals	Norms (in percent)											
Q ----	3.6	4.3	5.6	20.0	8.3	9.5	10.1	19.5	7.1	4.6	---	5.4
C ----	---	---	---	---	---	---	---	.3	---	---	---	---
OR ----	9.6	18.8	18.2	26.0	22.5	21.1	19.1	35.4	12.1	13.7	12.5	10.8
AB ----	28.5	29.5	27.7	29.3	33.3	32.8	32.5	34.4	29.5	31.6	24.1	30.0
AN ----	21.0	21.1	21.5	13.8	12.7	19.1	20.1	6.7	23.1	17.9	26.8	25.4
NE ----	---	---	---	---	---	---	---	---	---	---	---	---
WO ----	3.7	3.1	4.1	4.7	2.6	2.5	3.3	---	5.4	2.6	2.3	2.3
EN ----	18.3	11.2	11.2	2.8	8.5	7.4	6.5	1.2	12.8	15.1	21.2	14.4
FS ----	---	---	---	---	---	---	---	---	---	---	---	---
FO ----	---	---	---	---	---	---	---	---	---	---	.1	---
FA ----	---	---	---	---	---	---	---	---	---	---	---	---
MT ----	---	---	3.5	.9	---	1.7	1.4	.9	5.4	---	---	4.0
HM ----	10.2	7.4	3.4	1.6	7.3	3.3	3.3	.7	1.3	9.2	8.6	---
IL ----	---	2.2	2.5	.9	---	1.8	1.7	.8	2.3	---	2.0	2.1
TN ----	3.0	.5	---	---	3.0	---	---	---	---	3.4	1.0	---
RU ----	---	---	---	---	---	---	---	---	---	---	---	---
AP ----	1.9	2.1	1.5	.5	1.8	1.5	2.1	.2	1.0	1.8	1.4	1.0
FR ----	.1	---	---	---	.2	---	---	---	---	---	---	---

acteristics of the volcanic pile and of chemical trends and variations within the pile. The main purpose of the present report is to make such an appraisal and to compare the results with data from nearby volcanic suites. Unfortunately, chemical data on the associated plutonic rocks are unavailable, thus rendering the appraisal of major-element chemistry incomplete insofar as the Cenozoic igneous rocks are concerned.

Only a brief account of the geology of the area is presented in the present report. For more details, the reader is referred to the several reports discussed above and especially to those of Hansen (1962), Anderson (1971a), and Anderson and others (1972). An open-file report (Anderson, 1977), complementary to the present report, contains a detailed description of strata exposed in the Eldorado Mountains and includes descriptions of the chemically analyzed rocks.

Acknowledgments.—I thank W. L. Ellis for assistance in the field, R. P. Snyder and M. J. Adams for implementing computerized norm calculations as well as for assistance in the preparation of illustrations, F. M. Byers, Jr., for supplying petrographic data, and J. P. Thorson for supplying unpublished K-Ar data on rocks from the Oatman district, Arizona. Valuable criticism was received from F. M. Byers, Jr., E. B. Ekren, and Myron Best. I thank the Robert Littleton family, Boulder City, Nev., for their hospitality during this and other work done in southern Nevada.

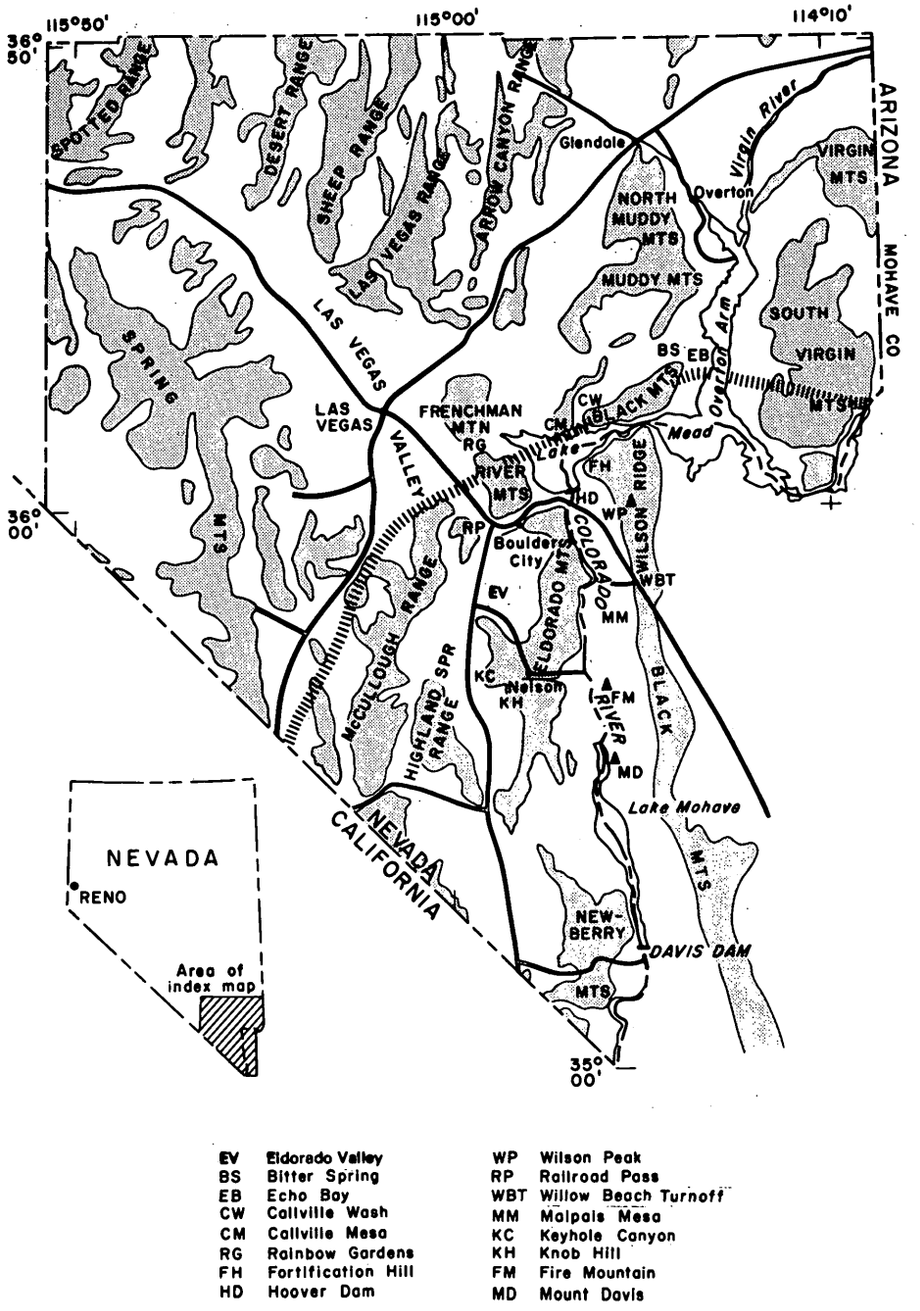

EV	Eldorado Valley	WP	Wilson Peak
BS	Bitter Spring	RP	Railroad Pass
EB	Echo Bay	WBT	Willow Beach Turnoff
CW	Callville Wash	MM	Malpais Mesa
CM	Callville Mesa	KC	Keyhole Canyon
RG	Rainbow Gardens	KH	Knob Hill
FH	Fortification Hill	FM	Fire Mountain
HD	Hoover Dam	MD	Mount Davis

FIGURE 1.—Index map showing location of Eldorado Mountains and major physiographic and cultural features in the area. Hachured line marks northern limit of area where the geology is characterized by basement rocks of Precambrian age overlain by volcanic rocks of Tertiary age (Anderson and others, 1972).

GEOLOGIC SETTING

The Eldorado Mountains are situated in the Basin and Range province about 60 kilometers west of the Colorado Plateaus province. They are part of a large area in southern Nevada and northwestern Arizona characterized by an absence of the thick sequences of Paleozoic, Mesozoic, and Cenozoic sedimentary rocks found to the north (fig. 1).

TABLE 2.—*Chemical analyses and norms of volcanic rocks that are not known to have erupted from the Eldorado Mountains*

[Sample BC168 is from an ash-flow tuff at the base of the Patsy Mine Volcanics. Plotting symbols are those used in figures 3–5. Analysis of field Nos. 2–93–3 and BC405: SiO_2, Al_2O_3, Fe_2O_3, P_2O_5 by X-ray fluorescence (values for Fe_2O_3 are total Fe expressed as Fe_2O_3) by J. S. Wahlberg; MgO, CaO, Na_2O, K_2O by atomic absorption by R. L. Rahill; TiO_2 by colorimetric method by R. L. Rahill; F by specific ion method by W. D. Goss and D. R. Norton. Analysis of field Nos. TP64, BC397, TP62, BC392, BC346, and BC168 performed in the U.S. Geological Survey rapid rock analysis laboratory under Leonard Shapiro; analysts: P. L. D. Elmore, G. W. Chloe, J. Kelsey, S. D. Botts, H. Smith, Lowell Artis, J. L. Glenn. Leaders indicate no data]

	Fortification Basalt		Tuff of Bridge Spring					Tuff
Plotting symbol	Y	Z	5					θ
Field no.	2-93-3	BC405	TP64	BC397	TP62	BC392	BC346	BC168
Laboratory no.	M60388	M60387	W170400	W170407	W170399	W170406	W170405	W170383
	Chemical analyses (in weight percent)							
SiO_2	51.1	49.7	66.1	67.8	66.9	68.2	68.2	77.6
Al_2O_3	14.2	17.1	16.0	13.9	15.6	14.9	14.8	10.6
Fe_2O_3	12.6	12.0	2.4	2.3	2.0	2.1	1.7	1.0
FeO	-----	-----	.12	.06	.04	.20	.12	.06
MgO	3.63	5.50	1.0	1.2	.96	.61	.61	.33
CaO	8.26	9.40	1.8	2.4	1.4	2.2	3.0	.90
Na_2O	3.48	3.43	3.5	4.0	3.8	3.6	4.1	2.4
K_2O	2.56	1.50	5.4	4.6	5.6	5.0	5.1	4.8
H_2O-	-----	-----	1.0	.51	1.3	.49	.36	.20
H_2O+	-----	-----	1.3	.79	1.5	.81	.59	.75
TiO_2	2.14	1.79	.55	.50	.44	.45	.40	.17
P_2O_5	1.6	.89	.13	.20	.07	.11	.06	.04
MnO	-----	-----	.03	.04	.06	.07	.06	-----
CO_2	-----	-----	.05	.85	<.05	.64	.84	.18
F	.13	.09	-----	-----	-----	-----	-----	-----
Total	100	100	99	99	100	99	100	99
	Norms (in percent)							
Q	5.7	1.2	20.7	22.1	19.8	23.5	19.7	43.9
C	----	----	1.5	----	1.0	----	----	----
OR	15.2	8.7	32.9	28.0	34.2	30.3	30.7	29.0
AB	29.5	28.6	30.5	34.9	33.2	31.3	35.3	20.7
AN	15.6	26.5	8.3	6.6	6.7	10.0	7.0	4.1
WO	3.1	3.2	----	1.2	----	----	2.9	----
EN	9.1	13.5	2.6	3.1	2.5	1.6	1.5	.8
HM	12.6	11.8	2.5	2.4	2.1	2.2	1.8	1.0
IL	----	----	.3	.2	.2	.6	.4	.1
TN	5.3	4.3	----	1.0	----	.3	.5	.2
RU	----	----	.4	----	.3	----	----	----
AP	3.8	2.1	.3	.5	.2	.3	.1	.1

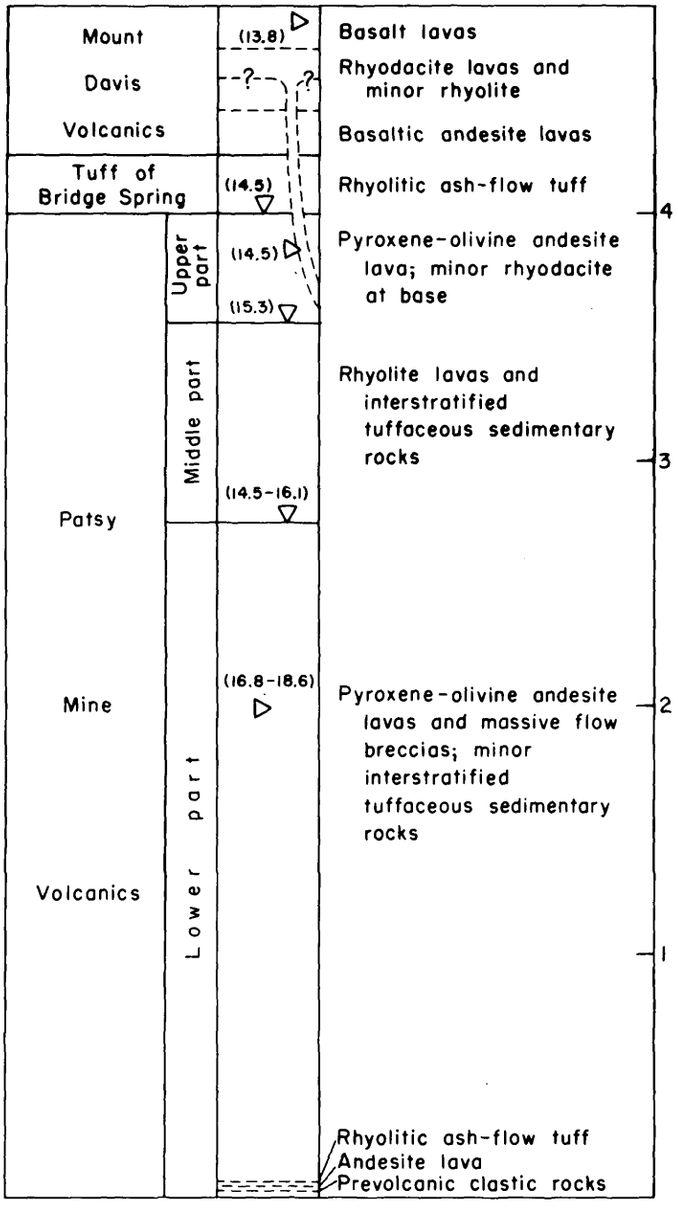

FIGURE 2.—Stratigraphic section of Tertiary rocks in the Eldorado Mountains showing stratigraphic position (triangles) of K-Ar ages in parentheses. Dashed form indicates schematic intrusive. Scale indicates thickness in kilometers. From Anderson and others (1972).

The three informally designated groups of rocks exposed in the Eldorado Mountains are as follows: (1) metamorphic rocks of Precambrian age, (2) volcanic, intrusive, and volcanogenic sedimentary rocks of late Tertiary age, and (3) volcanic and sedimentary rocks of latest Tertiary and Quaternary age. The volcanic rocks of group 2 are the main subject of this report. These rocks accumulated to a thickness of approximately 5000 meters on a surface of low relief cut on the crystalline rocks of group 1. They consist mostly of lava and flow breccia of mafic to intermediate composition, minor ash-flow tuff, bedded tuff, and lava of rhyolitic composition. In ascending order, they are divided into the Patsy Mine Volcanics (subdivided into lower, middle, and upper parts), the tuff of Bridge Spring, and the Mount Davis Volcanics. Their approximate thickness and age are shown in figure 2. The Patsy Mine Volcanics and the Mount Davis Volcanics probably vented from the Eldorado Mountains, but the source of the tuff of Bridge Spring is not known.

Eruption of the Mount Davis Volcanics was accompanied by widespread epizonal plutonism. Granitoid intrusive rocks representing two intrusive episodes are exposed in the Eldorado Mountains at Nelson, Knob Hill, and Keyhole Canyon (fig. 1). An early group of irregular plutons consisting predominantly of quartz monzonite but ranging to diorite is intruded by several bodies of later granodiorite and leucogranite (Hansen, 1962). These plutons have fine-grained to porphyritic border facies locally. Numerous aphanitic and porphyritic dikes, sills, and small plugs, some of which are apophyses related to the larger masses, are also exposed in the Eldorado Mountains. They range from rhyolite to basalt. Granitoid to subgranitoid plutons of similar age are also found at Railroad Pass, Boulder City, Wilson Ridge, and in the Newberry Mountains (fig. 1).

The plutonism and Mount Davis volcanism were accompanied by intense faulting and stratal rotation that Anderson (1971a, b) interpreted as thin-skin effects of extreme crustal stretching and attenuation. This brief episole of violent volcanic and structural activity was followed by high-angle normal faulting that blocked out the present range and basin system. The basins were partially filled with sedimentary rocks and occasional basaltic lavas of group 3. These late deposits include the Muddy Creek Formation and the Fortification Basalt Member of the Muddy Creek Formation.

MAJOR-ELEMENT CHEMISTRY

The chemical data and norms for rocks known or presumed to have been erupted from the Eldorado Mountains are given in table 1 and those for the other rocks are given in table 2. Descriptions of the rocks, their locations, and their relative stratigraphic positions and ages, where known, are given in a separate report (Anderson, 1977).

Nearly all rocks from the Eldorado Mountains are quartz normative, but a few lie just above the boundary between silica saturation and undersaturation

(tables 1, 2). A little corundum appears in the norms of a few samples. The ratio of normative magnetite to hematite shows extreme variation, owing to oxidation of iron, but for the most part normative magnetite is sparse or absent. For the purpose of classification, no attempt was made to correct the analyses for their indicated variations in oxidation state.

Standard silica variation diagrams based on percentages adjusted free of H_2O and CO_2 are presented in figure 3. The strata erupted from the Eldorado Mountains (Patsy Mine and Mount Davis Volcanics) have a 27-percent range in silica content from 50.5 to 77.5. Points for other analyses such as the Fortification Basalt Member, the ash-flow tuff at the base of the Patsy Mine Volcanics, and the average of five analyses of the tuff of Bridge Spring are also plotted. CaO, MgO, and ΣFe as FeO show a consistent decline with increasing SiO_2 and display little scatter. Na_2O shows very little increase; K_2O shows a small increase but with considerable scatter. MgO contents are gener-

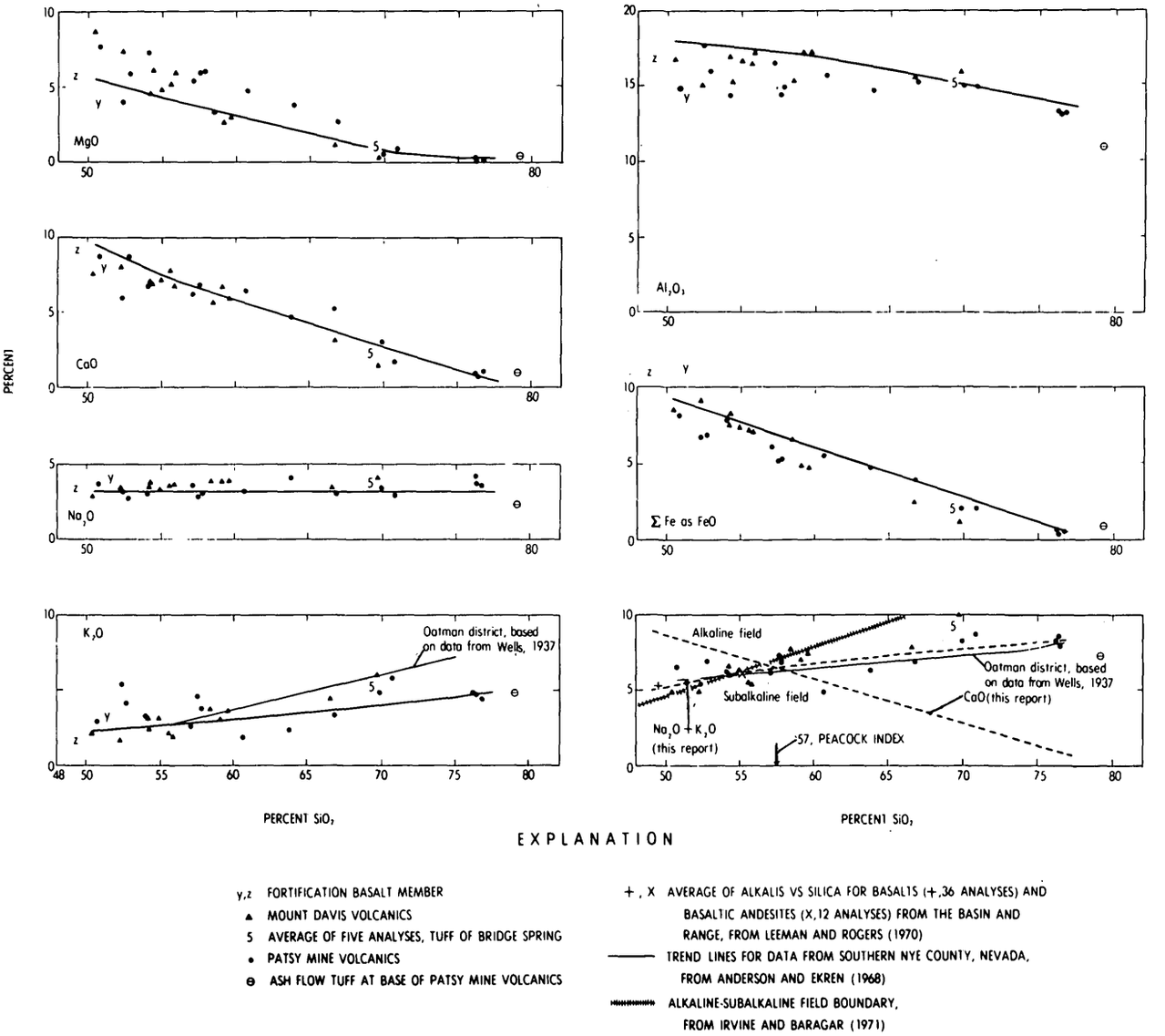

FIGURE 3.—Diagrams showing comparison of standard silica variation representing rocks from the Eldorado Mountains with variations representing rocks from southern Nye County. Also shown are plots of average oxides for basaltic rocks from the Basin and Range province and some trend lines for the Oatman district, Arizona. In the $K_2O + Na_2O$ versus CaO diagram, the short-dashed trend lines are visual best-fit curves to the data from table 1; the hachured line marks the boundary between alkaline and subalkaline composition fields as determined by Irvine and Baragar (1971).

ally lower and Na_2O and Al_2O_3 contents are generally higher for a given silica content in the Mount Davis rocks than in the Patsy Mine rocks. Data points plotted on the $Na_2O + K_2O$ versus silica diagram show considerable scatter and an average increase of about 3 percent alkalis over the full range of silica increase. There does not appear to be any basis for discriminating between the total alkali contents of the Patsy Mine Volcanics and the Mount Davis Volcanics.

When the chemical analyses of the rocks in the Eldorado Mountains are plotted on the three-axis orthogonal plot $Na_2O + K_2O$ versus $FeO + Fe_2O_3 + \frac{1}{2}(MgO + CaO)$ versus Al_2O_3/Si_2O_3, as suggested by Church (1975) for the classification of common volcanic rocks, they display a continuum of variation similar to the common basalt-andesite-dacite-rhyolite association, as indicated in figure 4 by bold letters positioned near Daly's (1933) averages for those rock types. The fields shown for each of the rock types represent contours within which two-thirds of the most common rocks cataloged by Washington (1917) plot as basalt, andesite, dacite, and rhyolite (Church, 1975). Not all of the rocks from the Eldorado Mountains plot within the fields on both projections, but more than two-thirds of them do; most of the others plot very close to the field boundaries. A tendency exists for the plotted points representing the rocks from the Eldorado Mountains to be displaced slightly toward the high-alkali and low-alumina side of the fields.

Ternary diagrams for selected groups of oxides and normative minerals are shown in figure 5. The distribution of points on the standard AMF diagram (fig. 5*A*) suggests a trend of greater iron enrichment in the Mount Davis Volcanics than in the Patsy Mine Volcanics. The Fortification Basalt Member has higher iron concentration than either of its volcanic predecessors, though the data are limited. As noted above, there is a corresponding discrimination between the Patsy Mine and Mount Davis rocks on the MgO versus SiO_2 diagram (fig. 3). The mafic Patsy Mine rocks have lower ratios of iron to magnesium compared with rocks from the Cactus Range, Nev., the Oatman district, Arizona, and other mafic volcanic rocks from the Basin and Range province for which data were compiled by Leeman and Rogers (1970).

On the $K_2O + Na_2O$ versus silica diagram (fig. 3), data points representing the mafic rocks (<57 percent silica) are scattered almost symmetrically along the discriminant line separating alkaline and subalkaline compositional fields taken from Irvine and Baragar (1971), whereas the more siliceous rocks fall within the subalkaline field. The mafic rocks share their position along the discriminant line with other upper Cenozoic mafic rocks from the Basin and Range prov-

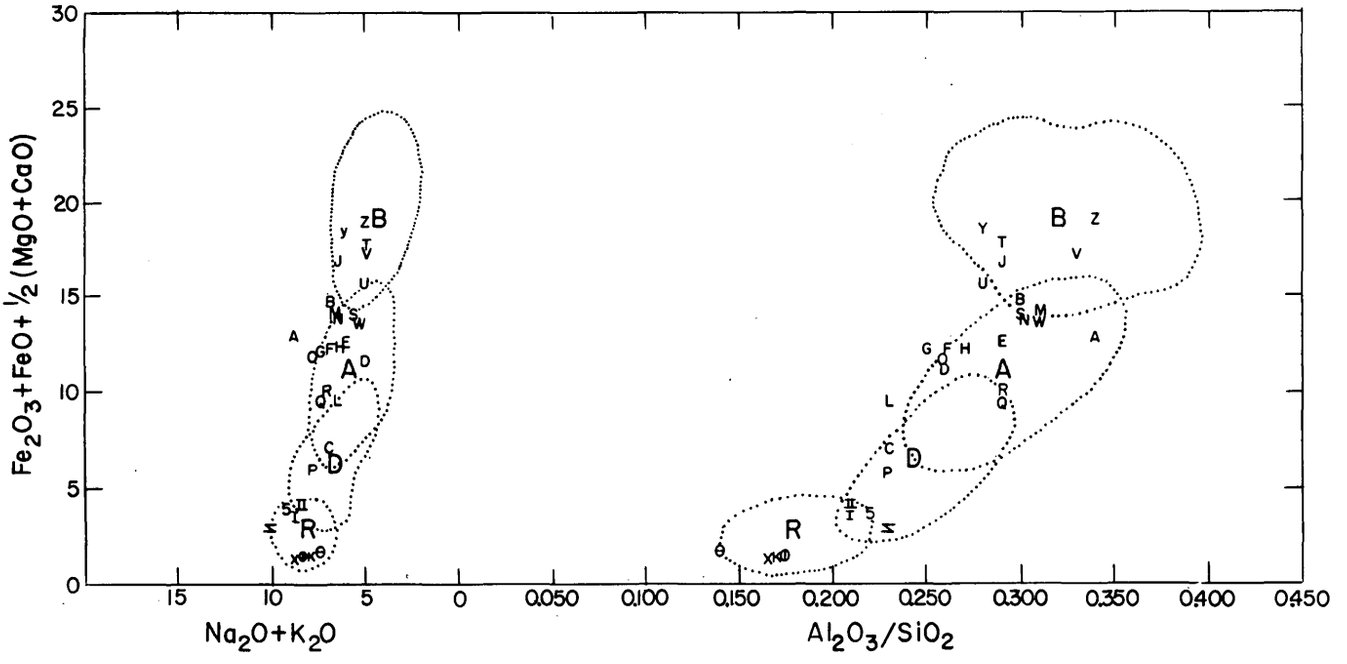

FIGURE 4.—Rock classification diagram, showing by dotted outline, the fields of concentration for common volcanic rocks of the basalt-andesite-dacite-rhyolite suite; bold letters are positioned near Daly's (1933) averages calculated from analyses of those rock types (modified from Church, 1975). Data from the Eldorado Mountains are indicated by symbols keyed to tables 1 and 2.

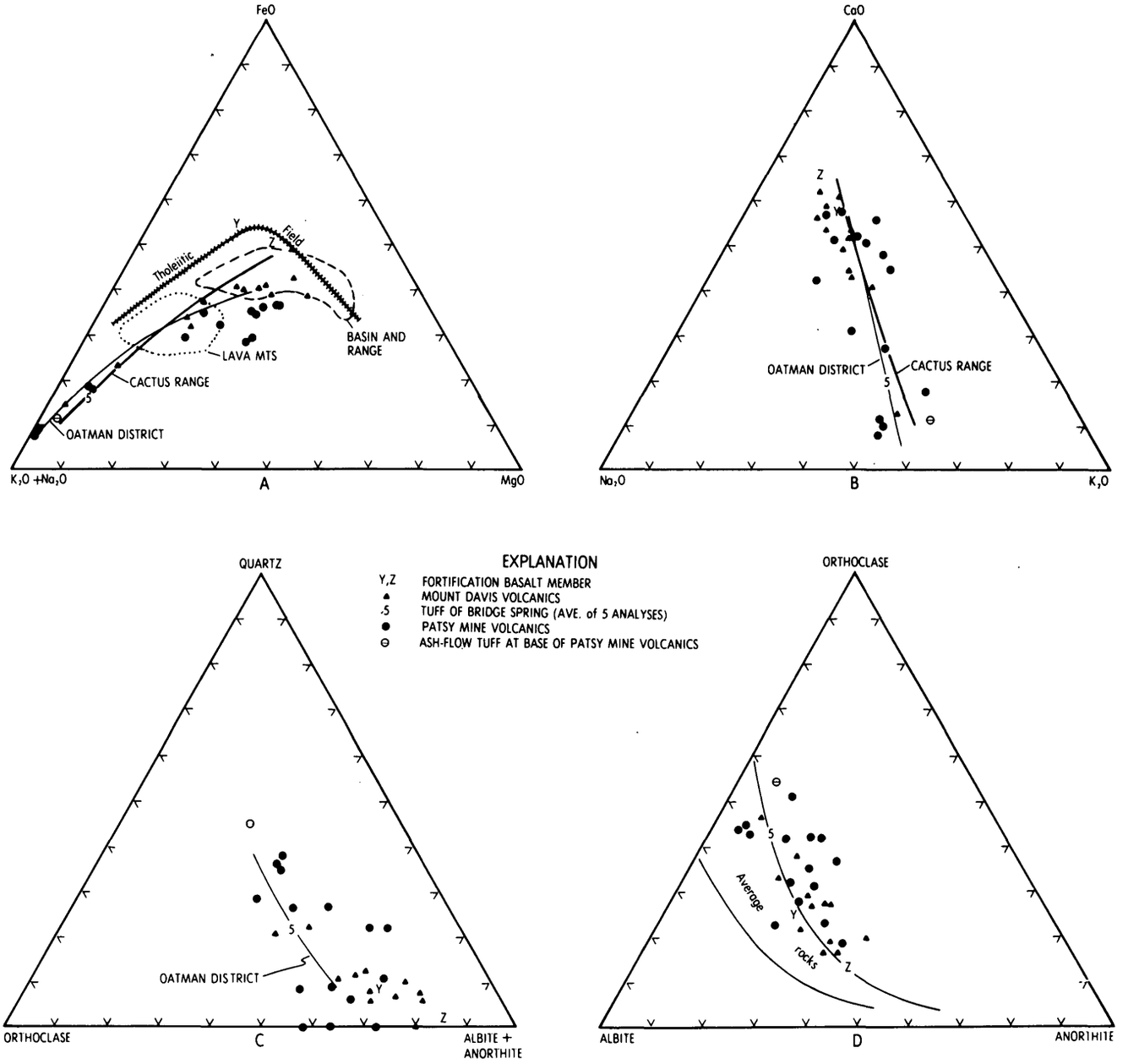

FIGURE 5.—Ternary diagrams of selected chemical and normative parameters showing variations in data from the Eldorado Mountains and comparisons with variations from other areas. In *A* the field outlined by a dotted line represents 22 analyses reported by Smith (1964) for the Lava Mountains, San Bernardino County, Calif., the dashed outline represents 34 analyses from the Basin and Range province summarized by Leeman and Rogers (1970); the hachured line marks the boundary between tholeiitic and calc-alkalic fields from Irvine and Baragar (1971). In *A* and *B*, the bold trend lines are taken from Ekren and others (1971) and are visual best-fit curves through 18 tightly grouped points representing intrusive rocks from the Cactus Range, Nye County, Nev. The lighter trend lines in *A*, *B*, and *C* are visual best-fit curves through points plotted from abundant chemical data reported by Wells (1937) and Thorson (1971) on rocks from the Oatman district, Arizona. In *D* the lines enclose a field considered by Irvine and Baragar (1971) to represent average subalkaline rocks.

ince, as determined from data assembled by Leeman and Rogers (1970). The intersection of the $Na_2O + K_2O$ versus silica curve with the CaO versus silica curve (fig. 3) yields a Peacock index of about 57, indicating that the rocks have a calc-alkalic characteristic. Also, data points plotted on the standard AMF diagram (fig. 5*A*) are situated well within the field of calc-alkalic suites as determined by Irvine and Baragar (1971). In other tests, however, the rocks from the Eldorado Mountains do not display obvious calc-alkalic

characteristics. For example, on the ternary feldspar diagram (fig. 5*D*) most of the normative data plot outside the boundaries of the field for average subalkaline rocks determined by Irvine and Baragar (1971), suggesting that the suite is richer in K_2O than normal subalkaline rocks. This agrees with the slight displacement of data points from Daly's average rocks to the high-alkali side on the rock classification diagram (fig. 4). Irvine and Baragar (1971) suggested that a plot of Al_2O_3 versus normative plagioclase composition (fig. 6) provides a significant discrimination between calc-alkalic and tholeiitic suites, especially among their more mafic variants. According to this discrimination (fig. 6), the Mount Davis Volcanics are more typically calc-alkalic than their Patsy Mine predecessors.

The data points on the alkali-lime diagram (fig. 5*B*) show considerable scatter, especially for the samples from the Patsy Mine Volcanics. Part of the scatter may reflect disturbance of alkali contents resulting from propylitic alteration in the voluminous mafic lower part of the Patsy Mine Volcanics or hydration and (or) ground-water disturbances in the glassy siliceous rocks, whose analyses were taken from Longwell (1963). In any case, the diagram illustrates the broad range in the ratio of K_2O to CaO in the rocks from the Eldorado Mountains and the conspicuous insensitivity of that ratio to Na_2O contents, especially for the relatively unaltered Mount Davis Volcanics. This is a predictable relationship in a series of rocks having a 30-percent range in SiO_2 contents and essentially no correlative variation in Na_2O contents (fig. 3). Though the data are more scattered on the ternary diagram showing normative feldspar (fig. 5*D*), the essential parallelism of the trend to the orthoclase-anorthite leg illustrates the same relationship.

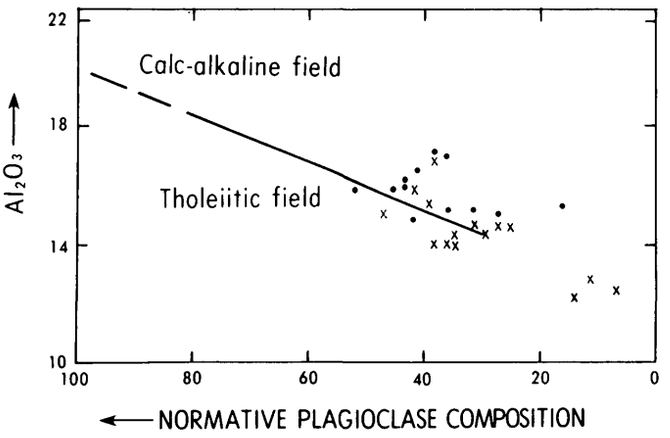

FIGURE 6.—Plot of Al_2O_3 versus normative plagioclase composition for Mount Davis Volcanics (dots) and Patsy Mine Volcanics (crosses). Dividing line between calc-alkalic and tholeiitic fields is that proposed by Irvine and Baragar (1971).

The data points on the normative plot of quartz-orthoclase-plagioclase (fig. 5*C*) are too scattered to yield a meaningful trend, but it is clear that no conspicuous enrichment in orthoclase accompanies increasing normative quartz. The lack of such a relationship is in keeping with petrographic data showing that quartz is sparse to absent and that potassium feldspar is not found in large quantities as phenocrysts in the siliceous representatives of these rocks.

In general, the lack of good correlations on the several variation diagrams that involve alkalis argues against derivation of the magmas from which these rocks crystallized by any process involving partial or total melting of sialic crust. That the suite as a whole is heavily weighted at the mafic end is, of course, an additional argument against such an origin. Data reported by Hedge and Noble (1971) indicated that the anomalously high Sr^{87}/Sr^{86} ratios of numerous, mostly upper Cenozoic basalts from the southern Great Basin could not have been produced by assimilation of crustal material by primary basaltic magma. One of the samples reported by Hedge and Noble (1971; table 1, field no. TP26) and another analyzed by them but not reported (TP57) are from the Eldorado Mountains (table 1). Both samples have anomalously high uncorrected Sr^{87}/Sr^{86} ratios (normalized to $Sr^{86}/Sr^{88}=0.1194$) of 0.7078 and 0.7088, respectively (D. C. Noble, written commun., 1971). Hedge and Noble concluded that such basalts must have been derived from unusual mantle material in which an originally high Rb/Sr ratio was markedly lowered during an earlier phase of magmatic activity.

Tuff of Bridge Spring

The tuff of Bridge Spring (dated at about 14.5 million years by Anderson and others, 1972) is a widespread quartz-free ash-flow tuff in which phenocrysts of plagioclase, sanidine, biotite, hornblende, clinopyroxene, sphene, and magnetite vary considerably in amount and relative proportions. Two cooling units are recognized locally. In general, the mafic mineral content increases upward in the lower cooling unit as does the ratio of plagioclase to sanidine.

Five analyses from three widespread locations of the tuff of Bridge Spring are available (table 2) and in each case the sample was collected from the crystalline (stony) interior of the cooling units. The five analyses are very similar to one another (table 2), indicating lithologic homogeneity for the interior of the tuffs, despite vertical lithologic variations observed

in some stratigraphic sections. Because they are similar, only the average of the analyses is shown on the variation diagrams (figs 3, 5). The location of the source for the tuffs is not known, and, therefore, the chemical data were not used in constructing curves showing chemical variation for the rocks from the Eldorado Mountains. However, it is clear from the diagrams that the tuff of Bridge Spring does plot on, near, or within the trends or fields of concentration defined by the suite of locally derived rocks and is not chemically anomalous with the Eldorado Mountains rocks. This is supported by petrographic studies that show that locally derived lavas of similar composition have mineral assemblages similar to those of the tuff of Bridge Spring.

A suggestion from the normative quartz-orthoclase-albite + anorthite diagram (fig. 5*C*) is that the average analysis accords more closely with the relatively more potassic rocks of the Oatman district than with the rocks of the Lake Mead area. However, this distinction cannot be seen on the oxide diagrams (figs. 5*A*,*B*).

Fortification Basalt Member of Muddy Creek Formation

Chemical analyses were obtained on two samples of alkali olivine basalt from the Fortification Basalt Member of the Muddy Creek Formation (samples BC405 and 2–93–3, table 2). Neither sample was collected from the Eldorado Mountains. Chemical analyses of many rocks would be needed to accurately characterize the widespread basalts of the Fortification. Although the two reported herein do not accomplish that, they do indicate that the Fortification contains lavas that are more iron-rich than any of their mafic predecessors (plots Y and Z, fig. 5*A*) and that alkali contents are not anomalous when compared with the older lavas (fig. 3).

COMPARISONS WITH OTHER AREAS

In recent comprehensive syntheses of available geologic data on suites of Cenozoic igneous rocks from many locations throughout the Western United States, Lipman, Prostka, and Christiansen (1972) and Christiansen and Lipman (1972) presented a clear, though tentative, picture of older predominantly calc-alkalic andesitic igneous activity succeeded by younger fundamentally basaltic suites associated with regional normal and strike-slip faulting. The data they synthesized also suggested a time pattern in which the transition from predominantly andesitic volcanism to fundamentally basaltic volcanism occurred across the region. Chemical and age data from the lower Colorado River area, which includes the Eldorado Mountains and the Oatman district, were used in those syntheses, as were data from nearby areas such as southern Nye County, Nev., and the Lava Mountains, Calif.

The intent in this report is to provide certain background information against which some of the conclusions and assumptions made for the lower Colorado River area in the excellent syntheses mentioned above can be evaluated in the light of new data. The data given in parentheses following the subheadings of this section are approximate distances and azimuths of the various areas measured from the Eldorado Mountains.

Oatman district, Mohave County, Ariz. (100 km SSE)

The Oatman mining district is located in the southern part of the Black Mountains, Ariz. The district, about 175 square kilometers in extent, was mapped in detail by Ransome (1923), who found that most of the area consists of trachyte, andesite, and latite flows and closely related quartz monzonite porphyry and granite porphyry intrusive masses. Other rock types present include volcanic breccia, tuffs, rhyolite, and basalt. Recent studies by Thorson (1971) have shown that the area contains no true andesite.

On the basis of stratigraphic position, thickness, and composition, Longwell (1963) suggested correlations of the Oatman district volcanic rocks with the volcanic rocks that he mapped to the north between Lake Mead and Davis Dam (including the Eldorado Mountains), as shown in figure 7. In a later report, Anderson (1971a) indicated that the rocks mapped by Longwell (1963) as Golden Door Volcanics are correlative with the middle part of the Patsy Mine Volcanics and abandoned the name Golden Door Volcanics. This change in stratigraphic assignment is indicated in figure 7. Unfortunately, the Oatman district was not visited for the purpose of evaluating these suggested correlations. The evaluation that follows is based on K-Ar determinations (Thorson, 1971, and written commun., 1976; Anderson and others, 1972), lithologic description, and major-element chemistry (Wells, 1937; Thorson, 1971).

Thorson (1971) retained most of the stratigraphic units mapped by Ransome (1923), although he made minor revisions in nomenclature and added two units not mapped by Ransome. In particular, Thorson (1971) recognized an erosional unconformity at the top of the Gold Road Latite of Ransome (1923) and attempted to date the hiatus by obtaining K-Ar age determinations on rocks from both sides of the unconformity. The rock dated from above the unconformity was collected from one of the units not mapped by Ransome (1923). The K-Ar data (Thorson, 1971; written

Oatman district, (Ransome, 1923)	Area between Lake Mead and Davis Dam
Basalt	Fortification Basalt Member of the Muddy Creek Formation
Cottonwood Rhyolite Sitgreaves Tuff Meadow Creek Trachyte Flag Spring Trachyte Gold Road Latite	Patsy Mine Volcanics Middle part (as redefined by Anderson, 1971a)
Oatman Andesite Esperanza Trachyte Alcyone Trachyte Bedded breccia	Patsy Mine Volcanics Lower part (as redefined by Anderson, 1971a)

FIGURE 7.—Correlation diagram showing correlations suggested by Longwell (1963) between rocks of the Oatman district and those to the north between Lake Mead and Davis Dam.

commun., 1976) suggest that the hiatus was brief and occurred approximately 18.5 m.y. ago. This age falls within the age range of the Patsy Mine Volcanics, estimated to be about 20 to 15 m.y. on the basis of isotopic data reported by Anderson and others (1972). Five age dates from two horizons (including the base) in the middle part of the Patsy Mine Volcanics range from 16.1 to 15.3 m.y. These data indicate that the only units mapped by Ransome (1923) in the Oatman district that could be as young as the middle part of the Patsy Mine Volcanics are the Flag Spring Trachyte and overlying units (fig. 7). All of those units are locally derived (Thorson, 1971) and do not resemble the middle part of the Patsy Mine Volcanics or any of the overlying units in the Eldorado Mountains area. Thus, the only possible direct correlation between the two areas is between the lower part of the Patsy Mine Volcanics in the Eldorado Mountains area and the Gold Road Latite and subadjacent strata of Ransome (1923). These strata all lack olivine. The Alcyone Trachyte contains phenocrysts of biotite and potassium feldspar, and the Esperanza Trachyte and Gold Road Latite contain biotite. Much of the lower part of the Patsy Mine Volcanics is olivine-bearing dark andesite. Except for a thin ash-flow tuff unit of unknown source near the base of the unit, the rocks in the lower part of the Patsy Mine lack alkali feldspar phenocrysts, and biotite is sparse or absent. Thus, lithologic contrasts argue strongly against direct correlation between the two areas.

Chemical analyses of 19 rocks from the Oatman district were reported by Wells (1937). More recently, Thorson (1971), apparently unaware of the existence of the earlier data, conducted complete and partial analyses of 134 samples from the Oatman district and reported the results in the form of averages for each of 22 volcanic and plutonic units that he recognized. Thus, major-element chemical data are available for all volumetrically significant rock units exclusive of the youngest lavas, which are basalt.

None of the analyzed rocks from the Eldorado Mountains area are as rich in K_2O or normative orthoclase as the trachyte welded tuffs of Thorson (1971) and some of the biotite latites of Wells (1937). Thorson suggested that these relatively potassic rocks resulted from potassium enrichment in the upper part of the magma chamber and that they are cogenetic with their less potassic neighbors. Using the data reported by Wells (1937), the K_2O–SiO_2 variation for rocks from the Oatman district (fig. 3) yields a trend line with a slope of $y=0.229x-10.0$ and a correlation coefficient of 0.79 at the 95-percent confidence limit. Potassium contents in the samples from the Eldorado Mountains are somewhat erratic and show less variation with silica than the Oatman district rocks (fig. 3). For silica contents higher than 65 percent, potassium contents in the Oatman rocks are higher than in the rocks from the Eldorado Mountains, but at 60 percent silica no apparent distinction occurs between the two suites; the potassium contents are about 3.5 percent.

Comparison of weight percentages of alkalis and lime between the Eldorado Mountains and Oatman district rocks (fig. 5*B*) is difficult because both groups show appreciable scatter in the low-calcium range. Although the Eldorado Mountain rocks extend to more calcium-rich (mafic) compositions than the Oatman suite, it is clear from figure 5*B* that in the high-calcium range of the ternary diagram the Eldorado Mountains rocks tend to be poorer in potassium and (or) richer in sodium than the Oatman rocks. If the normative Q–OR–Ab+An data, exclusive of the relatively potassic trachyte welded tuffs reported by Thorson (1971), are fitted by a trend line (fig. 5*C*), then the line is essentially parallel to the Q–Ab + An join, suggesting that potassium contents are insensitive to the other major sialic components and that the K_2O–SiO_2 trend shown in figure 3 is a fundamental aspect of the chemistry of the Oatman rocks.

The youngest volcanic rocks in the Oatman district are olivine basalt lavas that Longwell (1963) suggested are probably equivalent to the Fortification

Basalt Member of the Muddy Creek Formation (fig. 7). In the Eldorado Mountains area, the broad stratigraphic range of olivine basalts that are petrographically and chemically similar to the Fortification Basalt Member precludes correlation over long distances on the basis of lithology. Therefore, the correlation suggested by Longwell (1963), although very reasonable, cannot be confirmed.

No parts of the stratigraphic sequence in the Eldorado Mountains appear to be directly correlative with the Oatman strata, which is not surprising in view of the fact that the lava piles are separated by more than 80 km. Petrographic and chemical data indicate that the pre-Fortification rocks in the Eldorado Mountains area range to more mafic compositions and include large volumes of andesite and basaltic andesite not found in the Oatman area. Also, some of the Oatman rocks are conspicuously more potassic, and most are slightly more potassic than rocks of similar silica content in the Eldorado Mountains area. Thus, the data indicate not only separate and distinct magma chambers for the two suites but possibly also different courses of magma generation.

Central Nye County, Nev. (250 km NW)

In the Nellis Air Force Base Bombing and Gunnery Range, central Nye County, Nev., eruptions of large volumes of rhyolitic ash-flow tuff during the latest Oligocene and early Miocene were followed during the middle Miocene by widespread eruptions of lavas and hypabyssal intrusive masses of less siliceous composition ranging down to basaltic andesite and meladiorite (Ekren and others, 1971; Anderson and Ekren, 1968). The middle Miocene igneous rocks covered an area of about 5000 km^2, and the volcanic activity culminated with eruption of ash-flow tuffs, lavas, and intrusive masses of predominantly rhyolitic composition. These late siliceous rocks are closely related chemically and petrographically to their more mafic predecessors (Anderson and Ekren, 1968; Ekren and others, 1971). The entire suite has a calc-alkaline characteristic and a Peacock index of 59. The K_2O content at 60 percent SiO_2 is estimated at 3.2 percent. The K-Ar age data indicate that the widespread igneous rocks of intermediate composition and their less mafic counterparts range in age from about 21 to 15 m.y. (Ekren and others, 1971).

Curves that fit visually to data points plotted on standard silica-variation diagrams for the widespread Miocene rocks of intermediate composition from Nye County are shown in figure 3. No appreciable differences in alkali contents exist between the Nye County rocks and those from the Eldorado Mountains, over the full range in silica variation. Over most of the range, the two curves representing total alkalis are only separated by 0.5 percent. At equivalent silica contents, the amounts of Al_2O_3 and total iron are lower and that of MgO is higher in the rocks from the Eldorado Mountains than in those from Nye County. The conspicuous difference in the ratio of total iron to magnesia is seen best in the AMF diagram (fig. 5*A*). The anomalously weak iron-enrichment trend exhibited by the Patsy Mine Volcanics is conspicuously different from the trend representing 18 tightly grouped analyses of intrusive rocks from the Cactus Range in Nye County.

Lava Mountains, San Bernardino County, Calif. (220 km W)

Smith (1964) mapped the Lava Mountains and described the chemistry and petrography of a cogenetic suite of middle to upper Pliocene high-silica andesites that cover an area of about 350 km^2 at the north edge of the Mojave Desert, San Bernardino County, Calif. Compared to the rocks from the Eldorado Mountains, the Lava Mountains rocks have a narrow silica range of from 60 to 72 percent. The field enclosing points on an AMF diagram, representing 22 analyses from Smith (1964), is shown in figure 5*A*. The position of the field is nondiscriminant when compared with the other data shown in that figure. Smith (1964) noted that alkali abundances are similar to typical calc-alkalic suites. He extrapolated curves beyond the limited silica variation to estimate an alkali-lime index of 58, which was midway between the Eldorado Mountains rocks (57) and the Nye County rocks (59). However, the Lava Mountains rocks are slightly higher in Na_2O and lower in K_2O than the other two suites. The percentage of K_2O at 60 percent SiO_2 is approximately 2.5. Also, the Lava Mountains rocks are wholly younger than those of the other two suites.

SUMMARY AND INTERPRETATION

Volcanic activity in the Eldorado Mountains displays an episodic nature that is characteristic of many areas of Cenozoic igneous activity in the Basin and Range province (Anderson and others, 1972). Although the age of inception is not well established, Cenozoic volcanic activity in the Eldorado Mountains ranged from about 20 to 5 m.y. and had its maximum development between about 19 and 12 m.y. The latter half of the main phase of volcanism (16–12 m.y.) was also a period of climatic widespread hypabyssal intrusive activity of batholithic proportions that was

overlapped and outlasted by a period of extensional tectonism (15–11 m.y.) of colossal magnitude (Anderson and others, 1972; Anderson, 1971a).

Chemical analyses of volcanic rocks erupted from the Eldorado Mountains indicate a range in the uncorrected silica percentage from about 48 to 74. Andesites and dacites predominate, although the rocks range in composition from basalt to rhyolite. The suite has a slightly abnormal calc-alkaline characteristic, shows no tendency toward bimodality, and does not contain high-silica or alkali rhyolites. The inception of intense extensional tectonism at about 15 m.y. was marked by an abrupt shift to more iron-rich and more typically calc-alkalic volcanic products (Mount Davis Volcanics) than those erupted earlier (Patsy Mine Volcanics), but no corresponding shift in alkali contents or ratios is recognized nor is there any obvious shift toward bimodality in the post-15-m.y. rocks. The more iron-rich rocks erupted during the main phase of extensional tectonism are more similar to calc-alkaline suites in nearby areas and elsewhere in the Basin and Range province than are their more iron-poor predecessors (fig. 5*A*). In contrast, basalts (Fortification Basalt Member) erupted after the main phase of extensional tectonism are more iron-rich than either their predecessors (Mount Davis Volcanics) or typical basalts in the Basin and Range province. Without speculating on the cause of these differences depicted on the AMF diagram, it is clear that they represent the most obvious major-element variation with time discernible in these rocks.

Documentation of the age at which igneous activity in each major area of Cenozoic igneous rocks in the Western United States shifted from predominantly andesitic to fundamentally basaltic constitutes a critical factor in establishing the time pattern in which the shift occurred as depicted by Christiansen and Lipman (1972, fig. 5). They indicated that the shift occurred prior to 18 m.y. for the lower Colorado River area. The only shift from predominantly andesitic to fundamentally basaltic that can be rationalized with the new age and chemical data from the Eldorado Mountains is at about 10 m.y. when the relatively small volume eruptions of Fortification Basalt Member began. This event does not mark a shift to a bimodal assemblage nor does it herald the beginning of extensional tectonism; it does, however, mark a change in the style of extensional tectonism, which, prior to that time, featured closely spaced curved shingling normal faults that flattened with depth and, after that time, featured basin-range-forming, high-angle normal faults that may have penetrated deep into the crust (Anderson, 1971b).

Limited isotopic data suggest that the change in structural style was accompanied by a shift from eruption of lavas with high initial Sr^{87}/Sr^{86} ratios of about 0.708 (Hedge and Noble, 1971; D. C. Noble, written commun., 1971) to lavas with conspicuously lower ratios. Scott and others (1971) reported whole-rock Sr^{87}/Sr^{86} initial ratios of 0.7048 and 0.7035 for two rocks collected in Arizona a few kilometers east of the Eldorado Mountains. Although the rocks were not assigned to a stratigraphic unit, their locations and descriptions indicate that they are correlative with the Fortification Basalt Member. Throughout the Basin and Range province, the suggestion is that young Cenozoic rocks have lower Sr^{87}/Sr^{86} ratios than the older ones (Scott and others, 1971), and the rocks from the Eldorado Mountains seem to fit that pattern.

Presumably the 18 m.y. date for the shift from predominantly andesitic to fundamentally basaltic suites given by Christiansen and Lipman (1972, fig. 5) also was intended to apply to the Oatman district. Lipman, Prostka, and Christiansen (1972, table 1) included the Oatman rocks with other lower and middle Cenozoic suites of predominantly andesitic composition and suggested that the rocks may correlate with the Patsy Mine Volcanics. The suggested correlation seems highly unlikely in the light of new age and chemical data as noted above. Christiansen and Lipman (1972, fig. 5) indicated uncertainty as to the validity of placing the Oatman rocks with the older predominantly andesitic suites. According to Thorson (1971), andesite is sparse or absent in the Oatman district. He recognized basalt at the base of the volcanic sequence, but it is volumetrically insignificant and is, in large part, reworked material in sedimentary rocks. He designated all other rocks, exclusive of capping basalt lavas, as rhyolite, trachyte, and latite. The suite is not bimodal from the chemical standpoint of Christiansen and Lipman (1972). Thus, new age and chemical data do not clarify with which of the two groups established by Lipman, Prostka, and Christiansen (1972) and Christiansen and Lipman (1972) the Oatman district rocks should be ranked. The rocks do not seem to fit into either group. What does seem clear, however, is that no shift from predominance of one lithologic type to another occurred at 18 m.y. If any shift did occur, it was from early relatively siliceous igneous activity to later basaltic activity at a time possibly contemporaneous with the eruption of the Fortification Basalt Member in the Eldorado Mountains. Knowledge of the structural history of the Oatman district is insufficient to evaluate this possible shift in terms of a change in tectonic environment.

On the basis of the foregoing summary, the north-

ern part of the lower Colorado River area appears to represent an anomaly in terms of the patterns of Cenozoic igneous and tectonic evolution of the Western United States outlined by Lipman, Prostka, and Christiansen (1972) and Christiansen and Lipman (1972). The Pliocene andesites of the Lava Mountains, San Bernardino County, Calif., are a typical calc-alkaline suite with no bimodal tendency (Smith, 1964). They, too, represent an anomaly in the suggested pattern of evolution as recognized by Christiansen and Lipman (1972, p. 263). Relatively recent data from Nye County, Nev., suggest that the area may also be anomalous. Christiansen and Lipman (1972) suggested that the transition from predominantly andesitic to bimodal basalt-rhyolite volcanism occurred there during the interval 18–16 m.y. ago. Four K-Ar ages for Fraction Tuff (a unit with typical calc-alkaline characteristics) range from 17.8 ± 0.5 to 15.0 ± 0.6 (Ekren and others, 1971, table 5). Post-Fraction Tuff intrusive rocks are indistinguishable chemically from the Fraction Tuff and related andesitic lavas (Anderson and Ekren, 1968), suggesting that calc-alkaline igneous activity predominated until at least 15 m.y. ago. A recent compilation of chemical data from the Timber Mountain–Oasis Valley caldera complex (Quinlivan and Byers, 1977) a short distance to the south in Nye County indicates that calc-alkalic volcanism continued there at the Sleeping Butte and Silent Canyon calderas until about 13 m.y. ago. It is certainly not the intent herein to emphasize a refinement indicated by chemical and K-Ar data. It does seem important, however, to evaluate whether or not these ages represent corresponding changes from orogenic or anorogenic to extensional tectonism as suggested by Christiansen and Lipman (1972).

Ekren and others (1968) suggested that normal faults in the Nevada Test Site and in the bombing range north of the test site started to form during or shortly after the extrusion of the oldest welded tuff dated at 26.5 m.y. and that displacements on some of those faults range to over 1 km. This suggestion was substantiated by continued geologic mapping of the bombing range in southern Nye County, Nev. (Ekren and others, 1971; R. E. Anderson, unpub. mapping). Evidence for early stratal tilting and normal faulting comes from the Cactus Range and the Mellan Hills, among other areas.

In the Cactus Range, the oldest recognizable phase of strong stratal tilting postdates the tuff of Antelope Springs (dated at about 27 m.y.) and predates the tuff of White Blotch Springs (dated at about 22 m.y.). The tilting may be of volcanotectonic origin. Additional phases of stratal tilting on normal faults in the Cactus Range are bracketed between the tuff of White Blotch Springs (dated at about 22 m.y.) and the Fraction Tuff (the oldest age indicated is 17.8 m.y.) and between the Fraction Tuff and the Thirsty Canyon Tuff (dated at about 7 m.y.). This latter phase involved large normal displacements on faults that dip toward the range at moderate angles. Several contacts that were first interpreted by the writer to be intrusive (Ekren and others, 1971) are now known to be moderately to gently dipping normal faults.

Ekren and others (1971, p. 75) expressed uncertainty as to the significance of a structural discordance revealed by opposed dips in Tertiary strata separated by a low-angle fault in the northern part of the Mellan Hills, Nye County, Nev. Ash-flow tuffs ranging in age from about 27 to 22 m.y. beneath that fault were probably tilted to their present steep dips during an early episode of normal faulting, and the rocks with opposed dips above the fault were juxtaposed during a later episode of faulting. Lavas equivalent in age to those above the fault are dated at about 18 m.y. (Ekren and others, 1971). The second period of normal faulting probably correlates with an episode of well-documented intense normal faulting that occurred between about 18 and 14 m.y. ago elsewhere in the Mellan Hills (Ekren and others, 1971, p. 75–76). Displacements were on a system of gently to moderately dipping faults that are similar in style and age to those described from the Eldorado Mountains area by Anderson (1971a). The early faulting in the Cactus Range and the Mellan Hills reflects a control by more deeply seated processes than mere gravity sliding and indicates fundamental crustal extension during episodes of calc-alkaline igneous activity that cannot be classified as fundamentally basaltic or bimodal.

REFERENCES CITED

Anderson, R. E., 1971a, Thin skin distension in Tertiary rocks of southeastern Nevada: Geol. Soc. America Bull., v. 82, no. 1, p. 43–58.

——— 1971b, Thin skin distension in Tertiary rocks of southeastern Nevada—Reply: Geol. Soc. America Bull., v. 82, no. 12, p. 3533–3536.

——— 1977, Composite stratigraphic section of Tertiary rocks in the Eldorado Mountains, Nevada: U.S. Geol. Survey Open-File Rept. 77–483, 5 p.

Anderson, R. E., and Ekren, E. B., 1968, Widespread Miocene igneous rocks of intermediate composition, southern Nye County, Nevada, *in* Nevada Test Site: Geol. Soc. America Mem. 110, p. 57–63.

Anderson, R. E., Longwell, C. R., Armstrong, R. L., and Marvin, R. F., 1972, Significance of K–Ar ages of Tertiary rocks from the Lake Mead region, Nevada-Arizona: Geol. Soc. America Bull., v. 83, no. 2, p. 273–288.

Christiansen, R. L., and Lipman, P. W., 1972, Cenozoic volcanism and plate tectonic evolution of the Western United

States, pt. 2, Late Cenozoic, *in* A discussion on volcanism and the structure of the earth: Royal Soc. London Philos. Trans., Ser. A, v. 271, p. 249–284.

Church, B. N., 1975, Quantitative classification and chemical comparison of common volcanic rocks: Geol. Soc. America Bull., v. 86, p. 257–263.

Daly, R. A., 1933, Igneous rocks and the depths of the earth: New York, McGraw-Hill Book Co., 508 p.

Ekren, E. B., Rogers, C. L., Anderson, R. E., and Orkild, P. P., 1968, Age of Basin and Range normal faults in Nevada Test Site and Nellis Air Force Range, Nevada, *in* Nevada Test Site: Geol. Soc. America Mem. 110, p. 247–250.

Ekren, E. B., Anderson, R. E., Rogers, C. L., and Noble, D. C., 1971, Geology of northern Nellis Air Force Base bombing and gunnery range, Nye County, Nevada: U.S. Geol. Survey Prof. Paper 651, 91 p.

Hansen, S. M., 1962, The geology of the Eldorado mining district, Clark County, Nevada: Missouri Univ., Ph. D. thesis, 328 p.

Hedge, C. E., and Noble, D. C., 1971, Upper Cenozoic basalts with high Sr^{87}/Sr^{86} and Sr/Rb ratios, southern Great Basin, western United States: Geol. Soc. America Bull., v. 82, no. 12, p. 3503–3510.

Irvine, T. N., and Baragar, W. R. A., 1971, A guide to the chemical classification of the common volcanic rocks: Canadian Jour. Earth Sci., v. 8, no. 5, p. 523–548.

Leeman, W. P., and Rogers, J. J. W., 1970, Late Cenozoic alkali-olivine basalts of the Basin-Range province, U.S.A.: Contr. Mineralogy and Petrology, v. 25, no. 1, p. 1–24.

Lipman, P. W., 1965, Chemical comparison of glassy and crystalline volcanic rocks: U.S. Geol. Survey Bull. 1201–D, p. D1–D24.

Lipman, P. W., Christiansen, R. L., and Van Alstine, R. E., 1969, Retention of alkalis by calc-alkalic rhyolites during crystallization and hydration: Am. Mineralogist, v. 54, p. 286–291.

Lipman, P. W., Prostka, H. J., and Christiansen, R. L., 1972, Cenozoic volcanism and plate tectonic evolution of the Western United States, pt. 1, Early and middle Cenozoic, *in* A discussion on volcanism and the structure of the earth: Royal Soc. London Philos. Trans., Ser. A, v. 271, no. 1213, p. 217–248.

Longwell, C. R., 1963, Reconnaissance geology between Lake Mead and Davis Dam, Arizona-Nevada: U.S. Geol. Survey Prof. Paper 374–E, p. E1–E51.

Noble, D. C., 1965, Ground-water leaching of sodium from quickly cooled volcanic rocks: Am. Mineralogist, v. 50, p. 289.

——— 1967, Sodium, potassium, and ferrous iron contents of some secondarily hydrated natural silicic glasses: Am. Mineralogist, v. 52, p. 280–286.

Quinlivan, W. D., and Byers, F. M., Jr., 1977, Chemical data and variation diagrams of igneous rocks from the Timber Mountain—Oasis Valley caldera complex, southern Nevada: U.S. Geol. Survey Open-File Rept. 77–724, 24 p.

Ransome, F. L., 1907, Preliminary account of Goldfield, Bullfrog, and other mining districts in southern Nevada, *with notes on the Manhattan district* by G. H. Garrey and W. H. Emmons: U.S. Geol. Survey Bull. 303, 98 p.

——— 1923, Geology of the Oatman gold district Arizona—A preliminary report: U.S. Geol. Survey Bull. 743, 58 p.

Scott, R. B., Nesbitt, R. W., Dasch, E. J., and Armstrong, R. L., 1971, A strontium isotope evolution model for Cenozoic magma genesis, eastern Great Basin, U.S.A.: Bull. Volcanology, v. 35, p. 1–26.

Smith, G. I., 1964, Geology and volcanic petrology of the Lava Mountains, San Bernardino County, California: U.S. Geol. Survey Prof. Paper 457, 97 p.

Spurr, J. E., 1903, Descriptive geology of Nevada south of the fortieth parallel and adjacent portions of California: U.S. Geol. Survey Bull. 208, 229 p.

Thorson, J. P., 1971, Igneous petrology of the Oatman district, Mohave County, Arizona: Santa Barbara, California Univ., Ph. D. thesis, 173 p.

Vanderburg, W. O., 1937, Reconnaissance of mining districts in Clark County, Nevada: U.S. Bur. Mines Inf. Circ. 6964, 81 p.

Washington, H. S., 1917, Chemical analyses of igneous rocks published from 1884 to 1913: U.S. Geol. Survey Prof. Paper 99, 1201 p.

Wells, R. C., 1937, Analyses of rocks and minerals from the laboratory of the United States Geological Survey, 1914–1936: U.S. Geol. Survey Bull. 878, 134 p.

CHANGE OF ADDRESS FORM

NAME—FIRST, LAST

COMPANY NAME OR ADDITIONAL ADDRESS LINE

STREET ADDRESS

CITY | STATE | ZIP CODE

PLEASE PRINT OR TYPE

(or) COUNTRY

Mail this form to:

NEW ADDRESS
Journal of Research of the
U.S. Geological Survey
Superintendent of Documents
Government Printing Office SSOM
Washington, DC 20402

Attach last subscription label here.

(please detach here)

SUBSCRIPTION ORDER FORM

SUBSCRIPTION ORDER FORM

Enter my subscription to "Journal of Research of the U.S. Geological Survey" at $18.90 (domestic) or $23.65 (foreign). Domestic remittance should be made by money order or check. Foreign remittance should be made by international money order, draft on an American bank, or UNESCO coupons.

NAME—FIRST, LAST

COMPANY NAME OR ADDITIONAL ADDRESS LINE

STREET ADDRESS

CITY | STATE | ZIP CODE

PLEASE PRINT OR TYPE

(or) COUNTRY

☐ Remittance Enclosed (Make checks payable to Superintendent of Documents)

☐ Charge to my deposit Account No.....

MAIL ORDER FORMS TO:
Superintendent of Documents
Government Printing Office
Washington, DC 20402

ANNOUNCEMENT

DIRECT-MAIL SALES OF USGS OPEN-FILE REPORTS By the U.S. Geological Survey

Purpose of Program

- To furnish microfiche or paper-duplicate copies of open-file reports from a single, centrally located facility.
- To provide faster order-filling service to the public for copies of open-file reports.
- To increase the availability of earth-science information to the scientific community.

Order USGS Open-File Reports From:

Open-File Services Section, Branch of Distribution, U.S. Geological Survey, Box 25425, Federal Center, Denver, CO 80225. (Telephone: 303-234-5888.)

Price information will be published in the monthly listing "New Publications of the Geological Survey."

This facility will stock open-file reports only. Please do not mix orders for open-file reports with orders for any other USGS products. Checks or money orders, in exact amount for open-file reports ordered, should be made payable to U.S. Geological Survey. Prepayment is required.

Order by series and number (such as Open-File Report 77-123) and complete title.

Inquiries concerning this new program should be sent to the address given above.

☆U.S.GOVERNMENT PRINTING OFFICE: 1978--261-198/7

SHEET AT C-96 50%

RECENT PUBLICATIONS OF THE U.S. GEOLOGICAL SURVEY

The following books may be ordered from the Branch of Distribution, U.S. Geological Survey, 1200 South Eads Street, Arlington, VA 22202 (an authorized agent of the Superintendent of Documents, Government Printing Office). Prepayment is required. Remittances should be sent by check or money order payable to U.S. Geological Survey. Give series designation and number, such as Bulletin 1368–A, and the full title. Prices of Government publications are subject to change. Increases in costs make it necessary for the Superintendent of Documents to increase the selling prices of many publications offered. As it is not feasible for the Superintendent of Documents to correct the prices manually in all the previous announcements and publications stocked, the prices charged on your order may differ from the prices printed in the announcements and publications.

In addition to the publications mentioned below, other professional papers, water-supply papers, bulletins, circulars, single copies of the periodical "Earthquake Information Bulletin," maps, and items of general interest, such as leaflets, pamphlets, and booklets, are available at the above address. All new Survey publications are listed in a free monthly catalog, "New Publications of the Geological Survey"; to subscribe, send name and address to U.S. Geological Survey, 329 National Center, Reston, VA 22092. (Some reports that are now out of print at the Superintendent of Documents can also be obtained at the Branch of Distribution address.)

Professional Papers

P 373. Aerial photographs in geologic interpretation and mapping by R. G. Ray. 1960. 230 p. $5.25 (Reprint.)

P 676. Geology and fuel resources of the Fruitland Formation and Kirtland Shale of the San Juan Basin, New Mexico and Colorado, by J. E. Fassett and J. S. Hinds. 1971. 76 p.; plates in pocket. $1.80 (Reprint.)

P 942. Flood-prone areas and land-use planning—Selected examples from the San Francisco Bay region, California, by A. O. Waananen, J. T. Limerinos, W. J. Kockelman, W. E. Spangle, and M. L. Blair. 1977. 75 p. $2.20. (Reprint.)

P 956. Geology of the Minturn 15-minute quadrangle, Eagle and Summit Counties, Colorado, by Ogden Tweto and T. S. Lovering. 1977. 96 p.; plate in pocket. $3.50.

P 969. Some engineering geologic factors controlling coal mine subsidence in Utah and Colorado, by C. R. Dunrud. 1976. 39 p. $1.25. (Reprint.)

P 996. Upper Ordovician and Silurian stratigraphy in Sequatchie Valley and parts of adjacent valley and ridge, Tennessee, by R. C. Milici and Helmuth Wedow, Jr. 1977. 38 p.; plates in pocket. $2.10.

P 1009. Characteristic marine molluscan fossils from the Dakota Sandstone and intertongued Mancos shale, west-central New Mexico, by W. A. Cobban. 1977. 30 p., 21 plates. $2.50.

P 1022-B. Water-quality effects on Baker Lake of recent volcanic activity at Mount Baker, Washington, by G. C. Bortleson, R. T. Wilson, and B. L. Foxworthy. 1977. p. B1–B30; plate in pocket. $2.

P 1036. Steller's sea cow (*Hydrodamalis gigas*) of Late Pleistocene age from Amchitka, Aleutian Islands, Alaska, by F. C. Whitmore, Jr., and L. M. Gard, Jr. 1977. 19 p., 8 plates. $1.80.

P 1040. Stochastic analysis of particle movement over a dune bed, by B. K. Lee and H. E. Jobson. 1977. 72 p. $2.50. (Supersedes Open-File Report 75–358.)

Bulletins

B 1397-C. Mineral resources of the Ramseys Draft Wilderness Study Area, Augusta County, Virginia, by F. G. Lesure, P. J. Geraci, P. C. Mory, and B. B. Williams. 1977. p. C1–C42; plates in pocket. $2.50.

B 1421-B. Thermodynamic properties of the coexisting phases and thermochemical properties of the NaCl component in boiling NaCl solutions, by J. L. Haas, Jr. 1976. p. B1–B71. $2.10. (Revised 1977.)

B 1426. Bibliography of reports resulting from U.S. Geological Survey technical cooperation with other countries, 1967–74, by W. E. Bergquist. 1976 (1977). 68 p. 90¢.

B 1430. Mineral resources of the proposed additions to the Scapegoat Wilderness, Powell and Lewis and Clark Counties, Montana, by R. L. Earhart, D. J. Grimes, R. W. Leinz, and L. Y. Marks, *with a section on* Geophysical surveys, by D. L. Peterson. 1977. 62 p.; plates in pocket. $3. (Supersedes Open-File Report 76–438.)

B 1437. The Permian and Triassic Seven Devils Group, western Idaho and northeastern Oregon, by T. L. Vallier. 1977. 58 p. $1.90.

B 1439. Mineral resources of the Jarbidge Wilderness and adjacent areas, Elko County, Nevada, by R. R. Coats, R. C. Green, L. D. Cress, and L. Y. Marks, *with a section on* Interpretation of aeromagnetic data, by W. E. Davis. 1977. 79 p.; plates in pocket. $3.25.

B 1445. A manual on fire assaying and determination of the noble metals in geological materials, by Joseph Haffty, L. B. Riley, and W. D. Goss. 1977. 58 p. $2.

Water-Supply Papers

W 1608–P. Ground-water resources of Cambodia, by W. C. Rasmussen and G. M. Bradford. 1977. p. P1–P122; plates in pocket. $3.75.

W 1999–E. Mean annual runoff as related to channel geometry of selected streams in California, by E. R. Hedman. 1970. p. E1–E17. $1. (Reprint.)

W 2137. Surface water supply of the United States, 1966–70, pt. 16—Hawaii and other Pacific areas. 1977. 750 p. $5.85.

W 2161. Ground-water levels in the United States, 1971–74, northwestern States. 1977. 153 p. $2.50.

W 2164. Ground-water levels in the United States, 1973–74, northeastern States. 1977. 126 p. $2.50.

W 2165. Ground-water levels in the United States, 1974, southeastern States, 1977. 116 p. $2.25.

Techniques of Water Resources Investigations

TWI 3–A11. Measurement of discharge by the moving-boat method, by G. F. Smoot and C. E. Novak. 1969. 22 p. $1.20. (Reprint.)

TWI 3–C3. Computation of fluvial-sediment discharge, by George Porterfield. 1972. 66 p. $2.10. (Reprint.)

TWI 4–A1. Some statistical tools in hydrology, by H. C. Riggs. 1968. 39 p. $1.60. (Reprint.)

TWI 4–D1. Computation of rate and volume of stream depletion by wells, by C. T. Jenkins. 1968. 17 p. $1.10. (Reprint.)

TWI 5–C1. Laboratory theory and methods for sediment analysis, by H. P. Guy. 1969. 58 p. $2.10. (Reprint.)

TWI 8–B2. Calibration and maintenance of vertical-axis type current meters, by G. F. Smoot and C. E. Novak. 1968. 15 p. $1.10. (Reprint.)